



UvA-DARE (Digital Academic Repository)

Spatio-temporal organization of the lipid II flippase MurJ and the lateral wall synthesizing proteins RodA and PBP2

Liu, X.

Publication date

2019

Document Version

Final published version

License

Other

[Link to publication](#)

Citation for published version (APA):


Liu, X. (2019). *Spatio-temporal organization of the lipid II flippase MurJ and the lateral wall synthesizing proteins RodA and PBP2*. [Thesis, fully internal, Universiteit van Amsterdam].

General rights

It is not permitted to download or to forward/distribute the text or part of it without the consent of the author(s) and/or copyright holder(s), other than for strictly personal, individual use, unless the work is under an open content license (like Creative Commons).

Disclaimer/Complaints regulations

If you believe that digital publication of certain material infringes any of your rights or (privacy) interests, please let the Library know, stating your reasons. In case of a legitimate complaint, the Library will make the material inaccessible and/or remove it from the website. Please Ask the Library: <https://uba.uva.nl/en/contact>, or a letter to: Library of the University of Amsterdam, Secretariat, Singel 425, 1012 WP Amsterdam, The Netherlands. You will be contacted as soon as possible.

A microscopic view of numerous rod-shaped bacteria, likely Bacillus subtilis, showing their characteristic shape and some surface texture. The bacteria are distributed across the slide, with a higher density in the central and right-hand portions.

Spatio-temporal organization of the lipid II flippase MurJ and the lateral wall synthesizing proteins RodA and PBP2

Xiaolong Liu

University of Amsterdam

**Spatio-temporal organization of the lipid II flippase
MurJ and the lateral wall synthesizing
proteins RodA and PBP2**

ACADEMISCH PROEFSCHRIFT

ter verkrijging van de graad van doctor
aan de Universiteit van Amsterdam
op gezag van de Rector Magnificus
prof. dr. ir. K.I.J. Maex

ten overstaan van een door het College voor Promoties ingestelde
commissie,

in het openbaar te verdedigen in de Aula der Universiteit
op donderdag 5 december 2019, te 15:00 uur

door

Xiaolong Liu

geboren te Shanxi

Promotor:	dr. T. den Blaauwen	Universiteit van Amsterdam
Copromotor:	prof. dr. L. W. Hamoen	Universiteit van Amsterdam
Overigen leden:	prof. dr. W. Vollmer	Newcastle University
	prof. dr. G. van Wezel	Universiteit Leiden
	prof. dr. S. Brul	Universiteit van Amsterdam
	prof. dr. J. H. van Maarseveen	Universiteit van Amsterdam
	prof. dr. B. H. ter Kuile	Universiteit van Amsterdam
	dr. J. Luirink	Vrije Universiteit Amsterdam
	dr. E. Breukink	Universiteit Utrecht

Faculteit der Natuurwetenschappen, Wiskunde en Informatica

The research described in this thesis was conducted in the Bacterial Cell Biology and Physiology (BCBP) group at the Swammerdam Institute for Life Science (SILS), Faculty of Science, University of Amsterdam. The work was financially supported by the China Scholarship Council (File No. 201406220123) and the University of Amsterdam.

Table of Contents

CHAPTER 1	General introduction	5
	<i>Bacterial cell wall</i>	6
	<i>Peptidoglycan and antibiotic resistance</i>	6
	<i>Peptidoglycan biosynthesis</i>	8
	<i>Lipid II flippase</i>	9
	<i>PBPs and SEDS proteins</i>	11
	<i>Elongasome proteins and their interaction</i>	12
	<i>Assembling the Divisome</i>	15
	<i>Scope of this thesis</i>	16
	<i>References</i>	18
CHAPTER 2	FtsW activity and lipid II synthesis are required for recruitment of MurJ to midcell during cell division in <i>Escherichia coli</i>	27
	<i>Abstract</i>	28
	<i>Introduction</i>	29
	<i>Results</i>	31
	<i>Discussion</i>	46
	<i>Material and methods</i>	51
	<i>Acknowledgement</i>	57
	<i>Author contributions</i>	57
	<i>References</i>	58
	<i>Supplementary Information</i>	65
CHAPTER 3	MreC and MreD balance the interaction between the elongasome proteins PBP2 and RodA	82
	<i>Abstract</i>	83
	<i>Introduction</i>	84
	<i>Results</i>	86
	<i>Discussion</i>	99
	<i>Materials and Methods</i>	101
	<i>References</i>	107
	<i>Supplementary informations</i>	111

CHAPTER 4 Interaction between RodA and MreCD proteins is essential for MreB localization and elongasome function	128
<i>Abstract</i>	129
<i>Introduction</i>	130
<i>Results</i>	132
<i>Discussion</i>	143
<i>Materials and methods</i>	146
<i>Acknowledgements</i>	150
<i>References</i>	151
<i>Supplementary information</i>	155
CHAPTER 5 General Discussion	164
<i>Flipping lipid II across the cytoplasmic membrane</i>	165
<i>Interactions between elongasome proteins</i>	166
<i>Regulation of peptidoglycan synthesis by elongasome and divisome</i>	169
<i>References</i>	171
Summary	174

CHAPTER

1

General introduction

Bacterial cell wall

Peptidoglycan and antibiotic resistance

Peptidoglycan biosynthesis

Lipid II flippase

PBPs and SEDS proteins

Elongasome proteins and their interaction

Assembling the Divisome

Scope of this thesis

Bacterial cell wall

Bacteria belong to the kingdom of prokaryotic microorganisms¹. They exist almost everywhere on earth, including the environments with extreme temperatures and pressures², and can live with plants and animals in symbiotic and parasitic relationships^{3,4}. Although bacteria are generally small (*i.e.* of micrometer scale) and invisible to the unaided eyes, they play important roles in the entire ecology system. Despite the variations in shape, typical bacteria are single cell organisms surrounded by a cell wall (envelope) that is distinguishable from the cell wall of eukaryotic plant cells. Based on the structural differences of their cell walls, bacteria are classified into two main groups, the gram-positive and gram-negative bacteria. Gram-positive bacteria, such as *Bacillus subtilis*, possess a thick cell envelope that contains a cytoplasmic lipid membrane, multiple layers of peptidoglycan and teichoic acids, and a small periplasm space in between the cytoplasmic membrane and peptidoglycan layers (Fig. 1A). While gram-negative bacteria, such as *Escherichia coli*, possess a cell envelope composed of a cytoplasmic (inner) membrane, an outer membrane containing lipopolysaccharides on the outer leaflet, and in-between both membranes a wider periplasm that contains a thin peptidoglycan layer (Fig. 1B).

Peptidoglycan and antibiotic resistance

Peptidoglycan is a unique and important component of bacteria cell walls^{5,6}. It is a mesh-like macromolecular consisting of alternating *N*-acetylmuramic acid (MurNAc)–pentapeptide and *N*-acetylglucosamine (GlcNAc) residues that are connected by β -(1,4) glycosidic bonds and are cross-linked by peptide side chains (Fig. 1C)^{6,7}. In *E. coli*, the cross-links in peptidoglycan are mainly of the 4–3 type between the D-Ala⁴ and *meso*-DAP³ residues of two peptide side chains with a low percentage of 3–3 cross-links between the two *meso*-DAP³ residues^{6,8}. The peptidoglycan layer in gram-positive bacteria can be as thick as 20 to 80 nm, while in gram-negative bacteria it is only 7 to 8 nm in thickness. The peptidoglycan layer determines the shape of bacteria, protects

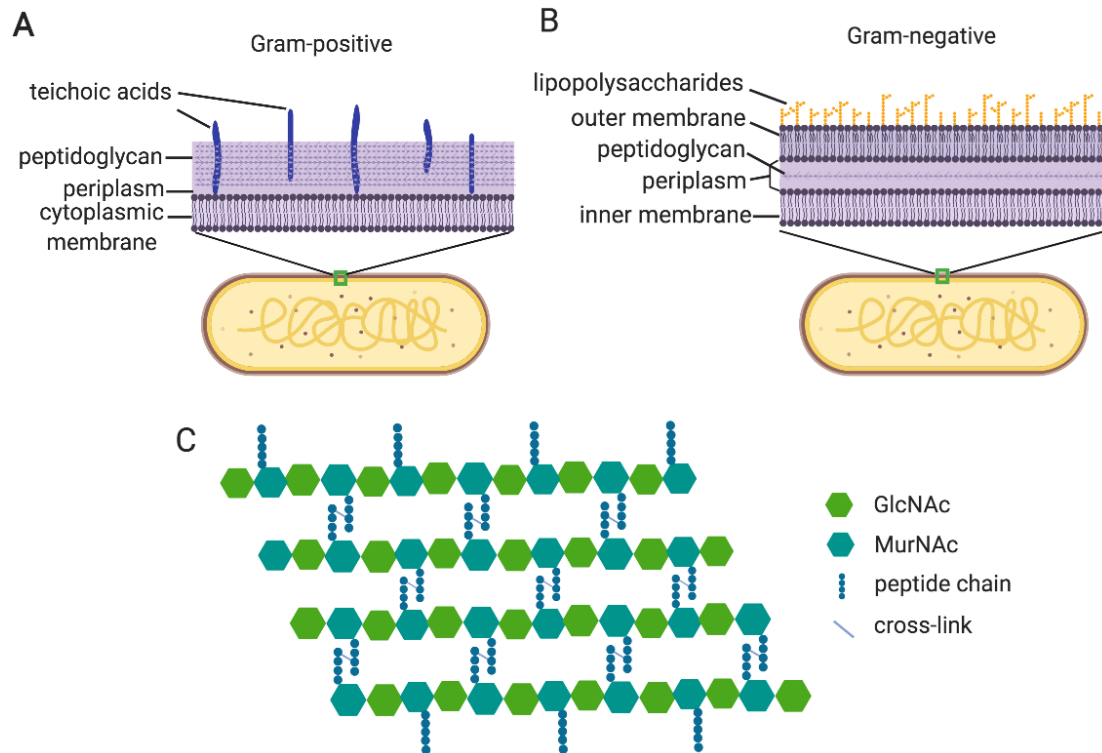


Figure 1. Schematic illustration of the architecture of the gram-positive and gram-negative bacterial cell envelope and peptidoglycan. (A) The cell envelope of gram-positive bacteria consists of a double-layered phospholipid cytoplasmic membrane, a thick layer of peptidoglycan and teichoic acids. The small space between the lipid membrane and peptidoglycan is the periplasm. (B) The cell envelope of gram-negative bacteria consists of an inner membrane, an outer membrane that contains an outer leaflet of lipopolysaccharides, and a wider periplasm accommodating a thin layer of peptidoglycan. (C) Structure of peptidoglycan. The mesh-like peptidoglycan layer is composed of glycan strands that are composed of repeating *N*-MurNAc-pentapeptide- β -(1.4)-*N*-GlcNAc dissacharides that are cross-linked through its peptide side chains.

them from osmotic lysis, and also functions as scaffold for many inner and/or outer membrane proteins^{9,10}. Defects in peptidoglycan biosynthesis results in irregular cell shape and eventual cell lysis^{11,12}. These essential roles of peptidoglycan make its biosynthesis pathway a key target of many antibiotics that are used in clinical therapy against bacterial infections^{13–16}.

A major group of antibiotics is the β -lactam family that inhibits the activity of penicillin binding proteins (PBPs) during peptidoglycan synthesis^{13,14,16,17}. However, over years, the widespread use (even abuse) of β -lactam antibiotics has led to a rapid increase in resistance to these

antibiotics in bacteria, while in contrast, the discovery of new antibiotics has largely fallen behind^{18–23}. Bacteria develop resistance to β -lactam antibiotics mainly in four different ways. (1) In the natural world, some gram-positive bacteria bear genes that encode the β -lactamases that are able to degrade β -lactam antibiotics. The transfer of these genes between species results into rapidly spreading of resistance²⁴. (2) More commonly, bacteria can eventually gain mutations in the target proteins of β -lactam antibiotics, and encode low affinity PBPs proteins¹⁸. (3) When exposed to β -lactam antibiotics, bacteria can employ unusual PBPs to bypass the steps that β -lactam antibiotics targets. For example, *E. coli* can use the LD-transpeptidase LdtD to catalyze 3–3 cross-linking in peptidoglycan, to compensate for the inhibition of D-D transpeptidase activity by ampicillin and aztreonam⁸. (4) Bacteria can develop strategies to pump out the antibiotics, and reduce the cellular concentrations^{19,25}.

Nowadays, antibiotic resistance has already become a serious public healthy issue that causes thousands of death each year^{20,22,26}. This situation calls urgently for developing of novel effective antibiotics that target essential process, for instance in the bacterial envelope, which is partly dependent on a better understanding of peptidoglycan synthesis in bacteria.

Peptidoglycan biosynthesis

Synthesis of peptidoglycan in bacteria is a complicated process catalyzed by many essential proteins, and can be divided into three stages: the cytoplasmic stage, the inner membrane stage and periplasmic stage (Fig. 2). (1) The cytoplasmic stage that begins with conversion of fructose-6-phosphate into UDP-GlcNAc by the enzymes GlmS, GlmU and GlmM. The produced UDP-GlcNAc is subsequently converted to UDP-MurNAc by the proteins MurA and MurB. After this, $_L$ -alanine, $_D$ -glutamic acid and diamino acid (generally meso-diaminopimelic acid or L-lysine) are added step by step to the UDP-MurNAc by the enzymes MurC, MurD and MurE, to generate UDP-MurNAc-tripeptide²⁷. A $_D$ -Ala- $_D$ -Ala dipeptide, which is catalyzed from $_L$ -alanine by the alanine racemase and $_D$ -alanine: $_D$ -alanine ligase, is then added to UDP-MurNAc-tripeptide to yield UDP-MurNAc-pentapeptide, which is the final

product of the cytoplasmic stage for peptidoglycan synthesis^{27,28}. (2) The inner membrane stage employs the enzymes that catalyze the formation of lipid II on the inner leaf of membrane and translocate it across the inner membrane^{29,30}. The first step of this stage is catalyzed by the essential inner membrane protein MraY that transfers phospho-MurNAc-pentapeptide moiety to the lipid carrier undecaprenyl phosphate (C₅₅-P), to yield the lipid-linked intermediate lipid I³¹⁻³⁴. Subsequently, lipid I is catalyzed by the membrane associated protein MurG that adds a unit of UDP-GlcNAc on lipid I, to form lipid II³⁵⁻³⁸, which is the building unit of peptidoglycan. Afterwards, lipid II is translocated by the flippase from the inner leaf to the outer leaf of the inner membrane³⁹⁻⁴¹, where it can be used to build the peptidoglycan layer. (3) In the periplasmic stage, the disaccharide-pentapeptide moiety of lipid II is polymerized and cross-linked into the existing peptidoglycan layer via the glycosyltransferase and transpeptidase activities of penicillin binding proteins (PBPs) and other PG synthesizing proteins.^{42,43} The cleaved lipid carrier moiety is then recycled⁴⁴.

Lipid II flippase

The discovery of the lipid II flippase is historical. The existence of this essential transporter has been hypothesized for decades⁴⁵ and for many years, two essential inner membrane proteins of the SEDS (Shape, Elongation, Division and Sporulation) family, RodA and FtsW, had been assumed to be the lipid II flippases. Both RodA and FtsW interact with their partner PBPs (PBP2 and PBP3, respectively) to form protein subcomplexes for peptidoglycan synthesis⁴⁶⁻⁵¹, and FtsW from *E. coli* has been shown to have lipid II flipping activity *in vitro*⁵². However, more and more evidence supports that MurJ, a member of the MOP (Multidrug/Oligosaccharidyl-lipid/Polysaccharide) exporter superfamily family, is the lipid II flippase during peptidoglycan synthesis³⁹.

MurJ is an essential inner membrane protein that contains 14 trans-membrane helices (TMHs)^{53,54}. It was firstly identified based on bioinformatic filtering of the essential inner membrane proteins in *E. coli*. Depletion of MurJ results in irregular cell shape and eventually cell lysis, and reduces

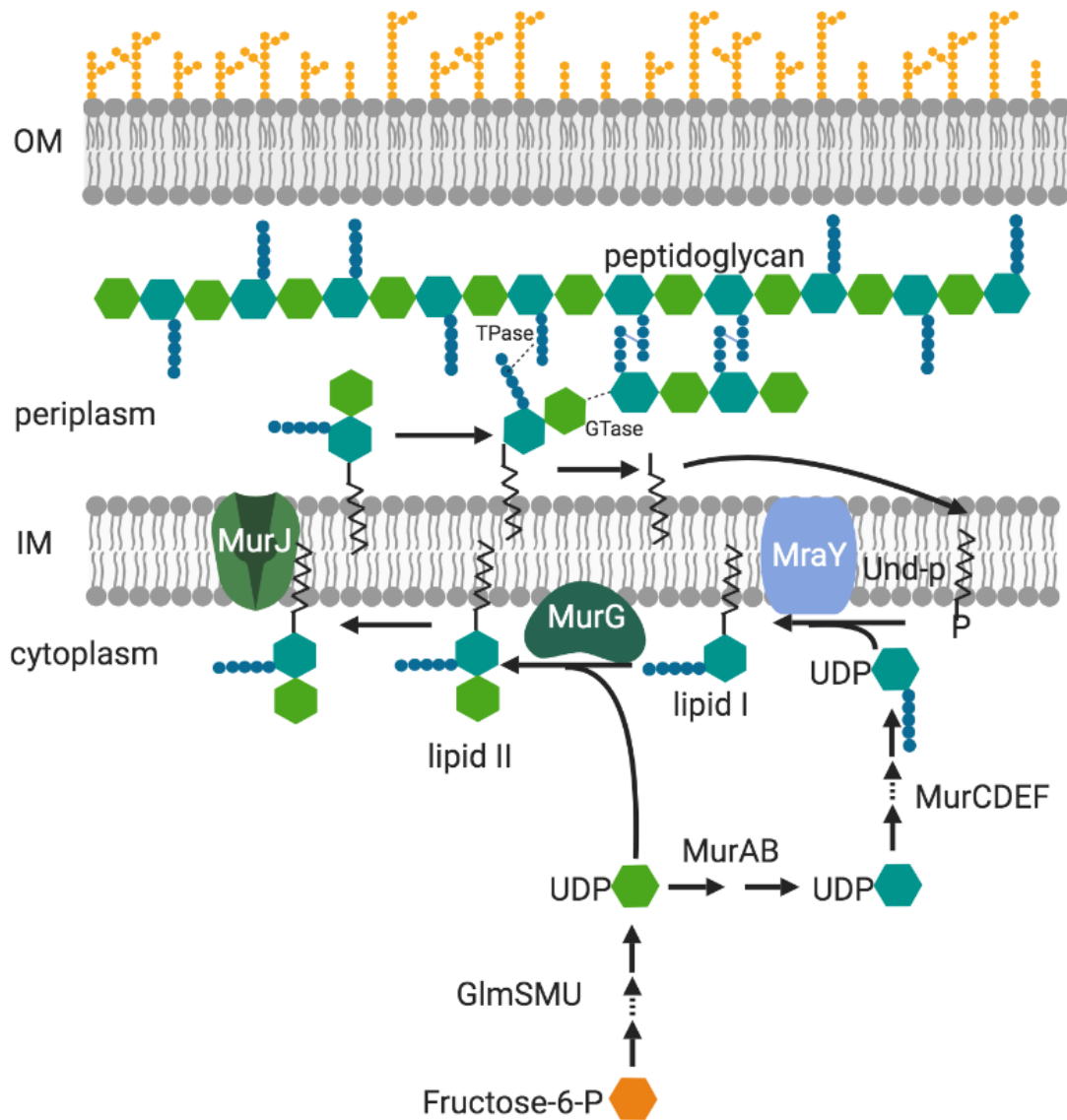


Figure 2. Schematic illustration of peptidoglycan synthesis in *E. coli*. Peptidoglycan synthesis initiates from the cytoplasm by converting fructose-6-P into UDP-GlcNAc and UDP-MurNAC-pentapeptide, which are subsequently combined to form lipid II by a following inner membrane stage. Lipid II is then flipped across the inner membrane by the flippase MurJ and is polymerized cross-linked and inserted into the murein layer in the periplasm. IM: inner membrane. OM: outer membrane. TPase: transpeptidase. GTase: glycosyltransferase.

peptidoglycan biosynthesis³⁹. More directly, only MurJ, but neither FtsW nor RodA, showed the *in vivo* lipid II flipping activity⁴⁰. Also, a viral inhibitory protein that targets MurJ has shown to abolish lipid II flipping⁵⁵. Early topological and functional studies of MurJ from *E. coli* have revealed an outward-facing central cavity that contains many essential residues^{56,57}, while

the later crystal structures of MurJ from *E. coli* and *Thermosipho africanus* both demonstrate the inward-facing conformation^{53,54}. According to its role as flippase, these results suggest potential conformational changes of MurJ during lipid II flipping. However, how MurJ performs its activity during peptidoglycan synthesis is not clear, and how these essential residues that are situated in the central cavity influence MurJ function is also a question to be answered.

PBPs and SEDS proteins

For peptidoglycan mesh assembly, the required glycosyltransferase and transpeptidase activities are mainly provided by the penicillin binding proteins⁴³. So far, there are 12 PBPs identified in *E. coli*. According to their structural features and functions, these PBPs are classified into three classes: class A, class B and class C PBPs^{42,43}.

Class A PBPs are the group of bifunctional proteins that possess both glycosyltransferase and transpeptidase activity. *E. coli* encodes three class A PBPs: PBP1a, PBP1b and PBP1c^{42,43}. These proteins have a cytoplasmic N-terminus, a trans-membrane helix and a large periplasmic domain. Their periplasmic domain can be further divided into the N-terminal domain and C-terminal domain that have glycosyltransferase activity and transpeptidase activity, respectively⁵⁸⁻⁶⁰. PBP1a and PBP1b function primarily in *E. coli* length growth and division, respectively, and they can replace each other function⁶⁰⁻⁶⁴. The role of PBP1c is not yet fully understood, as it cannot compensate the function of PBP1a or PBP1b. Also, PBP1c is not affected by most β -lactam antibiotics⁶⁵.

Class B PBPs are the group of monofunctional proteins that only have transpeptidase activity. *E. coli* encodes two class B PBPs: PBP2 and PBP3 that function during length growth and division, respectively^{42,59,66-70}. Topological and structural analysis indicate that class B PBPs also have a cytoplasmic N-terminus, a trans-membrane helix and a large periplasmic domain that can be divided into an N-terminal domain and a C-terminal domain. The C-terminal domain has transpeptidase activity, while the N-

terminal domain does not have any known activity^{42,59} but is believed to be important for the interactions with other proteins⁷¹⁻⁷³.

E. coli encodes seven class C PBPs that are mainly responsible for the modification, recycling or cleavage of peptidoglycan, during length growth, division and daughter cell separation. These proteins are generally functioning in the periplasmic space and not essential for growth because of their redundant activities. PBP4, PBP4b and PBP7 have endopeptidase activity that hydrolyzes the nascent cross-linked peptide side chains⁷⁴⁻⁷⁸. PBP5, PBP6a and PBP6b have carboxypeptidase activity that cleaves the terminal residue D -Ala from the pentapeptide side chains and make them unavailable for transpeptidation⁷⁹⁻⁸².

Recently, RodA and FtsW have been identified to be the essential glycosyltransferases that elongate the glycan strands during peptidoglycan synthesis, since both them have the lipid II polymerization activity *in vitro*^{63,83-85}. RodA from *B. subtilis* can perform this activity on its own, while FtsW proteins from *Streptococcus thermophilus* and *Staphylococcus aureus* require their cognate class B PBPs for this activity^{83,84}. Mutations in PBP2 have a stimulatory effect on RodA glycosyltransferase activity⁸⁶. Functional and topological studies of FtsW from *E. coli* have identified the essential residues for FtsW localization, interaction and function^{52,87}. The functional and structural studies of RodA from *B. subtilis* and *Thermus thermophilus* have also revealed many immutable residues^{84,85}.

Most rod-shaped bacteria employ two protein machineries, *i.e.* the elongasome and the divisome, to guide peptidoglycan synthesis during length growth and cell division, respectively. Both of them are composed of many important proteins, whose interactions and regulations are tightly controlled, to ensure the proper coordination of peptidoglycan synthesis with all other cell cycle events.

Elongasome proteins and their interaction

For *E. coli*, newborn cells start to grow firstly in length to enlarge the cell envelope for the duplication of cellular contents, such as chromosome and proteins (Fig. 1A). The length growth is controlled by the protein complex

called elongasome, which contains the core proteins MreB, MreC, MreD, RodA, PBP2, RodZ and PBP1a (function of PBP1a can be substituted by PBP1b) (Fig. 3B)^{66,88–93}. Defects in these proteins will block cell elongation and result into spherical phenotype and eventually cell lysis.

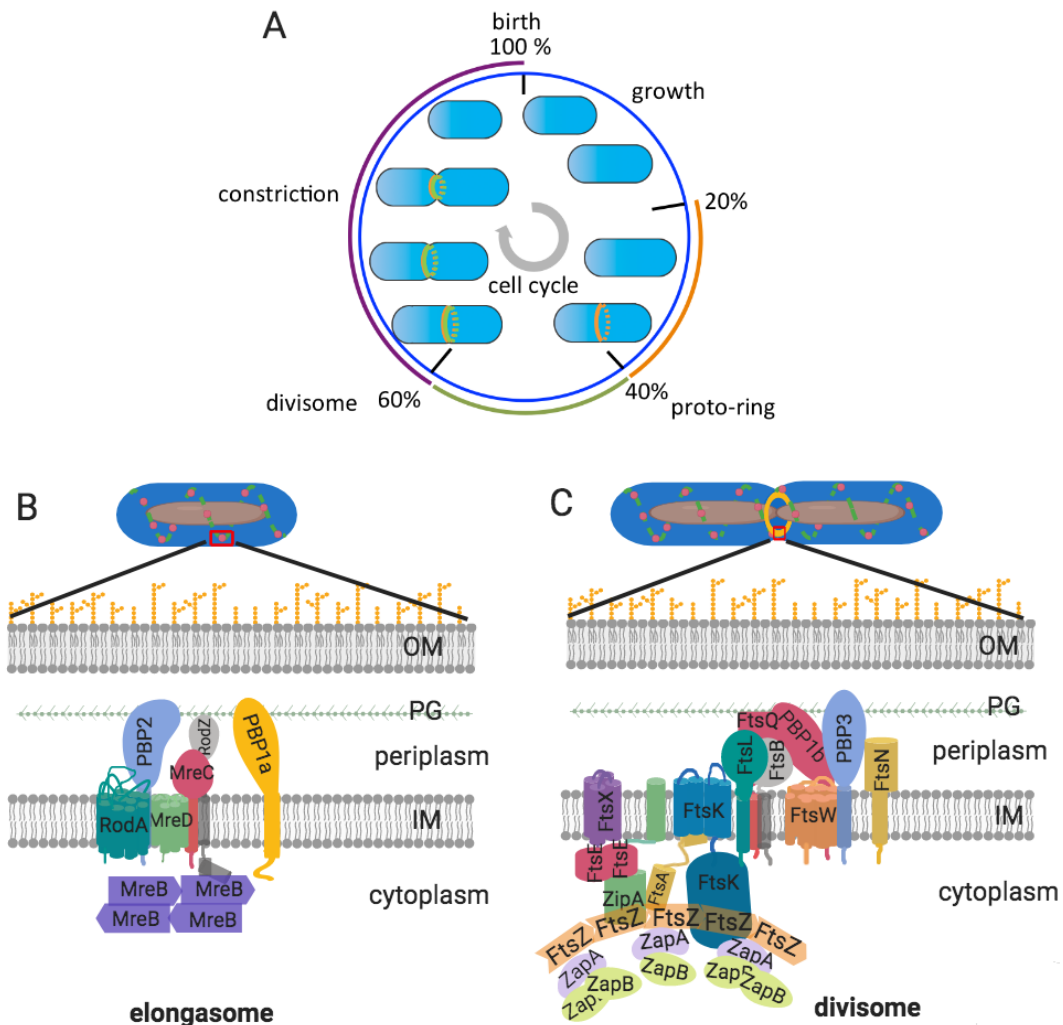


Figure 3. Schematic illustrations of *E. coli* cell cycle, elongasome and divisome. (A) Cell cycle of *E. coli*. Newborn cells start to grow in length that is controlled by the protein complex called elongasome. At about 20% to 40% of cell cycle, the proto-ring assembles at midcell to prepare for division, and eventually recruits later divisome components to form the mature complex during 40% to 60% of cell cycle. Next, septum synthesis is initiated, followed by envelope constriction and daughter cell separation. (B) and (C) Core components of elongasome and divisome, respectively.

MreB is the actin-like protein that can polymerize into short antiparallel filaments that associate to the inner membrane through its N-terminal

amphipathic helical domain^{94,95}. Localization and dynamic studies have revealed that MreB rotates along the cylindrical membrane in a circumferential motion, which is believed to organize the topology of the synthesis and insertion of peptidoglycan into the existing peptidoglycan layer⁹⁶⁻¹⁰⁰. MreB localization and rotation are abolished in the absence of MreC, MreD or RodA, but are not influenced by the absence of PBP2 transpeptidase activity when inhibited by mecillinam¹⁰¹.

MreC is a bitopic inner membrane protein that consists of a short cytoplasmic N-terminal tail, a TMH and a periplasmic domain. MreC interacts with itself, and is predicted to form a dimer or higher oligomer through its periplasmic domain⁸⁸. MreD is an integral inner membrane protein with multiple predicted TMHs. MreC and MreD have been shown to form an essential membrane-bound subcomplex with MreB. Interactions assayed by bacterial two-hybrid have revealed that MreC interacts with both MreB and MreD, while MreD only interacts with MreC⁸⁸. A recent structural study revealed different protein conformations of *Helicobacter pylori* PBP2 in the MreC bound and non-bound versions, suggesting a potential stimulation by MreC that switches PBP2 into a different functional state⁶⁹.

RodA and PBP2 interact with each other to form a stable subcomplex, and provide glycosyltransferase and transpeptidase activity for peptidoglycan synthesis, respectively^{50,63,84,102}. This subcomplex rotates with a similar motion as the MreB filaments⁶³. A structural study revealed 10 TMHs for RodA, with a potential lipid II binding groove and central substrate-binding cavity. TMH8 and TMH9 are likely involved in its interaction with PBP2⁸⁵. As mentioned above, structural study of PBP2 showed different conformations, which are likely corresponding to its active and inactive states^{69,86}. Although PBP1a is the primary class A PBP associated with the elongasome, its function can be replaced by PBP1b, whose primary function is associated with the divisome¹². Unlike RodA-PBP2 proteins, PBP1a likely functions outside of the core elongasome, as it has distinct dynamics compared to that of RodA-PBP2 and MreB proteins⁶³.

The bitopic inner membrane protein RodZ was identified relatively late as an essential component of the elongasome. It consists of a N-terminal helix-turn-helix domain, a juxta-membrane region, a TMH and large

periplasmic C-terminal domain^{91,103,104}. RodZ interacts strongly with MreB and MreC⁹¹. RodZ is reported to enhance MreB localization and links MreB to peptidoglycan synthesizing proteins (RodA and/or PBP2)¹⁰⁵. The helix-turn-helix region of RodZ is essential for its interaction with MreB and to maintain cell shape^{106,107}, while the periplasmic domain of RodZ is important for its self-interaction¹⁰⁸.

Assembling the Divisome

Bacterial cell division is controlled by the protein complex known as divisome. Assembly and maturation of the divisome can be divided into two steps¹⁰⁹: the assembly of the proto-ring (early divisome) and the recruitment of later localizing divisome proteins (Fig. 3A).

In *E. coli*, assembly of the proto-ring begins with the positioning of the FtsZ ring at the future division site (midcell) at about 20% of the cell cycle in glucose minimal medium grown cells¹⁰⁹. FtsZ is a tubulin homologue that can hydrolyze GTP and polymerize into protein filaments in a head-to-tail orientation^{110–113}. FtsZ filaments can further assemble into a dynamic ring structure that is attached to the inner membrane through the FtsZ anchor proteins FtsA and ZipA^{114–118}. The proper positioning of the Z-ring at midcell is regulated by two widely conserved systems: the Min system and nucleoid occlusion system. The Min system consists of the MinCDE proteins that oscillating from pole to pole to prevent the assembly of FtsZ ring at wrong positions^{119,120}, while the nucleoid occlusion factor SlmA inhibits FtsZ polymerization close to chromosomal DNA^{121–123}. Other early divisome proteins, such as ZapA, ZapB, FtsE and FtsX that are important for Z-ring stabilization and late divisome protein recruitment, are also recruited to the FtsZ ring^{124–129}, to form the early divisome at midcell at about 40% of cell cycle¹⁰⁹.

After formation of the proto-ring, the late localizing divisome proteins, FtsK, FtsBLQ, FtsW-PBP3(FtsI)-PBP1b and FtsN are recruited to division site, to form the complete core divisome (Fig. 3B). Although the recruitment of these proteins is largely in a linear order as the preceding one is required for recruiting of the next one, their assembly is more or less

simultaneously^{109,130,131}. FtsK is a DNA translocase that uses GTP to assist in the segregation of the terminus region of the sister chromosomes¹³². FtsBLQ form a subcomplex that plays an important role in divisome activity, as they are reported to inhibit the peptidoglycan synthesis activity of FtsW-PBP3-PBP1B till the maturation of the divisome is complete^{117,133,134}. FtsW, PBP3 and PBP1b are the group of peptidoglycan synthesizing proteins that can form a ternary subcomplex to provide glycosyltransferase and transpeptidase activities^{64,83,135}. FtsN is the last core protein that is recruited to the divisome. The arrival and accumulation of FtsN (self-interaction) is believed to relieve the inhibitory activity of FtsBLQ, which activates septum synthesis, and subsequently envelop constriction and daughter cell separation^{117,133,136,137}.

Scope of this thesis

To gain more insight into peptidoglycan synthesis *in vivo*, in this thesis, combining genetic, biochemical, microscopy and protein interaction approaches, we carried out several studies to unravel unclear key points of peptidoglycan synthesis in *E. coli*, and to reveal the regulation and coordination of peptidoglycan synthesis with bacterial cell growth and division.

As mentioned before, although the lipid II flipping activity of MurJ has been proved, how it functions together with other proteins during peptidoglycan synthesis was still not clear. In **chapter 2**, we constructed functional fluorescent protein fusions of MurJ, and showed that MurJ localizes both at the cylindrical membrane and at midcell. We further investigated the timing of MurJ recruitment to midcell and what determines its specific midcell localization. Based on functional studies, we also investigated how the activity of MurJ influences its cellular localization. This study visualized how and where MurJ performs its function together with other proteins that are involved in synthesis and regulation of peptidoglycan synthesis.

In **chapter 3**, we firstly investigated the peptidoglycan synthesizing protein subcomplex RodA and PBP2, which provide the glycosyltransferase activity and transpeptidase activity, during length growth. Through functionality, localization and interaction studies of their mutants, we verified what determines their interaction. Eventually, we introduced MreC and MreD

in this study. For the first time, we revealed an MreC-MreD balance dependent regulation of the PBP2 conformational changes, which are likely corresponding to the active and inactive state of PBP2. With great significance, our results indicate a potential activation mechanism of elongasome peptidoglycan synthesis that could be similar to the published regulation mechanism of divisome activation¹³³.

The study in **chapter 3** was mainly focused on PBP2. Our results suggested that the balance between MreC and MreD is important for the activation of PBP2. Whether these proteins also affect the function of RodA and its cooperation with other elongasome proteins is still largely unknown. Especially structural and functional studies of RodA from other species have revealed some essential residues that are not required for RodA glycosyltransferase activity. Therefore in **chapter 4**, we systematically investigated the essentialities of these residues in *E. coli* RodA, and how they influence RodA function. Our results revealed essential interactions between RodA and MreC and MreD proteins, which are important for elongasome (MreB) assembly and organization, and are also agreement with the regulation mechanism of the elongasome described in **chapter 3**.

References

1. Woese, C. R., Kandler, O. & Wheelis, M. L. Towards a natural system of organisms: proposal for the domains Archaea, Bacteria, and Eucarya. *Proc. Natl. Acad. Sci. U. S. A.* **87**, 4576–9 (1990).
2. Daly, M. J. *et al.* Geomicrobiology of High-Level Nuclear Waste-Contaminated Vadose Sediments at the Hanford Site, Washington State. *Appl. Environ. Microbiol.* **70**, 4230–4241 (2004).
3. Morley, N. J. Symbiotic bacteria of helminths: what role may they play in ecosystems under anthropogenic stress? *J. Helminthol.* **90**, 647–657 (2016).
4. Yurchenko, V., Luke, J. & Drzewiecka, D. Significance and Roles of *Proteus* spp. Bacteria in Natural Environments. *Microb. Ecol.* **72**, 741–758 (2016).
5. Vollmer, W. Morphogenesis of *Escherichia coli*. *Curr. Opin. Microbiol.* **4**, 625–633 (2002).
6. Glauner, B., Holtje, J. V. & Schwarz, U. The composition of the murein of *Escherichia coli*. *J. Biol. Chem.* **263**, 10088–10095 (1988).
7. Vollmer, W., Blanot, D. & De Pedro, M. A. Peptidoglycan structure and architecture. *FEMS Microbiol. Rev.* **32**, 149–167 (2008).
8. Silva, A. M. *et al.* The fluorescent D-Amino Acid NADA as a tool to study the conditional activity of transpeptidases in *Escherichia coli*. *Front. Microbiol.* **9**, 1–15 (2018).
9. Mattei, P. J., Neves, D. & Dessen, A. Bridging cell wall biosynthesis and bacterial morphogenesis. *Curr. Opin. Struct. Biol.* **20**, 749–755 (2010).
10. Demchick, P. & Koch, A. L. The permeability of the wall fabric of *Escherichia coli* and *Bacillus subtilis*. *J. Bacteriol.* **178**, 768 LP – 773 (1996).
11. Suzuki, H., Nishimura, Y. & Hirota, Y. On the process of cellular division in *Escherichia coli*: a series of mutants of *E. coli* altered in the penicillin-binding proteins. *Proc. Natl. Acad. Sci. U. S. A.* **75**, 664–668 (1978).
12. Lysis of *Escherichia coli* by beta-lactam antibiotics: deletion analysis of the role of penicillin-binding proteins 1A and 1B. *J Gen Microbiol.* **131**, 2839–45. (1985).
13. James T. Park, L. B. B. L. FL-1060: A new penicillin with a unique mode of action. *Biochem. Biophys. Res. Commun.* **51**, 863–868 (1973).
14. Raboisson, P. Ch 19: Discovery and development of TMC435. in *Reviews of infectious diseases* **7**, Noe (1985).
15. Zervosen, A., Sauvage, E., Frère, J. M., Charlier, P. & Luxen, A. Development of new drugs for an old target - The penicillin binding proteins. *Molecules* **17**, 12478–12505 (2012).
16. Jackson, M., Mcneil, M. R. & Brennan, P. J. Progress in targeting cell envelope biogenesis in *Mycobacterium tuberculosis*. *Futur. Microbiol* **8**, 1–32 (2013).
17. Jackson, M. *et al.* Development of new drugs for an old target - The penicillin binding proteins. *Molecules* **17**, 12478–12505 (2012).

18. Pernot, L. *et al.* A PBP2x from a Clinical Isolate of *Streptococcus pneumoniae* Exhibits an Alternative Mechanism for Reduction of Susceptibility to β -Lactam Antibiotics. *J. Biol. Chem.* **279**, 16463–16470 (2004).
19. Li, X. Z., Plésiat, P. & Nikaido, H. The challenge of efflux-mediated antibiotic resistance in Gram-negative bacteria. *Clin. Microbiol. Rev.* **28**, 337–418 (2015).
20. Dodds, D. R. Antibiotic resistance; a current epilogue. *Biochem. Pharmacol.* **134**, 139–146 (2016).
21. Neudorf, K. D. *et al.* Antibiotic resistance genes in municipal wastewater treatment systems and receiving waters in Arctic Canada. *Sci. Total Environ.* **598**, 1085–1094 (2017).
22. Foster, T. J. Antibiotic resistance in *Staphylococcus aureus*. Current status and future prospects. *FEMS Microbiol. Rev.* 430–449 (2017). doi:10.1093/femsre/fux007
23. Zapun, A., Contreras-Martel, C. & Vernet, T. Penicillin-binding proteins and β -lactam resistance. *FEMS Microbiol. Rev.* **32**, 361–385 (2008).
24. Barlow, M. What Antimicrobial Resistance Has Taught Us About Horizontal Gene Transfer. in *Horizontal Gene Transfer: Genomes in Flux* (eds. Gogarten, M. B., Gogarten, J. P. & Olendzenski, L. C.) 397–411 (Humana Press, 2009). doi:10.1007/978-1-60327-853-9_23
25. Livermore, D. M. Leading article Of. *J. Clin. Microbiol.* 247–250 (2001).
26. Ferri, M., Ranucci, E., Romagnoli, P. & Giaccone, V. Antimicrobial Resistance: A Global Emerging Threat to Public Health Systems. *Crit. Rev. Food Sci. Nutr.* **57**, 00–00 (2015).
27. Barreteau, H. *et al.* Cytoplasmic steps of peptidoglycan biosynthesis. *FEMS Microbiol. Rev.* **32**, 168–207 (2008).
28. Mengin-Lecreulx, D., Flouret, B. & Van Heijenoort, J. Cytoplasmic steps of peptidoglycan synthesis in *Escherichia coli*. *J. Bacteriol.* **151**, 1109–1117 (1982).
29. van Heijenoort, J. Lipid Intermediates in the Biosynthesis of Bacterial Peptidoglycan. *Microbiol. Mol. Biol. Rev.* **71**, 620–635 (2007).
30. Bouhss, A., Trunkfield, A. E., Bugg, T. D. H. & Mengin-Lecreulx, D. The biosynthesis of peptidoglycan lipid-linked intermediates. *FEMS Microbiology Reviews* **32**, 208–233 (2008).
31. Bouhss, A., Mengin-Lecreulx, D., Le Beller, D. & Van Heijenoort, J. Topological analysis of the *MraY* protein catalysing the first membrane step of peptidoglycan synthesis. *Mol. Microbiol.* **34**, 576–585 (1999).
32. Papers, J. B. C. *et al.* Purification and Characterization of the Bacterial *MraY* Translocase Catalyzing the First Membrane Step of Peptidoglycan Biosynthesis. *J. Biol. Chem.* **279**, 29974–29980 (2004).
33. Al-Dabbagh, B. *et al.* Active site mapping of *MraY*, a member of the polyprenylphosphate N-acetylhexosamine 1-phosphate transferase superfamily, catalyzing the first membrane step of peptidoglycan biosynthesis. *Biochemistry* (2008).

- doi:10.1021/bi8006274
34. Al-Dabbagh, B. *et al.* Active site mapping of MraY, a member of the polyprenyl-phosphate N-acetylhexosamine 1-phosphate transferase superfamily, catalyzing the first membrane step of peptidoglycan biosynthesis. *Biochemistry* **47**, 8919–8928 (2008).
 35. Mengin-Lecreux, D., Texier, L., Rousseau, M. & Van Heijenoort, J. The murG gene of *Escherichia coli* codes for the UDP-N-acetylglucosamine:N-acetylmuramyl-(pentapeptide) pyrophosphoryl-undecaprenol N-acetylglucosamine transferase involved in the membrane steps of peptidoglycan synthesis. *J. Bacteriol.* **173**, 4625–4636 (1991).
 36. Begg, K. J., Hatfull, G. F. & Donachie, W. D. Identification of new genes in a cell envelope cell-division gene cluster of *Escherichia Coli*: cell division gene *ftsQ*. *J. Bacteriol.* **144**, 435–437 (1980).
 37. Hu, Y. *et al.* Crystal structure of the MurG:UDP-GlcNAc complex reveals common structural principles of a superfamily of glycosyltransferases. *Proc Natl Acad Sci U S A* **100**, 845–849 (2003).
 38. Mohammadi, T. *et al.* The essential peptidoglycan glycosyltransferase MurG forms a complex with proteins involved in lateral envelope growth as well as with proteins involved in cell division in *Escherichia coli*. *Mol. Microbiol.* **65**, 1106–1121 (2007).
 39. Ruiz, N. Bioinformatics identification of MurJ (MviN) as the peptidoglycan lipid II flippase in *Escherichia coli*. *Proc. Natl. Acad. Sci. U. S. A.* **105**, 15553–7 (2008).
 40. Sham, L.-T. *et al.* MurJ is the flippase of lipid-linked precursors for peptidoglycan biogenesis. *Science (80-.)*. **345**, 220–222 (2014).
 41. Meeske, A. J. *et al.* MurJ and a novel lipid II flippase are required for cell wall biogenesis in *Bacillus subtilis*. *Proc. Natl. Acad. Sci. U. S. A.* **112**, 6437–42 (2015).
 42. Macheboeuf, P., Contreras-Martel, C., Job, V., Dideberg, O. & Dessen, A. Penicillin binding proteins: Key players in bacterial cell cycle and drug resistance processes. *FEMS Microbiol. Rev.* **30**, 673–691 (2006).
 43. Sauvage, E., Kerff, F., Terrak, M., Ayala, J. A. & Charlier, P. The penicillin-binding proteins: Structure and role in peptidoglycan biosynthesis. *FEMS Microbiol. Rev.* **32**, 234–258 (2008).
 44. Manat, G. *et al.* Deciphering the Metabolism of Undecaprenyl-Phosphate: The Bacterial Cell-Wall Unit Carrier at the Membrane Frontier. *Microb. Drug Resist.* **20**, 199–214 (2014).
 45. Pomorski, T. & Menon, A. K. Lipid flippases and their biological functions. *Cell. Mol. Life Sci.* **63**, 2908–2921 (2006).
 46. Sieger, B., Schubert, K., Donovan, C. & Bramkamp, M. The lipid II flippase RodA determines morphology and growth in *Corynebacterium glutamicum*. *Mol. Microbiol.* **90**, 966–982 (2013).
 47. Sieger, B. & Bramkamp, M. Interaction sites of DivIVA and RodA from

- Corynebacterium glutamicum. *Front. Microbiol.* **5**, 1–11 (2014).
48. Bendezú, F. O. & De Boer, P. A. J. Conditional lethality, division defects, membrane involution, and endocytosis in mre and mrd shape mutants of Escherichia coli. *J. Bacteriol.* **190**, 1792–1811 (2008).
 49. Henriques, a O., Glaser, P., Piggot, P. J. & Moran, C. P. Control of cell shape and elongation by the rodA gene in Bacillus subtilis. *Mol. Microbiol.* **28**, 235–247 (1998).
 50. van der Ploeg, R., Goudelis, S. T. & den Blaauwen, T. Validation of FRET assay for the screening of growth inhibitors of escherichia coli reveals elongasome assembly dynamics. *Int. J. Mol. Sci.* **16**, 17637–17654 (2015).
 51. Wang, L., Khattar, M. K., Donachie, W. D. & Lutkenhaus, J. FtsI and FtsW are localized to the septum in Escherichia coli. *J. Bacteriol.* **180**, 2810–2816 (1998).
 52. Mohammadi, T. *et al.* Specificity of the transport of lipid II by FtsW in Escherichia coli. *J. Biol. Chem.* **289**, 14707–14718 (2014).
 53. Zheng, S. *et al.* Structure and mutagenic analysis of the lipid II flippase MurJ from Escherichia coli. *Proc. Natl. Acad. Sci.* **115**, 6709–6714 (2018).
 54. Kuk, A. C. Y., Mashalidis, E. H. & Lee, S. Y. Crystal structure of the MOP flippase MurJ in an inward-facing conformation. *Nat. Struct. Mol. Biol.* **24**, 171–176 (2017).
 55. Chamakura, K. R. *et al.* A viral protein antibiotic inhibits lipid II flippase activity. *Nat. Microbiol.* (2017). doi:10.1038/s41564-017-0023-4
 56. Butler, E. K., Davis, R. M., Bari, V., Nicholson, P. A. & Ruiz, N. Structure-function analysis of MurJ reveals a solvent-exposed cavity containing residues essential for peptidoglycan biogenesis in Escherichia coli. *J. Bacteriol.* **195**, 4639–4649 (2013).
 57. Butler, E. K., Tan, W. B., Joseph, H. & Ruiz, N. Charge requirements of lipid II flippase activity in Escherichia coli. *J. Bacteriol.* **196**, 4111–4119 (2014).
 58. Goffin, C. & Ghuysen, J. M. Multimodular penicillin-binding proteins: an enigmatic family of orthologs and paralogs. *Microbiol. Mol. Biol. Rev.* **62**, 1079–93 (1998).
 59. Lovering, A. L., Castro, L. H. De, Lim, D. & Strynadka, N. C. J. Structural Insight into the Transglycosylation Step of Bacterial. *Science (80-.).* **315**, 1402–1405 (2007).
 60. Ranjit, D. K., Jorgenson, M. A. & Young, K. D. PBP1B Glycosyltransferase and Transpeptidase Activities Play Different Essential Roles during the De Novo Regeneration of Rod Morphology in Escherichia coli. *J Biol Chem* **199**, 1–17 (2017).
 61. Charpentier, X., Chalut, C., Rémy, M. H. & Masson, J. M. Penicillin-binding proteins 1a and 1b form independent dimers in Escherichia coli. *J. Bacteriol.* **184**, 3749–3752 (2002).
 62. Dion, M. F. *et al.* Bacillus subtilis cell diameter is determined by the opposing actions of two distinct cell wall synthetic systems. *Nat. Microbiol.* (2019). doi:10.1038/s41564-019-0439-0
 63. Cho, H. *et al.* Bacterial cell wall biogenesis is mediated by SEDS and PBP polymerase families functioning semi-Autonomously. *Nat. Microbiol.* **1**, (2016).
 64. Leclercq, S. *et al.* Interplay between Penicillin-binding proteins and SEDS proteins

- promotes bacterial cell wall synthesis. *Sci. Rep.* **7**, 43306 (2017).
65. Schiffer, G. & Höltje, J. V. Cloning and characterization of PBP 1C, a third member of the multimodular class A penicillin-binding proteins of *Escherichia coli*. *J. Biol. Chem.* **274**, 32031–32039 (1999).
 66. Den Blaauwen, T., Aarsman, M. E. G., Vischer, N. O. E. & Nanninga, N. Penicillin-binding protein PBP2 of *Escherichia coli* localizes preferentially in the lateral wall and at mid-cell in comparison with the old cell pole. *Mol. Microbiol.* **47**, 539–547 (2003).
 67. Bertsche, U. *et al.* Interaction between two murein (peptidoglycan) synthases, PBP3 and PBP1B, in *Escherichia coli*. *Mol. Microbiol.* **61**, 675–690 (2006).
 68. Van der Ploeg, R. *et al.* Colocalization and interaction between elongasome and divisome during a preparative cell division phase in *Escherichia coli*. *Mol. Microbiol.* **87**, 1074–1087 (2013).
 69. Contreras-Martel, C. *et al.* Molecular architecture of the PBP2-MreC core bacterial cell wall synthesis complex. *Nat. Commun.* **8**, 1–10 (2017).
 70. Piette, A. *et al.* Structural determinants required to target penicillin-binding protein 3 to the septum of *Escherichia coli*. *J. Bacteriol.* **186**, 6110–6117 (2004).
 71. Höltje, J. V. Growth of the stress-bearing and shape-maintaining murein sacculus of *Escherichia coli*. *Microbiol. Mol. Biol. Rev.* **62**, 181–203 (1998).
 72. Zapun, A., Vernet, T. & Pinho, M. G. The different shapes of cocci. *FEMS Microbiol. Rev.* **32**, 345–360 (2008).
 73. Den Blaauwen, T., De Pedro, M. A., Nguyen-Distèche, M. & Ayala, J. A. Morphogenesis of rod-shaped sacculi. *FEMS Microbiol. Rev.* **32**, 321–344 (2008).
 74. Henderson, T. A., Templin, M. & Young, K. D. Identification and cloning of the gene encoding penicillin-binding protein 7 of *Escherichia coli*. *J. Bacteriol.* **177**, 2074–2079 (1995).
 75. Obermann, W. & Holtje, J. V. Alterations of murein structure and of penicillin-binding proteins in minicells from *Escherichia coli*. *Microbiology* **140**, 79–87 (1994).
 76. Activity, C. I. A. Mutational Evidence for Identity of Penicillin-Binding. **137**, 644–647 (1979).
 77. Thunnissen, M. M., Fusetti, F., de Boer, B. & Dijkstra, B. W. Purification, crystallisation and preliminary X-ray analysis of penicillin binding protein 4 from *Escherichia coli*, a protein related to class A beta-lactamases. *J. Mol. Biol.* **247**, 149–153 (1995).
 78. Clarke, T. B. *et al.* Mutational analysis of the substrate specificity of *Escherichia coli* penicillin binding protein 4. *Biochemistry* **48**, 2675–2683 (2009).
 79. Chaput, C. *et al.* Septal and lateral wall localization of PBP5, the major D,D-carboxypeptidase of *Escherichia coli*, requires substrate recognition and membrane attachment. *Mol. Microbiol.* **77**, 300–323 (2010).
 80. Quintela, J. C., Baquero, M. R., Bouzon, M., Moreno, F. & Ayala, J. A. dacD, an *Escherichia coli* gene encoding a novel penicillin-binding protein (PBP6b) with DD-carboxypeptidase activity. *J. Bacteriol.* **178**, 7106–7111 (2016).

81. Nelson, D. E. & Young, K. D. Contributions of PBP 5 and dd-Carboxypeptidase Penicillin Binding Proteins to Maintenance of Cell Shape in *Escherichia coli* Contributions of PBP 5 and DD -Carboxypeptidase Penicillin Binding Proteins to Maintenance of Cell Shape in *Escherichia coli*. *J. Bacteriol.* **183**, 3055–3064 (2001).
82. Meiresonne, N. Y., van der Ploeg, R., Hink, M. A. & den Blaauwen, T. Activity-related conformational changes in D,D-carboxypeptidases revealed by in vivo periplasmic förster resonance energy transfer assay in *escherichia coli*. *MBio* **8**, 1–18 (2017).
83. Taguchi, A. *et al.* FtsW is a peptidoglycan polymerase that is functional only in complex with its cognate penicillin-binding protein. *Nat. Microbiol.* (2019). doi:10.1038/s41564-018-0345-x
84. Meeske, A. J. *et al.* SEDS proteins are a widespread family of bacterial cell wall polymerases. *Nature* 1–15 (2016). doi:10.1038/nature19331
85. Sjødt, M. *et al.* Structure of the peptidoglycan polymerase RodA resolved by evolutionary coupling analysis. *Nature* (2018). doi:10.1038/nature25985
86. Rohs, P. D. A. *et al.* A central role for PBP2 in the activation of peptidoglycan polymerization by the bacterial cell elongation machinery. *PLoS Genet.* **14**, 1–25 (2018).
87. Pastoret, S. *et al.* Functional Analysis of the Cell Division Protein FtsW of *Escherichia coli*. *J. Bacteriol.* **186**, 8370–8379 (2004).
88. Kruse, T., Bork-Jensen, J. & Gerdes, K. The morphogenetic MreBCD proteins of *Escherichia coli* form an essential membrane-bound complex. *Mol. Microbiol.* **55**, 78–89 (2005).
89. Fenton, A. K., Mortaji, L. El, Lau, D. T. C., Rudner, D. Z. & Bernhardt, T. G. CozE is a member of the MreCD complex that directs cell elongation in *Streptococcus pneumoniae*. *Nat. Microbiol.* **2**, 16237 (2016).
90. Shih, Y. L., Kawagishi, I. & Rothfield, L. The MreB and Min cytoskeletal-like systems play independent roles in prokaryotic polar differentiation. *Mol. Microbiol.* **58**, 917–928 (2005).
91. Bendezú, F. O., Hale, C. A., Bernhardt, T. G. & De Boer, P. A. J. RodZ (YfgA) is required for proper assembly of the MreB actin cytoskeleton and cell shape in *E. coli*. *EMBO J.* **28**, 193–204 (2009).
92. Matsuzawa, H. *et al.* Nucleotide sequence of the rodA gene, responsible for the rod shape of *Escherichia coli*: rodA and the pbpA gene, encoding penicillin-binding protein 2, constitute the rodA operon. *J. Bacteriol.* **171**, 558–560 (1989).
93. Wachi, M., Doi, M., Okada, Y. & Matsushashi, M. New mre genes mreC and mreD, responsible for formation of the rod shape of *Escherichia coli* cells. *J. Bacteriol.* **171**, 6511–6516 (1989).
94. van den Ent, F., Izoré, T., Bharat, T. A. M., Johnson, C. M. & Löwe, J. Bacterial actin MreB forms antiparallel double filaments. *Elife* **2014**, 1–22 (2014).
95. Salje, J., van den Ent, F., de Boer, P. & Löwe, J. Direct Membrane Binding by

- Bacterial Actin MreB. *Mol. Cell* **43**, 478–487 (2011).
96. Garner, E. C. *et al.* Coupled, circumferential motions of the cell wall synthesis machinery and MreB filaments in *B. subtilis*. *Science* (80-.). **333**, 222–5 (2011).
 97. van Teeffelen, S. *et al.* The bacterial actin MreB rotates, and rotation depends on cell-wall assembly. *Proc. Natl. Acad. Sci.* **108**, 15822–15827 (2011).
 98. Strahl, H., Bürmann, F. & Hamoen, L. W. The actin homologue MreB organizes the bacterial cell membrane. *Nat. Commun.* **5**, 1–11 (2014).
 99. Bratton, B. P., Shaevitz, J. W., Gitai, Z. & Morgenstein, R. M. MreB polymers and curvature localization are enhanced by RodZ and predict *E. coli*'s cylindrical uniformity. *Nat. Commun.* **9**, (2018).
 100. Kurita, K., Shin, R., Tabei, T. & Shiomi, D. Relation between rotation of MreB actin and cell width of *Escherichia coli*. *Genes to Cells* 259–265 (2019). doi:10.1111/gtc.12667
 101. Karczmarek, A. *et al.* DNA and origin region segregation are not affected by the transition from rod to sphere after inhibition of *Escherichia coli* MreB by A22. *Mol. Microbiol.* **65**, 51–63 (2007).
 102. Emami, K. *et al.* RodA as the missing glycosyltransferase in *Bacillus subtilis* and antibiotic discovery for the peptidoglycan polymerase pathway. *Nat. Microbiol.* **2**, 1–8 (2017).
 103. Shiomi, D., Sakai, M. & Niki, H. Determination of bacterial rod shape by a novel cytoskeletal membrane protein. *EMBO J.* **27**, 3081–3091 (2008).
 104. Alyahya, S. A. *et al.* RodZ, a component of the bacterial core morphogenic apparatus. *Proc. Natl. Acad. Sci.* **106**, 1239–1244 (2009).
 105. Morgenstein, R. M. *et al.* RodZ links MreB to cell wall synthesis to mediate MreB rotation and robust morphogenesis. *Proc Natl Acad Sci U S A* **112**, 12510–12515 (2015).
 106. Van Den Ent, F., Johnson, C. M., Persons, L., De Boer, P. & Löwe, J. Bacterial actin MreB assembles in complex with cell shape protein RodZ. *EMBO J.* **29**, 1081–1090 (2010).
 107. Colavin, A., Shi, H. & Huang, K. C. RodZ modulates geometric localization of the bacterial actin MreB to regulate cell shape. *Nat. Commun.* **9**, 1280 (2018).
 108. Ikebe, R., Kuwabara, Y., Chikada, T., Niki, H. & Shiomi, D. The periplasmic disordered domain of RodZ promotes its self-interaction in *Escherichia coli*. *Genes to Cells* **23**, 307–317 (2018).
 109. Aarsman, M. E. G. *et al.* Maturation of the *Escherichia coli* divisome occurs in two steps. *Mol. Microbiol.* **55**, 1631–1645 (2005).
 110. Mukherjee, A. Dynamic assembly of FtsZ regulated by GTP hydrolysis. *EMBO J.* **17**, 462–469 (2002).
 111. Mukherjee, A. & Lutkenhaus, J. Guanine nucleotide-dependent assembly of FtsZ into filaments. *J. Bacteriol.* **176**, 2754–8 (1994).
 112. Piet, de B., Robin, C. & Lawrence, R. The essential bacterial cell-division protein FtsZ

- is a GTPase. *Nature* **359**, 254–256 (1992).
113. Raychaudhuri, D. & Park, J. T. GYP-binding Escherichia coli cell-division gene *ftsZ* encodes a novel GYP-binding protein. *Nature* **359**, 251–254 (1992).
 114. Goate & APP. © 19 9 1 Nature Publishing Group. *Lett. To Nat.* (1991).
 115. Pichoff, S. & Lutkenhaus, J. Tethering the Z ring to the membrane through a conserved membrane targeting sequence in FtsA. *Mol. Microbiol.* **55**, 1722–1734 (2005).
 116. Pichoff, S., Du, S. & Lutkenhaus, J. The bypass of ZipA by overexpression of FtsN requires a previously unknown conserved FtsN motif essential for FtsA-FtsN interaction supporting a model in which FtsA monomers recruit late cell division proteins to the Z ring. *Mol. Microbiol.* **95**, 971–987 (2015).
 117. Liu, B., Persons, L., Lee, L. & de Boer, P. A. J. Roles for both FtsA and the FtsBLQ subcomplex in FtsN-stimulated cell constriction in Escherichia coli. *Mol. Microbiol.* **95**, 945–970 (2015).
 118. Hale, C. A. & De Boer, P. A. J. Direct binding of FtsZ to ZipA, an essential component of the septal ring structure that mediates cell division in E. coli. *Cell* **88**, 175–185 (1997).
 119. Ghosal, D., Trambaiolo, D., Amos, L. A. & Löwe, J. MinCD cell division proteins form alternating copolymeric cytomotive filaments. *Nat. Commun.* **5**, 5341 (2014).
 120. Rowlett, V. W. & Margolin, W. The Min system and other nucleoid-independent regulators of Z ring positioning. *Front. Microbiol.* **6**, 1–10 (2015).
 121. Tonthat, N. K. *et al.* Molecular mechanism by which the nucleoid occlusion factor, SlmA, keeps cytokinesis in check. *EMBO J.* **30**, 154–164 (2011).
 122. Cho, H. & Bernhardt, T. G. Identification of the SlmA Active Site Responsible for Blocking Bacterial Cytokinetic Ring Assembly over the Chromosome. *PLoS Genet.* **9**, (2013).
 123. Cho, H., McManus, H. R., Dove, S. L. & Bernhardt, T. G. Nucleoid occlusion factor SlmA is a DNA-activated FtsZ polymerization antagonist. *Proc. Natl. Acad. Sci.* **108**, 3773–3778 (2011).
 124. Ortiz, C., Natale, P., Cueto, L. & Vicente, M. The keepers of the ring: Regulators of FtsZ assembly. *FEMS Microbiol. Rev.* **40**, 57–67 (2015).
 125. Castillo, D. E., Yang, D., Siopsis, G. & Männik, J. The role of MatP, ZapA and ZapB in chromosomal organization and dynamics in Escherichia coli. *Nucleic Acids Res.* **44**, 1216–1226 (2016).
 126. Schmidt, K. L. *et al.* A Predicted ABC Transporter , FtsEX , Is Needed for Cell Division in Escherichia coli. *J. Bacteriol.* **186**, 785–793 (2004).
 127. Du, S., Pichoff, S. & Lutkenhaus, J. FtsEX acts on FtsA to regulate divisome assembly and activity. *Proc. Natl. Acad. Sci.* 201606656 (2016). doi:10.1073/pnas.1606656113
 128. Reddy, M. Role of FtsEX in cell division of Escherichia coli: Viability of *ftsEX* mutants is dependent on functional SufI or high osmotic strength. *J. Bacteriol.* **189**, 98–108

- (2007).
129. Arends, S. J. R., Kustus, R. J. & Weiss, D. S. ATP-Binding Site Lesions in FtsE Impair Cell Division. *J. Bacteriol.* **191**, 3772–3784 (2009).
 130. Goehring, N. W., Gonzalez, M. D. & Beckwith, J. Premature targeting of cell division proteins to midcell reveals hierarchies of protein interactions involved in divisome assembly. *Mol. Microbiol.* **61**, 33–45 (2006).
 131. Goehring, N. W., Gueiros-filho, F. & Beckwith, J. Premature targeting of a cell division protein to midcell allows dissection of divisome assembly in Escherichia coli. *Genes Dev.* **19**, 127–137 (2005).
 132. Stouf, M., Meile, J.-C. & Cornet, F. FtsK actively segregates sister chromosomes in Escherichia coli. *Proc. Natl. Acad. Sci.* **110**, 11157–11162 (2013).
 133. Boes, A., Olatunji, S., Breukink, E. & Terrak, M. Regulation of the peptidoglycan polymerase activity of PBP1b by antagonist actions of the core divisome proteins FtsBLQ and FtsN. *MBio* **10**, 1–16 (2019).
 134. den Blaauwen, T. & Luirink, J. Checks and Balances in Bacterial Cell Division. *MBio* **10**, 1–6 (2019).
 135. Fraipont, C. *et al.* The integral membrane FtsW protein and peptidoglycan synthase PBP3 form a subcomplex in Escherichia coli. *Microbiology* **157**, 251–259 (2011).
 136. Lutkenhaus, J. FtsN - Trigger for septation. *J. Bacteriol.* **191**, 7381–7382 (2009).
 137. Goehring, N. W., Robichon, C. & Beckwith, J. Role for the nonessential N terminus of FtsN in divisome assembly. *J. Bacteriol.* **189**, 646–649 (2007).

CHAPTER

2

FtsW activity and lipid II synthesis are required for recruitment of MurJ to midcell during cell division in *Escherichia coli*

Xiaolong Liu¹

Nils Y. Meiresonne¹

Ahmed Bouhss^{2,3}

Tanneke den Blaauwen^{1*}

¹*Bacterial Cell Biology and Physiology, Swammerdam Institute for Life Sciences, Faculty of Science, University of Amsterdam, Amsterdam, The Netherlands.*

²*Institute for Integrative Biology of the Cell (I2BC), CEA, CNRS, Univ Paris-Sud, Université Paris-Saclay, 91198, Gif-sur-Yvette, France.*

³*Laboratoire Structure-Activité des Biomolécules Normales et Pathologiques (SABNP), Univ Evry, INSERM U1204, Université Paris-Saclay, 91025 Evry, France*

*Corresponding author

This chapter has been published as:

Liu, X., Meiresonne, N. Y., Bouhss, A. & den Blaauwen, T. Mol. Microbiol. 109, 865–884 (2018).

Abstract

Peptidoglycan (PG) is the unique cell shape-determining component of the bacterial envelope, and is a key target for antibiotics. PG synthesis requires the transmembrane movement of the precursor lipid II, and MurJ has been shown to provide this activity in *E. coli*. However, how MurJ functions *in vivo* has not been reported. Here we show that MurJ localizes both in the lateral membrane and at midcell, and is recruited to midcell simultaneously with late-localizing divisome proteins and proteins MraY and MurG. MurJ septal localization is dependent on the presence of a complete and active divisome, lipid II synthesis and PBP3/FtsW activities. Inactivation of MurJ, either directly by mutation or through binding with MTSES, did not affect the midcell localization of MurJ. Our study visualizes MurJ localization *in vivo* and reveals a possible mechanism of how MurJ functions during cell division, which gives possibilities for future investigations and further antibiotics developments.

Introduction

Rod-shaped bacteria such as the Gram-negative bacterium *Escherichia coli* grow by elongation and binary fission. One of the requirements for proliferation is the enlargement of their cell envelope, which contains an inner membrane (IM) and an outer membrane (OM). The shape of the bacterium is determined by the shape of its peptidoglycan (PG) layer, which is attached to the outer membrane in the periplasmic space located between both membranes of the envelope¹. The PG layer is a mesh-like heteropolymeric macromolecule of alternating *N*-acetylmuramyl-peptides (MurNAc-pentapeptides) and *N*-acetylglucosamine (GlcNAc) disaccharides that are connected by a β -(1,4) bond forming glycan chains that are crosslinked between *meso* diaminopimelic acid (DAP) and D-Ala at the third and fourth position of the acceptor and donor stem peptide, respectively². The biosynthesis of PG is a complicated process that can be divided into 3 stages. In the cytoplasmic stage, the nucleotide precursors UDP-GlcNAc and UDP-MurNAc-pentapeptide are synthesized from fructose-6-phosphate by the GlmSMU and MurABCDEF proteins, respectively³. In the IM stage, the undecaprenyl-pyrophosphate- (C_{55}) linked intermediates lipid I (C_{55} -MurNAc-pentapeptide) and lipid II (C_{55} -MurNAc(-pentapeptide)-GlcNAc) are formed by the MraY and MurG proteins, respectively². During this stage, lipid II, the building unit of peptidoglycan, is translocated by a “flippase” across the IM³⁻⁷. In the periplasmic stage, the MurNAc-pentapeptide-GlcNAc component of lipid II is inserted into the PG layer by the glycosyltransferase and transpeptidase activities of various PBPs^{8,9}, and the lipoyl moiety C_{55} -PP is cleaved off and recycled¹⁰.

In *E. coli*, new PG-building units are inserted into the existing PG layer during length growth by a protein complex termed the elongasome, whereas during division new poles are synthesized from completely new material¹¹ by proteins that collectively have been termed the divisome¹². The elongasome is organized by the actin homolog MreB, which localizes underneath the IM in patches in a helix-like distribution. MreB is bound to the membrane by its amphipathic helix, and interacts with the bitopic membrane protein RodZ, the integral membrane proteins MreD and MreC, and the PG synthesis essential

proteins RodA and PBP2¹²⁻¹⁶. How the elongasome is regulated is not yet very clear whereas in contrast, cell division has been well investigated. During cell division, at least 20 proteins are recruited to midcell to form the divisome. The tubulin homologue FtsZ is attached to the IM at midcell by the anchor proteins FtsA and ZipA, and polymerizes to form the Z-ring^{17,18}. Simultaneously, other proteins, such as the Zap proteins and FtsEX, are recruited to the ring to form the early divisome or protoring. The protoring then recruits the later divisome proteins FtsK, FtsQ, FtsL, FtsB, FtsW, FtsI (PBP3), PBP1b, FtsN¹⁹, and a number of hydrolases and regulatory proteins²⁰ to form the mature divisome²¹. The arrival of FtsN completes the assembly of the core divisome, and signals to initiate septal PG synthesis²²⁻²⁴. The assembled divisome functions as a scaffold to initiate septal PG synthesis, OM constriction, and the cleavage of the PG layer to separate daughter cells²⁰. Septal PG synthesis is mainly orchestrated by PBP3 and PBP1b^{9,25}, but PBP1a can substitute for PBP1b^{26,27}. OM constriction is organized by the Tol/Pal system, which forms a complex connecting IM and OM^{28,29}. Tightly controlled amidase activity is involved in the separation of the daughter cells³⁰.

Although the stages of PG synthesis are well understood, conflicting information on the flipping of lipid II across the IM has been published over the last few years. In *E. coli*, RodA and FtsW that belong to the SEDS (shape, elongation, division, sporulation) family, and MurJ that belongs to the MOP (multidrug/oligo-saccharidyl-lipid/polysaccharide) export super family³¹, are reported as candidates of lipid II flippase, either functioning in elongation or division only or in both^{6,32,33}. An alternative activity as glycosyltransferase was recently reported for RodA in *Bacillus subtilis*³⁴, while the debate which protein is responsible for lipid II flipping is still going on. FtsW is an essential integral membrane cell division protein with 10 trans-membrane helices (TMHs) and is conserved in most bacterial species that have a PG cell wall³⁵. FtsW, PBP3 and PBP1b form a complex that is recruited to midcell at the later stage of divisome assembly³⁶⁻³⁸. FtsW was shown *in vitro* to have lipid II binding and flipping activity, for which two charged residues in TMH 4, arginine 145 and lysine 153, appeared to be essential³⁸⁻⁴⁰.

MurJ is an essential IM protein that contains 14 TMHs with both C- and

N-termini in the cytoplasm^{41,42}. Depletion of MurJ will cause irregularly shaped cell, and finally result into cell lysis³¹. Earlier functional and structural studies of MurJ reveal an outward-facing central cavity that is formed by TMHs 1, 2, 7 and 8, which contain several charged residues that are essential for MurJ function^{41,42}, while the observation of an open inward-facing conformation in the crystal structure of MurJ from *Thermosipho africanus* (MurJ_{TA}) suggests alternative conformational changes of MurJ⁴³. *In vivo* evidence favors MurJ over FtsW as the lipid II flippase, and depletion or inhibition of MurJ caused the accumulation of lipid II in cells^{31,32,44,45}, while *in vitro* flipping activity has thus far only be established for FtsW^{39,40}. Interestingly, the function of MurJ in *E. coli* can be replaced by other flippases that lack sequence similarity, such as the O-antigen flippase Wzk from *E. coli*, and Amj and YtgP from other species⁴⁶⁻⁴⁹. Two *in vitro* studies on lipid II binding of MurJ showed conflicting results, as one reported a higher lipid II binding affinity of MurJ compared with FtsW⁵⁰, while the other one showed lipid II binding only by FtsW but not by MurJ³⁸. Although these data support MurJ to be involved in flipping lipid II, it is still not clear where and how MurJ functions in bacterial cells. In this study, by visualizing the cellular localization of MurJ with functional fluorescent protein fusions, we provide new evidence on how MurJ performs its function during PG synthesis.

Results

Construct a functional fluorescent protein fusion to the N-terminus of MurJ

To investigate the MurJ function and localization *in vivo*, fluorescent protein (FP) fusions to either the N-terminus or the C-terminus of MurJ with different repeats of Gly-Gly-Ser (GGG) linkers were constructed⁵¹. Two low-copy-number plasmids, pTHV037 and pSAV057, were used to express the fused proteins under the control of a down-regulated $P_{trcdown}$ promoter⁵². Based on the physical properties of fluorescent proteins^{53,54}, green fluorescent protein mNeonGreen (mNG) and red fluorescent protein mCherry (mCh) were chosen for MurJ fusions. The functionality of the MurJ fusions was tested by a

complementation assay (Material and Methods).

As shown in Table 1, the N-terminal fusions of MurJ were fully functional, while C-terminal fusions were less functional or not functional at all. Among these, the N-terminal mNG fusion with a (GGS)₂ linker showed the most stable and strongest fluorescence signals. For mCh, the fusion without linker was the best. Thus they were chosen for further studies. The crystal structure of MurJ from *T. africanus* reveals that TMHs 13 and 14 form a hydrophobic groove, which penetrates into the central transport cavity and is hypothesized to be important for lipid II binding⁴³. The loss function of MurJ C-terminal fusions might due to the defects in folding and groove formation.

Table 1. Functionality and localization of MurJ fluorescence proteins fusions with different linkers at N- or C- terminus

Fusions	Plasmids	Complementation ^a	Localization ^b	Function ^c
No fusion	pTHV037-MurJ	≈16h	ND	+
	pSAV057-MurJ	≈16h	ND	+
N-terminus	pTHV037-mCh-(GGS) _n -MurJ	≈16h	+	+
	pSAV057-mNG-(GGS) _n -MurJ	≈16h	+	+
	pSAV057-mKO-MurJ	≈16h	+	+
C-terminus	pTHV037-MurJ-(GGS) _n -mCh	≥3 days	-	-
	pSAV057-MurJ-(GGS) _n -mNG	≥3 days	-	-

n: Number of GGS repeats (n = 0, 1, 2, 3)

^a after transformation, the time period needed for visible white colony appearance.

^b +, FP fused MurJ is fluorescent and localizes in the membrane; -, FP fused MurJ is fluorescent and localizes in the cytosol.

^c +, functional fusion; -, loss-of-function fusion.

MurJ localizes in the lateral wall and also at midcell

MurJ is reported to be present at 674 and 78 molecules per cell when grown in rich and minimal medium, respectively⁵⁵. In order to characterize MurJ at its endogenous expression level, the MurJ fusion was introduced into the *E. coli* chromosome at its native locus. The existence of the native promoter p_{murJ} was confirmed by inserting a divergently transcribed chloramphenicol cassette between the stop codon of gene *yceM* upstream of *murJ* and the putative

murJ promoter (Fig. S1A). However, attempts to introduce FP-fused MurJ under the native *murJ* promoter failed, apart from a mCh fusion, which yielded a strain with defects in cell morphology and growth (Fig. S1B). Since the plasmid expressed fusions were fully functional, a likely explanation for the morphological defect could be that the translation efficiency of the fused proteins was less than that of MurJ only. Consequently, the expression of the FP fused MurJ under the native *murJ* promoter was not enough to support growth. Therefore, we replaced the chromosomal *murJ* gene with *fp-murJ* constructs transcribed under the control of $p_{trcdown}$ promoter to generate strains XL08 and XL09 (Material and Methods). No defect on growth or cell morphology was observed even when grown without IPTG induction (Fig. S1 C and D).

Strain XL08 was grown to steady state in minimal glucose medium (Gb1) at 28°C to be able to correlate its length to its cell division cycle age^{18,56}, and the localization of MurJ in living *E. coli* cells was analyzed using ImageJ and the Coli-Inspector of ObjectJ⁵⁶. To avoid overexpression, no IPTG induction was applied. The mass double time (MD) of this strain is 83 minutes, which is close to 80 minutes of wild-type *E. coli*⁵⁶. MurJ localized in the cylindrical part of the cells as well as specifically at midcell in dividing cells (Fig. 1). After normalizing and plotting the fluorescence profiles into 10 age groups, a clear midcell localization was observed starting from 50% of the cell cycle. The septal proportion of MurJ, which is indicated as the “Ring fraction”, was analyzed as function of the division cell cycle, and a maximal proportion of 8.58% was observed at 82.5% of cell cycle (Fig. S2). To show that this accumulation was not an effect of double membrane formation during cell invagination, the localization of mNG-(GGS)₂-GlpT was introduced as control. GlpT (glycerol-3-phosphate transporter) is the major transporter for the uptake of *sn*-glycerol 3-phosphate in *E. coli*. It was reported to have 12 TMHs and to function as monomer⁵⁷, which diffuses homogenously in the IM⁵⁸. It was therefore expected to show homogenous membrane localization. Like for MurJ, the localization of mNG-(GGS)₂-GlpT was imaged and analyzed. As expected, GlpT localized homogenously in the membrane without midcell accumulation. After plotting into 10 age groups, GlpT showed a clear difference with MurJ, and no enhanced fluorescence was observed at midcell

during constriction (Fig. 1A and B). The differences between the localization patterns of the two proteins are also obvious in images of the cells (Fig. 1C). The specific localization pattern of MurJ suggests that MurJ is likely involved in both length growth and cell division.

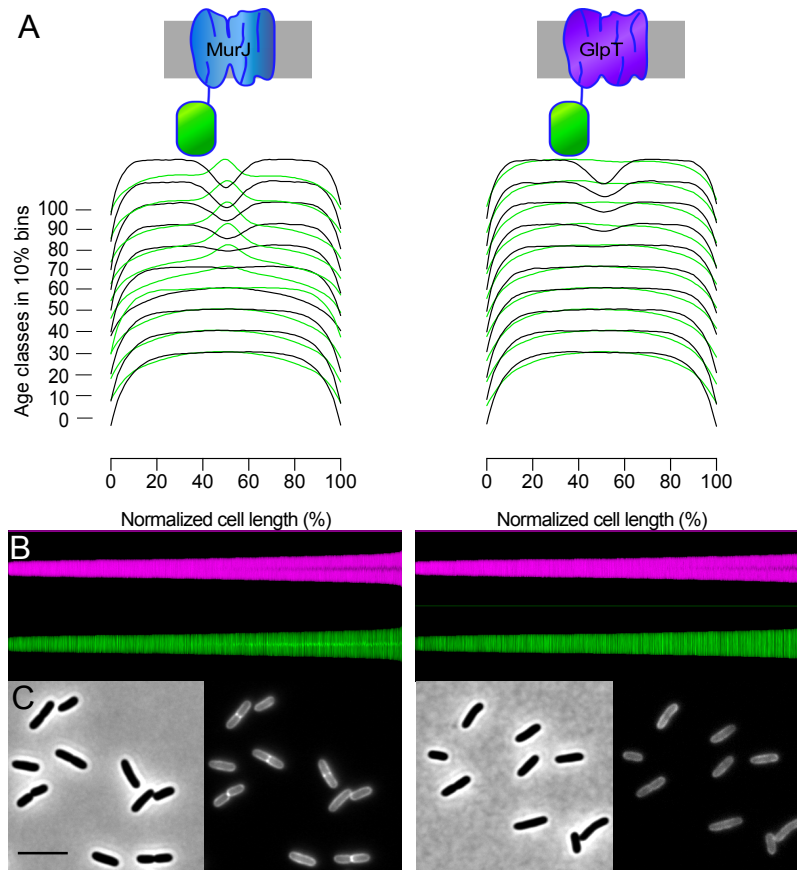


Fig. 1. MurJ localizes both in the lateral wall and at midcell. Strain XL08 containing the chromosomal mNG-MurJ fusion shows a cell-cycle-dependent localization in contrast to the homogeneously localizing integral membrane protein mNG-GlpT. Cells were grown in Gb1 minimal medium to steady state at 28°C. Left: MurJ profiles; Right: membrane control protein GlpT profiles. (A) Collective profiles of localization of MurJ and GlpT. For each protein, the diameter (black lines) and fluorescence (green lines) profiles along normalized cell length are shown in 10 % age class bins. (B) Maps of diameter profiles (magenta) and fluorescence profiles (green). Cells are plotted by length, ascending from left to right. (C) Phase contrast image (left) and the corresponding fluorescence image (right) for each protein. Scale bar equals 5 μ m. More than 1200 cells were included for both analyses.

MurJ is recruited to midcell simultaneously with the PG synthesis proteins

The observation of MurJ midcell localization prompted us to the next question: at which point of the cell division cycle MurJ is recruited. To reveal this, localization of MurJ, the early and late localizing proteins FtsZ and FtsN, respectively, and the proteins MraY and MurG, which synthesize Lipid I and lipid II, respectively^{21,23,59-62} was determined in steady-state grown strain XL08. Cells from the same culture and optical density were either imaged live for MurJ localization or were fixed with FGA (2.8% formaldehyde and 0.04% glutaraldehyde) and subsequently immunolabeled with antibodies specific for the above mentioned proteins⁶³. The early divisome protein FtsZ was recruited at midcell at about 25% of cell cycle, and the core divisome assembly was completed by the midcell arrival of FtsN at 40%-50% of the cell division cycle (Fig.2). The measured extra fluorescence at mid cell (FCplus) of these proteins plotted as function of the cell division cycle age (Fig. S3) is in agreement with a previous study⁶⁴. Interestingly, MraY, MurG and MurJ accumulated at midcell simultaneously at approximately 50% of cell cycle at the later stage of divisome assembly. These results indicate that MurJ is very likely functioning together with the PG synthesis complex, which would be in agreement with its function as a lipid II flippase.

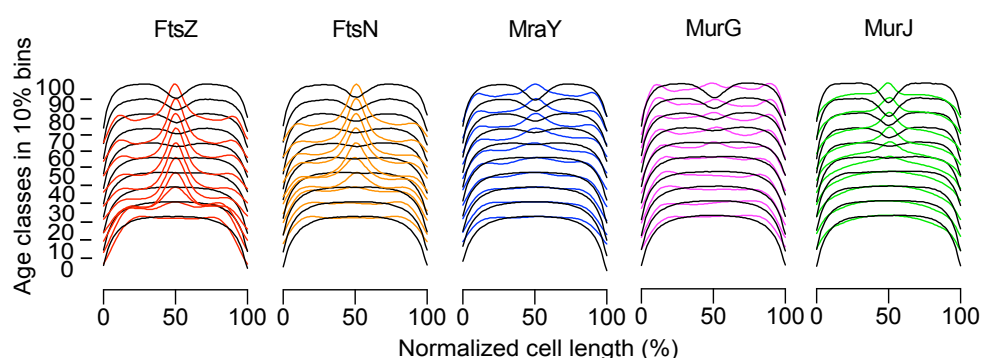


Fig. 2. Timing of MurJ midcell localization. mNG-(GGG)₂-MurJ cellular localization was compared with the localization of divisomal and PG precursor synthesizing proteins. XL08 strain was grown to steady state in Gb1 medium. MurJ localization was determined in living cells. After fixation with FGA, the rest of cells were immunolabeled with antibodies against FtsZ, FtsN, MraY and MurG. Diameter (black lines) and Fluorescence (colored lines) profiles were plotted into 10 % age class bins along the normalized cell length in %. More than 1200 cells were included.

MurJ requires a mature divisome for midcell localization

The timing of MurJ midcell localization raised the question whether its localization is dependent on particular divisome proteins. To answer this, the mNG-(GGS)₂-MurJ chromosomal fusion was introduced into a series of temperature-sensitive cell division mutant strains. FtsA is an essential early

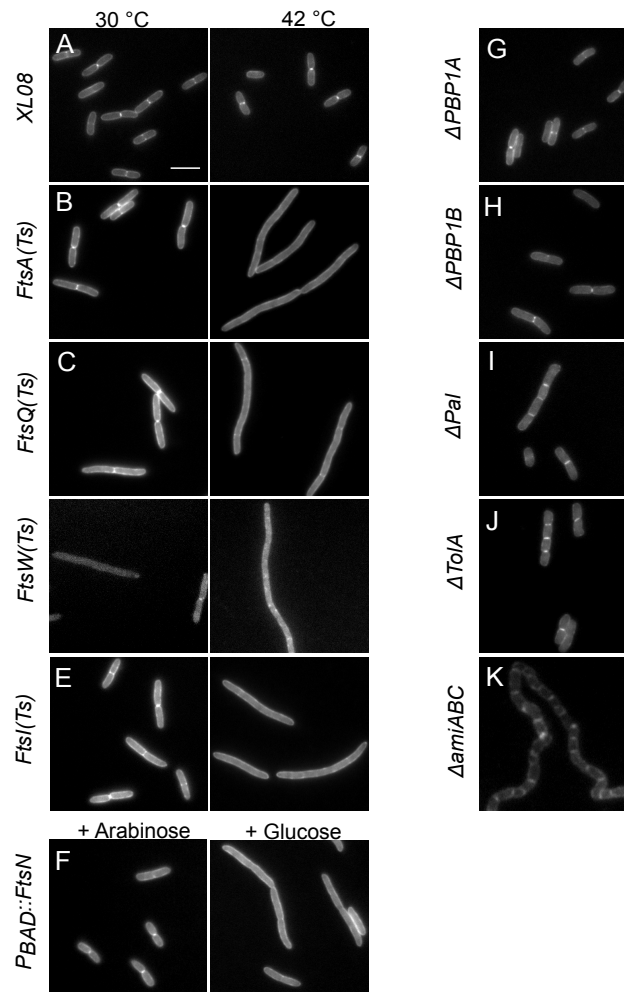


Fig. 3. MurJ requires the core divisome for its midcell localization. Chromosomal mNG-(GGS)₂-MurJ fusion was introduced into strains that harbor temperature sensitive, depletable, or deleted division proteins (except that the mNG-(GGS)₂-MurJ plasmid was expressed in *ΔtolA* and *Δpal* strains, and the mCherry-MurJ plasmid was expressed in *ΔamiABC* strain). (A-E) MurJ localization in XL08 (WT), *ftsA 1882* (Ts), *ftsQ1* (Ts), *ftsW* (Ts) and *ftsI/2185* (Ts) backgrounds. Left: Localization at permissive temperature of 28 °C. Right: Localization after growth at the non-permissive temperature of 42 °C for 2 mass doublings (MD)s. (F) MurJ localization in FtsN depletion background at 30 °C. Left: localization in the presence of 0.2% w/v arabinose. Right: Localization of MurJ in the absence of arabinose for 2 MDs. (G-H) mCh-MurJ localization in *ΔmrcA* (PBP1A), *ΔmrcB* (PBP1B), *Δpal*, *ΔtolA* and *ΔamiABC* background at 30 °C, respectively. Scale bar equals 5 μm.

divisome protein that anchors the Z-ring to the IM^{65,66}. The absence of FtsA causes filamentous growth of *E. coli*, as the downstream divisome proteins are not recruited to midcell⁶⁷. In the FtsA(*Ts*) background, MurJ showed normal midcell localization when grown at permissive temperature. However, when grown at 42 °C, MurJ midcell localization was lost, and MurJ only localized in the cylindrical membrane of the filamentous cells (Fig. 3B and Fig. S4). This indicates that MurJ midcell localization is dependent on the presence of the early divisome. Like in the FtsA(*Ts*) cells, depletion of the later divisome proteins, FtsQ, FtsW, FtsI or FtsN^{68,69}, abolished MurJ midcell localization in the filamentous cells (Fig. 3 C-F, and Fig. S4). To point out, some localization bands of MurJ were observed in FtsQ(*Ts*) filaments at 42 °C, which was likely caused by the relocalization of FtsQ proteins during the imaging at room temperature. As control, MurJ still localized at midcell in a wild-type background at 42 °C (Fig. 3A). These results suggest that MurJ requires a mature divisome for midcell localization. To determine to what extent MurJ is dependent on cell division, we also examined MurJ localization in strains that were deleted for PBP1a, PBP1b, Pal, TolA, or the amidases AmiABC. The observation of a clear MurJ midcell localization in the absence of these proteins, even when cells grow as chains, indicates that MurJ midcell localization is independent of these proteins (Fig. 3 G-K). All these results are consistent with the function of MurJ as the lipid II flippase during PG synthesis.

MurJ midcell localization requires PBP3 activity

After observation of MurJ midcell localization, the next obvious question would be whether this localization is dependent on septal PG synthesis. Septal PG synthesis requires the activity of PBP3 (FtsI) and PBP1b, although the latter can be replaced by PBP1a²⁶. The specific inhibition of PBP3 activity by aztreonam blocks septal PG synthesis without initially inhibiting the localization of the divisome, resulting in filamentous cells with divisomes localized at regular cell division distances^{61,70}. After growing the chromosomal mNG-MurJ containing strain XL08 at 28 °C to steady state in Gb1 medium,

MurJ localization was determined in the presence of 1 mg.L^{-1} aztreonam. A block of MurJ midcell localization was already observed after 30 min, without much change in cell morphology (Fig. S5). After 1 MD and 2 MDs, MurJ midcell localization was completely abolished in the typical filamentous cells (Fig. S5 and Fig. 4). Subsequently, cells were fixed and immunolabeled with antibodies against FtsZ and FtsN to show the localization of divisomes, and against MraY and MurG to show the localization of the lipid II-synthesizing complex. As expected, we found that FtsZ, FtsN, MurG and MraY localized at potential division sites in the filaments (Fig. 4). Likewise, MurJ localization was determined in the presence of elongasome inhibitors A22 and mecillinam for 2 MDs, which inactivate MreB and PBP2, respectively^{70–73}. No influence on MurJ midcell localization was observed although cells started to grow spherically (Fig. S6). Together, these results suggest that MurJ localization is specifically dependent on the activity of PBP3 and septal PG synthesis.

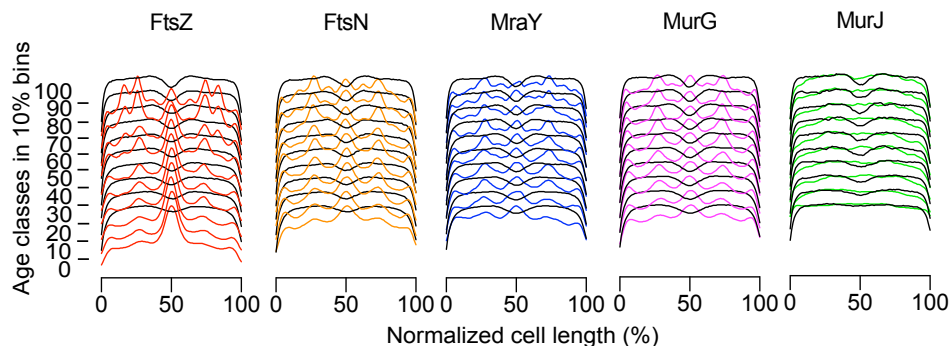


Fig. 4. Localization of cell division proteins in the presence of the PBP3 inhibitor aztreonam for 2 MDs. Cell division is inhibited but the localization and assemblage of the divisome continues, whereas the localization of MurJ is lost. In Gb1 at $28 \text{ }^{\circ}\text{C}$, steady state growing XL08 was treated with 1 mg.L^{-1} aztreonam, MurJ localization was determined in living cells, and FtsZ, FtsN, MraY and MurG were immunolabeled with antibodies after fixation. Diameter (black lines) and fluorescence (colored lines) profiles were plotted into 10 % age class bins along the normalized cell length. More than 1200 cells were included.

MurJ midcell localization requires lipid II synthesis

Next, we asked whether MurJ localization would be lipid II-dependent. The biosynthesis of lipid II requires the activity of two essential enzymes in the

cytoplasmic stage, the pyridoxal 5'-phosphate (PLP) dependent alanine racemase, Alr, which converts L-alanine into D-alanine^{3,74}, and the ATP-dependent D-ala:D-ala ligase, Ddl, which catalyzes the formation of D-alanyl-D-alanine from two molecules of D-alanine^{3,75}. D-cycloserine (DCS) is a structural analogue of D-alanine that inactivates Alr and Ddl, and causes rapid cell lysis⁷⁶⁻⁷⁹. A concentration of 1 $\mu\text{g}\cdot\text{ml}^{-1}$ DCS is sufficient to deplete the UDP-MurNac-pentapeptide pool in 30 minutes when *E. coli* is grown in minimal medium^{80,81}. Therefore, steady-state grown XL08 cells were treated with different concentrations of DCS, and MurJ localization was determined at 30 min after adding DCS. At concentrations of 0.5 $\mu\text{g}\cdot\text{mL}^{-1}$ DCS or higher, growth inhibition and rapid cell lysis was observed after 30 min, while lower concentrations of DCS caused lysis after 1 MD or even longer incubation periods (Fig. 5A). Interestingly, DCS also showed a concentration-dependent effect on MurJ localization. Increasing DCS concentrations eventually blocked the MurJ midcell localization, and when the DCS concentration was higher than 0.5 $\mu\text{g}\cdot\text{mL}^{-1}$, MurJ was mostly absent from midcell (Fig. 5B and Fig. S7A). In addition, localization of MraY and MurG was somewhat reduced at midcell in the presence of DCS (Fig. S7, B and C). On the contrary, the core divisome monitored by the presence of FtsN remained intact (Fig. S7D). Together, these results indicate that MurJ midcell localization is dependent on the synthesis of lipid II.

MurJ midcell localization requires FtsW activity

Our results so far showed that MurJ midcell localization is dependent on the assembly of the divisome, the activity of PBP3 and also the synthesis of lipid II. Previous investigation of divisome assembly and regulation suggests that FtsQLB normally keeps FtsW/PBP3 inactive, and once the divisome is completely assembled, the FtsW/PBP3 complex is somehow activated^{23,82}. Very recently, *in vitro* data showed that FtsW, PBP3 and PBP1b form a ternary complex, and the lipid II binding activity of FtsW inhibits the polymerization of lipid II by PBP1b in the absence of PBP3, while the presence of PBP3 stimulates the release of lipid II from FtsW, and activates its polymerization by PBP1b³⁸. These observations raised the possibility that

FtsW is needed to ensure the lipid II accessibility to MurJ, which implied that MurJ would not be able to localize at midcell in the presence of inactive FtsW.

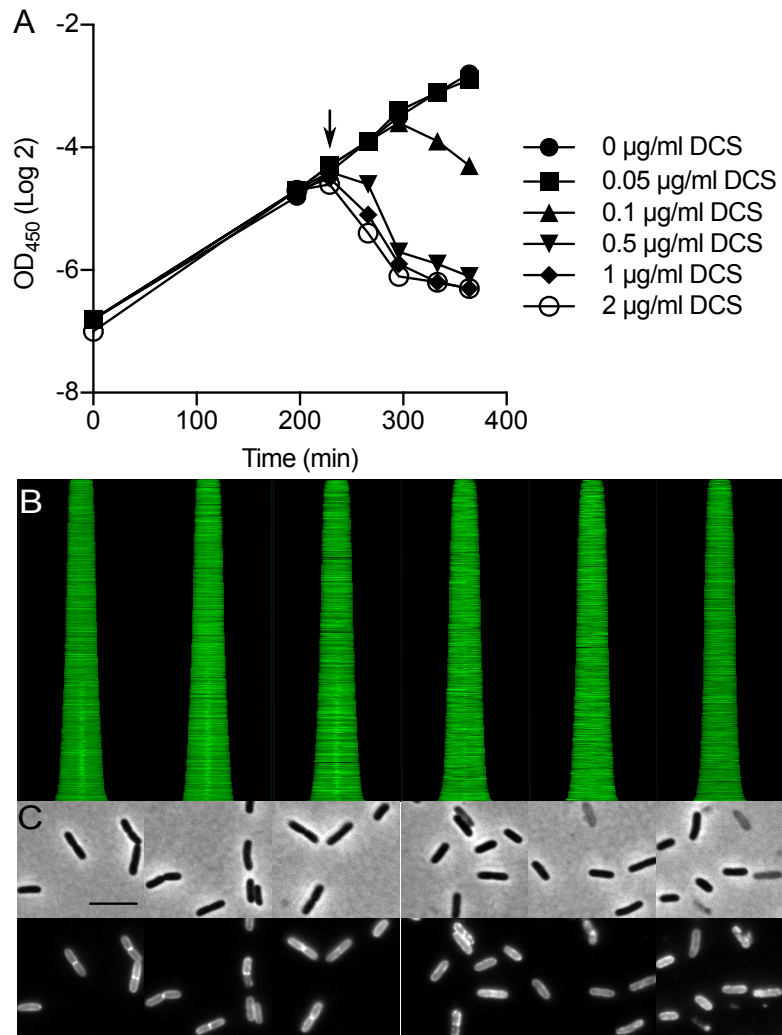


Fig. 5 Inhibition of lipid II biogenesis blocks MurJ midcell localization. In Gb1 at 28 °C, steady state growing XL08 was treated with increasing concentrations of D-cycloserine (DCS), and mNG-MurJ localization was determined at 30 minutes after addition of DCS. (A) Growth curves were plotted as time against the natural logarithm of the optical density of the cells. The black arrow indicates the addition of DCS. (B) Fluorescence maps profiles of MurJ localization. Cells are plotted according to increasing cell length from top to bottom. From left to right, the maps correspond to 0, 0.05, 0.1, 0.5, 1 and 2 µg.L⁻¹ of DCS concentrations. More than 1200 cells were included. (C) Phase contrast images (upper) and correspond fluorescence images (down) of cells treated with DCS. Scale bar equals 5 µm.

To validate this hypothesis, plasmids that expressed two non-functional FtsW mutants, FtsW R145A and FtsW K153N were introduced into strain XL08 to investigate the localization of MurJ. These two mutants were shown to localize at midcell but failed to complement the FtsW(*Ts*) strain at non-

permissive temperature, and their expression in LMC500 wild-type cells showed a dominant-negative filamentous morphology³⁹. In addition, *in vitro* data showed that these mutants lost the lipid II “flipping” activity of FtsW³⁹. In our study, to eliminate the role of the wild-type FtsW, 20 μ M IPTG was used to overexpress these two mutants, and thus diluted the functional wild type FtsW that expressed from the XL08 genome. When cells were grown to steady state in minimal medium, cell length increased due to the defect on cell division, especially in cells expressing mutant K153N (Fig. 6B). MurJ midcell localization was lost in the presence of non-functional FtsW mutants for 2 MDs, despite the overexpression of MurJ as it is also expressed under the IPTG inducible $P_{trcdown}$ promoter. In contrast, the divisome, which was monitored by immunolabeling of FtsN, was still localized at midcell (Fig. 6). Midcell localization of MurJ was not affected when wild type FtsW was overexpressed (Fig. S8), indicating that MurJ needs a functional FtsW for its localization at mid cell. Moreover, when grown in LB medium, strains expressing these mutants showed strong defects on morphology and MurJ localization. At early exponential phase ($OD_{600} = 0.2$), filamentous morphology was observed for all cultures, even for cells grown with glucose that suppressed the expression of the FtsW mutants (Fig. S9A). Interestingly, in cultures at late log phase expressing the FtsW K153N mutant or in cultures at stationary phase expressing the FtsW R145A mutant, some cells started to restore the MurJ localization, especially in the cells that were induced with IPTG (Fig. S9A). Since these mutants are toxic, we wondered whether the XL08 strain lost these FtsW expressing plasmids at high frequency, restoring MurJ localization. A spot assay was carried out to test our hypothesis: cells from each culture were diluted to the same OD_{600} value and spotted on LB and LB-ampicillin agar plates (these two plasmids expressing the FtsW mutants are ampicillin resistant). For both strains, no obvious growth difference was observed on both plates when grown with glucose, indicating that most cells still contained the mutant plasmids. However, for cells that had been induced with IPTG, a large population of cells had lost the FtsW mutant plasmids, as much less growth was observed on the ampicillin plate compared with LB plate (Fig. S9B). These results strongly suggest that MurJ midcell localization requires FtsW activity, rather than its physical presence.

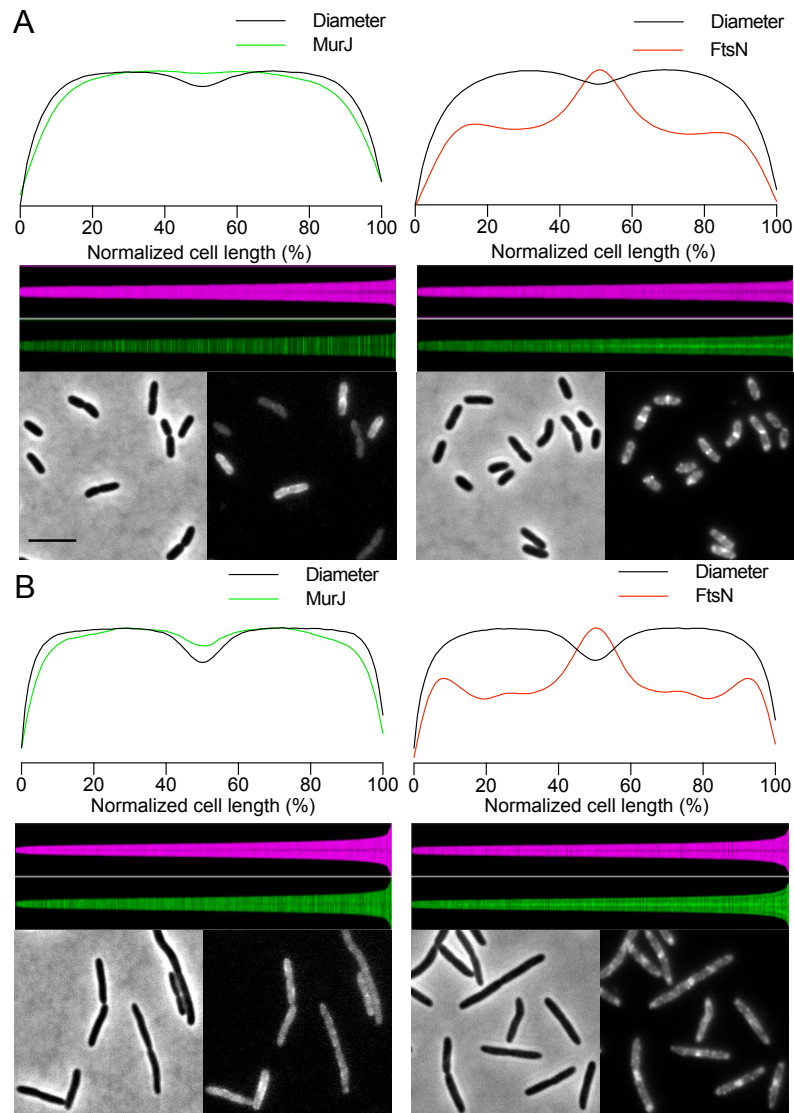


Fig. 6. Expression of non-functional FtsW mutants abolishes MurJ midcell localization. XL08 expressing mutant FtsW R145A or FtsW K153N was grown in Gb1 minimal medium to steady state at 28 °C. IPTG (20 μ M) was used to induce expression of the FtsW mutants from plasmid. MurJ localization was determined in living cells and the presence of the divisome was confirmed by immunolabeling of FtsN, after fixation. (A) Localization of MurJ and FtsN after expression of FtsW R145A. (B) Localization of MurJ and FtsN after expression of FtsW K153N. For each part: top, average localization profiles plotted along normalized cell length ($n \geq 1200$ cells). Black lines indicate cell diameter. Green lines and red lines indicate MurJ and FtsN localization, respectively. Middle, map profiles of cell diameter and MurJ or FtsN localization sorted by ascending cell length. Bottom, phase contrast and fluorescence microscopy images. Scale bar equals 5 μ m.

MurJ activity is not required for its localization

Earlier studies revealed several conserved charged residues, R18, R24, R52 and R270 in the central cavity of MurJ that are essential for its function^{41–43}. To verify whether MurJ needed to be functional to allow midcell localization, an mNG fused MurJ R18A mutant was expressed from plasmid in LMC500. The cells were grown in Gb1 and expression was induced with 20 μ M IPTG. As shown in Fig. 7A, the non-functional mutant R18A localized both in the lateral wall and at midcell as was observed for the wild type-MurJ fusion. Although MurJ is likely functional as a monomer based on its structure, the wild-type copy of MurJ from LMC500 genome might still contribute to the localization of this non-functional mutant. To eliminate this potential contribution, localization of the R18A mutant was also determined in strain XL30, a MurJ-depletion strain in which native MurJ production is under an arabinose-inducible promoter³¹. In the presence of arabinose, no growth defect was observed, and the R18A mutant showed the same localization as in the LMC500 strain (Fig. 7B, left). When grown in the presence of glucose, native MurJ was eventually depleted as morphology defects were observed after 3 hours, however, the mutant R18A was still localized in lateral wall and at midcell (Fig. 7B, right). The localization of the other loss-of-function-mutants showed the same results as R18A (see below). These results suggest that the MurJ function is not required for its localization.

MTSES does not influence the localization of MurJ single-cysteine variants

The function of a number of MurJ single-cysteine mutants, A29C, N49C, S263C and E273C, was reported to be sensitive (only partially in the case of E273C) to MTSES⁴¹. MTSES covalently modifies reduced cysteine residues that are exposed to the periplasm. In the absence of MTSES, these mutant proteins are functional, but not when MTSES is bound to their cysteine residues^{44,45,83}. To investigate whether MTSES affects the functionality of these mutants through the disruption of their recruitment, the localization of their mNG fusions was determined in the presence of MTSES. Having optimized the induction conditions, MurJ cysteine mutants were induced with

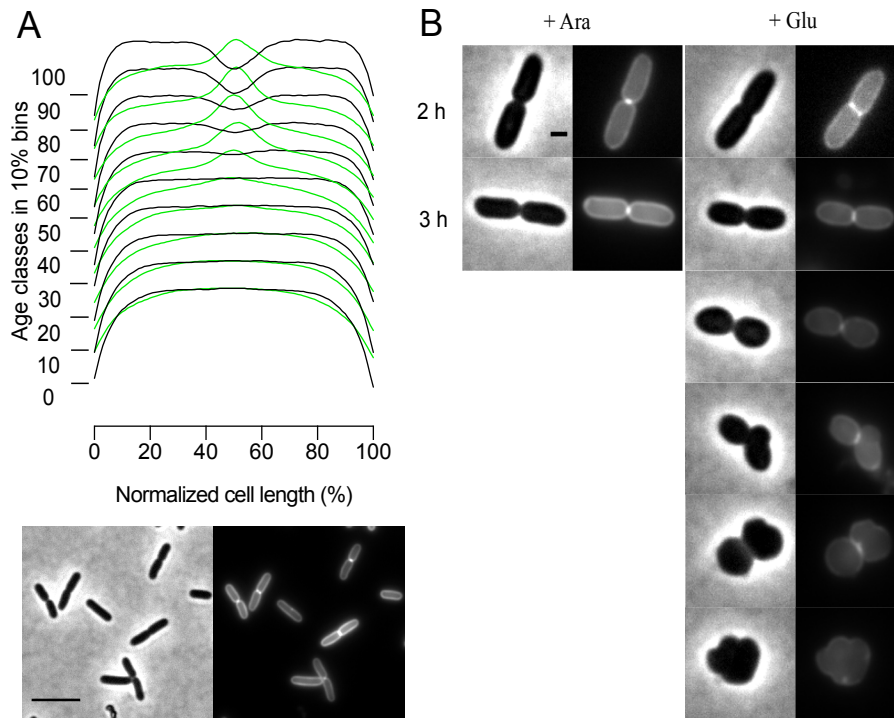


Fig. 7. MurJ non-functional mutant R18A does not influence its localization. (A) The plasmid expressing the mNG-MurJ R18A fusion was introduced into LMC500. This strain was grown in Gb1 minimal medium to steady state at 28 °C, and expression was induced with 20 μ M IPTG for 2 MDs. The diameter (black lines) and fluorescence (green lines) profiles along normalized cell length are shown in 10 % age class bins. More than 1200 cells were included. Scale bar equals 5 μ m. (B) The plasmid expressing the mNG-MurJ R18A fusion was introduced into the MurJ depletion strain XL20. Mutant localization was determined in the presence of arabinose (wild type MurJ expression) or glucose (wild type MurJ depletion). Scale bar equals 1 μ m.

40 μ M IPTG, and their localization was determined at 10 min and 40 min (20 min for S263C variant due to the higher sensitivity) after addition of 0.5 mM MTSES (Material and Methods and Fig. S10). We found that MTSES influences only the functionality but not the localization of these mutants, as MurJ midcell localization was still observed, in spite of cell lysis after MTSES addition (Fig. 8 A-D, and Fig. S11). As a control, neither the functionality nor localization of cysteine free variant (MurJ Cys⁻) was influenced by MTSES (Fig. 8 E).

Next, we also investigated whether MTSES influences the localization of the total-loss-of-function mutants, R18C, R24C, R52C, and R270C. Similar MTSES experiments were performed on these mNG-fused mutants in the LMC500 background. To eliminate the potential influence of MTSES on wild

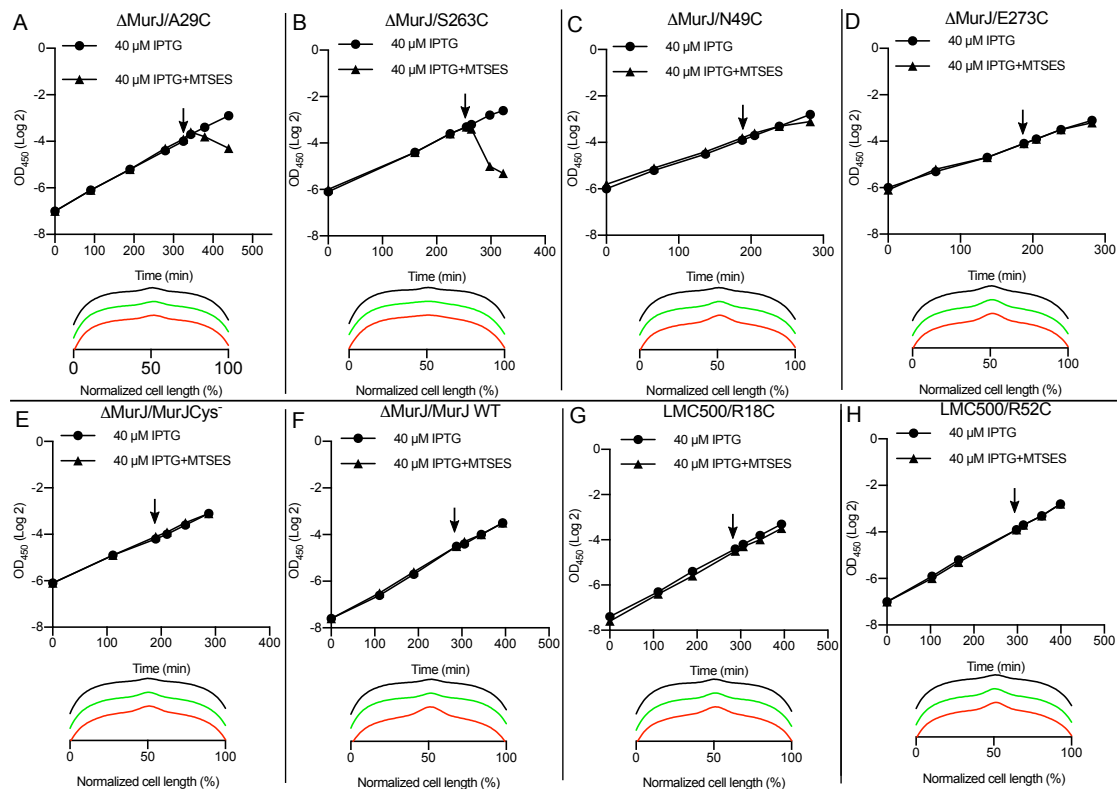


Fig. 8. Localization of MurJ cysteine mutants in the presence of MTSES. Strains expressing MurJ single-cysteine-mutants from plasmid were grown to steady state in Gb1 medium at 28 °C, and expression was induced with IPTG for 2 MDs. MurJ localization was determined at 10 min and 40 min after the addition of MTSES (for mutant S263C, localization was determined at 10 min and 20 min because of its higher sensitivity to MTSES), Average of MurJ localization profiles were plotted along normalized cell axis. Black lines indicate the MurJ localization in the absence of MTSES, green and red lines indicate the MurJ localization at 10 and 40 min in the presence of MTSES, respectively. More than 1200 cells were included for each experiment. (A-D) Only growth but not localization of functional mutants A29C, S263C, N49C and E273C is affected by MTSES. (E) Neither growth nor localization of cysteine free mutants is influenced by MTSES. (F) Neither growth nor localization of wild type MurJ is influenced by MTSES. (G and H) Localization of non-functional MurJ mutants R18C and R52C is not affected by MTSES.

type MurJ from the LMC500 genome, the MurJ deletion strain expressing mNG fused wild-type MurJ was firstly checked. In agreement with the evidence that the two native cysteine residues in wild-type MurJ are not labeled by MTSES⁴¹, no defect on cell growth, morphology or MurJ localization was observed when MTSES was added (Fig. 8F and Fig. S11F). Similarly, no growth or morphology defect was observed after addition of MTSES to the non-functional single cysteine mutants, and MurJ still localized

at midcell (Fig. 8G-H, Fig. S11, G-K and Fig. S12). To point out, when induced with 40 μ M IPTG, mutant R24C showed strongly reduced fluorescence and a cytoplasmic-like localization, compared to other mutants. However, when induced with 100 μ M IPTG, R24C showed a normal MurJ localization and comparable fluorescence, indicating that mutation R24C does not affect MurJ localization (Fig. S12C). Surprisingly, a spontaneous suppressor mutation R447H that is situated at the cytoplasmic end of TMH13 restored fluorescence and showed a typical MurJ localization when induced with 40 μ M IPTG (Fig. S7D-F). Since the R24C mutant was reported not to affect protein level⁴², R24C might slightly change the structure of MurJ, and affect mNG folding and fluorescence, while mutation R447H could somehow suppress this defect.

Together, the investigation of MTSES on MurJ cysteine variants supports the notion that MurJ activity is not essential for its localization.

Discussion

Recruitment of MurJ to midcell and the coordination of cell division and septal PG synthesis

The synthesis of PG has been studied for decades, and FtsW and RodA have been always considered as the lipid II flippases in elongasome and divisome, respectively^{12,33,39,40,84–86}. Only recently, MurJ was identified as the lipid II flippase^{31,44,45,47,48}. FtsW has been shown to bind and flip lipid II and other lipids *in vitro* but not *in vivo*^{39,40}, whereas evidence has been provided that MurJ has the lipid II flipping activity *in vivo*, but only lipid II binding activity so far *in vitro*^{38,44,45,50}. Our study indicates that these observations can be very well all valid, as both FtsW and MurJ are required for lipid II flipping during cell division.

Our results show for the first time the specific MurJ cellular localization in *E. coli*. Its midcell localization is critically dependent on maturation of the divisome, on PBP3 and FtsW activity, and lipid II synthesis. Interestingly, in *E. coli*, MurJ can be replaced by non-homologous flippases from other organisms^{43,46–48,87}. Probing the interaction of MurJ with cell division proteins

such as PBP3, FtsW, MurG using our cytoplasmic FRET assay⁸⁸ did not support interaction between these proteins and MurJ, which is also supported by the loss of MurJ localization in aztreonam treated cells that still have an intact divisome at mid cell (Fig. 4). Although negative FRET results are not at all a guarantee for the absence of protein interactions, together with the smoothly replacement of MurJ by other non-homologous flippases, it suggests that protein-protein interactions are likely not involved in MurJ recruitment, which implies that its localization at midcell is driven by its substrate lipid II. This is also in agreement with the delocalization of MurJ in the presence of D-cycloserine that inhibits the production of Lipid-II (Fig. 5). Inactivation of MurJ *In vivo* results in accumulation of lipid II^{31,45}, indicating that lipid II synthesis is independent of the flipping process and MurJ's presence is needed for lipid II translocation but not synthesis. The failure of MurJ to localize at an incomplete divisome or upon inactivation of PBP3 (by aztreonam) or FtsW (by mutation) signifies that lipid II is inaccessible to MurJ under these conditions (Fig 3, 4 and 6).

But why would lipid II not be accessible to MurJ under these conditions? One possible explanation could concern the regulation between PBP3 and FtsW to bind lipid II. We showed that MurJ requires FtsW activity for midcell localization. FtsW is clearly able to bind lipid II *in vitro*³⁸, and the absence of PBP3 causes FtsW to hold lipid II and prevents its polymerization by PBP1b, whereas presence of PBP3 stimulates the release of lipid II from FtsW and allows its polymerization by PBP1b³⁸. Adding that an incomplete divisome will keep the FtsW-PBP3 complex activity in check (probably) by the FtsQLB subcomplex^{23,82}, a logical explanation would be that the inactivated FtsW, either caused by the incomplete divisome assembly, or inactivation of PBP3, or mutations (FtsW R145A and FtsW K513N), is unable to release lipid II to MurJ, and thus blocks MurJ midcell recruitment. An alternative explanation could be that FtsW, stimulated by PBP3, is required to take over the flipped lipid II from MurJ to use it or present it for PG synthesis. The inactivated PBP3 and/or FtsW will keep MurJ from resuming its flipping cycle. In this scenario MurJ would diffuse away from the division site and would provide any available transglycosylase with lipid II. Taking over lipid II from MurJ would be in agreement with the suggested transglycosylase function of FtsW³⁴. The

requirement of FtsW/PBP3 activities would also explain why MurJ is not flipping lipid II *in vitro*. A third possibility, which we cannot exclude presently, is that FtsW and MurJ are both flipping lipid to insert multiple glycan stands simultaneously in the septum as was suggested in the three for one or four for two models of PG insertion during cell division⁸⁹.

Why would it be necessary to present lipid II at midcell to MurJ (or take it over from MurJ) and does this imply that RodA as an FtsW homolog is also presenting (or taking over) lipid II to/from MurJ during lateral growth? The midcell position is very precisely determined by the cell^{90,91}. If lipid II would be synthesized randomly and flipped randomly, it could lead to loss of precision of the binary fission into identical daughter cells. The observation that inhibition of the elongasome did not affect division or MurJ midcell localization, and the inhibition of the divisome did not influence cell length growth (Fig. 4 and Fig. S6), suggest that lipid II flipping is precisely organized at the position where new PG synthesis should occur. This can be achieved by allowing it only to flip as closely as possible where the substrate is needed, and by only allowing it to bind lipid II next to the proteins that are activated to synthesize the new cell wall.

Other studies suggested that MurJ alters between inward-facing and outward-facing conformations during substrate transport⁴³, and observed that cysteine mutations at the charged residues, R18, R24, R52 and R270, in the cavity center cause the loss function of MurJ, while some other cysteine mutants at position A29, N49, S263 and E273 are functional but not in the presence of cysteine-reactive agent MTSES^{42,44}. But how do these residues contribute to the function of MurJ is not clear. Our results show that the functionality of MurJ is not required for its midcell recruitment, despite the inactivation caused directly by mutation or by MTSES treatment (Fig. 7 and 8). As we mentioned above, MurJ midcell recruitment is likely driven by its substrate lipid II, our results on the MurJ mutants suggest that these mutants are able to recognize at least part of the substrate lipid II, but cannot flip. Also, these important residues are not conserved in other flippases that are able to replace MurJ and therefore more likely involved in the flipping mechanism than in initial substrate recognition (Fig. S13).

However, residues A29 and S263 are situated at the interface between

the two lobes of MurJ, and thus are predicted to be important for MurJ conformational changes from the outward-facing to the inward-facing state, and binding of MTSES at these two positions will trap the protein at the outward-facing state^{43,44}. Also, recent *in vitro* evidence suggests that binding of MTSES at A29C reduced the lipid II binding affinity of MurJ protein⁵⁰. This would predict delocalization for the MTSES bound A29C MurJ mutant, whereas we observe the typical midcell localization *in vivo*. If this MTSES bound mutant does not recognize lipid II, its localization would require protein-protein interaction, which is unlikely in view of MurJ's smoothly replacement by completely non-homologous flippases. It would also imply that the dependence of MurJ recruitment on divisome assembly, lipid II synthesis, FtsW activity and PBP3 activity would then be indirect, and that an important unknown factor that determines MurJ localization is missing. *In vitro* data are not always completely comparable to the *in vivo* situation, and given the conflicting lipid II binding evidences *in vitro*^{38,50}, we assume that the MurJ A29C MTSES mutant still has a partial ability to recognize lipid II. According to the present published models^{43,45,83}, this would require changing to the inward open conformation, which is the only conformation observed thus far in MurJ crystals⁴³.

Model of MurJ function in septal PG synthesis

Based on our evidence and that of others, we arrived at a model for the mechanism of MurJ recruitment and lipid II flipping during septal PG synthesis (Fig. 9). After maturation of the core divisome complex, MurJ is recruited to midcell through the recognition of its substrate lipid II (Fig. 9 A), and ensures the precise positioning of septal PG synthesis. Interruption of lipid II synthesis by D-cycloserine, or inactivation of PBP3 by aztreonam, or inactivation of FtsW will likely make lipid II inaccessible for MurJ, and block the recruitment of MurJ to midcell. Once recruited, MurJ flips lipid II by changing from the inward-facing state to an outward-facing conformation, and the flipped lipid II can be used for new PG synthesis (Fig. 9 B and C). Subsequently, the unloaded outward facing MurJ switches back to the inward-facing state, and can be recruited for new cycles (Fig. 9D). Inactivation of MurJ, either by direct

mutation at the charged residues R18, R24, R52, R270, or by binding of MTSES to residues A29C, N49C, S263C and E273C, will disrupt the translocation of lipid II across the membrane (Fig. 9B). Although we cannot totally rule out the possibility of involvement of protein-protein interaction recruitment of MurJ during septal PG synthesis, our data show a possible

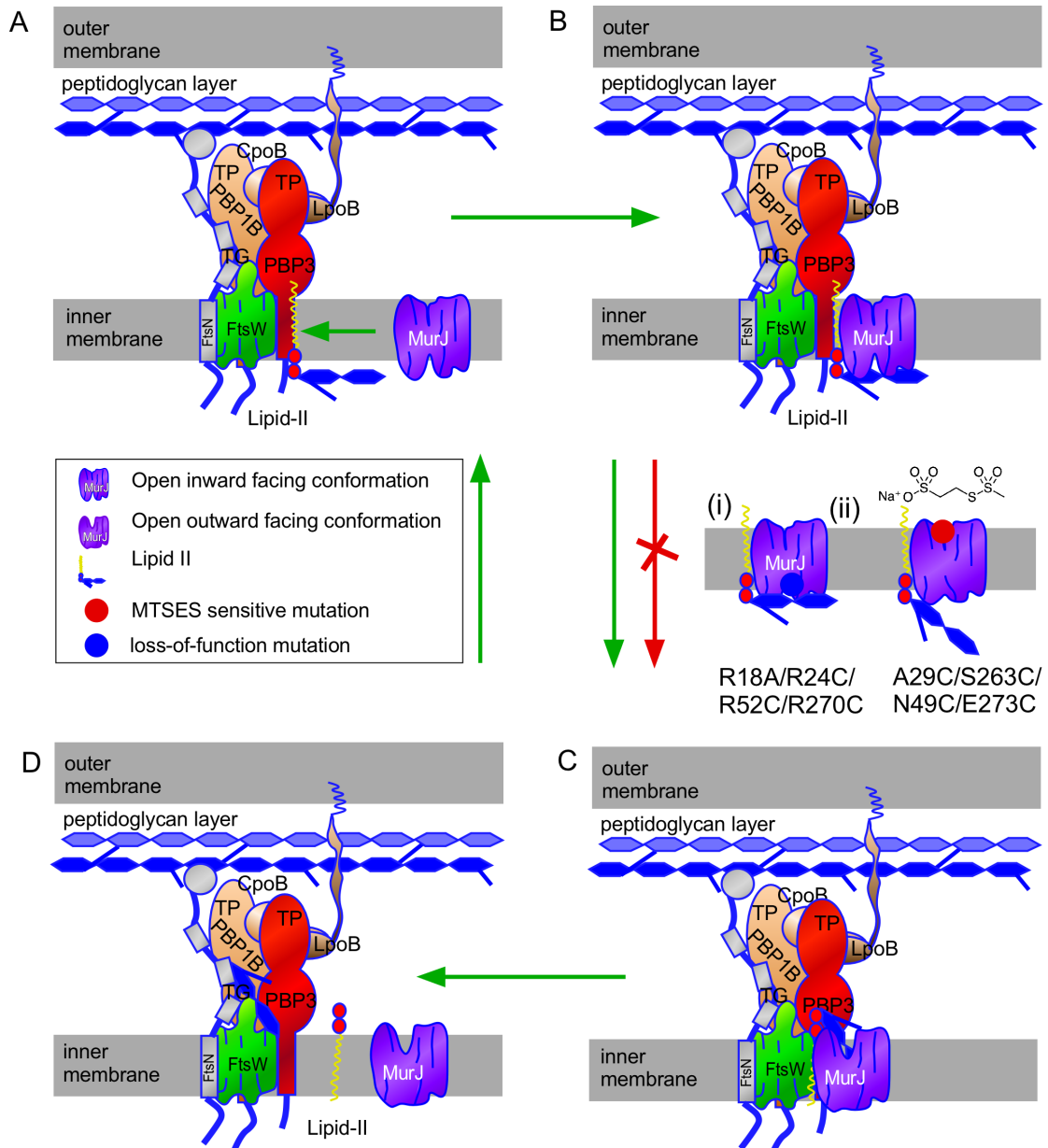


Fig. 9. Model of MurJ recruitment and function in septal peptidoglycan synthesis. (A) Recruitment of MurJ to midcell when FtsW is activated. (B) MurJ binds substrate. (C) MurJ flips lipid II across the IM by changing its structure from the inward-facing conformation into the outward-facing state. (D) Unloaded MurJ changes back into the default inward-facing state to participate in a new cycle. (i) Loss-of-function MurJ mutants that localize but are not able to flip lipid II. (ii) Functional MurJ mutants that are inactivated by MTSES still localize but are not able to flip lipid II.

mechanism of how MurJ functions during cell division *in vivo*, and visualize of MurJ localization will give possibilities for future investigations and further antibiotics developments. It should be noted that although we mainly focused on the septal MurJ, some evidence, like the D-cycloserine experiments, MurJ depletion experiment, and MTSES experiments, showed a global effect on *E. coli*, indicating that MurJ very likely works similarly in collaboration with the elongasome, likely with the FtsW homologous protein RodA.

Material and methods

Strains and plasmids construction

Strains and plasmids used in this study are listed in Table. S1. To construct the MurJ N-terminal fluorescent protein (FP) fusion plasmids, mCherry (mCh)⁵³ or *E. coli* codon optimized mNeonGreen mNG⁵⁴, were firstly cloned into plasmids pTHV037⁷⁰ and pSAV057⁸⁸ by restriction and ligation (*Nco*I and *Eco*RI), to generate plasmid pSAV047 and pSAV057-mNG, respectively. Subsequently, amplified MurJ fragments with different linkers were cloned into these two plasmids by restriction and ligation (*Eco*RI and *Hind*III), to generate the derived N-terminal fusion plasmids. To construct the MurJ C-terminal FP fusion plasmids, MurJ gene was firstly cloned into plasmids pTHV037 and pSAV057 with *Nco*I and *Bam*HI, to generate plasmids pXL09 and pXL10. Subsequently, FP genes with different linkers were cloned into these two plasmids with *Bam*HI and *Hind*III, to generate the derived C-terminal fusion plasmids. GlpT fusion plasmid pXL28 was constructed in the same way. To construct the MurJ mutant plasmids, QuickChange site directed mutagenesis (Agilent technologies, Santa Clara, CA) and Gibson assembly⁹⁴ approaches were applied. Plasmid pXL74 was firstly generated from pXL05 by replacing the wild type MurJ with the cysteine free mutant that was amplified from plasmid pFLAGMurJ Δ Cys⁴¹. Single-cysteine-mutant plasmids were constructed afterwards by replacing the original residues with cysteine. The double mutation plasmid pXL93 was constructed by introducing the additional R52C mutation into plasmid pXL82.

The MurJ deletion strain XL03 (LMC500 $\Delta murJ::FRT/pRC7MurJKan$) was constructed by λ -Red recombination⁹⁵ in the presence of the complementing plasmid pRC7MurJ⁴¹. Primers priXL17 and priXL18 were used to amplify the MurJ upstream homologous sequence region ahead of MurJ start codon from the *E. coli* genome, primers priXL19 and priXL20 were used to amplify the chloramphenicol (*cat*) cassette from plasmid pKD3⁹⁵, and primers priXL21 and priXL22 were used to amplify the downstream homologous sequence that comes after MurJ stop codon from the *E. coli* genome. An overlap PCR was performed using the obtained homologous sequences and *cat* gene with primers priXL17 and priXL21 to generate the final recombination fragment. This PCR product was used to generate the MurJ depletion strain sNM01 (LMC500 $\Delta murJ::cat$ pRC7MurJKan). Subsequently, the chloramphenicol resistance cassette was removed by plasmid pCP20⁹⁵, which resulted in the final *murJ* deletion strain XL03/pRC7MurJ Δ Kan (The kanamycin cassette on this plasmid is also removable).

To prove the existence of the native *murJ* promoter, a chloramphenicol cassette was inserted after the stop codon of *yceM* upstream of *murJ* with a similar strategy as above. Primers priXL49 and priXL50 were used to amplify the upstream homologous sequence from the *E. coli* genome, priXL54 and priXL52 were used to amplify the *cat* cassette from plasmid pKD3, and priXL45 and priXL48 were used to amplify the downstream homologous sequence from the *E. coli* genome. The amplified overlap PCR product with primers priXL49 and priXL48 was used to construct the recombinant strain XL04 that interrupted MurJ expression from the upstream gene cluster. To construct MurJ chromosomal fusion strains that are expressed under its native promoter, plasmids pXL36 and pXL37 were firstly constructed with Gibson assembly: primers priXL51 and priXL52 were used to amplify the pKD3 backbone, primers priXL45 and priXL46 were used to amplify the P_{murj} sequence from the *E. coli* genome, primers priXL53 and priXL47 were used to amplify FPs-MurJ sequence from plasmid pXL05 and pNM037. The final recombination fragments were generated by overlap PCR of 2 fragments with primers priXL17 and priXL48 from fragment *yceM-cat* amplified from the XL04 genome with primers priXL17 and priXL50, and fragment *cat-P_{murj}-FPs-murJ*

amplified from these assembled plasmids with primers priXL54 and priXL48. To construct the MurJ chromosomal FP fusion strains XL06 and XL07 expressing MurJ under control of the $P_{trcdown}$ promoter, fragment *yceM-cat* was amplified from the XL04 genome with primers priXL17 and priXL52, and fragment $P_{trcdown}$ -FPs-MurJ was amplified from plasmids pXL06 or pNM037 with primers priXL77 and priXL48. The two fragments were used for an overlap PCR with primers priXL17 and priXL48 and the resulting sequence was used to construct strains XL06 and XL07 from LMC500 by λ -Red recombination. To insert the mNG-MurJ fusion in the chromosomal of temperature sensitive strains and deletion strains, PCR fragment *yceM-cat-P_{trcdown}-NG-(GGS)₂-MurJ* was firstly amplified from the XL06 genome with primer priXL17 and priXL48, and subsequently introduced into other strains by λ -Red recombination.

To construct an FtsN depletion strain, primers priXL140 and priXL141 were used to amplify the upstream sequence of FtsN from the *E. coli* genome, priXL54 and priXL52 were used to amplify the *cat* cassette from plasmid pKD3, and priXL138 and priXL139 were used to amplify the *araC-P_{BAD}* region from plasmid pJC83⁹⁶. An overlap PCR with priXL140 and priXL138 was performed subsequently to generate the final product for recombination. The MurJ depletion strain was constructed in a similar way, primers priXL17 and priXL52 were used to amplify the *YceM-cat* region from the XL06 genome, priXL126 and priXL157 were used to amplify *araC-P_{BAD}* region from plasmid pKD46, priXL156 and priXL48 were used to amplify the MurJ region from the *E. coli* genome. The final PCR product for MurJ depletion was generated by an overlap PCR with primers priXL17 and priXL48.

All PCR amplifications were performed using the DNA polymerase pfuX7 prepared in our lab as described⁹⁷, and all restriction enzymes used were purchased from New England Biolabs Inc (NEB, Ipswich, MA).

Medium and growth conditions

LB medium (10 g of tryptone (Bacto laboratories, Australia), 10 g of NaCl (Merck, Kenilworth, NJ), 5 g of yeast extract (Duchefa, Amsterdam, The

Netherlands) per liter) was used for growth in rich medium at 30 °C, 37 °C and 42 °C. The FtsW(*Ts*) strain was grown in LBΔNaCl medium (LB without NaCl and containing 0.1% glucose and 20 mg thymine per liter) as described previously⁹⁸. Gb1 minimal medium (6.33 g of K₂HPO₄ (Merck), 2.95 g of KH₂PO₄ (Riedel de Haen, Seelze, Germany), 1.05 g of (NH₄)₂SO₄ (Sigma, St. Louis, MO), 0.10 g of MgSO₄·7H₂O (Roth, Karlsruhe, Germany), 0.28 mg of FeSO₄·7H₂O (Sigma), 7.1 mg of Ca(NO₃)₂·4H₂O (Sigma), 4 mg of thiamine (Sigma), 2 mg of uracil (Sigma), 2 mg of lysine (Sigma), 2 mg of thymine (Sigma), and 0.5 % glucose (Merck) per liter, pH 7.0) was prepared for steady state growth at 28 °C as described⁶⁴. Protein expression was induced with isopropyl β-D-1-thiogalactopyranoside (IPTG, Promega, Madison WI) or L-(+)arabinose (Sigma) at described concentrations. All antibiotics were purchased from Sigma Aldric, Working antibiotics concentrations were: 100 μg.mL⁻¹ ampicillin (10 μg.mL⁻¹ for Δ*tolA* and Δ*pal* strains), 25 μg.mL⁻¹ chloramphenicol, 50 μg.mL⁻¹ kanamycin, 10 μg.mL⁻¹ tetracycline (for chromosomal recombinant strains, half of the concentrations were used). Optical density (OD) was measured at 450 nm and 600 nm when grown in minimal medium and rich medium, respectively.

Testing functionality of MurJ fusions

Functionality experiments were performed as described previously^{41,42} using the MurJ depletion strain XL03 that expresses a functional MurJ copy from plasmid pRC7MurJΔKan. This plasmid has partitioning defects causing some of the daughter cells to lose this plasmid and die after division, unless they are complemented with a functional copy of MurJ since MurJ is essential for *E. coli*. In addition, pRC7MurJΔKan contains the *lacZ* operon and thus cells that lost the plasmid will also lose their ability to produce the blue color on 20 μg.L⁻¹ X-gal (Sigma) agar plates, as our pTHV and pSAV-based plasmids do not. The functional FPs fusions to MurJ were obtained by selecting the white colonies on Ampicillin or chloramphenicol X-gal agar dish after transformation. The growth and fluorescence intensity of strains containing a fusion expressing plasmid were investigated with Synergy Mx BioTek plate reader and microscopy.

Immunolocalization experiments

E. coli cells were fixed with FGA (2.8% formaldehyde and 0.04% glutaraldehyde final concentration) for 15-20 minutes in a shaking waterbath after steady state growth in Gb1 minimal medium at 28 °C⁷⁰. Subsequently, cells were permeabilized and immunolabeled with antibodies as described⁶³. The antibodies against FtsZ, FtsN, MurG used in this study were purified as described^{21,61}. Polyclonal antibodies against MraY were obtained from Rabbits that were injected with an antigenic peptide that was designed with the Epiros program (Biosiris). Based on the predicted topology by Bouhss et al (16,17) the peptide localizes in the cytoplasmic loop between TMH 1 and 2. The sequence was H2N-G54QVVRNDGPESHFS67C-COOH. The cysteine was added at the C-terminal to perform the coupling with the KLH carrier protein.

Depletion or inactivation of of divisome proteins

Strain XL17, XL15, XL13 and XL14 that contain a MurJ FP fusion and the temperature sensitive divisome mutant proteins FtsW, FtsI, FtsQ and FtsA, respectively, were diluted 1:1000 from overnight cultures (grown at 30 °C) into fresh LB medium (LBΔNaCl medium for XL13) with 12.5 µg.mL⁻¹ chloramphenicol, and grown at 30 °C to OD₆₀₀ of approximately 0.2. Cells were diluted 1:5 into the same fresh medium that was pre-warmed at 30 °C and 42 °C, respectively, and kept growing for 2 mass doublings. To deplete FtsN, strain XL23 was diluted 1:1000 from an overnight culture (grown at 30 °C) into fresh LB medium with 12.5 µg.mL⁻¹ chloramphenicol and 0.5% w/v glucose, and kept growing at 30 °C to OD₆₀₀ of approximately 0.2. Induced with 0.2% w/v arabinose was set as control. After growth, cells were immobilized on 1% agarose slides, and imaged live by phase contrast and epifluorescence microscopy.

MTSES assay

Sodium (2-sulfonatoethyl) methanethiosulfonate (MTSES) was purchased from Santa Cruz Biotechnology Company. A gradient assay on MTSES concentrations (0, 0.01, 0.05, 0.1 or 0.5 mg.mL⁻¹) was firstly applied on Gb1 steady state grown strain XL03 that expressed the MurJ A29C mutant. MurJ localization was determined by microscopy at 10 min and 40 min after addition of MTSES. Upon induction of expression with 20 μ M IPTG for 2 MDs rapid cell lysis was observed after adding MTSES for 10 min at concentrations 0.1mM or 0.5 mM. A pattern of MurJ midcell localization was observed despite the increase of MTSES concentrations (Fig. S7A). However, we noticed that lower concentration of MTSES (0.01 mM) was not sufficient to influence the cell growth, and cells lysed too fast at higher MTSES concentrations (above 0.05 mM) to determine MurJ localization at a longer time scale. Since MTSES targets MurJ A29C by covalent binding, we suspected that the higher expression of MurJ might help to increase the resistance to MTSES. Thus, 40 μ M IPTG was used for MurJ induction (2 MDs). Indeed, higher expression of A29C slightly improved the survival of cells, with a yield of better fluorescent signal, and MurJ midcell localization was able to be determined at both 10 min and 40 min after MTSES addition. In addition, 0.5 mM MTSES was sufficient to show the influence on cell growth. Thus, 0.5 mM MTSES and 40 μ M IPTG inductions were used for the investigation of MurJ localization in the presence of MTSES.

Microscope and image analysis

For localization imaging, cells were immobilized on 1.0% agarose (w/v in Gb1) pads and imaged immediately. Fluorescence microscopy was carried out either with an Olympus BX-60 fluorescence microscope equipped with a CoolSnap *fx* (Photometrics) CCD camera, a 100 \times /N.A. 1.35 oil objective, and software 'ImageJ-MicroManager', or with a Nikon Eclipse Ti microscope equipped with a C11440-22CU Hamamatsu ORCA camera, a CFI Plan Apochromat DM 100 \times oil objective, an Intensilight HG 130W lamp and the NIS elements software (version 4.20.01).

Images were analyzed with Coli-Inspector supported by the ObjectJ plugin for ImageJ (version 1.49v)⁵⁶. Briefly, the length and diameter of more

than 1200 individual cells were marked and analysis in the phase contrast images. Fluorescence and phase contrast images were aligned and fluorescence background was subtracted as described (18). The fluorescence of each cell was collected in a one pixel wide bar with the length of the cell. A map of the diameter or the fluorescence localization and intensity was generated with the cells sorted according to increasing cell from left to right. Because cells were grown to steady state, the length of the cells can be directly correlated to the cell division cycle age. A collective profile is created from all cell profiles in a map. They are first resampled to a normalized cell length of 100 data points, and then averaged to a single plot, in either 1 group or more age bins. The FCplus (the extra fluorescence at mid cell in comparison to the fluorescence in the rest of the cell) and Ringfraction (FCplus/Total cellular fluorescence) profiles were generated with the “graph assistant” macro in ObjectJ.

Acknowledgement

We would like to thank Dr. N. Ruiz for critically reading the manuscript and for the gift of plasmids pFLAGMurJ Δ Cys and pRC7MurJ for cloning and the functionality testing.

Author contributions

X.L. was supported by the Chinese Scholarship Council (File No.201406220123), and N.Y.M. by NWO ALW open program (822.02.019).

X.L. and T.B. designed most experiments. X.L performed most experiments and N.Y.M designed and performed some of the experiments. X.L and TdB analyzed the data and wrote the manuscript. A.B. isolated MraY and made antibodies against the protein. All authors critically read the manuscript and gave feedback.

References

1. Vollmer, W., Blanot, D. & De Pedro, M. A. Peptidoglycan structure and architecture. *FEMS Microbiol. Rev.* **32**, 149–167 (2008).
2. Bouhss, A., Trunkfield, A. E., Bugg, T. D. H. & Mengin-Lecreulx, D. The biosynthesis of peptidoglycan lipid-linked intermediates. *FEMS Microbiology Reviews* **32**, 208–233 (2008).
3. Barreteau, H. *et al.* Cytoplasmic steps of peptidoglycan biosynthesis. *FEMS Microbiol. Rev.* **32**, 168–207 (2008).
4. Pomorski, T. & Menon, A. K. Lipid flippases and their biological functions. *Cell. Mol. Life Sci.* **63**, 2908–2921 (2006).
5. Ruiz, N. Filling holes in peptidoglycan biogenesis of *Escherichia coli*. *Curr. Opin. Microbiol.* **34**, 1–6 (2016).
6. Ruiz, N. Lipid Flippases for Bacterial Peptidoglycan Biosynthesis. *Lipid Insights* **8**, 21–31 (2015).
7. Scheffers, D. J. & Tol, M. B. LipidII: Just Another Brick in the Wall? *PLoS Pathog.* **11**, 1–12 (2015).
8. Macheboeuf, P., Contreras-Martel, C., Job, V., Dideberg, O. & Dessen, A. Penicillin binding proteins: Key players in bacterial cell cycle and drug resistance processes. *FEMS Microbiol. Rev.* **30**, 673–691 (2006).
9. Sauvage, E., Kerff, F., Terrak, M., Ayala, J. A. & Charlier, P. The penicillin-binding proteins: Structure and role in peptidoglycan biosynthesis. *FEMS Microbiol. Rev.* **32**, 234–258 (2008).
10. Manat, G. *et al.* Deciphering the Metabolism of Undecaprenyl-Phosphate: The Bacterial Cell-Wall Unit Carrier at the Membrane Frontier. *Microb. Drug Resist.* **20**, 199–214 (2014).
11. Pedro, M. A. De, Quintela, J. C., Höltje, J. V & Schwarz, H. Murein segregation in *Escherichia coli*. *Microbiology* **179**, 2823–2834 (1997).
12. Den Blaauwen, T., De Pedro, M. A., Nguyen-Distèche, M. & Ayala, J. A. Morphogenesis of rod-shaped sacculi. *FEMS Microbiol. Rev.* **32**, 321–344 (2008).
13. van Teeffelen, S. *et al.* The bacterial actin MreB rotates, and rotation depends on cell-wall assembly. *Proc. Natl. Acad. Sci.* **108**, 15822–15827 (2011).
14. Morgenstein, R. M. *et al.* RodZ links MreB to cell wall synthesis to mediate MreB rotation and robust morphogenesis. *Proc Natl Acad Sci U S A* **112**, 12510–12515 (2015).
15. Fenton, A. K., Mortaji, L. El, Lau, D. T. C., Rudner, D. Z. & Bernhardt, T. G. CozE is a member of the MreCD complex that directs cell elongation in *Streptococcus pneumoniae*. *Nat. Microbiol.* **2**, 16237 (2016).
16. Contreras-Martel, C. *et al.* Molecular architecture of the PBP2–MreC core bacterial cell wall synthesis complex. *Nat. Commun.* **8**, 776 (2017).

17. Sun, Q. & Margolin, W. FtsZ Dynamics during the Division Cycle of Live Escherichia coli Cells. *J. Bacteriol.* **180**, 2050–2056 (1998).
18. Blaauwen, T. Den, Buddelmeijer, N., Aarsman, M. E. G., Hameete, C. M. & Nanninga, N. Timing of FtsZ assembly in Escherichia coli. *J. Bacteriol.* **181**, 5167–5175 (1999).
19. den Blaauwen, T., Hamoen, L. W. & Levin, P. A. The divisome at 25: the road ahead. *Curr. Opin. Microbiol.* **36**, 85–94 (2017).
20. Gray, A. N. *et al.* Coordination of peptidoglycan synthesis and outer membrane constriction during Escherichia coli cell division. *Elife* **4**, 1–29 (2015).
21. Aarsman, M. E. G. *et al.* Maturation of the Escherichia coli divisome occurs in two steps. *Mol. Microbiol.* **55**, 1631–1645 (2005).
22. Lutkenhaus, J. FtsN - Trigger for septation. *J. Bacteriol.* **191**, 7381–7382 (2009).
23. Weiss, D. S. Last but not least: New insights into how FtsN triggers constriction during Escherichia coli cell division. *Mol. Microbiol.* **95**, 903–909 (2015).
24. Gerding, M. A. *et al.* Self-enhanced accumulation of FtsN at division sites and roles for other proteins with a SPOR domain (DamX, DedD, and RlpA) in Escherichia coli cell constriction. *J. Bacteriol.* **191**, 7383–7401 (2009).
25. Bertsche, U. *et al.* Interaction between two murein (peptidoglycan) synthases, PBP3 and PBP1B, in Escherichia coli. *Mol. Microbiol.* **61**, 675–690 (2006).
26. Lysis of Escherichia coli by beta-lactam antibiotics: deletion analysis of the role of penicillin-binding proteins 1A and 1B. *J Gen Microbiol.* **131**, 2839–45. (1985).
27. Suzuki, H., Nishimura, Y. & Hirota, Y. On the process of cellular division in Escherichia coli: a series of mutants of E. coli altered in the penicillin-binding proteins. *Proc. Natl. Acad. Sci. U. S. A.* **75**, 664–668 (1978).
28. Derouichei, R., Bénédicti, H., Lazzaroni, J. C., Lazdunski, C. & Lloubès, R. Protein complex within Escherichia coli inner membrane: TolA N-terminal domain interacts with TolQ and TolR proteins. *J. Biol. Chem.* **270**, 11078–11084 (1995).
29. Dubuisson, J. F., Vianney, A. & Lazzaroni, J. C. Mutational Analysis of the TolA C-Terminal Domain of Escherichia coli and Genetic Evidence for an Interaction between TolA and TolB. *J. Bacteriol.* **184**, 4620–4625 (2002).
30. Priyadarshini, R., De Pedro, M. A. & Young, K. D. Role of peptidoglycan amidases in the development and morphology of the division septum in Escherichia coli. *J. Bacteriol.* **189**, 5334–5347 (2007).
31. Ruiz, N. Bioinformatics identification of MurJ (MviN) as the peptidoglycan lipid II flippase in Escherichia coli. *Proc. Natl. Acad. Sci. U. S. A.* **105**, 15553–7 (2008).
32. Young, K. D. A flipping cell wall ferry. *Microbiology* **345**, 139–140 (2014).
33. Ikeda, M. *et al.* Structural similarity among Escherichia coli FtsW and RodA proteins and Bacillus subtilis SpoVE protein, which function in cell division, cell elongation, and spore formation, respectively. *J. Bacteriol.* **171**, 6375–6378 (1989).
34. Meeske, A. J. *et al.* SEDS proteins are a widespread family of bacterial cell wall polymerases. *Nature* 1–15 (2016). doi:10.1038/nature19331

35. Khattar, M. M., Begg, K. J. & Donachie, W. D. Identification of FtsW and characterization of a new ftsW division mutant of Escherichia coli. *J. Bacteriol.* **176**, 7140–7147 (1994).
36. Goehring, N. W., Gueiros-filho, F. & Beckwith, J. Premature targeting of a cell division protein to midcell allows dissection of divisome assembly in Escherichia coli. *Genes Dev.* **19**, 127–137 (2005).
37. Goehring, N. W., Gonzalez, M. D. & Beckwith, J. Premature targeting of cell division proteins to midcell reveals hierarchies of protein interactions involved in divisome assembly. *Mol. Microbiol.* **61**, 33–45 (2006).
38. Leclercq, S. *et al.* Interplay between Penicillin-binding proteins and SEDS proteins promotes bacterial cell wall synthesis. *Sci. Rep.* **7**, 43306 (2017).
39. Mohammadi, T. *et al.* Specificity of the transport of lipid II by FtsW in Escherichia coli. *J. Biol. Chem.* **289**, 14707–14718 (2014).
40. Mohammadi, T. *et al.* Identification of FtsW as a transporter of lipid-linked cell wall precursors across the membrane. *EMBO J.* **30**, 1425–1432 (2011).
41. Butler, E. K., Davis, R. M., Bari, V., Nicholson, P. A. & Ruiz, N. Structure-function analysis of MurJ reveals a solvent-exposed cavity containing residues essential for peptidoglycan biogenesis in Escherichia coli. *J. Bacteriol.* **195**, 4639–4649 (2013).
42. Butler, E. K., Tan, W. B., Joseph, H. & Ruiz, N. Charge requirements of lipid II flippase activity in Escherichia coli. *J. Bacteriol.* **196**, 4111–4119 (2014).
43. Kuk, A. C. Y., Mashalidis, E. H. & Lee, S. Y. Crystal structure of the MOP flippase MurJ in an inward-facing conformation. *Nat. Struct. Mol. Biol.* **24**, 171–176 (2017).
44. Sham, L.-T. *et al.* MurJ is the flippase of lipid-linked precursors for peptidoglycan biogenesis. *Science (80-.)*. **345**, 220–222 (2014).
45. Qiao, Y. *et al.* Lipid II overproduction allows direct assay of transpeptidase inhibition by [beta]-lactams. *Nat. Chem. Biol.* **13**, 793–798 (2017).
46. Ruiz, N. Streptococcus pyogenes YtgP (Spy-0390) complements Escherichia coli strains depleted of the putative peptidoglycan flippase MurJ. *Antimicrob. Agents Chemother.* **53**, 3604–3605 (2009).
47. Meeske, A. J. *et al.* MurJ and a novel lipid II flippase are required for cell wall biogenesis in Bacillus subtilis. *Proc. Natl. Acad. Sci. U. S. A.* **112**, 6437–42 (2015).
48. Elhenawy, W. *et al.* The o-antigen flippase wzk can substitute for MurJ in peptidoglycan synthesis in helicobacter pylori and Escherichia coli. *PLoS One* **11**, 1–16 (2016).
49. Hong, Y., Liu, M. A. & Reeves, P. R. Progress in our understanding of Wzx flippase for translocation of bacterial membrane lipid-linked oligosaccharide. *J. Bacteriol.* **200**, 1–14 (2018).
50. Bolla, J. R. *et al.* Direct observation of the influence of cardiolipin and antibiotics on lipid II binding to MurJ. *Nat. Chem.* **10**, 363–371 (2018).
51. Chen, X., Zaro, J. L. & Shen, W. C. Fusion protein linkers: Property, design and

- functionality. *Advanced Drug Delivery Reviews* **65**, 1357–1369 (2013).
52. van der Ploeg, R., Goudelis, S. T. & den Blaauwen, T. Validation of FRET assay for the screening of growth inhibitors of escherichia coli reveals elongasome assembly dynamics. *Int. J. Mol. Sci.* **16**, 17637–17654 (2015).
 53. Cranfill, P. J. *et al.* Quantitative assessment of fluorescent proteins. *Nat. Methods* **13**, 557–562 (2016).
 54. Meiresonne, N. Y., van der Ploeg, R., Hink, M. A. & den Blaauwen, T. Activity-Related Conformational Changes in d,d-Carboxypeptidases Revealed by In Vivo Periplasmic Förster Resonance Energy Transfer Assay in Escherichia coli. *MBio* (2017). doi:10.1128/mBio.01089-17
 55. Li, G. W., Burkhardt, D., Gross, C. & Weissman, J. S. Quantifying absolute protein synthesis rates reveals principles underlying allocation of cellular resources. *Cell* **157**, 624–635 (2014).
 56. Vischer, N. O. E. *et al.* Cell age dependent concentration of Escherichia coli divisome proteins analyzed with ImageJ and ObjectJ. *Front. Microbiol.* **6**, 1–18 (2015).
 57. Huang, Y. Structure and Mechanism of the Glycerol-3-Phosphate Transporter from Escherichia coli. *Science (80-.)*. **301**, 616–620 (2003).
 58. Oswald, F., Varadarajan, A., Lill, H., Peterman, E. J. G. & Bollen, Y. J. M. MreB-Dependent Organization of the E. coli Cytoplasmic Membrane Controls Membrane Protein Diffusion. *Biophys. J.* **110**, 1139–1149 (2016).
 59. Mengin-Lecreux, D., Texier, L., Rousseau, M. & Van Heijenoort, J. The murG gene of Escherichia coli codes for the UDP-N-acetylglucosamine:N-acetylmuramyl-(pentapeptide) pyrophosphoryl-undecaprenol N-acetylglucosamine transferase involved in the membrane steps of peptidoglycan synthesis. *J. Bacteriol.* **173**, 4625–4636 (1991).
 60. Bouhss, A., Mengin-Lecreux, D., Le Beller, D. & Van Heijenoort, J. Topological analysis of the MraY protein catalysing the first membrane step of peptidoglycan synthesis. *Mol. Microbiol.* **34**, 576–585 (1999).
 61. Mohammadi, T. *et al.* The essential peptidoglycan glycosyltransferase MurG forms a complex with proteins involved in lateral envelope growth as well as with proteins involved in cell division in Escherichia coli. *Mol. Microbiol.* **65**, 1106–1121 (2007).
 62. Bisson Filho, A. W. *et al.* Treadmilling by FtsZ filaments drives peptidoglycan synthesis and bacterial cell division. *Science (80-.)*. **355**, 739–743 (2017).
 63. Buddelmeijer, N., Aarsman, M. & Blaauwen, T. den. Immunolabeling of Proteins in situ in Escherichia coli K12 Strains. *Bio-Protocol* **3**, 1–5 (2013).
 64. Van der Ploeg, R. *et al.* Colocalization and interaction between elongasome and divisome during a preparative cell division phase in Escherichia coli. *Mol. Microbiol.* **87**, 1074–1087 (2013).
 65. Pichoff, S. & Lutkenhaus, J. Tethering the Z ring to the membrane through a conserved membrane targeting sequence in FtsA. *Mol. Microbiol.* **55**, 1722–1734

- (2005).
66. Rico, A. I., García-Ovalle, M., Mingorance, J. & Vicente, M. Role of two essential domains of Escherichia coli FtsA in localization and progression of the division ring. *Mol. Microbiol.* **53**, 1359–1371 (2004).
 67. Pichoff, S. & Lutkenhaus, J. Unique and overlapping roles for ZipA and FtsA in septal ring assembly in Escherichia coli. *EMBO J.* **21**, 685–693 (2002).
 68. Taschner, P. E., Huls, P. G., Pas, E. & Woldringh, C. L. Division behavior and shape changes in isogenic ftsZ, ftsQ, ftsA, pbpB, and ftsE cell division mutants of Escherichia coli during temperature shift experiments. *J. Bacteriol.* **170**, 1533–1540 (1988).
 69. Ishino, F. *et al.* New mutations fts-36, lts-33, and ftsW clustered in the mra region of the Escherichia coli chromosome induce thermosensitive cell growth and division. *J. Bacteriol.* **171**, 5523–5530 (1989).
 70. Den Blaauwen, T., Aarsman, M. E. G., Vischer, N. O. E. & Nanninga, N. Penicillin-binding protein PBP2 of Escherichia coli localizes preferentially in the lateral wall and at mid-cell in comparison with the old cell pole. *Mol. Microbiol.* **47**, 539–547 (2003).
 71. White, C. L. & Gober, J. W. MreB: Pilot or passenger of cell wall synthesis? *Trends Microbiol.* **20**, 74–79 (2012).
 72. Moreno, E. *et al.* Surgical treatment of Zenker's diverticulum: Review of our experience. *Gullet* **2**, 19–23 (1992).
 73. Shih, Y. L., Kawagishi, I. & Rothfield, L. The MreB and Min cytoskeletal-like systems play independent roles in prokaryotic polar differentiation. *Mol. Microbiol.* **58**, 917–928 (2005).
 74. Wood, B. W. A. & Gunsalus, I. C. D-Alanine formation; a racemase in Streptococcus faecalis. *J. Biol. Chem.* **190**, 403–416 (1959).
 75. Neuhaus, F. C. The enzymatic synthesis of D-alanyl-D-alanine. I. Purification and properties of D-alanyl-D-alanine synthetase. *J. Biol. Chem.* **237**, 778–786 (1962).
 76. Wang, E., Walsh, C. & Walsh, C. Suicide substrates for the alanine racemase of Escherichia coli. *Biochemistry* **17**, 1313–1321 (1978).
 77. Neuhaus, F. C. & Lynch, J. L. Studies on the inhibition of D-alanyl-D-alanine synthetase by the antibiotic D-cycloserine. *Biochem. Biophys. Res. Commun.* **8**, 377–382 (1972).
 78. Azam, M. A. & Jayaram, U. Inhibitors of alanine racemase enzyme: a review. *J. Enzyme Inhib. Med. Chem.* **6366**, 1–10 (2015).
 79. Prosser, G. a & de Carvalho, L. P. S. Kinetic mechanism and inhibition of Mycobacterium tuberculosis D-alanine:D-alanine ligase by the antibiotic D-cycloserine. *FEBS J.* **280**, 1150–66 (2013).
 80. de Roubin, M. R., Mengin-Lecreulx, D. & van Heijenoort, J. Peptidoglycan biosynthesis in Escherichia coli: variations in the metabolism of alanine and D-alanyl-D-alanine. *J. Gen. Microbiol.* **138 Pt 8**, 1751–7 (1992).
 81. Mengin-lecreulx, D. *et al.* Pool Levels of UDP N-Acetylglucosamine and UDP N-

- Acetylglucosamine-Enolpyruvate in *Escherichia coli* and Correlation with Peptidoglycan Synthesis. *J. Bacteriol.* **154**, 1284–1290 (1983).
82. Liu, B., Persons, L., Lee, L. & de Boer, P. A. J. Roles for both FtsA and the FtsBLQ subcomplex in FtsN-stimulated cell constriction in *Escherichia coli*. *Mol. Microbiol.* **95**, 945–970 (2015).
 83. Chamakura, K. R. *et al.* A viral protein antibiotic inhibits lipid II flippase activity. *Nat. Microbiol.* (2017). doi:10.1038/s41564-017-0023-4
 84. Matsuzawa, H., Hayakawa, K., Sato, T. & Imahori, K. Characterization and genetic analysis of a mutant of *Escherichia coli* K-12 with rounded morphology. *J. Bacteriol.* **115**, 436–442 (1973).
 85. Sieger, B., Schubert, K., Donovan, C. & Bramkamp, M. The lipid II flippase RodA determines morphology and growth in *Corynebacterium glutamicum*. *Mol. Microbiol.* **90**, 966–982 (2013).
 86. Dai, K. & Lutkenhaus, J. *ftsZ* is an essential cell division gene in *Escherichia coli*. *J. Bacteriol.* **173**, 3500–3506 (1991).
 87. Fay, A. & Dworkin, J. *Bacillus subtilis* homologs of MviN (MurJ), the putative *Escherichia coli* lipid II flippase, are not essential for growth. *J. Bacteriol.* **191**, 6020–6028 (2009).
 88. Alexeeva, S., Gadella, T. W. J., Verheul, J., Verhoeven, G. S. & Den Blaauwen, T. Direct interactions of early and late assembling division proteins in *Escherichia coli* cells resolved by FRET. *Mol. Microbiol.* **77**, 384–398 (2010).
 89. Egan, A. J. F. & Vollmer, W. The stoichiometric divisome: A hypothesis. *Front. Microbiol.* **6**, 1–6 (2015).
 90. Rowlett, V. W. & Margolin, W. The Min system and other nucleoid-independent regulators of Z ring positioning. *Front. Microbiol.* **6**, 1–10 (2015).
 91. Ortiz, C., Natale, P., Cueto, L. & Vicente, M. The keepers of the ring: Regulators of FtsZ assembly. *FEMS Microbiol. Rev.* **40**, 57–67 (2015).
 92. Tsang, M. J. & Bernhardt, T. G. Guiding divisome assembly and controlling its activity. *Curr. Opin. Microbiol.* **24**, 60–65 (2015).
 93. Du, S., Pichoff, S. & Lutkenhaus, J. FtsEX acts on FtsA to regulate divisome assembly and activity. *Proc. Natl. Acad. Sci.* 201606656 (2016). doi:10.1073/pnas.1606656113
 94. Gibson, D. G. *et al.* Enzymatic assembly of DNA molecules up to several hundred kilobases. *Nat. Methods* **6**, 343–345 (2009).
 95. Datsenko, K. & Wanner, B. One-step inactivation of chromosomal genes in *Escherichia coli* K-12 using PCR products. *Proc. Nat. Acad. Sci.* **97**1242, 6640–6645 (2000).
 96. Chen, J. C. & Beckwith, J. FtsQ, FtsL and FtsI require FtsK, but not FtsN, for co-localization with FtsZ during *Escherichia coli* cell division. *Molecular Microbiology* **42**, 395–413 (2008).
 97. Nørholm, M. H. H. A mutant Pfu DNA polymerase designed for advanced uracil-

- excision DNA engineering. *BMC Biotechnol.* **10**, 21 (2010).
98. Pastoret, S. *et al.* Functional Analysis of the Cell Division Protein FtsW of *Escherichia coli*. *J. Bacteriol.* **186**, 8370–8379 (2004).
 99. Al-Dabbagh, B. *et al.* Active site mapping of MraY, a member of the polyprenyl-phosphate N-acetylhexosamine 1-phosphate transferase superfamily, catalyzing the first membrane step of peptidoglycan biosynthesis. *Biochemistry* **47**, 8919–8928 (2008).

Supplementary Information

Table S1. Strains and plasmids used in this study.

<i>E.coli</i> strain	Relevant properties	References
LMC500	<i>F araD139 Δ(argF-lac)U169 deoC1 flbB5301 ptsF25 rbsR relA1 rpsL150 lysA1</i>	¹
LMC510	<i>LMC500 FtsI2158 (Ts)</i>	²
LMC512	<i>LMC500 ftsA1882 (Ts)</i>	²
LMC531	<i>LMC500 ftsQ1(Ts)</i>	²
JLB17	<i>F, thr trp his thy ara lac gal xyl mtl rspL tonA ftsW(Ts)</i>	³
LMC1783	<i>BW25113 ΔtolA::kan</i>	⁴
LMC1784	<i>BW25113 Δpal::kan</i>	⁴
LMC3346	<i>BW25113 ΔmrcA::tet</i>	⁵
BCB676	<i>BW25113 ΔmrcB::tet</i>	⁵
LMC2028	<i>aph araD139 Δ (ara-leu)7696 galE15 galK16 D(lac)X74 rpsL hsdR2 urA mcrBΔamiA::cat ΔamiB ΔamiC::kan</i>	⁶
sNM01	<i>LMC500 ΔmurJ::cat pRC7MurJ</i>	This study
XL03	<i>LMC500 ΔmurJ::FRT/pRC7MurJΔKan</i>	This study
XL04	<i>LMC500::cat-P_{murJ}-MurJ</i>	This study
XL05	<i>LMC500::cat-P_{murJ}-mCh-MurJ</i>	This study
XL06	<i>LMC500::cat-P_{trcdwn}-NG-(GGS)₂-MurJ</i>	This study
XL07	<i>LMC500::cat-P_{trcdwn}-mCh-MurJ</i>	This study
XL08	<i>LMC500::FRT-P_{trcdwn}-NG-(GGS)₂-MurJ</i>	This study
XL09	<i>LMC500::FRT-P_{trcdwn}-mCh-MurJ</i>	This study
XL13	<i>ftsW(Ts):: cat-P_{trcdwn}-NG-(GGS)₂-MurJ</i>	This study
XL14	<i>ftsI(Ts):: cat-P_{trcdwn}-NG-(GGS)₂-MurJ</i>	This study
XL15	<i>ftsQ1(Ts):: cat-P_{trcdwn}-NG-(GGS)₂-MurJ</i>	This study
XL17	<i>ftsA12(Ts):: cat-P_{trcdwn}-NG-(GGS)₂-MurJ</i>	This study
XL23	<i>XL08::cat-araC-P_{BAD}-FtsN</i>	This study
XL28	<i>ΔmrcA:: P_{trcdwn}-NG-(GGS)₂-MurJ</i>	This study
XL29	<i>ΔmrcB:: P_{trcdwn}-NG-(GGS)₂-MurJ</i>	This study
XL30	<i>LMC500::araC-P_{BAD}- MurJ</i>	This study
Plasmids		
pRC7MurJKan	<i>pRC7 plasmid expressing MurJ, for complementation assay</i>	⁷
pFLAGMurJΔCys	<i>Plasmid contains functional MurJ cysteine free mutant</i>	⁷

pJC83	<i>pBAD33-ftsN</i>	8
pTHV037	<i>pTRC99A with a weakened promoter $P_{trcdown}$ and a multiple cloning site, pBR322 ori, ampicillin resistance</i>	9
pSAV047	<i>pTHV037-NcoI-mCh-HindIII</i>	9
pSAV057	<i>pTRC99A with a weakened promoter $P_{trcdown}$ and a multiple cloning site, p15A ori, chloramphenicol resistance</i>	9
pNM036	<i>pSAV057-NcoI-mNG-EcoRI-HindIII</i>	This study
pNM037	<i>pSAV047-mCh-EcoRI-MurJ-HindIII</i>	This study
pNM038	<i>pSAV057-mNG-EcoRI-MurJ-HindIII</i>	This study
pXL01	<i>pSAV047-GGS-MurJ</i>	This study
pXL02	<i>pSAV047-(GGS)₂-MurJ</i>	This study
pXL03	<i>pSAV047-(GGS)₃-MurJ</i>	This study
pXL04	<i>pSAV057-mNG-GGS-MurJ</i>	This study
pXL05	<i>pSAV057-mNG-(GGS)₂-MurJ</i>	This study
pXL06	<i>pSAV057-mNG-(GGS)₃-MurJ</i>	This study
pXL09	<i>pTHV037-MurJ</i>	This study
pXL10	<i>pSAV057-MurJ</i>	This study
pXL11	<i>pTHV037-MurJ-GGS-mCh</i>	This study
pXL12	<i>pTHV037-MurJ-(GGS)₂-mCh</i>	This study
pXL13	<i>pTHV037-MurJ-(GGS)₃-mCh</i>	This study
pXL14	<i>pTHV037-MurJ-GGS-mNG</i>	This study
pXL15	<i>pTHV037-MurJ-(GGS)₂-mNG</i>	This study
pXL16	<i>pTHV037-MurJ-(GGS)₃-mNG</i>	This study
pXL17	<i>pSAV057-MurJ-GGS-mCh</i>	This study
pXL18	<i>pSAV057-MurJ-(GGS)₂-mCh</i>	This study
pXL19	<i>pSAV057-MurJ-(GGS)₃-mCh</i>	This study
pXL20	<i>pSAV057-MurJ-GGS-mNG</i>	This study
pXL21	<i>pSAV057-MurJ-(GGS)₂-mNG</i>	This study
pXL22	<i>pSAV057-MurJ-(GGS)₃-mNG</i>	This study
pXL28	<i>pSAV057-NG-(GGS)₂-GlpT</i>	This study
pXL36	<i>pKD3-cat-Pmurj-mNG-(GGS)₂-MurJ</i>	This study
pXL37	<i>pKD3-cat-PmurJ-MC-MurJ</i>	This study
pXL70	<i>pSAV057-mNG-(GGS)₂-MurJR18A</i>	This study
pXL71	<i>pSAV057-mNG-(GGS)₂-MurJR18C</i>	This study
pXL72	<i>pSAV057-mNG-(GGS)₂-MurJD39C</i>	This study
pXL73	<i>pSAV057-mNG-(GGS)₂-MurJD39A</i>	This study
pXL74	<i>pSAV057-mNG-(GGS)₂-MurJCys⁻</i>	This study
pXL79	<i>pSAV057-mNG-(GGS)₂-MurJCys⁻R24C</i>	This study

pXL80	<i>pSAV057-mNG-(GGS)₂-MurJCys⁻R52C</i>	This study
pXL81	<i>pSAV057-mNG-(GGS)₂-MurJCys⁻R270C</i>	This study
pXL82	<i>pSAV057-mNG-(GGS)₂-MurJCys⁻A29C</i>	This study
pXL83	<i>pSAV057-mNG-(GGS)₂-MurJCys⁻N49C</i>	This study
pXL84	<i>pSAV057-mNG-(GGS)₂-MurJCys⁻S263C</i>	This study
pXL85	<i>pSAV057-mNG-(GGS)₂-MurJCys⁻E273C</i>	This study
pXL87	<i>pSAV057-mNG-(GGS)₂-MurJCys⁻R18C</i>	This study
pXL90	<i>pSAV057-mNG-(GGS)₂-MurJCys⁻R24C-R447H</i>	This study
pXL93	<i>pSAV057-mNG-(GGS)₂-MurJCys⁻A29C-R52C</i>	This study

Table S2. Primers used in this study. Restriction sites are underlined, mutations are indicated by lowercase letters.

Primer	Sequence 5'-3'	Purpose
priXL1	GCGCGAATTC <u>CGG</u> AGGATCTGGAGGATCTGGAGGA TCTATGAATTTATTA AAAATCGCTGG	EcoRI-3GGS- MurJ
priXL2	GCGCGAATTC <u>CGG</u> AGGATCTGGAGGATCTATGAATT TATTA AAAATCGCTGG	EcoRI-2GGS- MurJ
priXL3	GCGCGAATTC <u>CGG</u> AGGATCTATGAATTTATTA AAAAT CGCTGG	EcoRI-GGS-MurJ
priXL4	GCGCGCAAGCTTGAATGCATTGTTACACCGTC	HindIII-stop-MurJ
priXL5	GCGCGGATCC <u>GAG</u> AGGATCTGGAGGATCTGGAGGA TCTATGGTGAGCAAGGGCGAGGAG	BamHI-3GGS- mNG/mCh
priXL6	GCGCGGATCC <u>GAG</u> AGGATCTGGAGGATCTATGGTG AGCAAGGGCGAGGAG	BamHI-2GGS- mNG/mCh
priXL7	GCGCGGATCC <u>GAG</u> AGGATCTATGGTGAGCAAGGGC GAGGAG	BamHI-GGS- mNG/mCh
priXL8	GCGCGCAAGCTT ACTTGACAGCTCGTCCATGCC	HindIII-stop- mNG/mCh
priXL17	CGACATTACGGATATGCGCGAAT	MurJ-dele-FA-F
priXL18	GAAAGTATAGGAACTTCGAAGCAGCTCCAGCCTAC ACCGGTGTTCTAATCCAGACCCAC	MurJ-dele-FA-R
priXL19	TTGCAGGCGTTTTGCCCGTGGGTCTGGATTAGAAC ACCGGTGTAGGCTGGAGCTGCTTC	MurJ-dele-F
priXL20	AGATTATCTCCGGCCTGCACTGCAGGCCGGAATG CATTGATGGGAATTAGCCATGGTCC	MurJ-dele-R
priXL21	TAAGGAGGATATTCATATGGACCATGGCTAATTCC CATCAATGCATTCCGGCCTGCAGT	MurJ-dele-BA-F
priXL22	ACGGCAGCCAGTTGCAATGGAT	MurJ-dele-BA-R

priXL45	ATAGGAACTAAGGAGGATATTCATATGGACCCTGT AACATCTGGCGGTAG	GA-Pmurj-F
priXL46	GTTATCCTCCTCGCCCTTGCTCACCATCGGTGTTT TAATCCAGACCCA	GA-Pmurj-R
priXL47	ACGGCTGACATGGGAATTAGCCATGGTCATAAGAG ACAAAGACCCGCGTG	GA-FP-inMurJ-R
priXL48	CATAAGAGACAAAGACCCGCGTG	PCR-inmur-R
priXL49	GACGGTGCCTCATCGACATT	PCR-FA-inYceM
priXL50	ATAGGAACTTCGAAGCAGCTCCAGCCTACACTTAT TCACTCATCGCATCGCGC	PCR-FA-inYceM- R
priXL51	ACCATGGCTAATTCCCATGTCAG	GA-pkd3-F
priXL52	CCATATGAATATCCTCCTTAGTTC	GA-pkd3-R
priXL53	ATGGTGAGCAAGGGCGAGGAG	GA-FP-F
priXL54	GTGTGGCTGGAGCTGCTTC	PCR-pkd3-F
priXL77	ATAGGAACTAAGGAGGATATTCATATGGACAGCTT ATCATCGACTGCACG	GA-Ptrc-thsa-F
priXL138	GATGCGTAATGAAGTACAGACC	inFtsN-R
priXL139	GAATAGGAACTAAGGAGGATATTCATATGGTTATG ACAACCTTGACGGCTACATC	In-araC-Pbad-F
priXL140	GACGCAATTTTGTGATCCGCC	FA-FtsN-F
priXL141	TATAGGAACTTCGAAGCAGCTCCAGCCTACACTCA GCCCCGCATGTTACTTAAG	FA-FtsN-R
priXL148	CGTGCGAAGC <u>CtAGg</u> ACACaCGAAAACATGGT	R18C-AvrII-R
priXL149	ACCATGTTTTCGtGTGT <u>cCTa</u> GGCTTCGCACG	R18C-AvrII-F
priXL150	TGGCAAC <u>Ctg</u> CGCCTTTTTCGTCGCTTTTT <u>AAgCTTC</u> CTAACTTG	D39C-HindIII-F
priXL151	CAAGTTAGG <u>AAgCTT</u> AAAAGCGACGAAAAGGCGc aGGTTGCCATCC	D39C-HindIII-R
priXL152	ATGTTTTCGgcTGT <u>cCTa</u> GGCTTCGCA	MurJR18A-F
priXL153	TGCGAAGCC <u>tAGc</u> ACAgcCGAAAACAT	MurJR18A-R
priXL154	GGGATGGCAACCGcgGCCTTTTTCGTC	MurJD39A-F
priXL155	GACGAAAAAGGCCgcGGTTGCCATCCC	MurJD39A-R
priXL156	ATGAATTTATTAATAATCGCTGGCCGC	MurJ-deple-F
priXL157	GCTGACGGCGGCCAGCGATTTTAATAAATTCATTT TTTATAACCTCCTTAGAGCTCGA	MurJ-deple-Pbad- R
priXL158	CACGAGACGCAATTGT <u>Ctg</u> CAGAATCTTTGG	MurJA29C-PstI-F
priXL159	CCTGCGCCAAAGATT <u>CTGca</u> GACAATTGCGTC	MurJA29C-PstI-R
priXL173	CTTGGCTTCGAtGcGACGCAATTGTCTG	MurJR24C-F
priXL174	CGACAATTGCGTCgCaTGCGAAGCCAAG	MurJR24C-R
priXL175	CTAACTTGTTAtGCCGaATaTTTGCCGAAGG	MurJR52C-F

Chapter 2

priXL176	CCTTCGGCAAAATtCGGCaTAACAAGTTAG	MurJR52C-R
priXL177	ACGCCGACTGCTTAATGGAaTTcCCGTCCGGTG	MurJR270C-F
priXL178	GGACGGgAAAtTCCATTAAGCaGTCGGCGTAATAC	MurJR270C-R
priXL181		MurJN49C-
	CGTCGCTTTTAAgCTTCCTtgCTTGTTAC	HindIII-F
priXL182		MurJN49C-
	GTAACAAGcaAGGAAGcTTAAAAGCGACG	HindIII -R
priXL183		MurJS263C-
	GCTTCGGaTCcGTGTgTTGGATGTATTA	BamHI-F
priXL184		MurJS263C-
	TAATACATCCAACACACgGAtCCGGAAGC	BamHI -R
priXL185	CCGCTTAATGtgtTTTCCGTCCGGT	MurJE273C-F
priXL186	ACCGGACGGAAAacaCATTAAAGCGG	MurJE273C-R

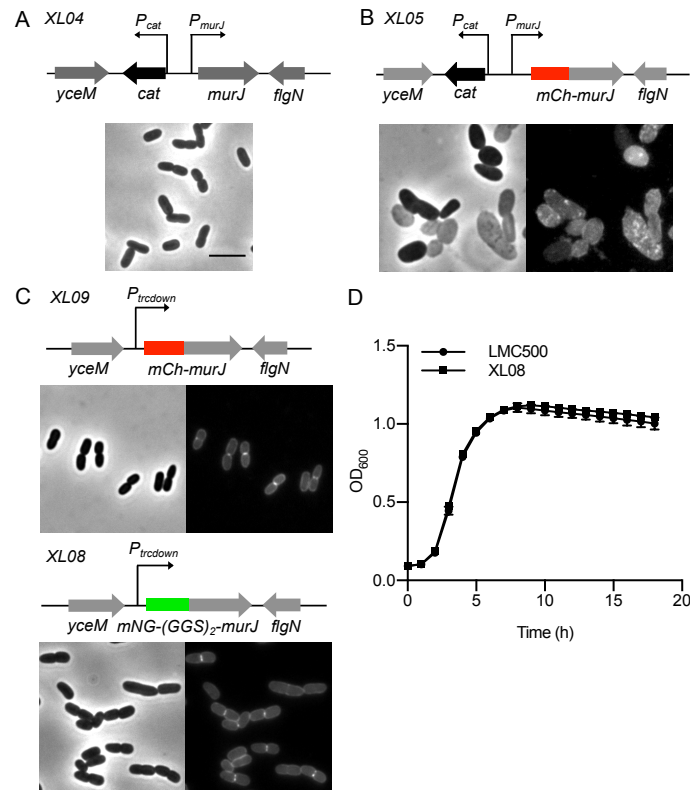


Figure S1. Construction of MurJ chromosomal fusions. (A) Genomic structure and morphology of strain XL04. MurJ expression is not interrupted by the insertion of chloramphenicol cassette in between *yceM* and the putative promoter of *murJ*, confirming the activity of the *murJ* promoter. (B) Genomic structure and morphology of strain XL05. Chromosomal mCh-MurJ was constructed under control of the native *murJ* promoter, which resulted in insufficient MurJ production. (C) Genomic structure and localization of MurJ chromosomal fusion strains XL08 and XL09. MurJ was fused with mCh or mNG under control of the $p_{trcdown}$ promoter, which allowed enough MurJ to be produced and give a wild type phenotype. (D) XL08 and wild type LMC500 strain grow in LB medium at 37 °C show very similar growth patterns. The scale bar equals 5 μ m.

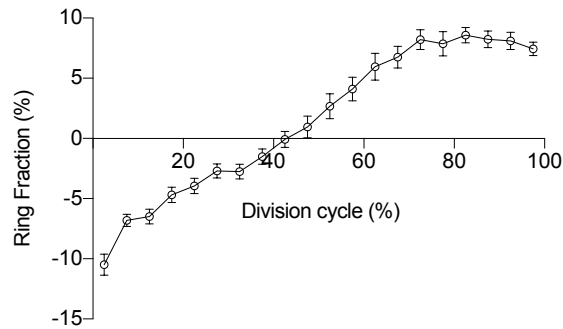


Figure S2. Septal proportion of MurJ during the cell division cycle. The MurJ chromosomal fusion strain XL08 was grown to steady state in Gb1 medium at 28 °C. The total number of cells is (> 1200) divided in age classes of 5%, the error bars indicate the 95% confidence interval. Midcell proportion (Ringfraction) of MurJ protein was calculated by dividing the FCplus (the extra amount of fluorescence in a rectangle of 0.4 μm times the width of the cell, at mid cell in comparison to the fluorescence in the rest of the cell) by the total fluorescence of each analyzed cell, and as a function of the division cycle time in percentages (18). The negative value indicates absence of mid cell in the beginning of the cell cycle.

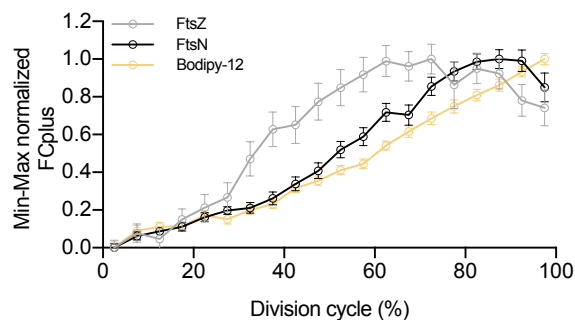


Figure S3. The quantified signal (FCplus) of midcell fluorescence of immunolabelled or Bodipy 12-stained XL08 cells. Cells were grown to steady state in Gb1 medium at 28°C. The total number of cells (>1200) is divided in age classes of 5%, the error bars indicate the 95% confidence interval. The extra amount of fluorescence in a rectangle of 0.4 μm times the width of the cell, at mid cell in comparison to the fluorescence in the rest of the cell (FCplus) is plotted as a function of the division cycle time in percentages (18). For concentration-independent comparison the data are normalized between their minimum and maximum values.

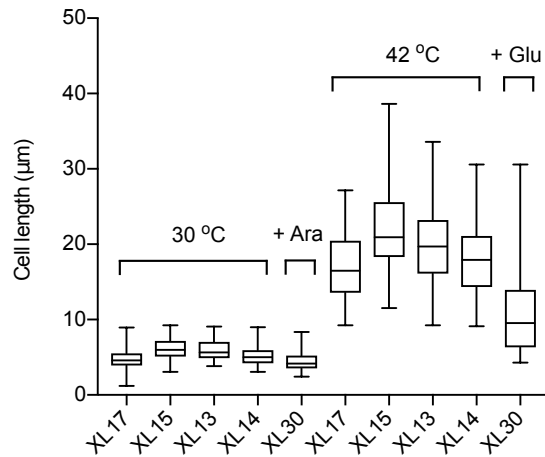


Figure S4. Cell length measurements after depletion or inactivation of divisome components. Depletion of divisome proteins FtsA, FtsQ, FtsW, FtsI and FtsN were performed as mentioned in supplementary data. More than 200 cells were quantified for each culture. Error bars represent 5-95% percentiles.

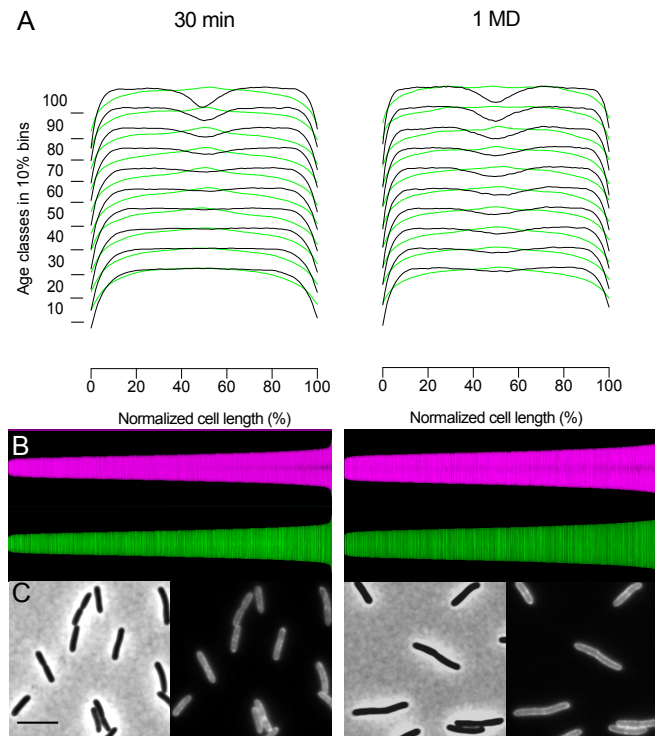


Figure S5. mNG-MurJ midcell localization in XL08 growing in Gb1 at 28 °C is strongly reduced at 30 min and absence at 1 MD after adding 1 mg.L⁻¹ aztreonam. (A) The diameter (black lines) and fluorescence (green lines) profiles as function of normalized cell length are shown in 10 % age class bins. (B) Map of diameter profiles (magenta) and fluorescence profiles (green). Cells are plotted sorted by increasing cell length from left to right. (C) Phase contrast image and the corresponding fluorescence images of cells treated with aztreonam for the 30 min and 1 MD time points. Scale bar equals 5 μm. More than 1200 cells were included.

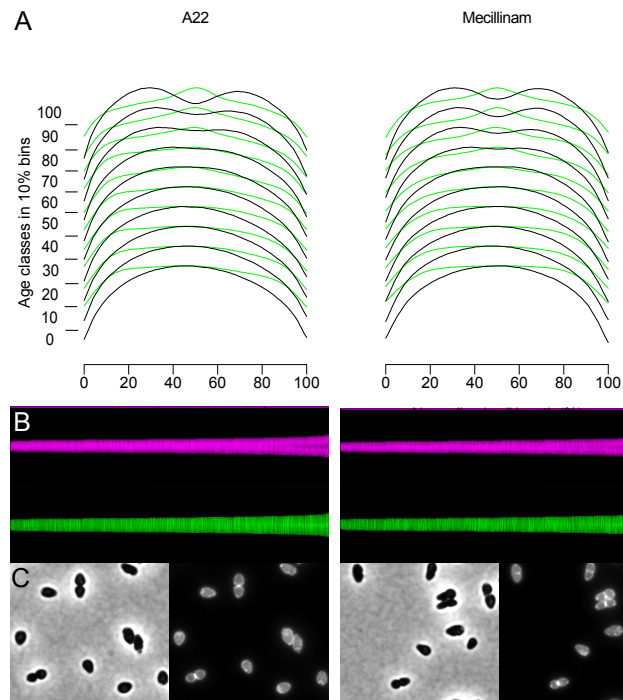


Figure S6. MreB inhibitor A22 and PBP2 inhibitor mecillinam do not influence MurJ midcell localization. In Gb1 at 28 °C, steady state growing strain XL08 was treated with 5 mg.L⁻¹ of A22 or 2 mg.L⁻¹ of mecillinam for 2 MD. (A) The diameter (black lines) and fluorescence (green lines) profiles along cell length are shown in 10 % age class bins. (B) Maps of diameter profiles (magenta) and fluorescence profiles (green). Cells are plotted by cell length, ascending from left to right. (C) Phase contrast image (left) and the corresponding fluorescence image (right) of antibiotic treated cells. Scale bar equals 5 μ m. More than 1200 cells were included for each experiment.

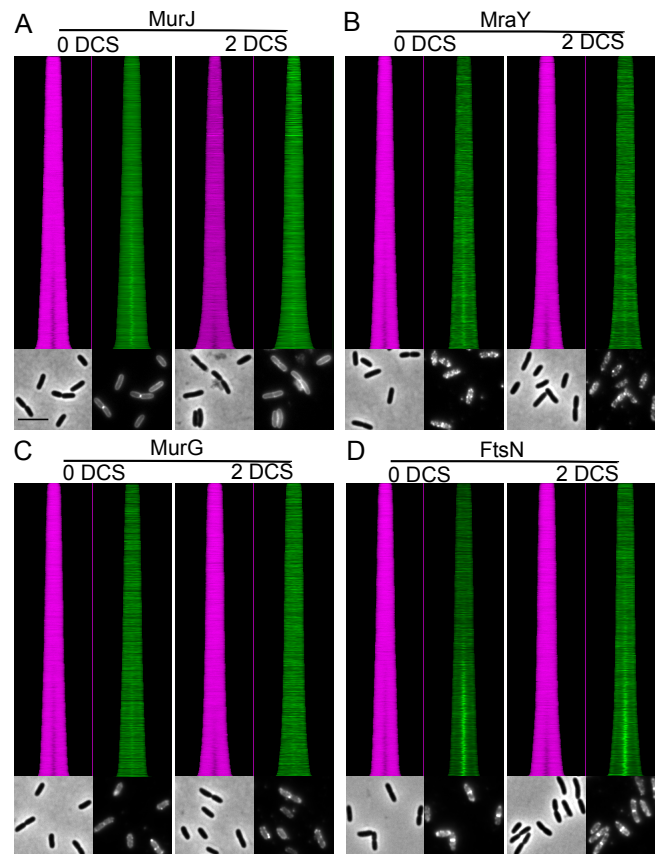


Figure S7. Localization of MurJ, MraY, MurG and FtsN in the absence and presence of D-cycloserine. In Gb1 medium at 28 °C, steady state growing strain XL08 was treated with or without 2 $\mu\text{g}\cdot\text{L}^{-1}$ of D-cycloserine for 30 min. MurJ localization was determined in living cells. After fixation with FAGA, the rest of cells were immunolabeled with antibodies against MraY, MurG and FtsN, respectively. Maps of according to cell length sorted profiles and microscopy images of each protein are shown. For each growth condition, left: map profile of diameters and phase contrast image, right: map profiles of fluorescence and fluorescence image. More than 1200 cells were included for each experiment. (A) MurJ map profiles and images. (B) MraY map profiles and images. (C) MurG map profiles and images. (D) FtsN map profiles and images. Scale bar equals 5 μm .

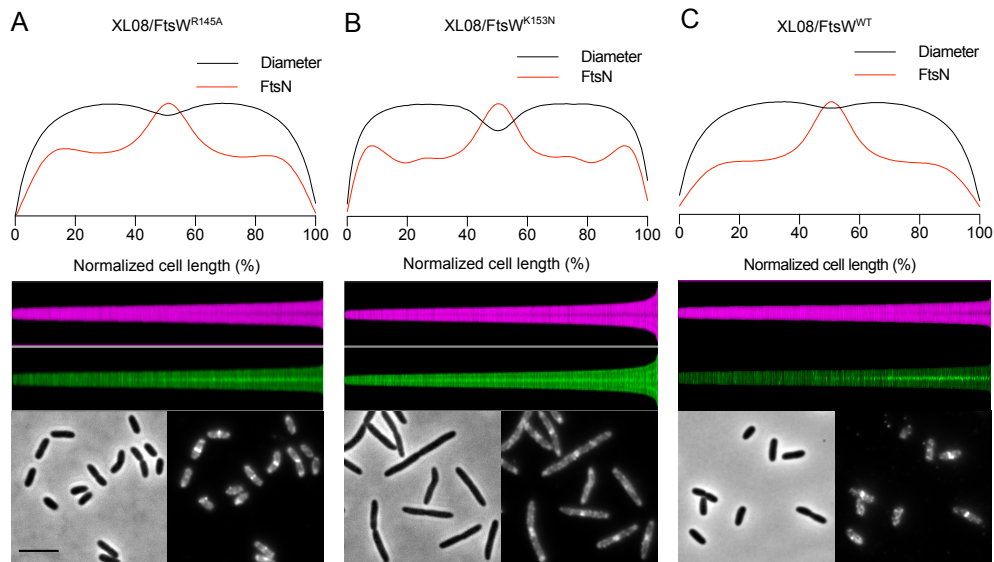


Figure S8. Expression of non-functional FtsW mutants does not influence divisome assembly. XL08 expressing mutant FtsW R145A, FtsW K153N or wild type FtsW was grown in Gb1 minimal medium to steady state at 28 °C. IPTG (20 μ M) was used to induce expression of the FtsW mutants from plasmids. The presence of the divisome was confirmed by immunolabeling of FtsN after fixation. (A) Localization of FtsN after expression of FtsW R145A. (B) Localization of FtsN after expression of FtsWK153N. (C) Localization of FtsN after expression of wild type FtsW. For each part: top, average localization profiles plotted along normalized cell length ($n \geq 1200$ cells). Black lines and red lines indicate cell diameter and FtsN localization, respectively. Middle, map of profiles of cell diameter and FtsN localization sorted by ascending cell length. Bottom, phase contrast and fluorescence microscopy images. Scale bar equals 5 μ m.

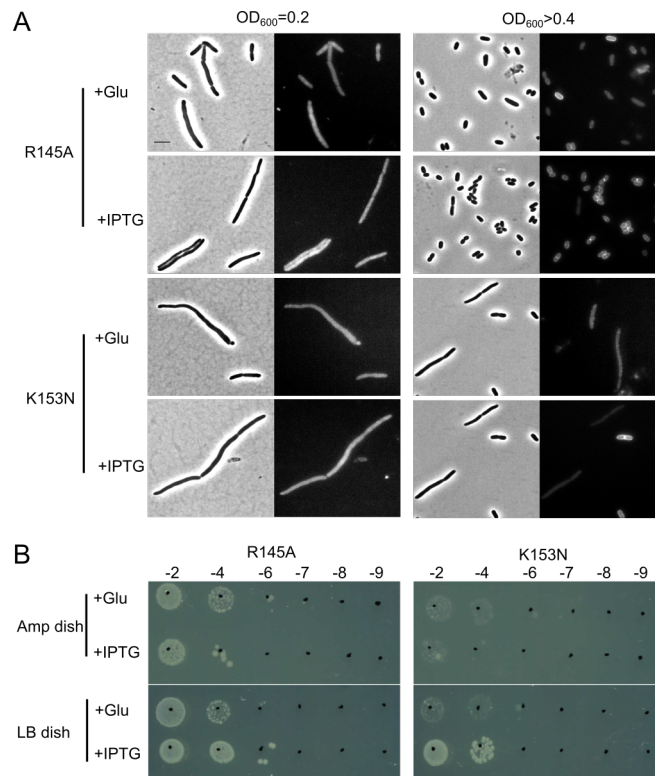


Figure S9. MurJ localization is restored when non-functional FtsW mutants are depleted. XL08 strain expressing the ampicillin plasmid that contains FtsW mutant R145A or K153N was grown in ampicillin-LB rich medium at 37 °C. (A) MurJ localization was determined at the early exponential phase ($OD_{600} = 0.2$) and late exponential phase ($OD_{600} > 0.4$), in the presence of either 0.5% glucose or 20 μ M IPTG to suppress or induce expression, respectively. (B) Spot assay of strain XL08 that expressed the FtsW mutants. Cells from late exponential phase were diluted into fresh LB medium to the same OD, and subsequently diluted to the concentrations as indicated in the figure. Ten μ L aliquots of each dilution was spotted on LB-ampicillin and LB plates, and incubated at 37°C overnight. Less growth is observed on the Amp LB plate comparing to LB only indicates the loss of FtsW mutant plasmids, especially when induced with IPTG because of the toxicity of these mutants. Scale bar equals 5 μ m.

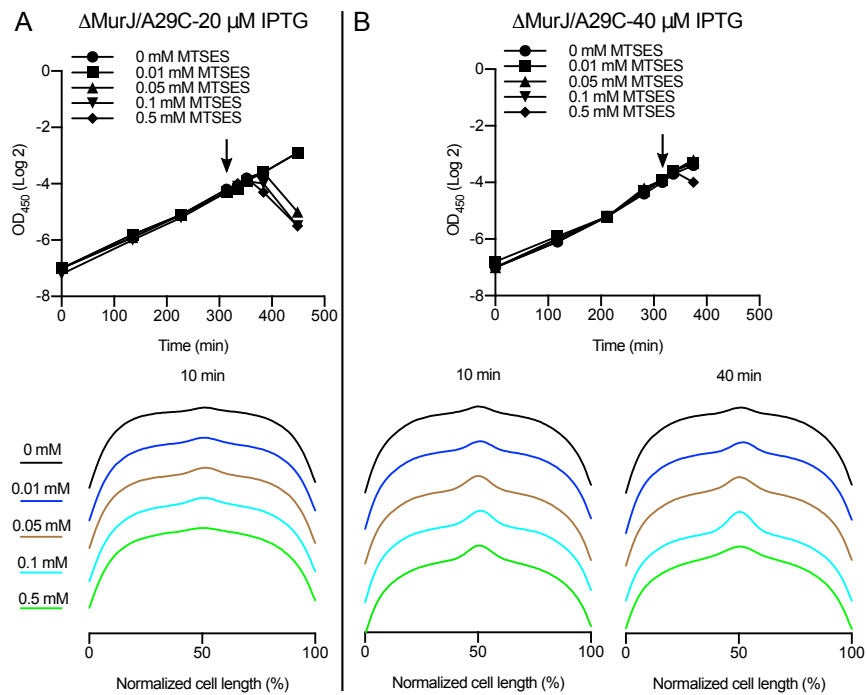


Figure S10. Gradient assay to optimize the MTSES concentration and IPTG induction for the MurJ A29C mutant. Strain XL03 expressing mutant A29C was grown in Gb1 medium to steady state, and induced with IPTG and treated with indicated concentrations of MTSES. MurJ localization was determined at 10 and 40 min after MTSES addition. The normalized average fluorescence intensity of MurJ localization was plotted along the normalized cell length for each condition. More than 1200 cells were included for each experiment. (A) Mutant expression was induced with 20 μ M IPTG for 2MDs. (B) mutant expression was induced with 40 μ M IPTG for 2 MDs.

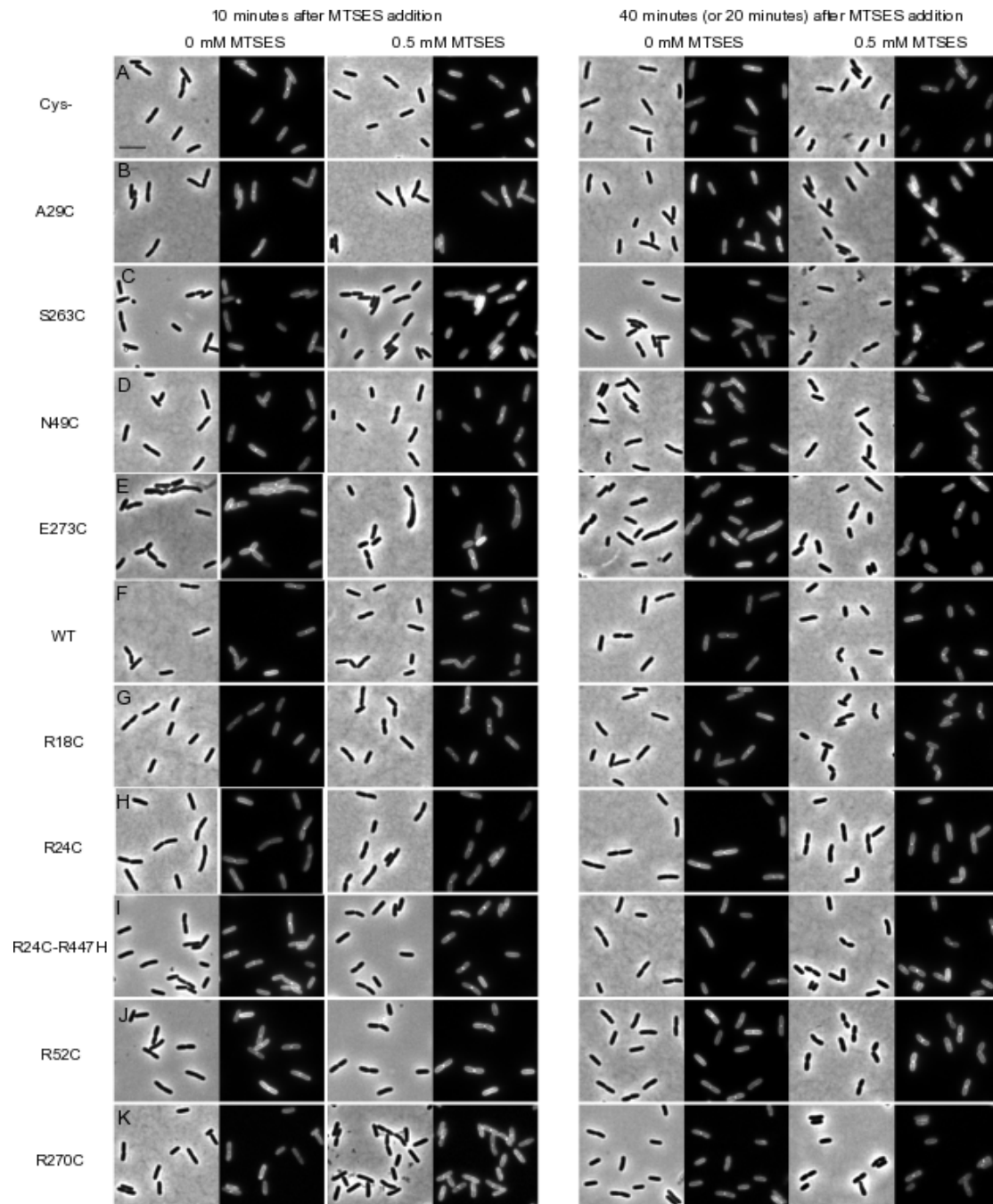


Figure S11. Microscopy images of the morphology and localization of MurJ mutants in the presence of MTSES. Images were taken from the in Gb1 steady state growing cells at 10 min and 40 min (20 min for mutant S263C) after MTSES addition. (A-F) Functional mNG-MurJ mutants were expressed from plasmid in the XL03 MurJ deletion strain. (G-K) Non-functional mutants were expressed in the LMC500 wild type strain. Scale bar equals 5 μ m.

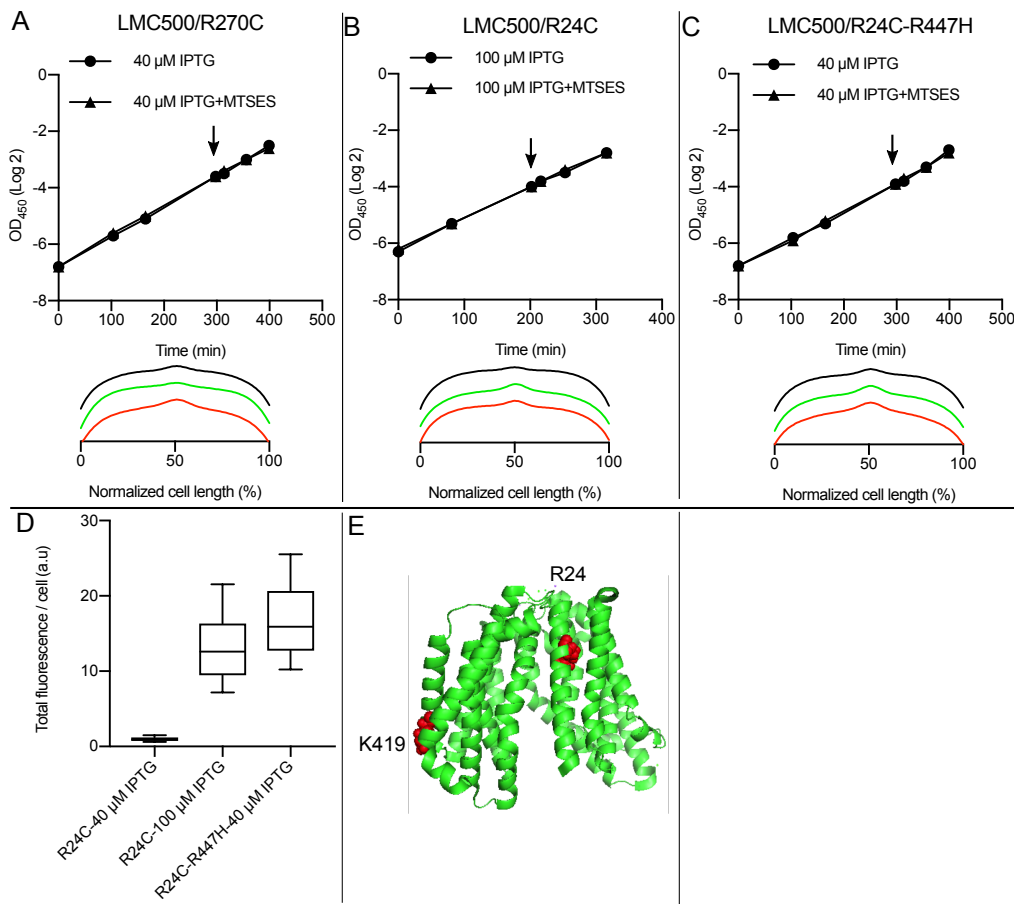


Figure S12. Localization of MurJ non-functional single cysteine mutants is not sensitive to MTSES. Strains expressing each mutant were grown to steady state in Gb1 medium at 28 °C. After induction of the mutant protein expression with IPTG for 2 MDs, cells were treated without and with 0.5 mM MTSES. Localization was determined after 10 min and 40 min of growth in the presence of MTSES. Black lines indicate the MurJ localization in the absence of MTSES, green and red lines indicate the MurJ localization at 10 and 40 min in the presence of MTSES, respectively. (A-C) Growth curves and localization of MurJ mutants R270C, R24C, and R24C-R447H in the presence and absence of MTSES. Black arrows indicate the addition of MTSES. (D) The extra spontaneous suppressor mutation R447H restores the fluorescence of MurJ mutant R24C. Error bars represent 5-95% percentiles (E). Position of the residues R24 and K419 in the structure of MurJ_{TA} that correspond to the mutated residues R24 and R447 in *E. coli* MurJ. The structure of MurJ_{TA} was generated using PyMol and [PDB 5T77](#) from previous study¹⁰.

WZK_HP	1	-----MAKKKHKIPTLKYFLRSLKQIYYRLITFEKEKMIFLLVLMVFFSSFVE	47
AMJ_BS	1	-----VHVITTOVLE-----IFCFLLL	17
YTGP_SP	1	MSTEKKQLTQEELMVOGAAWSTAGNFISRLLG-VLYIIPWYIWMQYATQANALFNMGYN	59
MURJ_BS	1	MSSK-----LLRGTFFVLTGLTYISRLG-MVYLIPFSIMVGA---TGGALFQYGYN	47
MURJ_TA	1	MS-----ILFSSILFSIATFFSRILG-LFRDVLFAKYFGV-SYELDAYFTIAMF	47
MURJ_EC	1	MN-----LLKSLAAVSSMTMESRVLG-PA ^{red} DAI ^{red} VAR ^{red} IFGA-GMAT ^{red} AF ^{red} VAFKL	47
WZK_HP	48	VMSLTLMPFITLASDPSRA ^{red} DDDKDWKVMVYD--FFHFSPPVRLMYFFSFCLVGLVYLF ^{red} FRMF	105
AMJ_BS	18	IHSIETLAYATRLSGARV ^{red} G-----FIASALSFLFNVMVIVSRMSNMVQOP	61
YTGP_SP	60	VYAYFLLISTTGLNVAIAKQVAKYNSMGQTEHSYQLERS ^{red} TLKMLGLGLFSAI ^{red} MYLGSP	129
MURJ_BS	48	QYTLFLNIATMGPPAAVSKFVSKYNSKGDYETSRKMLKAGMSVMLVTGMTAFFL ^{red} LYLSAP	107
MURJ_TA	48	PF ^{red} FLR ^{red} KV ^{red} FE ^{red} GEGAMSSAFVPL--YSEKSGEEKDKFLSSVINGFSLI ^{red} LLALVILSYFFPEL	104
MURJ_EC	48	<u><u>PNLLR^{red}RI^{red}FAEGAFSQA^{red}VFV^{red}ILAE^{red}YKSKQGEDATRV^{red}FVS^{red}YVSG^{red}LLTLALAV^{red}TVAG^{red}MLA^{red}AP</u></u>	107
WZK_HP	106	YGVFFTYLRGRFSNKKAYQIKQQLFLQHIKNNYLSH ^{red} LNNH ^{red} LDL ^{red} SRD ^{red} I ^{red} IN ^{red} KAEGMFMSFN	165
AMJ_BS	62	FTGHLIDDAGKNA-----LAI ^{red} VGE ^{red} QER-----	83
YTGP_SP	130	LFASLS-G-DDDT-----LVPI ^{red} MHSLSLAV ^{red} FE ^{red} PPV--MSVIR ^{red} CF ^{red} QH ^{red} NN--IKPY	164
MURJ_BS	108	MFAEISLG-KDNNCLTIDHVVYVIRMVSLALLV ^{red} VPI--MSLVRG ^{red} FFOG ^{red} HOM--MGPT	160
MURJ_TA	105	IINLE--GAGSSHE ^{red} TKILAKKLL ^{red} LITSPSYFIFL--WAI ^{red} SYSL ^{red} NTN ^{red} KK--FFWP	154
MURJ_EC	108	WVIMV ^{red} TAP-G ^{red} FADTADK ^{red} FAL ^{red} TSQL ^{red} LKIT ^{red} TPPY ^{red} LL ^{red} LSH--ASL ^{red} VGA ^{red} IL ^{red} NT ^{red} WR--ESIP	160
WZK_HP	166	<u><u>AF^{red}LSL^{red}TE^{red}IV^{red}IV^{red}FE-----FYSTL^{red}L^{red}TN^{red}WK^{red}IL^{red}V-FT^{red}L^{red}AL^{red}Q^{red}IFF---</u></u>	205
AMJ_BS	84	-----FLI ^{red} EG ^{red} TV ^{red} G-----TIL ^{red} G ^{red} IT ^{red} L---	99
YTGP_SP	165	AV ^{red} SOIAE ^{red} QL ^{red} IR ^{red} V ^{red} IM ^{red} LL ^{red} T ^{red} FF ^{red} IM ^{red} KL ^{red} GS ^{red} GD ^{red} YASAV ^{red} TQST ^{red} FA ^{red} PI ^{red} GM ^{red} VAS ^{red} MG ^{red} V ^{red} LY ^{red} YLW--K	222
MURJ_BS	161	AV ^{red} SOV ^{red} VEQ ^{red} IV ^{red} RI ^{red} IF ^{red} LESAT ^{red} FL ^{red} IL ^{red} KV ^{red} FN ^{red} GGL ^{red} VIA ^{red} VGYAT ^{red} PAAL ^{red} IG ^{red} AG ^{red} GL ^{red} V ^{red} VL--Y ^{red} Y ^{red} WN ^{red} KR	219
MURJ_TA	155	AL ^{red} FP ^{red} SI ^{red} NI ^{red} TI ^{red} IG ^{red} TFL ^{red} ST ^{red} KY-----GI ^{red} IS ^{red} PT ^{red} IG ^{red} FL ^{red} IG-----SIL ^{red} MF ^{red} FS---	194
MURJ_EC	161	<u><u>AF^{red}APT^{red}IL^{red}NI^{red}SI^{red}MG^{red}AL^{red}FA^{red}APY-----FN^{red}PPV^{red}IL^{red}AL^{red}AW^{red}AV^{red}TV^{red}G-----GV^{red}L^{red}Q^{red}LV^{red}Y---Q</u></u>	204
WZK_HP	206	--IVKKV ^{red} TVL ^{red} IKK ^{red} KGEMAA ^{red} Ks-KA ^{red} Q ^{red} TL ^{red} KV ^{red} SK ^{red} FFS-----NFK ^{red} IT ^{red} KL ^{red} KN ^{red} HEEA ^{red} HKL	254
AMJ_BS	100	-----LPS ^{red} FVA ^{red} LES ^{red} RA ^{red} I ^{red} HL ^{red} AGG ^{red} GS ^{red} V ^{red} Q ^{red} VF-----	125
YTGP_SP	223	QGL ^{red} LAAL ^{red} FSK ^{red} PD ^{red} HT ^{red} VS ^{red} ID ^{red} IK ^{red} GL ^{red} LE ^{red} TL ^{red} KES ^{red} IF ^{red} IV-----TGS ^{red} AI ^{red} QAF ^{red} OL ^{red} D ^{red} Q ^{red} W ^{red} FV ^{red} NTM	277
MURJ_BS	220	KGSL ^{red} LAMP ^{red} NT ^{red} GPT ^{red} ANLS ^{red} YKKM ^{red} FFEL ^{red} FSYA ^{red} APY ^{red} VF--VGL ^{red} AI ^{red} PL ^{red} Y ^{red} NY ^{red} ID ^{red} NT ^{red} FN ^{red} KAM	274
MURJ_TA	195	-----I ^{red} IKS ^{red} I ^{red} KK ^{red} Y ^{red} FT ^{red} IKH-PP ^{red} H ^{red} KL ^{red} FP ^{red} PT ^{red} M-----TM ^{red} V ^{red} SO ^{red} INT ^{red} V ^{red} VD ^{red} MN---	237
MURJ_EC	205	<u><u>L^{red}PL^{red}KK^{red}IG^{red}ML^{red}V^{red}LP^{red}RI^{red}N^{red}F^{red}HD^{red}AG-AM^{red}R^{red}V^{red}V^{red}K^{red}OM^{red}GA^{red}IL-----G^{red}V^{red}S^{red}Q^{red}IS^{red}L^{red}I^{red}INT^{red}I-----</u></u>	252
WZK_HP	255	----FGENS ^{red} RKA ^{red} HD ^{red} TE ^{red} I ^{red} Y ^{red} ST----LQ ^{red} V ^{red} V ^{red} PR ^{red} YS ^{red} IE ^{red} TV ^{red} GF ^{red} SLL ^{red} L ^{red} AV ^{red} AY ^{red} IL ^{red} F ^{red} KY ^{red} GE ^{red} ARMV	305
AMJ_BS	126	----RK ^{red} GF ^{red} SK ^{red} Q ^{red} GF ^{red} KNAL ^{red} SY ^{red} LR-----L ^{red} PS ^{red} IS ^{red} Y ^{red} -V ^{red} KG ^{red} FM ^{red} RL ^{red} IP ^{red} KRL-----	161
YTGP_SP	278	TL--PT ^{red} D ^{red} YS ^{red} RS ^{red} QL ^{red} LV ^{red} LF ^{red} GY ^{red} FNAN ^{red} PA ^{red} K ^{red} IT ^{red} MV ^{red} L-IA ^{red} V-AAS ^{red} IG ^{red} V ^{red} GT ^{red} ALL ^{red} TEN ^{red} Y ^{red} V ^{red} KK ^{red} DM ^{red} AAA	333
MURJ_BS	275	IEAG ^{red} HQA ^{red} IS ^{red} Q ^{red} MD ^{red} LAIL ^{red} TV ^{red} VO---KL ^{red} VM ^{red} IP-VSL-ATA ^{red} F ^{red} GL ^{red} T ^{red} L ^{red} PT ^{red} TES ^{red} TS ^{red} GN ^{red} Y ^{red} KL	328
MURJ_TA	238	----V ^{red} VS ^{red} F ^{red} Y ^{red} D ^{red} K ^{red} GS ^{red} IS ^{red} YL ^{red} Q ^{red} VAS---RF ^{red} Y ^{red} LL ^{red} P ^{red} Y ^{red} GLF-AV ^{red} SV ^{red} TV ^{red} VL ^{red} SK ^{red} IS---N ^{red} DR ^{red} KN ^{red} L	283
MURJ_EC	253	----FA ^{red} S ^{red} FL ^{red} AS ^{red} GS ^{red} V ^{red} W ^{red} MY ^{red} Y ^{red} AD---R ^{red} IME ^{red} FP ^{red} SG ^{red} VL-GVA ^{red} L ^{red} GT ^{red} IL ^{red} LS ^{red} LS ^{red} KS ^{red} FAS ^{red} GN ^{red} H ^{red} DEY	303
WZK_HP	306	LPT ^{red} IS-MYAL ^{red} AL ^{red} Y ^{red} RI ^{red} L ^{red} PS ^{red} VT ^{red} GV ^{red} IS ^{red} Y ^{red} NE ^{red} IAY ^{red} N ^{red} QL ^{red} AT ^{red} N ^{red} V ^{red} E ^{red} KS ^{red} LS ^{red} K ^{red} TIVE ^{red} ED ^{red} L ^{red} V ^{red} PL ^{red} DF ^{red} NEK	364
AMJ_BS	162	-----F ^{red} VIN ^{red} ML ^{red} ITS ^{red} Y ^{red} TIG ^{red} VL ^{red} SA-LY-----AG ^{red} LL ^{red} AP ^{red} ERS ^{red} TA--VM ^{red} AS ^{red} GL ^{red} TV	202
YTGP_SP	334	ARL ^{red} I ^{red} NN ^{red} TE ^{red} ML ^{red} VM ^{red} ELL ^{red} PAL ^{red} TGAI ^{red} ILAR ^{red} PLY-----SV ^{red} FY ^{red} GASE--E--RA ^{red} I ^{red} HL ^{red} VA	380
MURJ_BS	329	NQ ^{red} IQ ^{red} NOT ^{red} Q ^{red} TIL ^{red} FLI ^{red} IPAV ^{red} GIS ^{red} LL ^{red} SG ^{red} PTY-----TF ^{red} FY ^{red} GES ^{red} SL ^{red} HP ^{red} E--IG ^{red} AN ^{red} IL ^{red} W	378
MURJ_TA	284	NY ^{red} HL ^{red} ND ^{red} ALK ^{red} T ^{red} FL ^{red} FT ^{red} IL ^{red} PS ^{red} MV ^{red} GL ^{red} IF ^{red} LS ^{red} TP ^{red} II-----RF ^{red} FY ^{red} EH ^{red} GA ^{red} FT ^{red} SK ^{red} TL ^{red} TS ^{red} K ^{red} IL ^{red} IA	335
MURJ_EC	304	<u><u>N^{red}RL^{red}MD^{red}W^{red}CL^{red}RL^{red}C^{red}FL^{red}AL^{red}PSA^{red}VAL^{red}GL^{red}SC^{red}PLT-----VS^{red}L^{red}E^{red}OY^{red}CK^{red}FT^{red}AP^{red}D^{red}AL^{red}M^{red}TORAL^{red}IA</u></u>	356
WZK_HP	365	IT ^{red} LQ ^{red} NIS ^{red} FAY ^{red} KS ^{red} K ^{red} HP ^{red} V ^{red} L ^{red} KN ^{red} FL ^{red} NT ^{red} IQ ^{red} G ^{red} Q ^{red} K ^{red} IAL ^{red} I ^{red} GH ^{red} SG ^{red} CG ^{red} KS ^{red} T ^{red} LAD ^{red} I ^{red} IM ^{red} GL ^{red} TY ^{red} PK ^{red} SGE ^{red} IFI	424
AMJ_BS	203	IA ^{red} TML ^{red} LAI ^{red} FV--DP ^{red} K ^{red} V ^{red} SL ^{red} ADD ^{red} VAK ^{red} G ^{red} K ^{red} RS ^{red} Y ^{red} YL ^{red} KWT--SV ^{red} TM ^{red} VT ^{red} S-----RV	245
YTGP_SP	381	VLF ^{red} Q ^{red} TLL ^{red} LAL--Y ^{red} TL ^{red} FS ^{red} P ^{red} ML ^{red} QAL ^{red} FN ^{red} KAI ^{red} Y ^{red} FAY ^{red} G---L ^{red} IL ^{red} KL ^{red} V ^{red} L ^{red} Q ^{red} IP ^{red} L--Y ^{red} LL ^{red} LHA	431
MURJ_BS	379	YSP ^{red} VA ^{red} IL ^{red} FS ^{red} T--FT ^{red} Y ^{red} NA ^{red} AIL ^{red} Q ^{red} GN ^{red} K ^{red} FA ^{red} V ^{red} SV ^{red} L ^{red} VIG--V ^{red} V ^{red} IK ^{red} L ^{red} V ^{red} LN ^{red} V ^{red} PL--IK ^{red} LM ^{red} QA	429
MURJ_TA	336	Y ^{red} TL ^{red} GL ^{red} LP ^{red} FY ^{red} CI--Y ^{red} ST ^{red} IS ^{red} RS ^{red} Y ^{red} HA ^{red} TK ^{red} N ^{red} KT ^{red} PP ^{red} IAAT ^{red} IV ^{red} SL ^{red} SN ^{red} I ^{red} LD ^{red} IF ^{red} GL ^{red} KY--G ^{red} PT--	388
MURJ_EC	357	<u><u>Y^{red}SV^{red}GL^{red}IG^{red}LIV--VK^{red}V^{red}LAP^{red}GE^{red}Y^{red}SR^{red}Q^{red}IK^{red}TP^{red}V^{red}KIA^{red}IVT---L^{red}IT^{red}TO^{red}LM^{red}N^{red}LA^{red}F--IG^{red}PL^{red}KH</u></u>	407
WZK_HP	425	DN ^{red} TLL ^{red} TS ^{red} EN ^{red} RR ^{red} SR ^{red} WK ^{red} K ^{red} IGY ^{red} IP ^{red} Q ^{red} NI ^{red} Y ^{red} LD ^{red} GT ^{red} V ^{red} GD ^{red} N ^{red} IF ^{red} AG ^{red} SA ^{red} ID ^{red} E ^{red} K ^{red} RL ^{red} IK ^{red} V ^{red} CK ^{red} MA ^{red} H ^{red} I ^{red} Y ^{red} DF ^{red} LC	484
AMJ_BS	246	AG ^{red} TLLAQ-----LM ^{red} F ^{red} IP ^{red} GAY ^{red} Y ^{red} IA ^{red} WL ^{red} TK-----	267
YTGP_SP	432	Y ^{red} G ^{red} PL ^{red} LAT ^{red} T-----I ^{red} AL ^{red} V ^{red} PI ^{red} Y ^{red} LM ^{red} Y ^{red} RR ^{red} LY ^{red} QVT--HF ^{red} NR ^{red} KL ^{red} Q ^{red} RL ^{red} LL ^{red} TL ^{red} ET ^{red} LLM	473
MURJ_BS	430	DGAILATA-----L ^{red} GY ^{red} IAS ^{red} LL ^{red} Y ^{red} GE ^{red} IM ^{red} IK ^{red} RHA--G ^{red} SY ^{red} K ^{red} IL ^{red} V ^{red} K ^{red} RT ^{red} V ^{red} LM ^{red} V ^{red} LSA ^{red} IM	476
MURJ_TA	389	-GVALATS-----I ^{red} AG ^{red} I ^{red} GV ^{red} LY ^{red} LF ^{red} SVK-----TF ^{red} PI ^{red} K ^{red} DF ^{red} L ^{red} K ^{red} ISE ^{red} NS ^{red} L ^{red} IM ^{red} L ^{red} V ^{red} TI	431
MURJ_EC	408	<u><u>AG^{red}LS^{red}L^{red}SIG-----LA^{red}ACL^{red}NAS^{red}LL^{red}Y^{red}W^{red}OL^{red}R^{red}K^{red}Q^{red}IT^{red}PT^{red}Q^{red}PG^{red}WMA^{red}FL^{red}RL^{red}V^{red}V^{red}AV^{red}VM^{red}SG^{red}VL</u></u>	459
WZK_HP	485	EHEGLK ^{red} TQ ^{red} VGE ^{red} GAK ^{red} LSGG ^{red} Q ^{red} K ^{red} RI ^{red} GI ^{red} ARAL ^{red} Y ^{red} DN ^{red} PE ^{red} IL ^{red} VL ^{red} DEATSAL ^{red} DN ^{red} ETES ^{red} K ^{red} IM ^{red} DE ^{red} I ^{red} YO	544
AMJ_BS	268	-----WF-----	269
YTGP_SP	474	-----G ^{red} LV ^{red} VF ^{red} VAN--W ^{red} LL ^{red} GYA ^{red} -FK-PT ^{red} G ^{red} RL ^{red} TS ^{red} LL ^{red} Y ^{red} LL ^{red} TI	508
MURJ_BS	477	-----G ^{red} IA ^{red} V ^{red} K ^{red} IV ^{red} Q--W ^{red} VL ^{red} GF ^{red} -IS ^{red} Y ^{red} Q ^{red} D ^{red} G ^{red} OM ^{red} QA ^{red} IV ^{red} V ^{red} VIA	507
MURJ_TA	432	-----Y ^{red} L ^{red} TD--F ^{red} T ^{red} D ^{red} NE ^{red} F-WF-----L ^{red} IQ	446
MURJ_EC	460	<u><u>-----L^{red}GM^{red}L^{red}HT^{red}MP^{red}E--W^{red}SL^{red}GT^{red}MP^{red}WR-----L^{red}RL^{red}MA^{red}V</u></u>	484
WZK_HP	545	IAK ^{red} N ^{red} KL ^{red} IVIA ^{red} AH ^{red} RL ^{red} ST ^{red} IER ^{red} CE ^{red} VID ^{red} MS ^{red} QH ^{red} K ^{red} DN ^{red} LG----	578
AMJ_BS			
YTGP_SP	509	GGL ^{red} GM ^{red} TV ^{red} TAL ^{red} TL ^{red} TH ^{red} Q ^{red} L ^{red} D ^{red} KL ^{red} IG ^{red} SK ^{red} AS ^{red} RL ^{red} R ^{red} Q ^{red} KL ^{red} GW--	544
MURJ_BS	508	AA ^{red} V ^{red} CG ^{red} AV ^{red} LY ^{red} CG ^{red} Y ^{red} RL ^{red} GF ^{red} L ^{red} Q ^{red} KL ^{red} GR ^{red} RL ^{red} PG ^{red} FR ^{red} K-GR ^{red} HAG	544
MURJ_TA	447	IL ^{red} IG ^{red} IL ^{red} V ^{red} YL ^{red} IF ^{red} SS ^{red} TFY--R ^{red} DL ^{red} IR ^{red} RF ^{red} LY ^{red} ARKK----	475
MURJ_EC	485	<u><u>VL^{red}GI^{red}AA^{red}Y^{red}FA^{red}AL^{red}AV^{red}L^{red}GF^{red}K^{red}V^{red}KE^{red}FARR^{red}TV-----</u></u>	511

Figure S13. Alignment of *E. coli* MurJ (EC) with the flippases that are reported to complement MurJ depletion in *E. coli*. Definition of listed species: *HP: Helicobacter pylori*, *BS: Bacillus subtilis*, *SP: Streptococcus pyogenes*, *TA: Thermosipho africanus*. Essential residues in MurJ_{EC} are colored red, and the MTSES sensitive residues are colored green. Double-underlined regions indicate the transmembrane helices of MurJ_{EC}. A given column has one color which indicates the average BLOSUM62 score of pairs of letters in the column: light blue >= 3, dark blue >= 1, light gray >= 0.2, no color otherwise.

References

1. Taschner, P. E., Verest, J. G. & Woldringh, C. L. Genetic and morphological characterization of *ftsB* and *nrdB* mutants of *Escherichia coli*. *J. Bacteriol.* **169**, 19–25 (1987).
2. Taschner, P. E., Huls, P. G., Pas, E. & Woldringh, C. L. Division behavior and shape changes in isogenic *ftsZ*, *ftsQ*, *ftsA*, *pbpB*, and *ftsE* cell division mutants of *Escherichia coli* during temperature shift experiments. *J. Bacteriol.* **170**, 1533–1540 (1988).
3. Ishino, F. *et al.* New mutations *fts-36*, *fts-33*, and *ftsW* clustered in the *mra* region of the *Escherichia coli* chromosome induce thermosensitive cell growth and division. *J. Bacteriol.* **171**, 5523–5530 (1989).
4. Gray, A. N. *et al.* Coordination of peptidoglycan synthesis and outer membrane constriction during *Escherichia coli* cell division. *Elife* **4**, 1–29 (2015).
5. Banzhaf, M. *et al.* Cooperativity of peptidoglycan synthases active in bacterial cell elongation. *Mol. Microbiol.* **85**, 179–194 (2012).
6. Heidrich, C. *et al.* Involvement of N -acetylmuramyl- L -alanine amidases in cell separation and antibiotic-induced autolysis of *Escherichia coli*. *Mol. Microbiol.* **41**, 167–178 (2001).
7. Butler, E. K., Davis, R. M., Bari, V., Nicholson, P. A. & Ruiz, N. Structure-function analysis of MurJ reveals a solvent-exposed cavity containing residues essential for peptidoglycan biogenesis in *Escherichia coli*. *J. Bacteriol.* **195**, 4639–4649 (2013).
8. Chen, J. C. & Beckwith, J. *FtsQ*, *FtsL* and *FtsI* require *FtsK*, but not *FtsN*, for co-localization with *FtsZ* during *Escherichia coli* cell division. *Molecular Microbiology* **42**, 395–413 (2008).
9. Alexeeva, S., Gadella, T. W. J., Verheul, J., Verhoeven, G. S. & Den Blaauwen, T. Direct interactions of early and late assembling division proteins in *Escherichia coli* cells resolved by FRET. *Mol. Microbiol.* **77**, 384–398 (2010).
10. Kuk, A. C. Y., Mashalidis, E. H. & Lee, S. Y. Crystal structure of the MOP flippase MurJ in an inward-facing conformation. *Nat. Struct. Mol. Biol.* **24**, 171–176 (2017).

CHAPTER

3

MreC and MreD balance the interaction between the elongasome proteins PBP2 and RodA

Xiaolong Liu¹

Jacob Biboy²

Waldemar Vollmer²

Tanneke den Blaauwen^{1*}

¹ *Bacterial Cell Biology and Physiology, Swammerdam Institute for Life Science, Faculty of Science, University of Amsterdam, 1098 XH, Amsterdam, The Netherlands.*

² *Centre for Bacterial Cell Biology, Institute for Cell and Molecular Biosciences, Newcastle University, NE2 4AX, Newcastle upon Tyne, United Kingdom.*

**Corresponding author*

Manuscript in preparation

Abstract

Rod-shape of most bacteria is maintained by the elongasome, which mediates the synthesis and insertion of peptidoglycan into the cylindrical part of the cell wall. The elongasome contains several essential proteins, such as RodA, PBP2, and the MreBCD proteins, but how its activities are regulated remains poorly understood. Using *E. coli* as a model system, we investigated the interactions between core elongasome proteins *in vivo*. Our results show that PBP2 and RodA form a complex mediated by their transmembrane and periplasmic parts and independent of their catalytic activity. MreC and MreD also interact directly with PBP2. MreC elicits a change in the interaction between PBP2 and RodA, which is suppressed by MreD. The cytoplasmic domain of PBP2 is required for this suppression. We hypothesize that the *in vivo* measured PBP2-RodA interaction change induced by MreC corresponds to the conformational change in PBP2 as observed in the MreC-PBP2 crystal structure, which was suggested to be the “on state” of PBP2. Our results indicate that the balance between MreC and MreD determines the activity of PBP2, which could open new strategies for antibiotic drug development.

Introduction

Bacterial cells are surrounded by a peptidoglycan layer that maintains their shape and protects them from bursting due to the osmotic pressure. The biosynthesis of peptidoglycan is the target of many antibiotics that are used in clinical therapies for bacterial infections. The spread of antibiotic resistant pathogens calls urgently for the development of novel antibiotics. In depth knowledge on peptidoglycan synthesis will aid in the development of effective screening assays to select cell wall synthesis inhibitors. Peptidoglycan is a mesh-like heteropolymer of glycan chains of GlcNAc-MurNAc-peptide subunits that are connected by peptide cross-links¹. Peptidoglycan synthesis begins in the cytoplasm with synthesis of UDP-GlcNAc and UDP-MurNAc-pentapeptide². Two following membrane steps, catalyzed by MraY and MurG, assemble the precursor lipid II^{3,4}, which is flipped to the periplasmic side of the cytoplasmic membrane by lipid II flippase(s) MurJ and/or FtsW⁵⁻⁷. GlcNAc-MurNAc pentapeptide units are polymerized into glycan chains and the peptides are cross-linked to bridge the glycan stands by peptidoglycan synthases to expand the peptidoglycan layer while the lipid carrier is recycled⁸⁻¹⁰. Most rod-shaped bacteria employ two protein complexes, elongasome and divisome, to guide peptidoglycan synthesis during lateral growth and cell division, respectively¹¹.

In *E. coli*, the divisome contains more than twenty proteins. Assembly of the divisome starts with positioning the FtsZ ring at midcell together with other early divisome proteins, such as FtsA, ZipA, ZapA and FtsEX, to form the early divisome¹²⁻¹⁴. Subsequently, the late divisome proteins, FtsK, FtsBLQ, FtsW, PBP3 and FtsN, are recruited¹⁵. These proteins localize to midcell in an interdependent order^{15,16}. Among these proteins, FtsW, PBP3 and PBP1B provide the peptidoglycan synthesis activity during septum synthesis^{10,17,18}. PBP1B has both glycosyltransferase (GTase) and transpeptidase (TPase) activity¹⁹, while FtsW and FtsI only have GTase activity and TPase activity, respectively¹⁰. Although it is still not yet fully understood, recent studies showed that the peptidoglycan synthesis during division is regulated by competition between the FtsBLQ complex and FtsN, which have inhibitory and elevating effects, respectively, on the activities of

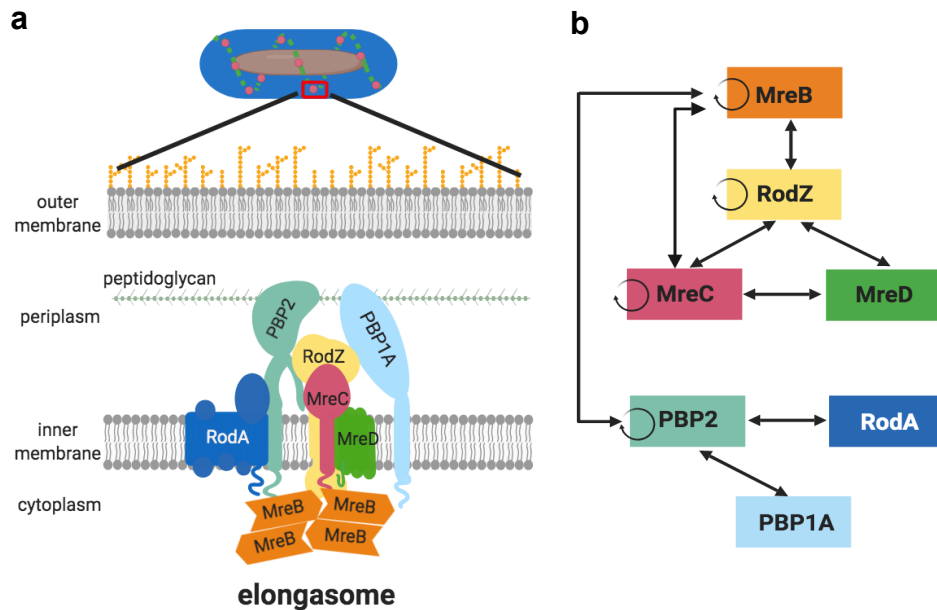
FtsW-PBP3-PBP1B^{20–22}.

Figure 1. Core proteins in elongasome and their interactions in *E. coli*. a. Schematic representation of the *E. coli* cell envelope and elongasome. MreB localizes in patches underneath the cytoplasmic membrane and recruits the other elongasome proteins of which PBP2-RodA and PBP1A peptidoglycan synthases. The peptidoglycan layer is sandwiched by the cytoplasmic membrane and the outer membrane. b. Identified interactions between elongasome proteins from previous interaction studies. Double arrowed lines represent the interaction between different proteins. Circular arrows indicate the reported self-interaction.

Proteins that are known to be part of the elongasome are the cytoplasmic membrane associated actin homologue MreB, the bitopic membrane proteins RodZ, MreC and PBP2, and the integral membrane proteins MreD and RodA (Fig. 1a). MreB polymerizes into short filaments that rotate around the cylindrical membrane^{23,24}. The rotation of MreB is believed to drive the topography of the insertion of peptidoglycan into the lateral wall^{23,25–27}. Bacterial two hybrid analysis showed that MreB interacts with MreC, but not with MreD²⁸, while RodZ interacts strongly with itself and MreB and MreC^{28,29} (Fig. 1b), and these interactions are essential to maintain bacterial morphology^{28,30–32}. RodA and PBP2 form a stable subcomplex³³ and provide GTase and TPase activity, respectively, during cylindrical peptidoglycan synthesis^{9,34,35}. This subcomplex also shows a circumferential

motion that is similar to that of MreB. The bifunctional PBP1A with glycosyltransferase (GTase) and transpeptidase (TPase) activities was shown to interact with PBP2 (Fig.1b) and stimulate its activity¹⁸. Because PBP1A moves independently of the rotation of PBP2 and MreB, it is thought not to be part of the core elongasome^{18,36}. However, the function and role of most elongasome proteins are still poorly understood. How peptidoglycan synthesis is activated and regulated during elongation is still the key question. In this study, combining genetics, microscopy and Förster Resonance Energy Transfer (FRET), we investigated the functions of, and interactions between, these core elongasome proteins. The transfer of energy between a donor fluorescent-protein fusion and an acceptor fluorescent-protein fusion (FRET) is very sensitive to distance, which allows the detection of conformational changes that affect this distance⁷. Our results indicate that MreC and MreD modulate the interaction between PBP2 and RodA in oppositely, which likely reflects a mechanism of elongasome activation and regulation.

Results

RodA and PBP2 activities are not essential for their interaction

RodA and PBP2 form a stable peptidoglycan synthesizing subcomplex in the cytoplasmic membrane, and show a strong interaction as detected by FRET³³. To investigate whether this interaction relies on their enzymatic activities, RodA^{R109A} and RodA^{Q207R} versions, which were predicted to be inactive based on studies on its homologue FtsW, were constructed (Supplementary Fig. 1)^{5,38}. As expected, these mutants could not complement the temperature sensitive RodA strain LMC882 at the non-permissive temperature, and the RodA^{Q207R} variant even showed dominant negative effects at the permissive temperature (Fig. 2a). Subsequently, N-terminal mCherry fused versions^{33,34} of the inactive RodA proteins were expressed to test their interaction with mKO-PBP2^{WT} by FRET (Fig. 2b). In our FRET system, the direct fused mCherry-mKO tandem was used as positive control³³. To account for possible interactions between proteins due to

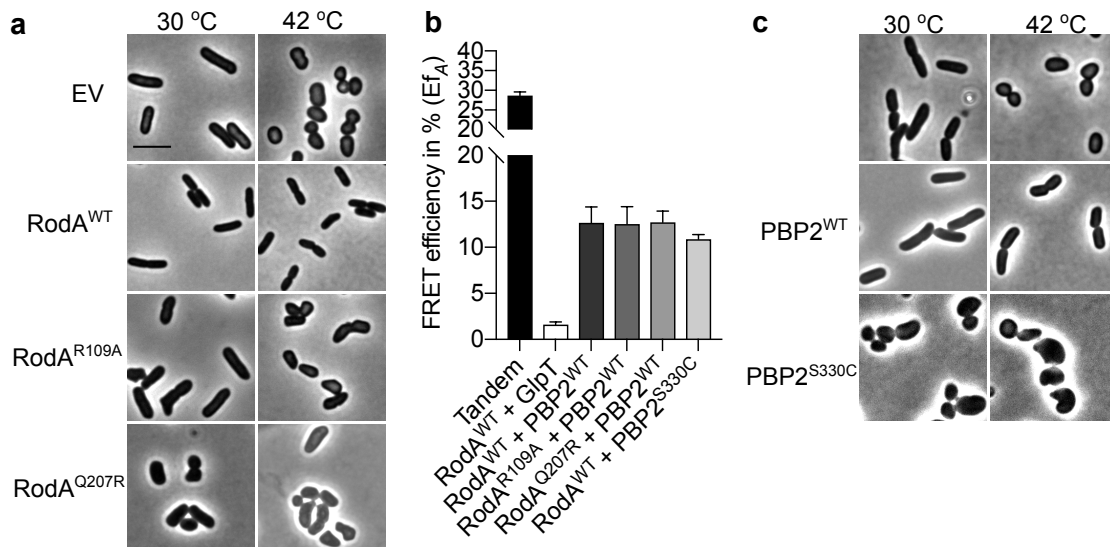


Figure 2. Activity of RodA and PBP2 are not required for their interaction. **a**, Phase contrast images of the complementation of RodA variants. RodA temperature sensitive strain LMC882 was transformed with plasmids expressing RodA variants and grown in LB medium at 30 °C (left panel) and 42 °C (right panel) for 2 mass doublings (with 15 μ M IPTG induction). **b**, Calculated acceptor FRET efficiencies (E_{fA}) between PBP2 and RodA variants from spectral FRET measurements. RodA and its variants are fused with mCherry. PBP2 and its variants are fused with mKO. **c**, Phase contrast images of the complementation of PBP2 variants. The PBP2 temperature sensitive strain LMC582 was transformed with PBP2^{WT} or PBP2^{S330C}, and grown in LB medium at 30 °C (left panel) and 42 °C (Right panel) for 2 mass doublings (with 15 μ M IPTG induction). Scale bar equals 5 μ m. All the results in the figure are representative of at least three independent experiments.

crowding in the cytoplasmic membrane, a peptidoglycan synthesis unrelated integral membrane protein GlpT^{3,34} was fused to mKO, and its interaction with mCh-RodA was detected as negative control. The acceptor FRET efficiency (E_{fA}) of all FRET samples were calculated using our previously published mKO-mCh FRET algorithm (Supplementary Fig. 2)³³. An E_{fA} value of $31.0 \pm 4.0\%$ was observed for the tandem control (Fig. 2b and Table 1), which is comparable to the published data³³. An E_{fA} value of $1.1 \pm 3.5\%$ was observed for the RodA-GlpT negative control (Fig. 2b and Table 1). FRET experiments with PBP2^{WT} and RodA^{R109A} or RodA^{Q207R} yielded calculated E_{fA} values of $12.5 \pm 1.9\%$ and $12.7 \pm 1.2\%$, respectively, which are comparable to the E_{fA} value of $12.7 \pm 1.7\%$ of wild type RodA (Fig. 2b and Table 1). To determine whether the activity of PBP2 was required for the interaction with RodA, we expressed the inactive variant PBP2^{S330C}, which is not able to bind

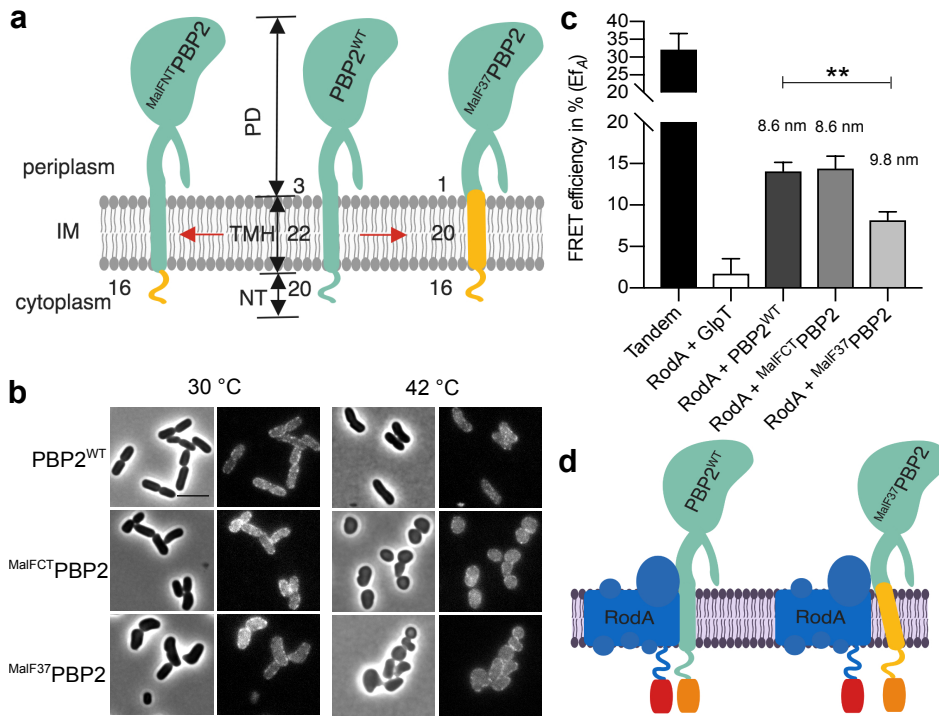


Figure 3. Functionality and interaction of PBP2 domain swap mutants. **a.** Schematic illustration of PBP2 domain-swap mutants. NT: N-terminus; TMH: transmembrane helix; PD: periplasmic domain; PBP2^{WT}: wild type PBP2; MalF^{NT}PBP2: the cytoplasmic N-terminus of PBP2 was replaced with the MalF cytoplasmic N-terminus; MalF³⁷PBP2: the NT and THM domains of PBP2 were replaced with corresponding domains of MalF. Numbers indicate the residues involved in replacements in each domain of the proteins. **b.** Phase contrast and fluorescence images of the complementation of PBP2 mutants. The PBP2 temperature sensitive strain LMC582 was transformed with the PBP2 variants, and grown in LB medium at 30 °C (left panels) and 42 °C (right panels) for 2 mass doublings (with 15 μM IPTG induction). Scale bar equals 5 μm. **c.** Calculated acceptor FRET efficiencies (E_{fA}) between PBP2 and RodA variants from spectral FRET measurements. RodA and its variants are fused with mCherry. PBP2 and its variants are fused with mKO. P value determined with Student's t-test (**: p<0.001). Distances between the two proteins (fluorophores) were calculated using the equation, $E = (1+(r/R_0)^6)^{-1}$, where r is the distance between the chromophores and R₀ of 6.4 nm is the Förster distance of for the mCh-mKO pair. **d.** Schematic illustration of the interaction between RodA and PBP2 variants. After replacement, the TMH domain of MalF³⁷PBP2 is not interacting with RodA, which increases its distance to RodA. All the results in the figure are representative of at least three independent experiments. Models were created with BioRender.

benzylpenicillin³⁵. This inactive mutant showed a strong dominant negative effect during the complementation in the PBP2 temperature sensitive strain LMC582 (Fig. 2c), while the detected E_{fA} value of PBP2^{S330C}-RodA^{WT}

remained $10.9 \pm 0.5\%$, which was slightly below the Ef_A value of PBP2^{WT}-RodA^{WT} (Fig. 2d and Table 1). These results imply that the activity of RodA and PBP2 are not needed for their interaction.

Table 1. Summary of the calculated acceptor FRET efficiencies (Ef_A) from spectral FRET measurements for listed samples.

Parameter	Proteins expressed		Ef_A (%)	SD (%)	No ¹
	pTHV037	pSAV057			
Positive control²					
Tandem	Empty plasmid	mKO-mCh	31.0	4.0	22
Negative control³					
RodA-GlpT	mCh-RodA	mKO-(GGG) ₂ -GlpT	1.1	3.5	24
Biological interactions					
RodA ⁴ -PBP2 ⁵	mCh-RodA	mKO-PBP2	12.7	1.7	16
RodA ^{R109A} -PBP2	mCh-RodA ^{R109A}	mKO-PBP2	12.5	1.9	4
RodA ^{Q207R} -PBP2	mCh-RodA ^{Q207R}	mKO-PBP2	12.7	1.2	4
RodA-PBP2 ^{S330C}	mCh-RodA	mKO-PBP2 ^{S330C}	10.9	0.5	3
RodA ^{MalFNT} -PBP2	mCh-RodA	mKO ^{MalFNT} -PBP2	14.4	1.7	4
RodA ^{MalF37} -PBP2	mCh-RodA	mKO ^{MalF37} -PBP2	8.2	1.3	3
RodA-PBP2 ^{L61R}	mCh-RodA	mKO-PBP2 ^{L61R}	12.8	2.8	8
RodA-RodA ^{WT}	mCh-RodA	mKO-RodA	5.5	1.4	4
MreB ^{SW} -RodA	mCh-MreB ^{SW}	mKO-RodA	7.2	3.4	4
PBP2-PBP2	mCh-PBP2	mKO-PBP2	9.2	0.5	4
PBP2 ^{MalFNT} -PBP2	mCh-PBP2	mKO ^{MalFNT} -PBP2	10.5	2.0	4
MreC-PBP2	mCh-MreC	mKO-PBP2	5.1	1.2	6
MreC ^{MalFNT} -PBP2	mCh-MreC	mKO ^{MalFNT} -PBP2	5.4	1.7	6
MreC-PBP2 ^{L61R}	mCh-MreC	mKO-PBP2 ^{L61R}	5.3	0.6	2
MreD-PBP2	mCh-MreD	mKO-PBP2	4.3	1.2	10
MreD ^{MalFNT} -PBP2	mCh-MreD	mKO ^{MalFNT} -PBP2	5.3	1.6	10
MreCD ⁶ -PBP2	mCh-MreCD	mKO-PBP2	3.3	0.5	6
MreCD ⁷ ^{MalFNT} -PBP2	mCh-MreCD	mKO ^{MalFNT} -PBP2	5.4	1.1	5
+ mecillinam					
Positive control					
Tandem	Empty vector	mKO-mCh	31.0	31.2	2
Negative control					
RodA-GlpT	mCh-RodA	mKO-(GGG) ₂ -GlpT	3.1	0.1	2
Biological interactions					
RodA-PBP2	mCh-RodA	mKO-PBP2	8.6	1.1	6
RodA ^{MalF37} -PBP2	mCh-RodA	mKO ^{MalF37} -PBP2	3.0	2.0	4
RodA-PBP2 ^{S330C}	mCh-RodA	mKO-PBP2 ^{S330C}	7.9	1.0	2
RodA-PBP2 ^{L61R}	mCh-RodA	mKO-PBP2 ^{L61R}	9.7	2.2	3

¹ No, number of biological repeats;

^{2,3} Here all measured positive and negative controls are averaged. In the figures the controls are included that belong to the corresponding measurements.

^{4,5} RodA and PBP2 without superscript represent the wild type version.

^{6,7} MreC and MreD were expressed from one plasmid, and MreC was fused to mCherry while MreD was non-fused.

The transmembrane and periplasmic parts of PBP2 contribute to its interaction with RodA

To reveal which part of PBP2 interacts with RodA, two domain swap mutants of PBP2 were constructed. The cytoplasmic N-terminus (NT) and NT-transmembrane-helix (NT-TMH) of PBP2 were replaced by the N-terminus and first 37 residues of MalF, a bitopic membrane protein that has been used for domain swap studies^{39–41}, to yield ^{MalFNT}PBP2 and ^{MalF37}PBP2, respectively (Fig. 3a). Both versions were able to localize in the membrane but showed dominant negative effects, indicating the essentiality of these parts of PBP2 (Fig. 3b). The replacement of the NT of PBP2 did not change its interaction with RodA, as the detected E_{fA} value remained $14.4 \pm 1.1\%$, which was not significantly different compared to that of the interaction between RodA and wild type PBP2 (Fig. 3c, Table 1 and Supplementary Fig. 3). However, replacement of the TMH of PBP2 significantly reduced the E_{fA} value between PBP2 and RodA to $8.2 \pm 1.3\%$, which reflected an apparent distance increase from 8.6 nm to 9.8 nm between these two proteins⁴² (Fig. 3c and Table 1). This decrease in distance was not caused by a change in the expression levels of RodA and PBP2 in the cells (Supplementary Fig. 3), or due to the shorter transmembrane helix after replacement (Fig. 3a). The average rise per residue in transmembrane helices is 0.15 nm, therefore a two amino acid residues shorter helix (Fig. 3a) would cause a change of only 0.3 nm in distance between donor and acceptor fluorophores. The still considerably higher E_{fA} value compared to the negative control indicates that the transmembrane helix alone is not sufficient for the interaction between PBP2 and RodA. Apparently, the periplasmic domain of PBP2 is also involved in this interaction (Fig. 3d).

MreC interacts with PBP2 and affects PBP2-RodA interaction

A recent study of PBP2-MreC from *Helicobacter pylori* showed two different structural conformations of PBP2 in the MreC bonded and non-bonded forms (Fig. 4 a), and the authors proposed that MreC changes PBP2 from an off-state into an on-state by binding the periplasmic hydrophobic zipper of

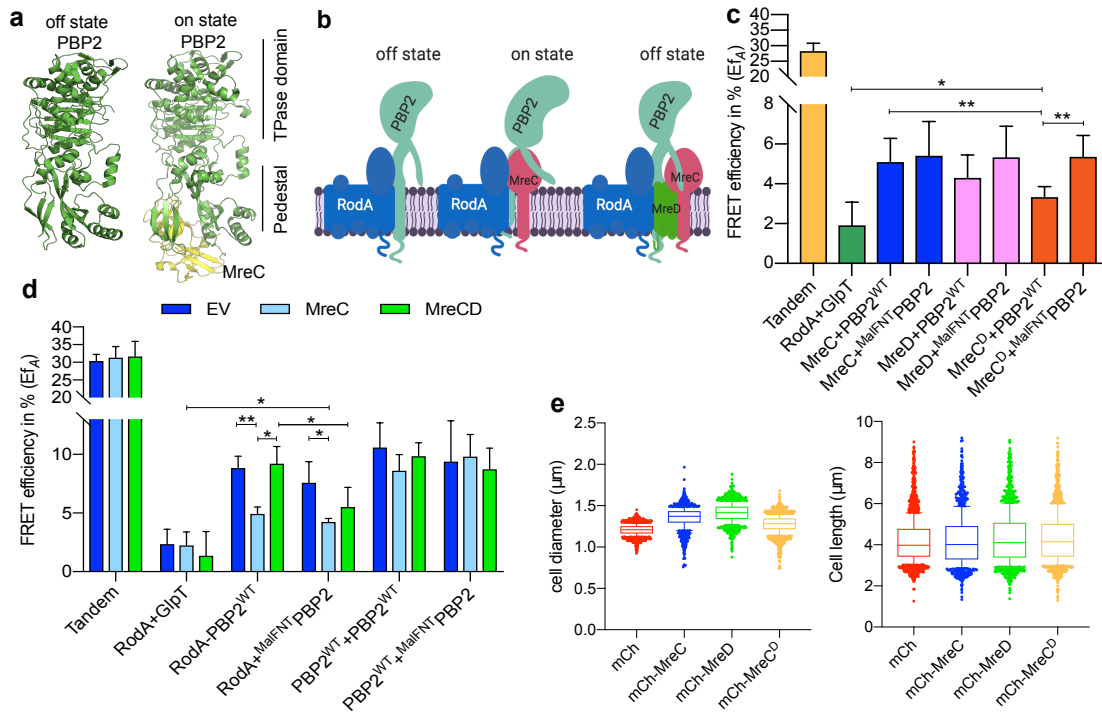


Figure 4. MreC and MreD balance the interaction between RodA and PBP2. **a.** Crystal structures of *Helicobacter pylori* PBP2 in different conformations¹. The structural information lacks the juxta-membrane, transmembrane helix and cytoplasmic regions of PBP2. MreC binds to PBP2 and was proposed to switch PBP2 from the “off state” to the “on state”¹. **b.** Schematic representation of PBP2 conformational changes caused by MreC. Left panels: PBP2 stays at the “off-state” in the absence of MreC (the distance between cytoplasmic terminus of RodA and PBP2 is small); middle panels: PBP2 switches to the “on-state” after binding with MreC (the distance between cytoplasmic terminus of RodA and PBP2 is larger), right panels: MreD suppresses the MreC-mediated conformational change of PBP2 and keeps PBP2 at the “off-state”. **c.** Calculated acceptor FRET efficiencies (E_f) between MreCD proteins and RodA variants from spectral FRET measurements. MreC: mCherry fused MreC; MreD: mCherry fused MreD; MreC^D: MreCD co-expressed from the same plasmid, and MreC is fused with mCherry while MreD is non-fused. PBP2 and its variants are fused with mKO. **d.** Calculated acceptor FRET efficiencies (E_f) between RodA and PBP2 variants from spectral FRET measurements in the three-plasmids FRET experiments. EV: a third empty vector; MreC: a third plasmid expressing non-fused MreC; MreCD: a third plasmid expressing non-fused MreCD. **e.** Cell length and diameter changes after expressing MreC, MreD or MreCD together. LMC500 strain was transformed with each construct and grown in LB medium at 37 °C and induced with 15 μ M IPTG for 2 mass doublings. Proteins were expressed from the pSAV057 derived plasmids (mKO: control; MreC: mKO fused MreC; MreD: mKO fused MreD; MreC^D: co-expression of MreC and MreD, MreC is fused with mKO while MreD is not fused). About 1000 cells were analyzed. P value determined with Student’s t-test (*: $p < 0.05$;; **: $p < 0.01$:). Models were created with BioRender.

PBP2⁴³. In our FRET system about 1000 mKO fusion proteins are expressed from plasmid⁴⁴ in the a wild type background. The ± 180 endogenous MreC⁴⁵ molecules are not sufficient to have a significant impact on the by plasmid expressed PBP2 molecules. Therefore the mildly overexpressed PBP2 versions mostly remain in the off state conformation (Fig. 4b, left). We reasoned that the interaction between PBP2 and RodA could be sensitive to possible conformational changes of PBP2, if we would additionally express MreC to balance the molecule numbers of both proteins. Firstly, the interaction between a functional mCh-MreC²⁸ fusion and mKO-PBP2 was tested *in vivo* by FRET measurements. The observed E_{fA} value of $5.1 \pm 1.2\%$ indicates a direct interaction between PBP2 and MreC (Fig. 4c, Table 1 and Supplementary Fig. 4), which is in agreement with the structural study of PBP2-MreC from *Helicobacter pylori*⁴³.

Table 2. Summary of the calculated acceptor FRET (E_{fA}) efficiencies from spectral FRET measurements for listed samples.

Parameter	FRET pairs		Third plasmid								
			EV			MreC			MreCD		
	pTHV037	pSAV057	E_{fA} (%)	SD (%)	No.	E_{fA} (%)	SD (%)	No.	E_{fA} (%)	SD (%)	No.
Positive control											
Tandem	Empty vector	mKO-mCh	30.4	1.9	4	31.3	3.2	3	31.7	4.3	2
Negative control											
RodA-GlpT	mCh-RodA	mKO-(GGG) ₂ -GlpT	2.4	1.3	7	2.2	1.1	2	1.4	2.1	4
Biological interactions											
RodA-PBP2 ^{WT}	mCh-RodA	mKO-PBP2 ^{WT}	8.8	1.1	6	4.9	0.6	2	9.2	1.5	4
RodA ^{-MalFNT} PBP2	mCh-RodA	mKO ^{-MalFNT} PBP2	7.6	1.8	5	4.2	0.3	2	5.5	1.7	4
PBP2 ^{WT} -PBP2 ^{WT}	mCh-PBP2 ^{WT}	mKO-PBP2 ^{WT}	10.6	2.1	6	8.6	1.4	2	9.8	1.2	4
PBP2 ^{WT} -MalFNT PBP2	mCh-PBP2 ^{WT}	mKO ^{-MalFNT} PBP2	9.4	3.5	5	9.8	1.9	2	8.7	1.8	4

No., number of samples measured.

Next we employed a three-plasmids-FRET system that expressed MreC from a third plasmid to test the interaction between PBP2 and RodA in the presence of enhanced levels of MreC (Fig. 4d, Table 2 and Supplementary Fig. 5). A control strain contained an empty plasmid instead of the MreC-expression plasmid. In the presence of the empty plasmid, the calculated E_{fA} values for the tandem (positive control) and RodA-GlpT (negative control) were $30.4 \pm 1.8\%$ and $2.3 \pm 1.3\%$, respectively (Fig. 4d and Table 2). These E_{fA} values remained unchanged in the presence of MreC expressed from the third plasmid (Fig. 4d and Table 2). Interestingly, the E_{fA}

value for the RodA-PBP2 interaction was significantly reduced to $4.9 \pm 0.6\%$ in the presence of MreC, compared with the Ef_A of $8.8 \pm 1.1\%$ in the presence of empty plasmid (Fig. 4d and Table 2). These results indicate that MreC changes the interaction between PBP2 and RodA, which would be consistent with a conformational change of PBP2 from the off-state to the on-state proposed from the crystal structures⁴³ (Fig. 4a, middle).

MreD suppresses the MreC-mediated change in the PBP2-RodA interaction

During our study, we noticed that overexpression of MreC caused morphological defects of the wild type strain, increasing the diameter of *E. coli* cells (Fig. 4e and Supplementary Fig. 6). Interestingly, the co-expression of MreD together with MreC suppressed these morphological defects and restored the wild type phenotype (Fig. 4e and Supplementary Fig. 6). To further investigate this effect, an N-terminal functional mCherry fusion of MreD³⁰ was expressed. Topological analysis predicted 6 transmembrane helices for MreD with both its N-terminus and C-terminus in the cytoplasm (Supplementary Fig. 7). This topology model is consistent with the fluorescence signals readily observed for N-terminal fused GFP-MreD³⁰ and mKO-MreD versions (data not shown), which could not be observed if the N-terminus of MreD would localize in the oxidative periplasm where GFP and mKO do not mature³⁷. Similarly as for MreC, over-expression of MreD alone also resulted in morphological defects of *E. coli* (Fig. 4e and supplementary Fig. 6).

To study the role of MreD in the elongasome, FRET experiments were applied to detect a possible interaction with PBP2. The calculated Ef_A value of $4.3 \pm 1.1\%$ indicated a direct interaction between MreD and PBP2 (Fig. 4c, Table 1 and Supplementary Fig. 4). Subsequently, the interaction between MreC and PBP2 was measured by FRET in the presence of MreD. The calculated Ef_A between MreC and PBP2 was significantly reduced from $5.1 \pm 1.2\%$ to $3.3 \pm 0.5\%$ ($p=0.0078$) when MreD was co-expressed (Fig. 4c, Table 1 and Supplementary Fig. 4). Since MreC reduced the Ef_A of RodA-PBP2 from $8.8 \pm 1.1\%$ to $4.9 \pm 0.5\%$, it was possible that MreD also influences the

effect of MreC on the interaction between RodA and PBP2. Therefore, the three-plasmid FRET experiment was applied to detect the interaction between RodA and PBP2 in the presence of MreCD. Interestingly, the E_{f_A} value of RodA-PBP2 was restored to $9.2 \pm 1.5\%$, which was comparable with the E_{f_A} in the presence of the third empty plasmid (Fig. 4d, Table 2 and Supplementary Fig. 5). Our combined results suggest a regulatory mechanism by which MreC interacts with PBP2 and changes its conformation, while MreD interacts with MreC and PBP2 to prevent this conformational change PBP2. These conformational changes could correspond the proposed on and off states of PBP2 as published⁴³ (Fig. 4 a and b).

The cytoplasmic part of PBP2 is important for the interplay with the MreCD proteins

As showed before, the cytoplasmic NT part of PBP2 has an essential unknown function rather than being involved in RodA-PBP2 interaction (Fig. 3). We considered that the NT of PBP2 might be important for its self-interaction and or interactions with other partner proteins. However, the E_{f_A} values of MalFNT PBP2 with wild type PBP2, MreC and MreD were not different from those of the wild type PBP2 (Fig. 4d, Supplementary Fig. 8 and Table 1). Interestingly, the E_{f_A} value of the interaction between MreC and wild type PBP2, but not the MalFNT PBP2, was reduced by the co-expression of MreD (Fig. 4d, Table 2 and Supplementary Fig. 5c). Similarly, in the three-plasmid FRET experiments, MreD was not able to suppress the MreC-mediated change in the $PBP2^{MalFNT}$ -RodA interaction. Because the E_{f_A} value of RodA- MalFNT PBP2 FRET remained at $5.5 \pm 1.7\%$ in presence of MreCD, rather than being restored to $9.2 \pm 1.5\%$ as in the RodA-PBP2^{WT} experiments (Fig. 4d, Table 2 and Supplementary Fig. 5c). Together, these results indicate that the cytoplasmic part of PBP2 plays an important role in the MreCD-mediated regulation of the alteration of PBP2's interaction with RodA.

MreCD proteins do not influence PBP2 self-interaction

So far our results has shown that MreC and MreD have clearly opposite effects on the interaction between RodA and PBP2. In contrast, the interaction between two PBP2 molecules¹⁷ was not significantly affected by the overexpressed MreC or of MreCD together, as the calculated E_{fA} values for the PBP2-PBP2 interaction remained unchanged compared to the values for the expression of the third empty plasmid (Fig. 4d and Table 2). RodA was also found to interact with itself (Table 1 and Supplementary Fig. 9). Likely PBP2 and RodA function as a complex of dimers, which might also allow simultaneously insertion of multiple glycan strand as has been proposed⁴⁶⁻⁴⁸.

Effect of mecillinam on the interaction between RodA and PBP2

As showed above, both the transmembrane helix and periplasmic part of PBP2 contribute to its interaction with RodA (Fig. 3). The binding of MreC to the periplasmic hydrophobic zipper domain of PBP2, which presumably changes the conformation of PBP2 from off-state to on-state, reduces the detected E_{fA} between RodA and PBP2 (Fig. 4 d and e). Interestingly, the PBP2 specific inhibitor mecillinam, also caused a reduction in the FRET efficiency of the interaction between RodA and PBP2. The RodA-PBP2^{WT} interaction pair yielded a reduced E_{fA} of $8.6 \pm 1.1\%$ in the presence of mecillinam³³, comparing with the E_{fA} of $12.7 \pm 1.7\%$ without mecillinam (Fig. 2, Table 1 and Supplementary Fig. 10). Since mecillinam binds specifically to the periplasmic TPase active site of PBP2, a possible explanation could be that binding of mecillinam reduces the affinity between the periplasmic parts of PBP2 and RodA, but allows their transmembrane helices interaction to maintain the interaction. Indeed, after replacing the transmembrane helix of PBP2 to abolish this part of the interaction (RodA-^{MalF37}PBP2), the E_{fA} value was further reduced to $3.0 \pm 2.0\%$ in the presence of mecillinam (Supplementary Fig. 10 and Table 1), consistent with an almost complete loss of interaction between RodA and ^{MalF37}PBP2. This possible mechanism of mecillinam is also in agreement with the published data that, mecillinam treatment only inhibited peptidoglycan synthesis (spherical phenotype) but did

not disrupt the structure of the elongasome⁴⁹. The inactive mutant PBP2^{S330C}, which was reported not to be able to covalently bind benzylpenicillin³⁵, was still responding to mecillinam and showed a similar Ef_A reduction as PBP2^{WT} (Supplementary Fig. 10 and Table 1).

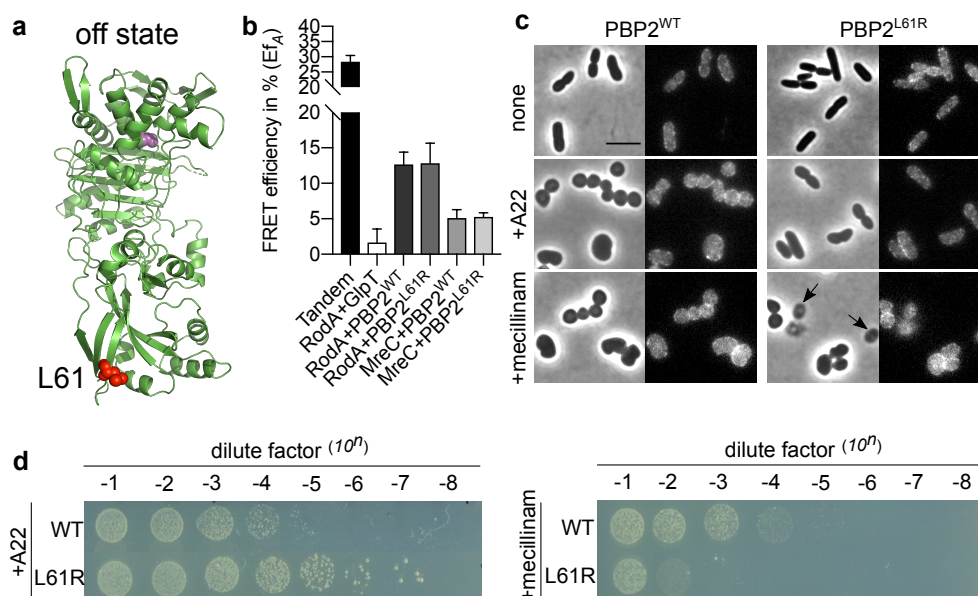


Figure 5. Hyperactive mutant PBP2^{L61R} is more sensitive to mecillinam. **a.** Modeled “off state” structure of *E. coli* PBP2 from *H. pylori* PBP2 using Phyre 2. Structural information lacks the juxta-membrane, transmembrane helix and cytoplasmic regions of PBP2. Residue L61 is colored in red and shown as spheres. Active site S330 is colored in pink and shown as spheres. **b.** Hyperactive mutant PBP2^{L61R} interacts similar like PBP2^{WT} with RodA and MreC. RodA and MreC were fused with mCherry, and PBP2^{WT} and PBP2^{L61R} were fused with mKO. **c.** Phase contrast and fluorescence images of cells expressing PBP2^{L61R} were less sensitive to A22 but hypersensitive to mecillinam in liquid culture. LMC500 strain expressing nothing, or PBP2^{WT}, or PBP2^{L61R} were grown in LB medium at 37 °C. IPTG induction (15 μM), and A22 treatment (10 mg·L⁻¹) or mecillinam treatment (2 mg·L⁻¹) were applied to each culture for 2 mass doublings. Arrows indicate the cell lyse after mecillinam treatment in the PBP2^{L61R} culture. Scale bar equals 5 μm. **d.** Spot assay to test the sensitivities of PBP2^{WT} and PBP2^{L61R} to A22 (10 mg·L⁻¹) and mecillinam (2 mg·L⁻¹).

PBP2^{L61R} stays in the off-state and activates RodA

A recent study reported a version of PBP2 in which Leu61 was replaced by Arg (PBP2^{L61R}) that could suppress an MreC defect, and was proposed to stay in the on state conformation mimicking the MreC activation⁵⁰. If this would be the case, the RodA-PBP2^{L61R} pair would be expected to have a

reduced FRET efficiency, since the MreC activated RodA-PBP2^{WT} pair resulted in a reduction of their FRET efficiency (Fig 4d). Therefore, an N-terminal mKO fusion of PBP2^{L61R} was constructed to test the interactions with its partner proteins. Surprisingly, the Ef_A for RodA-PBP2^{L61R} remained 12.8 ± 2.8%, which was comparable with the Ef_A of RodA-PBP2^{WT} that was presumably in the off state (Fig. 5 a and b, Table 1 and Supplementary Fig. 11). The RodA-PBP2^{L61R} interaction was reduced to an Ef_A of 9.7 ± 2.2% in the presence of mecillinam, which was also comparable with that of PBP2^{WT} (Table 1 and Fig. S10), indicating that the TPase active side is still accessible as in the wild type protein. Unfortunately, the co-expression of PBP2^{L61R} together with either MreC or MreD alone, or both together, was not possible in most cases, as FRET cells repeatedly lost the mKO-PBP2^{L61R} signal upon induction (Table 1), suggesting toxicity of these combinations. Out of 6 attempts to co-express MreC and PBP2^{L61R} only two times the cells did not lose the mKO signal. Of those samples the calculated Ef_A value of the MreC and PBP2^{L61R} pair remained 5.4 ± 1.7%, which was comparable with MreC-PBP2^{WT} (Fig. 4a and Table 1). These results suggest that the hyperactive mutant PBP2^{L61R} likely behaves similarly as wild type PBP2 in the interaction with its partner proteins.

Having observed these unexpected results, we continued to further characterize the hyperactive PBP2^{L61R}. Although the protein was reported to be functional⁵⁰, we confirmed that mKO-PBP2^{L61R} was able to complement the PBP2(TS) strain LMC582 at the non-permissive temperature (Supplementary Fig. 12a). Its expression resulted in longer and thinner cells (Fig. 5c and Supplementary Fig. 12b), and reduced the sensitivity of cells to the MreB inhibitor A22 (Fig. 5c) as reported⁵⁰. Interestingly, cells expressing PBP2^{L61R} were hypersensitive to mecillinam (Fig. 5 c and d). These results indicate potential defects in the peptidoglycan layer of cells expressing PBP2^{L61R}, and these defects may be tolerable in general growth conditions but are exacerbated in the presences of mecillinam. Considering the fact that PBP2^{L61R} stimulates the GTase activity of RodA *in vitro*⁵⁰ and our results on the cellular interactions, it is possible that the L61R exchange in PBP2 enhances only the activity of RodA and has no effect on PBP2's TPase activity. Given the fact that *in vitro* peptidoglycan synthesis experiments

Table 3. Muropeptide composition of LMC500 strains carrying no plasmid or different plasmids.

Muropeptide ² or feature	Percent peak area (%) ¹				
	LMC500	LMC500 mKO	LMC500 mKO-GlpT	LMC500 mKO-PBP2	LMC500 mKO-PBP2 ^{L61R}
Chain ends (anhydro)	2.7 ± 0.0	2.8 ± 0.0	2.7 ± 0.0	3.0 ± 0.0	2.2 ± 0.0
Glycan chain length (DS) ³	36.9 ± 1.7	34.9 ± 0.4	35.9 ± 0.3	32.7 ± 0.4	45.3 ± 0.1
Degree of cross-linkage	23.2 ± 0.1	23.4 ± 0.0	23.3 ± 0.0	23.3 ± 0.1	23.3 ± 0.2
% Peptides in cross-links	47.4 ± 0.1	48.0 ± 0.0	47.8 ± 0.0	48.0 ± 1.1	47.8 ± 0.9

¹ values are mean ± variation of two biological replicates.

² muropeptide names according to Glauner, 1988.

³ average glycan chain length in disaccharide (DS) units calculated from the percentage of anhydro-MurNAc containing muropeptides.

showed that inactivation of PBP2 by the specific antibiotic mecillinam resulted in longer glycan chains synthesized by a PBP1A-PBP2 complex¹⁸, we wondered whether the presence of PBP2^{L61R} affected peptidoglycan synthesis in the cell. We prepared peptidoglycan and analyzed its composition from cells expressing PBP2^{L61R}, wild type PBP2, and the control membrane protein GlpT. As predicted, the peptidoglycan from all strains retained a similar extent of peptide cross-linkage, only the peptidoglycan from the PBP2^{L61R}-expressing cells contained unusually long glycan chains with a mean length ~45 disaccharide units (Table 3). The peptidoglycan of the strain overexpressing wild-type PBP2 had a mean glycan chain length of ~33, and the mean glycan chain length of the peptidoglycan of the other strains was between 34-37 disaccharide units (Supplementary Table 3). Such an effect of enhanced RodA GTase activity would be in agreement with the fact that a mutation in RodA could also suppress the morphological defects of MreC mutants, and would explain why PBP2^{L61R} could only poorly restore survival and rod-shape in cells depleted of MreCD or RodZ⁵⁰. The tolerance to A22 and changes in MreB dynamics in the PBP2^{L61R} background⁵⁰ could also be explained by the enhanced RodA GTase activity by PBP2^{L61R}, since a direct interaction between RodA and MreB was detected with a Ef_A value of 5.5% ± 1.7% (Table 1 and Supplementary Fig. 13). Together these results indicate

that the hyperactive PBP2^{L61R} likely behaves as PBP2^{WT} with respect to its TPase activity, and is probably in the off state conformation in the absence of MreC⁴³. All these changes in morphology, resistance to A22, sensitivity to mecillinam, partially compensation of MreCD-RodZ depletion and MreB dynamic changes are likely due to the enhanced RodA GTase activity (and perhaps PBP1A) as reported^{18,50}, which results into longer glycan chains in the peptidoglycan mesh.

In conclusion, our data show that the interaction between PBP2 and RodA is not dependent on their enzymatic activity. It is dependent on the substrate binding (mecillinam) and the periplasmic and transmembrane part of PBP2 and the balance between the presence of MreC and MreD.

Discussion

Peptidoglycan synthesis by the elongasome and divisome

In this work we aimed to reveal the regulation of peptidoglycan synthesis during length growth. Recent studies revealed a possible mechanism for the regulation of septal peptidoglycan synthesis by FtsBLQ and FtsN proteins^{19–21,51–53}. In this model, the FtsBLQ subcomplex inhibits the activities of PBP3 (consequently also inhibiting FtsW) and PBP1B, and keeps septal peptidoglycan synthesis in check. A small amount of FtsN is already present at pre-septal sites together with ZipA and the class A PBPs, PBP1A and PBP1B⁵⁴. However, only once FtsN accumulates at higher levels it is able to relieve the suppression of FtsBLQ on the peptidoglycan synthases, thereby activating septal peptidoglycan synthesis. During length growth, the elongasome proteins, such as MreC, MreD, PBP2, RodA and RodZ, localize in the lateral membrane, which makes it a challenge to investigate their cellular dynamics. Thus, it is still largely unknown how the elongasome regulates and coordinates peptidoglycan synthesis.

MreCD proteins regulate the interaction between RodA and PBP2

In this study, we showed that RodA and PBP2 form a subcomplex independent of their biochemical activities (Fig. 2). This interaction requires

the transmembrane helix and periplasmic parts of PBP2 (Fig. 3). *In vivo* FRET experiments revealed that MreC interacts directly with PBP2, which modulated the interaction between PBP2 and RodA (Fig. 4). Surprisingly, MreD also interacts with PBP2 and but has an opposite effect, as it reverses the PBP2-RodA interaction change stimulated by MreC (Fig. 4). This is similar to the regulation of septal peptidoglycan synthesis by the FtsN and FtsBLQ proteins. When comparing the cellular numbers of these proteins synthesized per generation⁴⁵, we noticed that the average number of FtsN molecules per cell is about 2 times higher than FtsBLQ and FtsW-PBP3 proteins (Supplementary table 4). FtsN is reported to interact with itself and accumulates at midcell^{55,56}, and this accumulation is assumed to finally abolish the suppression of FtsBLQ on the peptidoglycan synthesis complex FtsW-PBP3-PBP1B. The number of MreC molecules is also about 2 times higher than MreD and PBP2-RodA proteins (Supplementary table 4)⁴⁵. MreC, but not MreD, is also reported to interact with itself, and the structural data showed that two molecules of MreC bind to one PBP2 molecule⁵⁷. Together with the published data, our results indicate that the balance between the MreC and MreD determines the nature of the interaction between PBP2 and RodA. Structural data show that the interaction between MreC and PBP2, causes a conformational change in PBP2 that was suggested to correspond to its activation from the off state to the on state⁴³. This conformational change could correspond to the change in the interaction between PBP2 and RodA induced by the presences of MreC. And likely, when MreD is co-expressed with MreC, the reversed change in the interaction between PBP2 and RodA could correspond to the PBP2 conformational change from the on state to the off state. This potential MreC and MreD balances dependent activation mechanism likely reflects the regulation of elongasome activity and peptidoglycan synthesis during length growth. The overexpression of either MreC or MreD would shift this balance and result in over activation or suppression of PBP2-RodA activities, and cause morphological defects (Fig. 4e and Supplementary Fig. 7).

Based on our observations, we propose a model for the regulation of PBP2 (elongasome) activity and cylindrical peptidoglycan synthesis (Fig. 6). The peptidoglycan synthases RodA and PBP2 form a stable subcomplex.

MreC stimulates and activates PBP2 and RodA, while MreD interferes with the PBP2 MreC interaction to keep PBP2 activity and peptidoglycan synthesis in check. The further binding and accumulation of MreC to PBP2 would finally outcompete MreD, which will activate PBP2 and consequently initiate peptidoglycan synthesis. Because hydrolytic activity is required to allow insertion of newly synthesized peptidoglycan into the existing mesh^{58,59}, a balanced regulation is likely needed to avoid premature glycan strand synthesis. Consequently, the elongasome must like the divisome have a mechanism to sense whether all partners are at the right position to act. A well-regulated moment for the switching on of peptidoglycan synthesis by balancing the MreCD ratio is likely part of such a regulatory system.

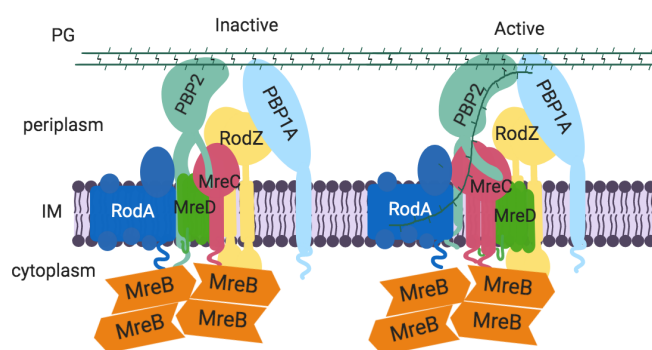


Figure 6. Model for regulation of elongasome and PG synthesis. RodA and PBP2 interact with each other and form a stable subcomplex. MreC and RodZ interact strongly with MreB filaments that likely link MreB to the PG synthesis proteins. MreC interacts with PBP2 that could stimulate and activate PBP2, while MreD, which interacts with both PBP2 and MreC, suppresses the activation of PBP2 by MreC, and keeps PG synthesis under control. The accumulation of MreC to the elongasome will finally abolish the inhibition of MreD and activate PBP2 by changing its conformation from the “off-state” to the “on-state”, and subsequently activate the elongasome and PG synthesis. Models were created with BioRender.

Materials and Methods

Media, strains, plasmids and primers

LB (10 g tryptone, 5 g yeast extract and 10 g NaCl, per liter) and Gb4 (6.33g $K_2HPO_4 \cdot 3H_2O$, 2.95g KH_2PO_4 , 1.05 g $(NH_4)_2SO_4$, 0.10 g $MgSO_4 \cdot 7H_2O$, 0.28

mg FeSO₄·7H₂O, 7.1 mg Ca(NO₃)₂·4H₂O, 4 mg thiamine, 2 mg uracil, 2 mg lysine, 2 mg thymine, and 0.5 % glucose, per liter, pH 7.0) were used for cell cultures in rich and minimal medium, respectively, as indicated. Final concentrations for antibiotics were: 100µg·L⁻¹ ampicillin, 50µg·L⁻¹ kanamycin and 25µg·L⁻¹ chloramphenicol.

E. coli strains and plasmids used in this study are listed in supplementary Table 1. Primers used in this study were listed in supplementary Table 2. The plasmids were constructed as following:

pXL29. Plasmid pXL28 and pWA004 were digested with *EcoRI* and *HindIII* restriction enzymes, the generated (GGG)₂-GlpT expressing gene and pSAV057-mKO linear vector were ligated together to generate the mKO-(GGG)₂-GlpT expressing plasmid.

pXL36, pXL40, pXL44, pXL48, pXL56 and pXL63. Plasmids pXL36 and pXL40 that expressing mCherry-fused RodA^{R109A} and RodA^{Q207R} were generated from pSAV047-RodA by mutagenesis PCR using primer pairs priXL61-priXL61 and priXL69-priXL70, respectively. To construct non-fused version of RodA variants, wild type *rodA* gene was amplified using primer priXL59 and priXL60 from the MG1655 genomic DNA and ligated into empty pSAV057 vector, to generate plasmid pXL63. The two mutants plasmids were generated in the same way as described above from pXL63. mKO fused RodA plasmid pXL56 was constructed by cutting and pasting the *rodA* gene from pSAV047-RodA to the pSAV058 plasmid with *EcoRI* and *HindIII* restriction enzymes.

pXL148, pXL149, pXL158 and pXL159. The PBP2 domain swap plasmids were constructed by Gibson assembly⁶⁰. For N-terminus replacement, primer pairs priXL146-priXL258 and priXL147-priXL259 were used for PCR from plasmid pWA004. The PCR products were purified after *DpnI* digestion and assembled to generated pXL148 that excludes the N-terminus of PBP2. For pXL149, the primer pair priXL258-priXL260 was used to amplify the entire pWA004 plasmid excluding the first 45 residues. Primer pair priXL261 and priXL263 was use to amplify the first 37 residues of MalF from MG1655 genome. The PCR products were purified after *DpnI* digestion and assembled to generate pXL149 plasmid. The PBP2^{S330C} and PBP2^{L61R}

plasmids were constructed with mutagenesis PCR from the pWA004 plasmid using primer pairs priXL274-priXL275 and priXL276-priXL277, respectively.

pXL165, pXL166 and pXL169. *mreC*, *mreCD* and *mreD* genes were amplified from MG1655 genome using primer pairs priXL282-priXL286, priXL282-priXL283 and priXL299-priXL283, respectively, and cloned into plasmid pSAV047 with *EcoRI* and *HindIII* restriction enzymes, to generate the mCherry fused version of these genes.

pXL167 and pXL168. The third plasmids used in the three-plasmids FRET experiments. *mreC* and *mreCD* genes were cloned into plasmid pSG4K5⁶¹ with Gibson assembly, respectively, and the *p_{trcdown}* promoter was introduced to control the protein expression. Primer pair priXL294-priXL295 was used to amplify the linear vector from pSG4K5. Primer pair priXL296-pp15 was used to amplify the *p_{trcdown}* promoter. Primer pairs pXL284-priXL297 and priXL284-priXL298 were used to amplify the *mreCD* and *mreD* genes, respectively.

Bacterial growth, morphology and protein localization

For general growth experiments in rich medium, overnight cultures (37 °C) were diluted 1:1000 into fresh LB medium with 0.5% glucose and the required antibiotics, and grew to OD₆₀₀ around 0.2 at 37 °C. Cultures were further diluted 1:5 into fresh LB medium with required antibiotics, and induced with 15 µM IPTG for 2 mass doubling at 37 °C (OD₆₀₀ reached around 0.2).

For complementation experiments, temperature sensitive strains expressing the mutant plasmids were grown as described above at 30 °C. Cultures were further diluted 1:5 into fresh LB medium with required antibiotics, and induced with 15 µM IPTG for 2 mass doubling at 30 °C and 42 °C, respectively (OD₆₀₀ reached around 0.2).

After induction, cells were fixed with FGA (2.8% formaldehyde and 0.04% glutaraldehyde, final concentration) for 15 minutes and centrifuged at 7000 rpm for 10 min at room temperature. Cell pellets were suspended and washed 3 times with PBS (pH7.2) buffer. Subsequently, bacterial morphology and protein localization were imaged by wide field phase contrast and

fluorescence microscopy. Specially, cells expressing the mKO fused proteins were firstly matured at 37 °C overnight before imaging by microscopy.

FRET experiment and data analysis

Protein interactions were detected by FRET as described previously^{33,37,62}. For the FRET experiments, mCherry and mKO fluorescent proteins were used as acceptor and donor fluorophores, respectively. LMC500 strain was co-transformed with the FRET pairs that were to be detected. In each FRET experiment, the empty-vector reference, mCherry reference, mKO reference were included to be able to calculate the E_{fA} by unmixing of the measured FRET pair spectrum in its individual components; background, mCherry, mKO and sensitized emission spectra. A tandem fusion of mKO-mCherry was used as positive control, and the mCherry-RodA and mKO-GlpT pair was used as negative control. After transformation, FRET strains were firstly grown in LB medium (with antibiotics and 0.5% glucose) overnight at 37 °C, and diluted 1:1000 into fresh medium and grown to OD_{600} around 0.2 at 37 °C. Subsequently, FRET strains were diluted 1:500 into Gb4 medium and grown to steady state at 28 °C (OD_{450} was kept below 0.2). All FRET strains were induced with 15 μ M IPTG (and treated with mecillinam at 2 $mg \cdot L^{-1}$ concentration as indicated) for two mass doubling before FAGA fixation. After fixation, FRET cells were pelleted by centrifugation at 7000rpm at room temperature and washed 3 times with PBS buffer (pH 7.2). Then all samples were incubated at 37 °C overnight and stored at 4 °C for 1 extra day before measured with spectrofluorimeter (Photon Technology International, NJ). Emission spectra of acceptor and donor fluorophores were measured through 6-nm slit widths with 1 second integration time per scanned nm for 3 times averaging. Filters f 587/11 nm (587/11 nm BrightLine single band-pass filter, Semrock, New York, NY, USA) and 600nm long-pass (LP) filter (Chroma Technology Corp., Bellows Falls, VT) were used for excitation and emission of acceptor fluorophore (mCherry), while 541/12 nm (Semrock) and 550 nm long pass (Chroma) filters were used for mKO excitation and emission, respectively. For calculation, measurement of PBS buffer was subtracted from all samples, and the empty-cell reference was subtracted from the donor and

acceptor spectra. The FRET efficiencies were calculated as described previously^{37,62}.

For three plasmids FRET, a third plasmid (expressing MreC or expressing MreCD both) was introduced into the whole two plasmids FRET system. Empty pSG4K5 vector was also introduced as a control to correct for the reduction in FRET efficiency due to the burden of maintaining three plasmids.

Spot assay

To test the sensitivity of *E. coli* strains to A22 and mecillinam, LMC500 strain was transformed with pWA004 (PBP2^{WT}) or pXL159 (PBP2^{L61R}). Strains expressing each construct were grown in LB medium as described above without induction. Cell cultures were diluted with varying dilution factors (Fig. 4C). A drop of 10 μl cell culture from each dilution was loaded on the LB agar dish (with chloramphenicol, 15 μM IPTG, 10 $\mu\text{g}\cdot\text{mL}^{-1}$ A22 or 2 $\mu\text{g}\cdot\text{mL}^{-1}$ mecillinam) and incubated overnight at 37 °C.

Peptidoglycan analysis

Peptidoglycan sacculi were prepared from *E. coli* cells, digested with cellosyl (kind gift from Hoechst, Germany), reduced with sodium borohydride and analyzed by high pressure liquid chromatography as described (Separation and quantification of muropeptides with high-performance liquid chromatography)⁶³.

Microscopy

Bacterial cell samples were immobilized on 1.3% agarose pads (w/v in Gb4 medium) and imaged under microscopy. Fluorescence microscopy was carried out either with an Olympus BX-60 fluorescence microscope equipped with an UPlanApo 100 \times /N.A. 1.35 oil Iris Ph3 objective, or with a Nikon Eclipse Ti microscope equipped with a C11440-22CU Hamamatsu ORCA camera, a CFI Plan Apochromat DM 100 \times oil objective, an Intensilight HG 130W lamp and the NIS elements software (version 4.20.01). Images were

acquired using the Micro Manager 1.4 plugin for ImageJ, and analyzed with Coli-Inspector supported by the ObjectJ plugin for ImageJ (version 1.49v)⁶⁴.

Acknowledgements

X.L. was supported by the Chinese Scholarship Council (File No.201406220123). W.V. received funding from the Wellcome Trust (101824/Z/13/Z). We thank Lisa Atkinson for preparation of peptidoglycan sacculi.

Author contributions

X.L and T.B. designed all the experiments. X.L. performed all experiments. Jacob Biboy and Waldemar Vollmer performed the peptidoglycan analysis experiment and analyzed the data. X.L. and T.B. analyzed all FRET data and wrote the manuscript.

Conflicting interests

The authors declare no conflicting interests.

References

1. Vollmer, W., Blanot, D. & De Pedro, M. A. Peptidoglycan structure and architecture. *FEMS Microbiol. Rev.* **32**, 149–167 (2008).
2. Mengin-Lecreux, D., Flouret, B. & Van Heijenoort, J. Cytoplasmic steps of peptidoglycan synthesis in *Escherichia coli*. *J. Bacteriol.* **151**, 1109–1117 (1982).
3. Bouhss, A., Trunkfield, A. E., Bugg, T. D. H. & Mengin-Lecreux, D. The biosynthesis of peptidoglycan lipid-linked intermediates. *FEMS Microbiology Reviews* **32**, 208–233 (2008).
4. van Heijenoort, J. Lipid Intermediates in the Biosynthesis of Bacterial Peptidoglycan. *Microbiol. Mol. Biol. Rev.* **71**, 620–635 (2007).
5. Mohammadi, T. *et al.* Specificity of the transport of lipid II by FtsW in *Escherichia coli*. *J. Biol. Chem.* **289**, 14707–14718 (2014).
6. Sham, L.-T. *et al.* MurJ is the flippase of lipid-linked precursors for peptidoglycan biogenesis. *Science (80-.)*. **345**, 220–222 (2014).
7. Sieger, B., Schubert, K., Donovan, C. & Bramkamp, M. The lipid II flippase RodA determines morphology and growth in *Corynebacterium glutamicum*. *Mol. Microbiol.* **90**, 966–982 (2013).
8. Sauvage, E., Kerff, F., Terrak, M., Ayala, J. A. & Charlier, P. The penicillin-binding proteins: Structure and role in peptidoglycan biosynthesis. *FEMS Microbiol. Rev.* **32**, 234–258 (2008).
9. Meeske, A. J. *et al.* SEDS proteins are a widespread family of bacterial cell wall polymerases. *Nature* 1–15 (2016). doi:10.1038/nature19331
10. Taguchi, A. *et al.* FtsW is a peptidoglycan polymerase that is functional only in complex with its cognate penicillin-binding protein. *Nat. Microbiol.* (2019). doi:10.1038/s41564-018-0345-x
11. Den Blaauwen, T., De Pedro, M. A., Nguyen-Distèche, M. & Ayala, J. A. Morphogenesis of rod-shaped sacculi. *FEMS Microbiol. Rev.* **32**, 321–344 (2008).
12. Pichoff, S. & Lutkenhaus, J. Tethering the Z ring to the membrane through a conserved membrane targeting sequence in FtsA. *Mol. Microbiol.* **55**, 1722–1734 (2005).
13. Schmidt, K. L. *et al.* A Predicted ABC Transporter , FtsEX , Is Needed for Cell Division in *Escherichia coli*. *J. Bacteriol.* **186**, 785–793 (2004).
14. Hale, C. A. & De Boer, P. A. J. Direct binding of FtsZ to ZipA, an essential component of the septal ring structure that mediates cell division in *E. coli*. *Cell* **88**, 175–185 (1997).
15. Aarsman, M. E. G. *et al.* Maturation of the *Escherichia coli* divisome occurs in two steps. *Mol. Microbiol.* **55**, 1631–1645 (2005).
16. den Blaauwen, T., Hamoen, L. W. & Levin, P. A. The divisome at 25: the road ahead. *Curr. Opin. Microbiol.* **36**, 85–94 (2017).
17. Van der Ploeg, R. *et al.* Colocalization and interaction between elongasome and

- divisome during a preparative cell division phase in *Escherichia coli*. *Mol. Microbiol.* **87**, 1074–1087 (2013).
18. Banzhaf, M. *et al.* Cooperativity of peptidoglycan synthases active in bacterial cell elongation. *Mol. Microbiol.* **85**, 179–194 (2012).
 19. Ranjit, D. K., Jorgenson, M. A. & Young, K. D. PBP1B Glycosyltransferase and Transpeptidase Activities Play Different Essential Roles during the De Novo Regeneration of Rod Morphology in *Escherichia coli*. *J Biol Chem* **199**, 1–17 (2017).
 20. den Blaauwen, T. & Luirink, J. Checks and Balances in Bacterial Cell Division. *MBio* **10**, 1–6 (2019).
 21. Boes, A., Olatunji, S., Breukink, E. & Terrak, M. Regulation of the peptidoglycan polymerase activity of PBP1b by antagonist actions of the core divisome proteins FtsBLQ and FtsN. *MBio* **10**, 1–16 (2019).
 22. Egan, A. J. F., Biboy, J., van't Veer, I., Breukink, E. & Vollmer, W. Activities and regulation of peptidoglycan synthases. *Philos. Trans. R. Soc. B Biol. Sci.* **370**, 20150031 (2015).
 23. van Teeffelen, S. *et al.* The bacterial actin MreB rotates, and rotation depends on cell-wall assembly. *Proc. Natl. Acad. Sci.* **108**, 15822–15827 (2011).
 24. Errington, J. Bacterial morphogenesis and the enigmatic MreB helix. *Nat Rev Micro* **13**, 241–248 (2015).
 25. White, C. L. & Gober, J. W. MreB: Pilot or passenger of cell wall synthesis? *Trends Microbiol.* **20**, 74–79 (2012).
 26. Strahl, H., Bürmann, F. & Hamoen, L. W. The actin homologue MreB organizes the bacterial cell membrane. *Nat. Commun.* **5**, 1–11 (2014).
 27. Garner, E. C. *et al.* Coupled, circumferential motions of the cell wall synthesis machinery and MreB filaments in *B. subtilis*. *Science (80-.)*. **333**, 222–5 (2011).
 28. Bendezú, F. O., Hale, C. A., Bernhardt, T. G. & De Boer, P. A. J. RodZ (YfgA) is required for proper assembly of the MreB actin cytoskeleton and cell shape in *E. coli*. *EMBO J.* **28**, 193–204 (2009).
 29. Ikebe, R., Kuwabara, Y., Chikada, T., Niki, H. & Shiomi, D. The periplasmic disordered domain of RodZ promotes its self-interaction in *Escherichia coli*. *Genes to Cells* **23**, 307–317 (2018).
 30. Kruse, T., Bork-Jensen, J. & Gerdes, K. The morphogenetic MreBCD proteins of *Escherichia coli* form an essential membrane-bound complex. *Mol. Microbiol.* **55**, 78–89 (2005).
 31. Colavin, A., Shi, H. & Huang, K. C. RodZ modulates geometric localization of the bacterial actin MreB to regulate cell shape. *Nat. Commun.* **9**, 1280 (2018).
 32. Morgenstein, R. M. *et al.* RodZ links MreB to cell wall synthesis to mediate MreB rotation and robust morphogenesis. *Proc Natl Acad Sci U S A* **112**, 12510–12515 (2015).
 33. van der Ploeg, R., Goudelis, S. T. & den Blaauwen, T. Validation of FRET assay for

- the screening of growth inhibitors of *Escherichia coli* reveals elongasome assembly dynamics. *Int. J. Mol. Sci.* **16**, 17637–17654 (2015).
34. Emami, K. *et al.* RodA as the missing glycosyltransferase in *Bacillus subtilis* and antibiotic discovery for the peptidoglycan polymerase pathway. *Nat. Microbiol.* **2**, 1–8 (2017).
 35. Takasuga, A. *et al.* Identification of the penicillin-binding active site of penicillin-binding protein 2 of *Escherichia coli*. *J. Biochem.* **104**, 822–826 (1988).
 36. Cho, H. *et al.* Bacterial cell wall biogenesis is mediated by SEDS and PBP polymerase families functioning semi-Autonomously. *Nat. Microbiol.* **1**, (2016).
 37. Meiresonne, N. Y., van der Ploeg, R., Hink, M. A. & den Blaauwen, T. Activity-related conformational changes in D,D-carboxypeptidases revealed by in vivo periplasmic Förster resonance energy transfer assay in *Escherichia coli*. *MBio* **8**, 1–18 (2017).
 38. Pastoret, S. *et al.* Functional Analysis of the Cell Division Protein FtsW of *Escherichia coli*. *J. Bacteriol.* **186**, 8370–8379 (2004).
 39. Oldham, M. L., Khare, D., Quiocho, F. A., Davidson, A. L. & Chen, J. Crystal structure of a catalytic intermediate of the maltose transporter. *Nature* **450**, 515–521 (2007).
 40. Goehring, N. W., Robichon, C. & Beckwith, J. Role for the nonessential N terminus of FtsN in divisome assembly. *J. Bacteriol.* **189**, 646–649 (2007).
 41. Meiresonne, N. Y. *et al.* Superfolder mTurquoise2 optimized for the bacterial periplasm allows high efficiency in vivo FRET of cell division antibiotic targets. *Mol. Microbiol.* **111**, 1025–1038 (2019).
 42. Müller, S. M., Galliardt, H., Schneider, J., Barisas, B. G. & Seidel, T. Quantification of Förster resonance energy transfer by monitoring sensitized emission in living plant cells. *Front. Plant Sci.* **4**, 1–20 (2013).
 43. Contreras-Martel, C. *et al.* Molecular architecture of the PBP2–MreC core bacterial cell wall synthesis complex. *Nat. Commun.* **8**, 776 (2017).
 44. Alexeeva, S., Gadella, T. W. J., Verheul, J., Verhoeven, G. S. & Den Blaauwen, T. Direct interactions of early and late assembling division proteins in *Escherichia coli* cells resolved by FRET. *Mol. Microbiol.* **77**, 384–398 (2010).
 45. Li, G. W., Burkhardt, D., Gross, C. & Weissman, J. S. Quantifying absolute protein synthesis rates reveals principles underlying allocation of cellular resources. *Cell* **157**, 624–635 (2014).
 46. Scheffers, D.-J. & Pinho, M. G. Bacterial Cell Wall Synthesis: New Insights from Localization Studies. *Microbiol. Mol. Biol. Rev.* **69**, 585 LP – 607 (2005).
 47. Holtje, J. V. Growth of the stress-bearing and shape-maintaining murein sacculus of *Escherichia coli*. *Microbiol. Mol. Biol. Rev.* **62**, 181–203 (1998).
 48. Holtje, J.-V. A hypothetical holoenzyme involved in the replication of the murein sacculus of *Escherichia coli*. *Microbiology* **142**, 1911–1918 (1996).
 49. Karczmarek, A. *et al.* DNA and origin region segregation are not affected by the transition from rod to sphere after inhibition of *Escherichia coli* MreB by A22. *Mol.*

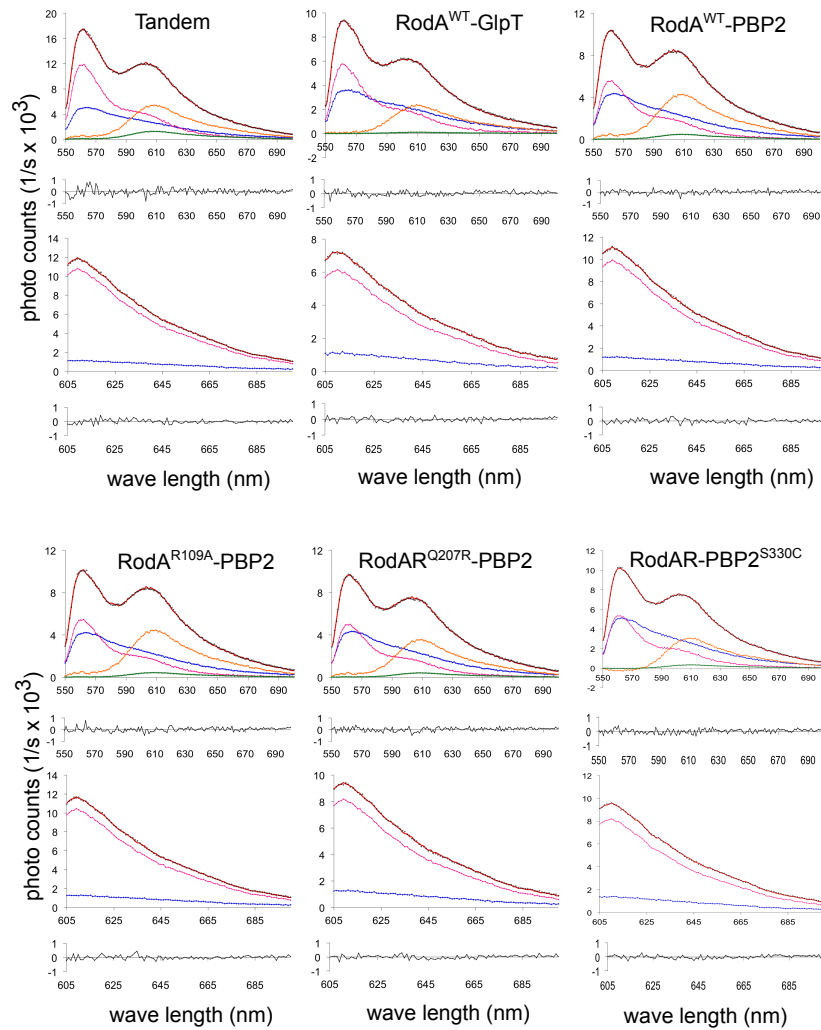
- Microbiol.* **65**, 51–63 (2007).
50. Rohs, P. D. A. *et al.* A central role for PBP2 in the activation of peptidoglycan polymerization by the bacterial cell elongation machinery. *PLoS Genet.* **14**, 1–25 (2018).
 51. Kureisaite-Ciziene, D. *et al.* Structural Analysis of the Interaction between the Bacterial Cell Division Proteins FtsQ and FtsB. *MBio* **9**, (2018).
 52. Egan, A. J. F. *et al.* Outer-membrane lipoprotein LpoB spans the periplasm to stimulate the peptidoglycan synthase PBP1B. *Proc. Natl. Acad. Sci. U. S. A.* **111**, 8197–202 (2014).
 53. Müller, P. *et al.* The essential cell division protein FtsN interacts with the murein (peptidoglycan) synthase PBP1B in *Escherichia coli*. *J. Biol. Chem.* **282**, 36394–36402 (2007).
 54. Pazos, M. *et al.* Z-ring membrane anchors associate with cell wall synthases to initiate bacterial cell division. *Nat. Commun.* **9**, 5090 (2018).
 55. Lutkenhaus, J. FtsN - Trigger for septation. *J. Bacteriol.* **191**, 7381–7382 (2009).
 56. Gerding, M. A. *et al.* Self-enhanced accumulation of FtsN at division sites and roles for other proteins with a SPOR domain (DamX, DedD, and RlpA) in *Escherichia coli* cell constriction. *J. Bacteriol.* **191**, 7383–7401 (2009).
 57. Contreras-Martel, C. *et al.* Molecular architecture of the PBP2-MreC core bacterial cell wall synthesis complex. *Nat. Commun.* **8**, 1–10 (2017).
 58. Singh, S. K., Parveen, S., SaiSree, L. & Reddy, M. Regulated proteolysis of a cross-link-specific peptidoglycan hydrolase contributes to bacterial morphogenesis. *Proc. Natl. Acad. Sci.* **112**, 10956–10961 (2015).
 59. Singh, S. K., Saisree, L., Amrutha, R. N. & Reddy, M. Three redundant murein endopeptidases catalyse an essential cleavage step in peptidoglycan synthesis of *Escherichia coli* K12. *Mol. Microbiol.* **86**, 1036–1051 (2012).
 60. Gibson, D. G. *et al.* Enzymatic assembly of DNA molecules up to several hundred kilobases. *Nat. Methods* **6**, 343–345 (2009).
 61. Standage-Beier, K., Zhang, Q. & Wang, X. Targeted Large-Scale Deletion of Bacterial Genomes Using CRISPR-Nickases. *ACS Synth. Biol.* **4**, 1217–1225 (2015).
 62. Meiresonne, N. Y., Alexeeva, S., van der Ploeg, R. & den Blaauwen, T. Detection of Protein Interactions in the Cytoplasm and Periplasm of *Escherichia coli* by Förster Resonance Energy Transfer. *Bio-protocol* **8**, e2697 (2018).
 63. Glauner, B. Separation and quantification of mucopeptides with high-performance liquid chromatography. *Anal. Biochem.* **172**, 451–464 (1988).
 64. Vischer, N. O. E. *et al.* Cell age dependent concentration of *Escherichia coli* divisome proteins analyzed with ImageJ and ObjectJ. *Front. Microbiol.* **6**, 1–18 (2015).

Supplementary informations

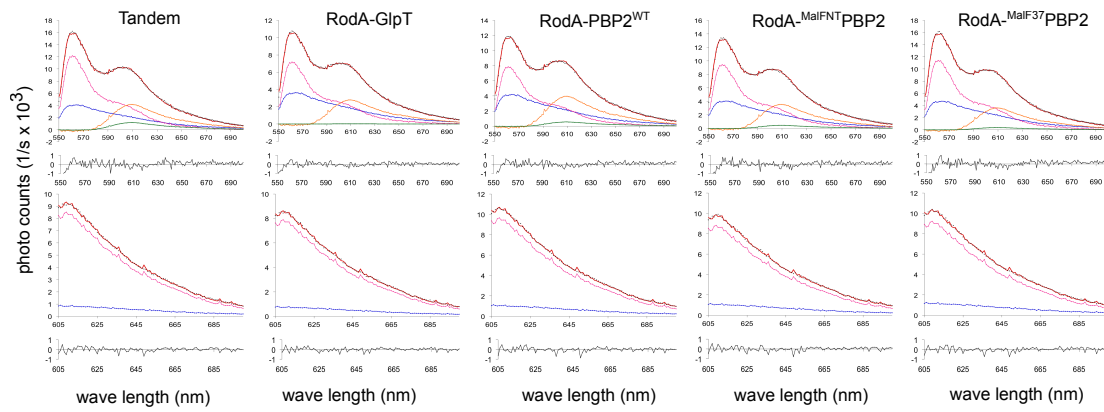
FtsW_EC	0	MRLSLPRLKMPRLPGFSILVWISTALKGWVMGSREKDTDSLIMYDRTLLWLTFLGLAAIGF	60
RodA_EC	0	-----MTDNPKNKTFWDKVLHDPFMLLILL-----ALLVYSALVIVSASG-QDIGM	45
FtsW_EC	61	IMVTSASMP IG QRLTNDPFFFAKRDGVYLILAFILAIITLRLPMEFWQRYSATMLLGSII	120
RodA_EC	46	M-----ERKIGQ-----IAMGLVIMVMAQIPPRVYEGWAPYLYIICII	84
		*	
FtsW_EC	121	LLMIVLVVVGSSVKGASRWIDLGLLR IQ PAELTKLSLFCYIANYLVRKGDEVRRNLRGFLK	180
RodA_EC	85	LLVAVDAF GA ISKGAQRWLDLGI VR F QP SEIAKIAVPLMVARF INR --DVCPPSLKNTGI	142
FtsW_EC	181	PMGVILVLAVLLLAQPDLTGVVVFVTTLAMLFLAGAKLWQFIAIIGMGISA---VLLI	237
RodA_EC	143	ALVLI F MP T LLVAAQ P DLG T SILVALSGLFVLFSLGLS-WRLIGVAVVLVAAFIPILWFF	201
		*	
FtsW_EC	238	LAEPY R IRRVTAFWNPWEDPF G SGYQ L TQSLMAFGRGELWGQ-LGNSVQKLEYLPEAHT	296
RodA_EC	202	LMHDYQRQRVMMLLD P ESD P L G AGYHIIQ S KIAIGSGGLRGK G WLHGTQ S Q L E F LP R HT	261
FtsW_EC	297	DFIFAI T GEELGYVGVVLAALLMVFFVAFRAMS I GRKALEIDHRFSGFLAC S IGIWF S FQA	356
RodA_EC	262	DFIFAVLA E E L GLV G IL L LLALY I LLIMRGLWIAARA---Q T FGRVMAGGLMLILFVYV	318
FtsW_EC	257	LNVN G AA G M L P T K L T L PLISYGGSSLLIMSTAIMMLLRIDYETRLEKAQAFV R GS R	414
RodA_EC	319	FVN I GMV S G I LPV V GV L PL V SYGG S AL I VLMAGFG I VMS I H T HR K MLS K SV-----	370

Supplementary Figure 1. Alignment of homologous proteins RodA and FtsW from *E.coli*.

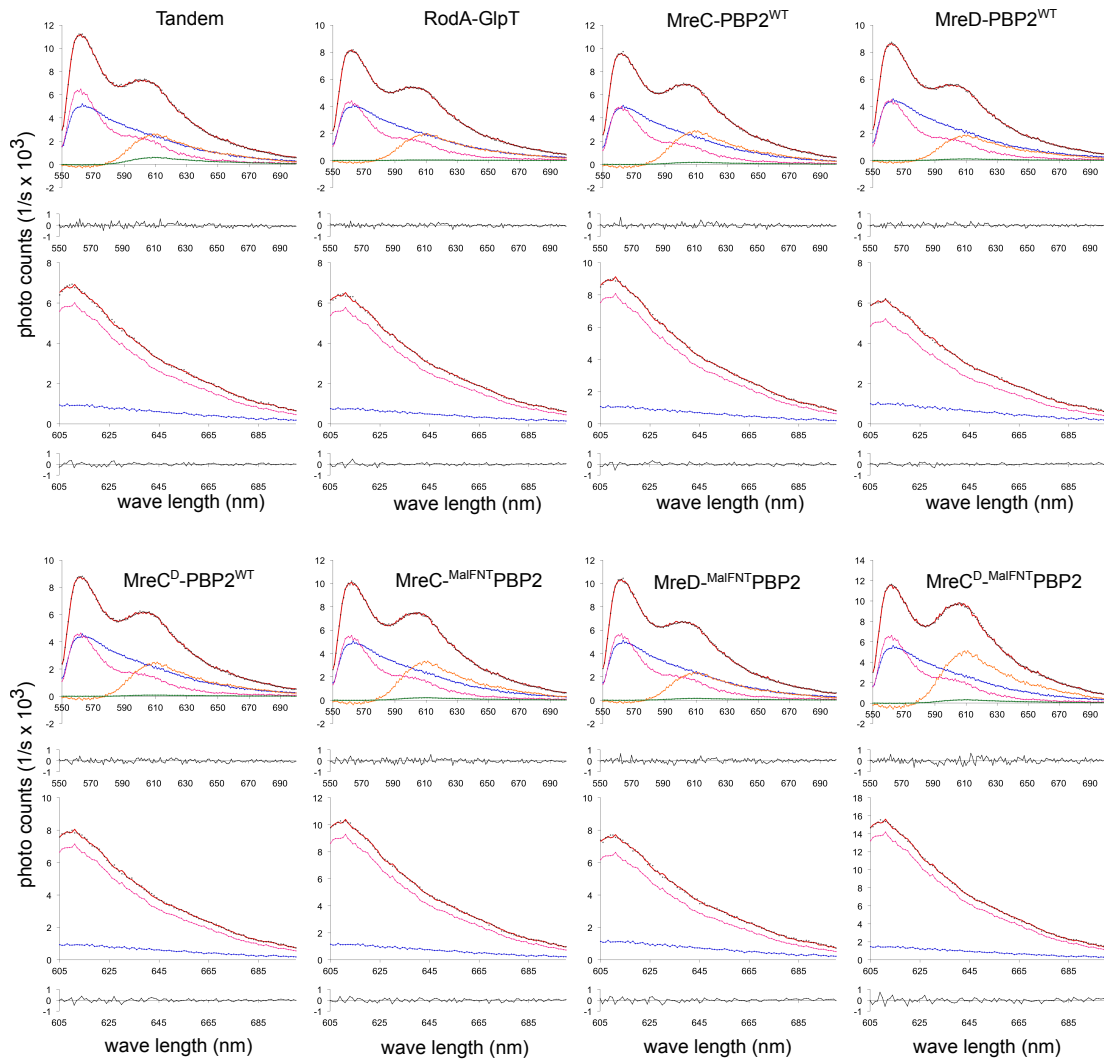
The two inactive RodA mutants were constructed based on the previous functional studies of FtsW^{1,2} (bold in red and labeled with *). The protein sequences alignment was generated with the online tool Multiple Sequence Alignment (MUSCLE). A given column has one color which indicates the average BLOSUM62 score of the paired residues in each protein: light blue>=3 identical, light gray>=2 similar, no color otherwise.



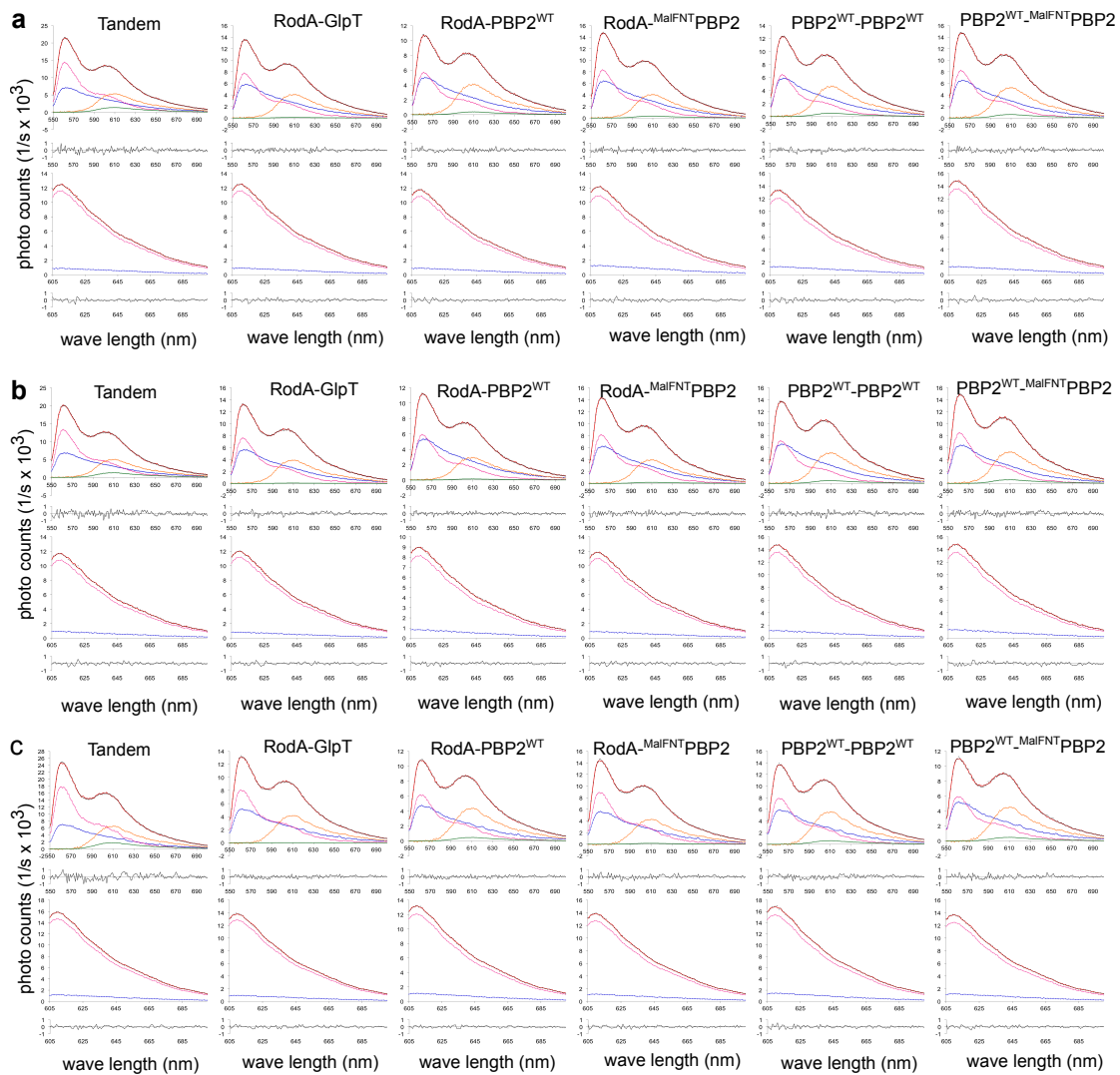
Supplementary Figure. 2. Overview of the unmixing data of all the FRET groups showed in the list in Fig. 2b. LMC500 strain expressing each FRET pair was grown in Gb4 medium to steady state at 28 °C and induced with 15 μ M IPTG for 2 mass doublings. The FRET pairs listed above the graphs apply to the spectra data beneath them. For each pair the upper panel contains the measured spectrum excited at 538 nm in black dots, the calculated spectrum and its unmixed components; blue is background, magenta is mKO, orange is mCherry and green is the sensitized emission. The middle panel is the measured spectrum of mCherry excited at 590 nm in black dots, the calculated spectrum and its unmixed components; blue is background and magenta is mCherry. The bottom panel shows the residuals of the measured and calculated spectrum.



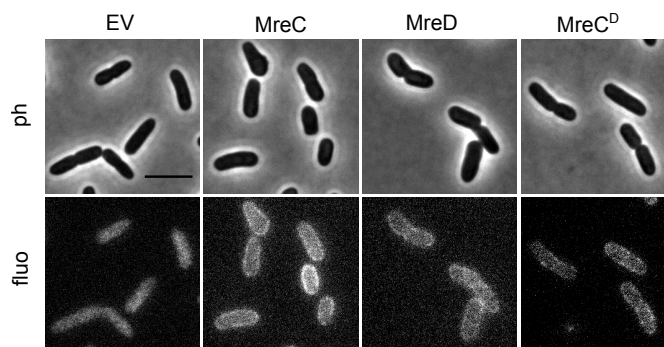
Supplementary Figure 3. Overview of the unmixing data of all the FRET groups between RodA and PBP2 domain swap variants that are listed in Fig. 3c. LMC500 strain expressing each FRET pair was grown in Gb4 medium to steady state at 28 °C and induced with 15 μ M IPTG for 2 mass doublings. The FRET pairs listed above the graphs apply to the spectra data beneath them. The FRET pairs listed above the graphs apply to the spectra data beneath them. Panels as in figure S2.



Supplementary Figure 4. Overview of the unmixing data of all the FRET groups between MreCD and PBP2 variants that are listed in Fig. 4c. LMC500 strain expressing each FRET pair was grown in Gb4 medium to steady state at 28 °C and induced with 15 μ M IPTG for 2 mass doublings. The FRET pairs listed above the graphs apply to the spectra data beneath them. MreC^D, MreC and MreD were expressed from one same plasmid, and MreC was fused with mCherry while MreD was not fused. Panels as in figure S2.



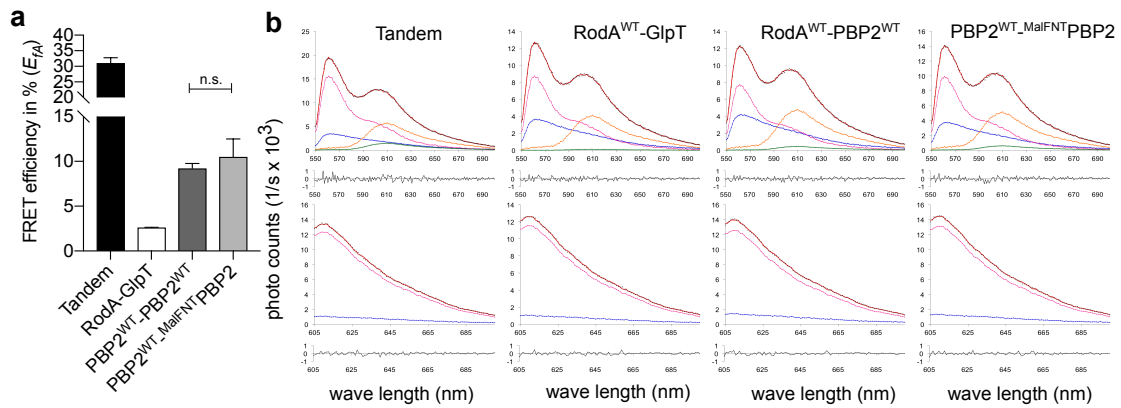
Supplementary figure 5. Overview of the unmixing data of all the three plasmids FRET groups that are listed in Fig. 4d. LMC500 strain containing three plasmids (FRET pairs and the third plasmid) was grown in Gb4 medium to steady state at 28 °C and induced with 15 μ M IPTG for 2 mass doublings. **a, b and c.** Unmixing data of FRET experiments in the presence of the third: empty vector (EV), or MreC (expressing MreC alone from the third plasmid under a $P_{trcdown}$ promoter) or MreCD (expressing MreCD together from the third plasmid under a $P_{trcdown}$ promoter), respectively. The FRET pairs listed above the graphs apply to the spectra data beneath. Panels as in figure S2.



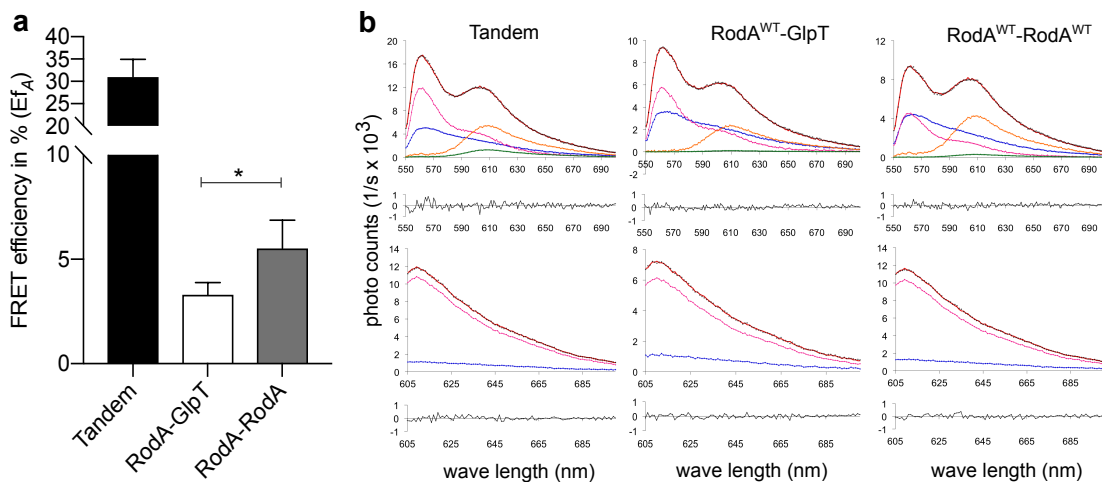
Supplementary figure 6. Co-expression of MreD suppresses the morphological defects of MreC overexpression. Phase contrast (upper panels) and fluorescent (bottom panels) images of morphology and FP-protein localization of LMC500 strain expressing the mCherry (control), mCherry-MreC, mCherry-MreD or mCherry-MreCD (MreCD were expressed from one plasmid and MreC was fused with mCherry, while MreD was non-fused). Cells were growth in LB medium at 37 °C and induced with 15 μM IPTG for 2 mass doublings. Scale bar equals 5 μm.

	1				50
Seq.	MASYRSQGRW	VIWLSFLIAL	LLQIMPWPDN	LIVFRPNWVL	LILLYWILAL
TOPCONS	iiiiiiiMMM	MMMMMMMMMM	MMMMMMMMoM	MMMMMMMMMM	MMMMMMMMMM
OCTOPUS	iiiiiiiMMM	MMMMMMMMMM	MMMMMMMMoo	oooooooooMM	MMMMMMMMMM
Philius	iiiiiiiim	MMMMMMMMMM	MMMMMMooo	ooooooooooo	MMMMMMMMMM
PolyPhobius	oooooooooM	MMMMMMMMMM	MMMMMMiii	iiiiiiiMMM	MMMMMMMMMM
SCAMPI	iiiiiiiMMM	MMMMMMMMMM	MMMMMMMMoM	MMMMMMMMMM	MMMMMMMMMM
SPOCTOPUS	iiiiiiiMMM	MMMMMMMMMM	MMMMMMMMoo	oooooooooMM	MMMMMMMMMM
HMMTOP	iiiiiiiim	MMMMMMMMMM	MMMMooMM	MMMMMMMMMM	MMMMMMMMMM
	51				100
Seq.	PHRVNVGTGF	VMGAILDLIS	GSTLGVRVLA	MSIIAYLVAL	KYQLFRNLAL
TOPCONS	iMMMMMMMMM	MMMMMMMMMM	MMoMMMMMM	MMMMMMMMMM	MMMMiiiiim
OCTOPUS	MMMiMMMMMM	MMMMMMMMMMo	MMMMMMMMMM	MMMMMMMMMM	Miiiiiiiim
Philius	oooooooooo	ooMMMMMMMM	MMMMMMMMMM	MMMMMMMMMM	iiiiiiiMM
PolyPhobius	MMMMMMMMMM	MMMoMMMM	MMMMMMMMMM	MMMMMMMMMM	Miiiiiiiim
SCAMPI	iiMMMMMMMM	MMMMMMMMMM	MMMoMMMM	MMMMMMMMMM	MMMMMiiim
SPOCTOPUS	MMMiMMMMMM	MMMMMMMMMMo	MMMMMMMMMM	MMMMMMMMMM	Miiiiiiiim
HMMTOP	iiMMMMMMMM	MMMMMMMMMMo	ooMMMMMMMM	MMMMMMMMMM	iiiiiiiim
	101				150
Seq.	WQQALVVMLL	SLVVDIIVFW	AEFLVINVSF	RPEVFWSSV	NGVLWPWIFL
TOPCONS	MMMMMMMMMM	MMMMMMMMMM	oooooooooo	oMMMMMMMM	MMMMMMMMMM
OCTOPUS	MMMMMMMMMM	MMMMMMMMMM	oooooooooo	oMMMMMMMM	MMMMMMMMMM
Philius	MMMMMMMMMM	MMMMMMMMMM	MMMoooooo	ooMMMMMM	MMMMMMMMMM
PolyPhobius	iMMMMMMMMM	MMMMMMMMMM	Mooooooooo	oMMMMMMMM	MMMMMMMMMM
SCAMPI	MMMMMMMMMM	MMMMMMMMMM	oooooooooo	oMMMMMMMM	MMMMMMMMMM
SPOCTOPUS	MMMMMMMMMM	MMMMMMMMMM	oooooooooo	oMMMMMMMM	MMMMMMMMMM
HMMTOP	iiMMMMMMMM	MMMMMMMMMM	oooooooooo	ooMMMMMM	MMMMMMMMMM
	151	162			
Seq.	LMRKVRQQFA	VQ			
TOPCONS	MMiiiiiii	ii			
OCTOPUS	MMiiiiiii	ii			
Philius	Miiiiiii	ii			
PolyPhobius	MMiiiiiii	ii			
SCAMPI	MMiiiiiii	ii			
SPOCTOPUS	MMiiiiiii	ii			
HMMTOP	Miiiiiii	ii			

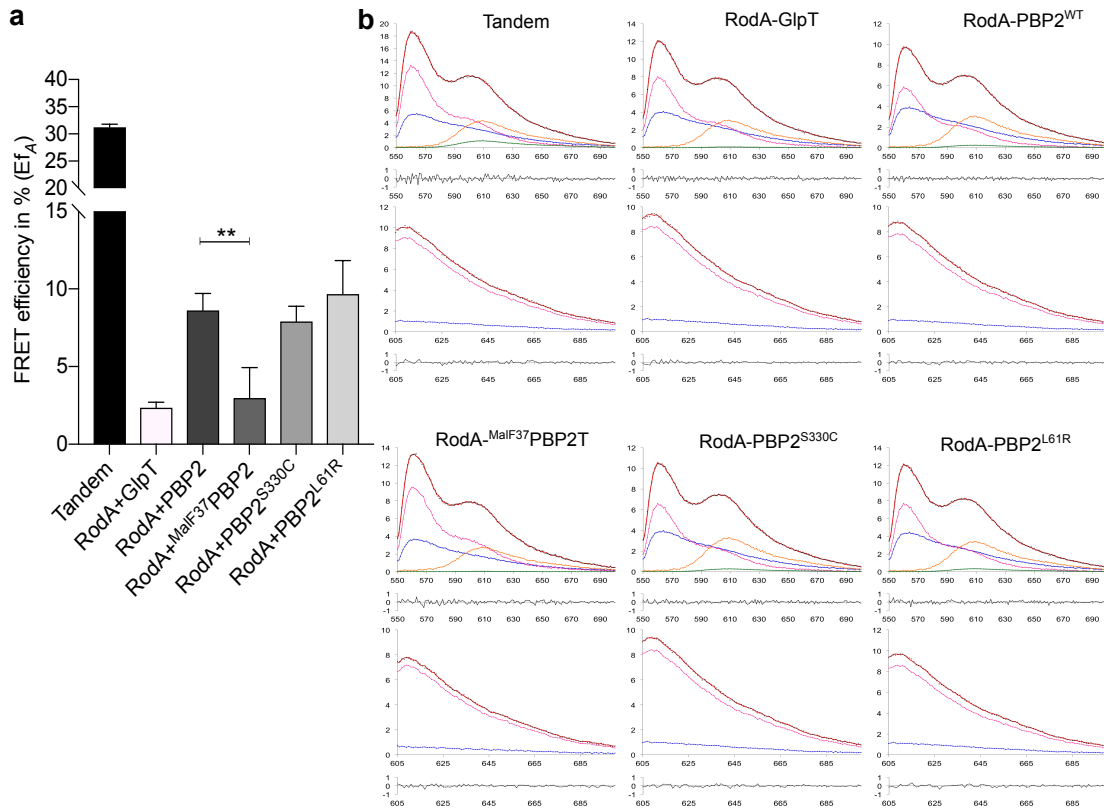
Supplementary figure 7. MreD topology predictions generated from various services as indicated. Numbers: MreD amino acid position. i: in the cytoplasm. o: in the periplasm. M: transmembrane sequences.



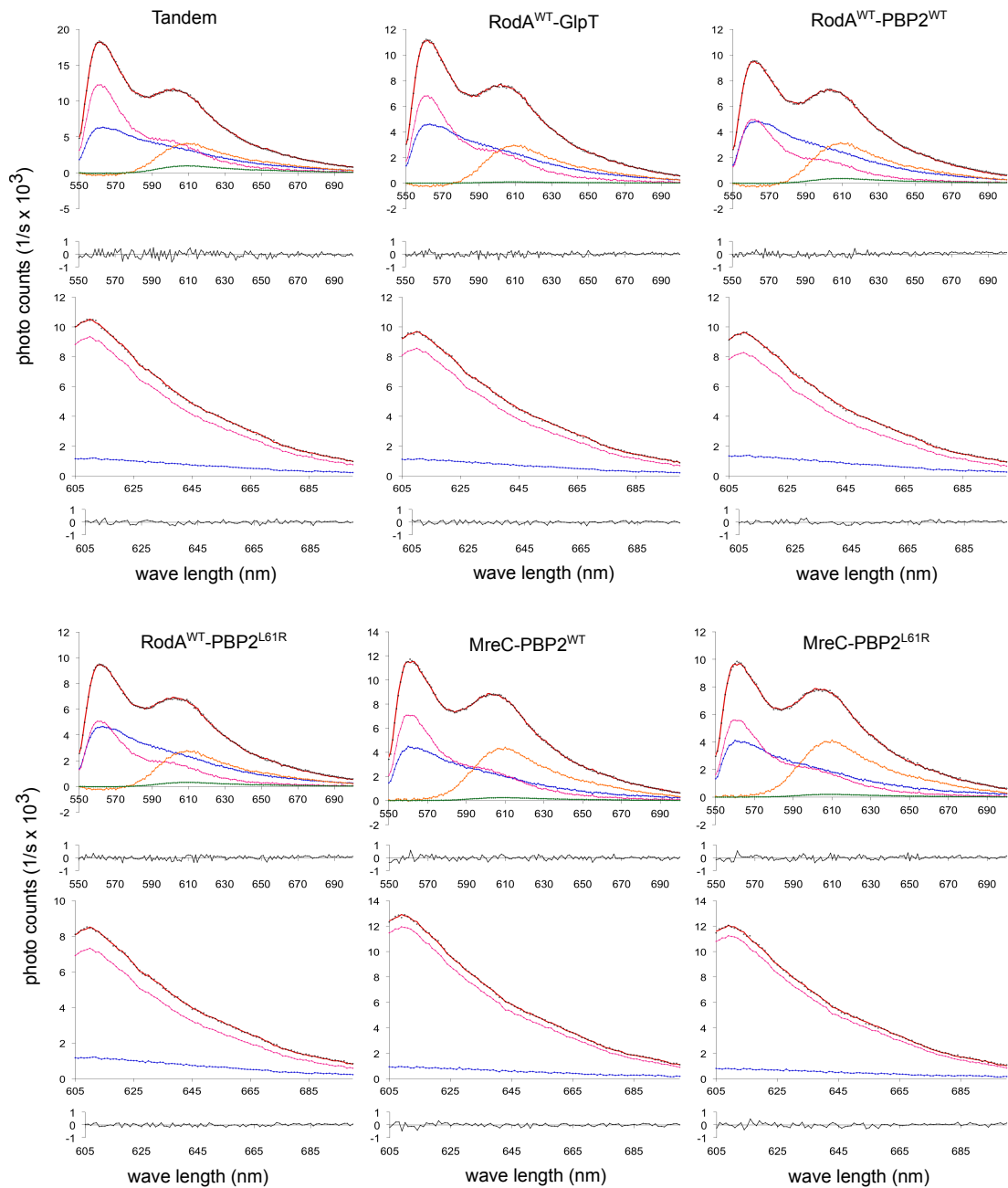
Supplementary figure 8. The cytoplasmic N-terminus of PBP2 is not essential for its self-interaction. LMC500 strain expressing each FRET pair was grown in Gb4 medium to steady state at 28 °C and induced with 15 μ M IPTG for 2 mass doublings. **a.** Acceptor FRET efficiency (E_{FA}) between PBP2 and PBP2 calculated from the spectral FRET measurements. P value determined with Student's t-test (n.s.: not significant). **b.** Overview of the unmixing data of all the FRET pairs showed in this figure. The FRET pairs listed above the graphs apply to the spectra data beneath them. Panels as in figure S2.



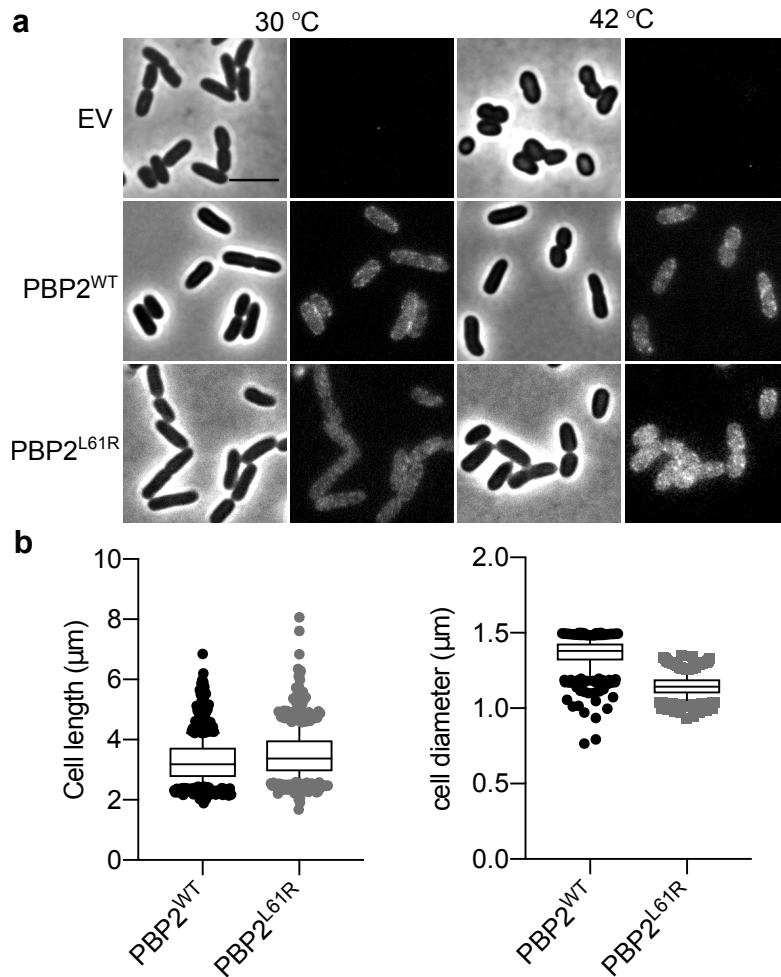
Supplementary figure 9. Self-interaction of RodA detected by FRET. LMC500 strain expressing each FRET pair was grown in Gb4 medium to steady state at 28 °C and induced with 15 μ M IPTG for 2 mass doublings. **a.** Acceptor FRET efficiency (E_{FA}) between RodA and RodA calculated from the spectral FRET measurements. P value determined with Student's t-test (*: $p < 0.05$). **b.** Overview of the unmixing data of all the FRET pairs showed in this figure. The FRET pairs listed above the graphs apply to the spectra data beneath them. Panels as in figure S2.



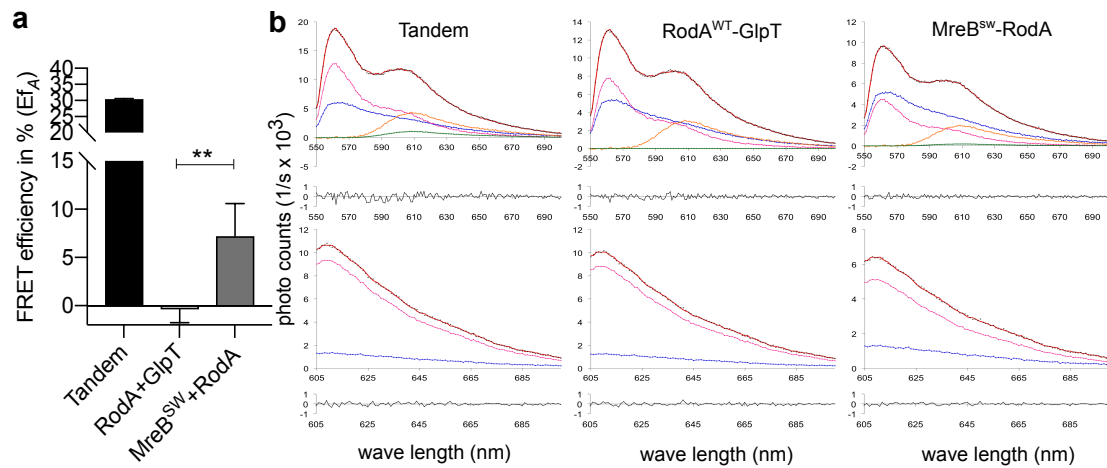
Supplementary figure 10. Interaction between RodA and PBP2 variants detected with FRET in the presence of mecillinam. LMC500 strain expressing each FRET pair was grown in Gb4 medium to steady state at 28 °C, and induced with 15 μ M IPTG and treated with mecillinam (2 μ g·mL⁻¹) for 2 mass doublings. **a.** Acceptor FRET efficiency (E_{f_A}) calculated from the spectral FRET measurements. P value determined with Student's t-test (**: $p < 0.001$). **b.** Overview of the unmixing data of all the FRET sample showed in Figure 10a. The FRET pairs listed above the graphs apply to the spectra data beneath them. Panels as in figure S2.



Supplementary figure 11. Overview of the unmixing data of all the FRET groups between hyperactive PBP2^{L61R} and its interaction partners that are listed in Fig. 4a. LMC500 strain expressing each FRET pair was grown in Gb4 medium to steady state at 28 °C and induced with 15 μ M IPTG for 2 mass doublings. The FRET pairs listed above the graphs apply to the spectra data beneath them. Panels as in figure S2.



Supplementary figure 12. Hyperactive mutant PBP2^{L61R}. **a.** Phase contrast and fluorescence images of the complementation of PBP2^{WT} and hyperactive PBP2^{L61R}. PBP2 temperature sensitive strain LMC582 was transformed with empty vector (EV), or mKO-PBP2^{WT} plasmid, or mKO-PBP2^{L61R} plasmid and grown in LB medium at 30 °C (left panels) and 42 °C (right panels), respectively, and induced with 15 μM IPTG for 2 mass doublings. Scale bar equals 5 μm. **b.** Expression of the hyperactive PBP2^{L61R} results into longer (slightly) and thinner cells. LMC500 strain was transformed with plasmid expressing either mKO-PBP2^{WT} or mKO-PBP2^{L61R}, and grown in LB at 37 °C and induced with 15 μM IPTG for 2 mass doublings. Cells were fixed and imaged by microscopy. Over 1000 cells were measured for statistical analysis.



Supplementary figure 13. Direct interaction between RodA and MreB detected with FRET. LMC500 strain expressing each FRET pair was grown in Gb4 medium to steady state at 28 °C and induced with 15 μ M IPTG for 2 mass doublings. **a.** Acceptor FRET efficiency (E_{fA}) calculated from the spectral FRET measurements. P value determined with Student's t-test ($p < 0.01$.: very significant). **b.** Overview of the unmixing data of all the FRET sample showed in Figure 12a. The FRET pairs listed above the graphs apply to the spectra data beneath them. Panels as in figure S2.

Supplementary table 1. Strains and plasmids used in this study.

	Relevant properties	References
Strains		
DH5 α	<i>supE44 ΔlacU169 (Φ80lacZΔM15) hsdR17 recA1 endA1 gyrA96 thi-1 relA1</i>	Lab stock
LMC500 (MC4100 <i>lysA</i>)	<i>F araD139 Δ(argF-lac)U169 deoC1 flbB5301 ptsF25 rbsR relA1 rpsL150 lysA1</i>	Lab stock ³
LMC882	<i>his,purB,proA,thi,lacY,rpsL,rodA(Ts)-52,zbe::Tn10</i>	Lab stock ⁴
LMC582	<i>LMC500 pbpa137 (ts)</i>	Lab stock ⁵
Plasmids		
pTHV037	pTRC99A with a weakened P _{trcdown} promoter. pBR322 ori, ampicillin resistance	Lab stock ⁶
pSAV057	pTRC99A with a weakened P _{trcdown} promoter. p15A ori, chloramphenicol resistance	Lab stock ⁶
pSG4K5	The empty third plasmid used for three-plasmids FRET. pSC101 ori, Kanamycin resistance	Lab stock ⁷
pSAV047	pTHV037 expressing with mcherry gene	Lab stock ⁶
pSAV058	pSAV057 expressing mKO gene	Lab stock ⁶
pSAV050	pSAV057 expressing mCherry-mKO tandem gene	Lab stock ⁶
pSAV047-RodA	pTHV037 expressing mCh-RodA fusion gene linked with five codons	Lab stock ⁶
pWA003	pTHV037 expressing mCh-PBP2 fusion gene	Lab stock ⁶
pWA004	pSAV057 expressing mKO-PBP2 fusion gene	Lab stock ⁶
pRP058	pTHV037 expressing mCh-MreB sandwich fusion gene	Lab stock ⁶
pXL28	pSAV057 expressing mNG-(GGG) ₂ -GlpT fusion gene	Lab stock ⁶⁸
pXL29	pSAV057 expressing mKO-(GGG) ₂ -GlpT fusion gene	This study
pXL36	pTHV037 expressing mCh-RodA ^{R109A} fusion gene	This study
pXL40	pTHV037 expressing mCh-RodA ^{Q207R} fusion gene	This study
pXL44	pSAV057 expressing RodA ^{R109A} gene	This study
pXL48	pSAV057 expressing RodA ^{Q207R} gene	This study
pXL56	pSAV057 expressing mKO-RodA fusion gene linked with five codons	This study
pXL63	pSAV057 expressing RodA ^{V1} gene	This study
pXL148	pSAV057 expressing mKO-MalI ^{N1} PBP2 fusion gene	This study
pXL149	pSAV057 expressing mKO-MalI ³⁷ PBP2 fusion gene	This study
pXL158	pSAV057 expressing mKO-PBP2 ^{S330C} fusion gene	This study
pXL159	pSAV057 expressing mKO-PBP2 ^{L61R} fusion gene	This study
pXL165	pTHV037 expressing mCh-MreC fusion gene that linked with 5 codons	This study

pXL166	pTHV037 expressing mCh-MreCD genes. MreC is fused to mCh with 5 codons. MreD is not fused	This study
pXL167	pSG4K5-derivative that expressing MreC genes under the $P_{trcdwon}$ promoter. Used for three plasmids FRET	This study
pXL168	pSG4K5-derivative that expressing MreCD genes under the $P_{trcdwon}$ promoter. Used for three plasmids FRET	This study
pXL169	pTHV037 expressing mCh-MreD fusion gene that linked with 5 codons	This study

Supplementary table 2. Primers used in this study.

Primer	Sequence 5'-3'	Description
priXL59	GCGCGAATTCATGACGGATAATCCGAATAAA	EcoRI-RodA-F
priXL60	GCGCAAGCTTTTACACGCTTTTCGACAACAT	HindIII-RodA-R
priXL61	CGACGGCTGAAAGGCAACAATACCTAGGTCCAG CC	RodA-R109A-R
priXL69	ATGCATGATTACCGTCGCCAGCGC	RodA-Q207R-F
priXL70	GCGCTGGCGACGGTAATCATGCAT	RodA-Q207R-R
priXL146	TGCTGCCAGTGGTGCTTTTGCAT	GA-57bone-F
priXL147	CTTGAGTCCAACCCGAAAGACA	GA-57bone-R
priXL258	TCGCTTTGCCACCAATGTTTCTTTTAAATGACATC CATGTTGTTGTTGAATTCGGAATG	GA-mKO-NNN-MalF-R
priXL259	ATTAAAAAGAAACATTGGTGGCAAAGCGACGCG CTGAAAGCGCTGGTCGCCTTTTTGGG	GA-PBP2-del-NT-F
priXL260	GCTGGTGGGTTACCTTGTGTTTAAATGTATGGC CAGCGCTTACCGACTACCAGACC	GA-PBP2-del42-F
priXL261	ATGGATGTCATTA AAAAGAAAC	MalF-F
priXL263	CTGGCCATACATTA AAAACAAC	MalF-NTTMH1-R
priXL274	GTTTATCCGCCGCGGTGTACAGTTAAACC	PBP2-S330C-F
priXL275	GGTTAACTGTACACGCCGCGGATAAACCCCC T	PBP2-S330C-R
priXL276	CGCATTAAGCGGGTGCCGATCGCGCC	PBP2-L61R-F
priXL277	TGGGCGCGATCGGCACCCGCTTAATGCGGT	PBP2-L61R-R
priXL282	CCCGAATTCAACAACAACATGAAGCCAATTTTAA GCCGTGG	EcoRI-MreCD-F
priXL283	GCGCAAGCTTTTATTGCACTGCAAACCTGCTGAC	HindIII-MreCD-R

MreC and MreD balance RodA-PBP2 interaction

priXL284	TGAGCGGATAACAATTTACACAGGAAACAGACC ATGAAGCCAATTTTTAGCCGTGG	MreCD-GA-F
priXL286	GCGCAAGCTTTATTGCCCTCCCGGCACG	HindIII-MreC-R
priXL299	GCGCGAATTCAACAACAACGTGGCGAGCTATCG TAGCCA	EcoRI-NNN-MreD-F
priXL294	CTAGATAATTGGAGACCGAGCT	GA-pXL167-168-F1
priXL295	CGAATTCGAGTCACTAAGGGCT	GA-pXL167-168-R1
priXL296	GTAATTAGTTAGTTAGCCCTTAGTGACTCGAATT CGCTGGCAAATATTCTGAAATGAGC	GA-pXL167-168-F2
priXL297	ACATCCTAGAGAGACCAGCTCGGTCTCCAATTAT CTAGCTATTGCCCTCCCGGCACG	GA-pXL167-R
priXL298	ATCCTAGAGAGACCAGCTCGGTCTCCAATTATCT AGTTATTGCACTGCAAAGTCTGAC	GA-pXL168-R
PP15	GGTCTGTTTCCTGTGTGAAATTGTTATCCGC	p _{trcd} down-R

Supplementary table 3. Details of muropeptide composition of LMC500 strains carrying no plasmid or different plasmids.

Muropeptide ² or Feature	Percent peak area (%) ¹				
	LMC500	LMC500 mKO	LMC500 mKO- GlpT	LMC500 mKO-PBP2	LMC500 mKO- PBP2 ^{L61R}
Tri	5.0 ± 0.2	4.9 ± 0.0	4.7 ± 0.1	5.0 ± 0.4	4.0 ± 0.2
TetraGly	1.0 ± 0.0	1.0 ± 0.0	1.1 ± 0.1	1.5 ± 0.0	1.2 ± 0.1
Tetra	41.5 ± 0.2	40.8 ± 0.0	42.8 ± 0.2	41.0 ± 0.2	43.1 ± 1.3
Di	1.4 ± 0.0	1.6 ± 0.1	1.4 ± 0.0	1.3 ± 0.1	1.2 ± 0.0
TriLysArg	3.7 ± 0.4	3.4 ± 0.2	3.4 ± 0.5	3.5 ± 0.5	3.0 ± 1.2
TetraTri(Dap)	1.4 ± 0.2	1.5 ± 0.0	1.8 ± 0.2	2.1 ± 0.2	2.4 ± 0.3
TetraTetraGly	0.2 ± 0.1	0.4 ± 0.0	0.2 ± 0.1	0.2 ± 0.1	0.2 ± 0.1
TetraTri	3.1 ± 0.3	2.9 ± 0.2	2.9 ± 0.1	3.0 ± 0.1	2.2 ± 0.0
TetraTetra	33.6 ± 0.8	33.6 ± 0.4	33.8 ± 0.3	32.4 ± 2.1	35.1 ± 2.2
TetraAnh	0.9 ± 0.0	1.0 ± 0.0	1.0 ± 0.0	1.0 ± 0.0	0.7 ± 0.0
TetraTri Lys Arg	1.5 ± 0.1	1.7 ± 0.1	1.6 ± 0.1	1.5 ± 0.2	1.2 ± 0.2
TetraTetraTetra	3.3 ± 0.0	3.4 ± 0.0	3.4 ± 0.0	3.4 ± 0.0	2.9 ± 0.0
TetraTetraAnh I	1.1 ± 0.0	1.1 ± 0.0	1.1 ± 0.0	1.2 ± 0.1	1.0 ± 0.0
TetraTetraAnh II	0.9 ± 0.0	1.0 ± 0.0	0.9 ± 0.0	1.0 ± 0.0	0.7 ± 0.0
TetraTetraTetra Anh	1.1 ± 0.0	1.2 ± 0.0	1.1 ± 0.0	1.3 ± 0.0	0.8 ± 0.0
Sum of all known	99.6 ± 0.3	99.4 ± 0.1	100 ± 0.0	99.2 ± 0.4	99.6 ± 0.4
Monomers (total)	52.6 ± 0.1	52.0 ± 0.0	52.2 ± 0.0	52.1 ± 1.1	52.2 ± 0.9
di peptides	1.4 ± 0.0	1.6 ± 0.1	1.4 ± 0.0	1.3 ± 0.1	1.2 ± 0.0
tri peptides	5.0 ± 0.2	5.0 ± 0.0	4.7 ± 0.1	5.0 ± 0.5	4.0 ± 0.3
tetra peptides	41.6 ± 0.0	41.0 ± 0.0	41.8 ± 0.2	41.3 ± 0.5	43.3 ± 2.0
anhydro	0.9 ± 0.0	1.0 ± 0.0	1.0 ± 0.0	1.0 ± 0.0	0.7 ± 0.0
LysArg	3.7 ± 0.4	3.4 ± 0.2	3.4 ± 0.5	3.5 ± 0.5	3.0 ± 1.2
Dimers (total)	40.5 ± 0.0	40.8 ± 0.0	40.7 ± 0.1	40.2 ± 0.7	41.7 ± 0.9
tetratri peptide	3.1 ± 0.3	3.0 ± 0.2	2.9 ± 0.1	3.0 ± 0.1	2.2 ± 0.0
tetratetra peptide	36.0 ± 1.0	36.3 ± 0.2	36.0 ± 0.9	35.0 ± 2.6	37.1 ± 2.7
anhydro	2.0 ± 0.0	2.1 ± 0.0	2.0 ± 0.0	2.2 ± 0.0	1.7 ± 0.0
LysArg	1.6 ± 0.0	1.7 ± 0.1	1.6 ± 0.1	1.5 ± 0.2	1.2 ± 0.2
Trimers (Total)	4.4 ± 0.1	4.6 ± 0.1	4.5 ± 0.1	4.8 ± 0.0	3.8 ± 0.0
Dipeptides (total)	1.4 ± 0.0	1.6 ± 0.1	1.4 ± 0.0	1.3 ± 0.1	1.2 ± 0.0
Tripeptides (total)	7.2 ± 0.9	7.2 ± 0.2	7.0 ± 0.3	7.6 ± 1.1	6.3 ± 0.7
Tetrapeptides (total)	85.8 ± 0.1	85.8 ± 0.0	86.2 ± 0.0	85.3 ± 0.1	87.7 ± 0.0

¹ values are mean ± variation of two biological replicates.

² muropeptide names according to Glauner, 1988.

³ average glycan chain length in disaccharide (DS) units calculated from the percentage of anhydro-MurNAc containing muropeptides.

Supplementary table 4. Molecular number^a of elongasome and divisome proteins in *E.coli*.

Protein	MOPS complete	MOPS minimal	MOPS complete without methionine
FtsQ	336	147	172
FtsL	416	201	423
FtsB	487	140	173
FtsN	871	269	405
FtsW	293	117	169
PBP3	349	144	226
PBP1B	521	139	259
MreC	738	176	333
MreD	367	71	148
RodA	435	103	156
PBP2	324	76	148
PBP1A	554	116	135

^a. Molecular number of each protein are published in previous research⁹.

References

1. Pastoret, S. *et al.* Functional Analysis of the Cell Division Protein FtsW of Escherichia coli. *J. Bacteriol.* **186**, 8370–8379 (2004).
2. Mohammadi, T. *et al.* Specificity of the transport of lipid II by FtsW in Escherichia coli. *J. Biol. Chem.* **289**, 14707–14718 (2014).
3. Taschner, P. E., Huls, P. G., Pas, E. & Woldringh, C. L. Division behavior and shape changes in isogenic ftsZ, ftsQ, ftsA, pbpB, and ftsE cell division mutants of Escherichia coli during temperature shift experiments. *J. Bacteriol.* **170**, 1533–1540 (1988).
4. Matsuzawa, H., Hayakawa, K., Sato, T. & Imahori, K. Characterization and genetic analysis of a mutant of Escherichia coli K-12 with rounded morphology. *J. Bacteriol.* **115**, 436–442 (1973).
5. Van der Ploeg, R. *et al.* Colocalization and interaction between elongasome and divisome during a preparative cell division phase in Escherichia coli. *Mol. Microbiol.* **87**, 1074–1087 (2013).
6. van der Ploeg, R., Goudelis, S. T. & den Blaauwen, T. Validation of FRET assay for the screening of growth inhibitors of escherichia coli reveals elongasome assembly dynamics. *Int. J. Mol. Sci.* **16**, 17637–17654 (2015).
7. Standage-Beier, K., Zhang, Q. & Wang, X. Targeted Large-Scale Deletion of Bacterial Genomes Using CRISPR-Nickases. *ACS Synth. Biol.* **4**, 1217–1225 (2015).
8. To Sham, L., Zheng, S., Yakhnina, A. A., Kruse, A. C. & Bernhardt, T. G. Loss of specificity variants of WzxC suggest that substrate recognition is coupled with transporter opening in MOP-family flippases. *Mol. Microbiol.* 1–33 (2018). doi:10.1111/mmi.14002
9. Li, G. W., Burkhardt, D., Gross, C. & Weissman, J. S. Quantifying absolute protein synthesis rates reveals principles underlying allocation of cellular resources. *Cell* **157**, 624–635 (2014).

CHAPTER

4

Interaction between RodA and MreCD proteins is essential for MreB localization and elongasome function

Xiaolong Liu

Tanneke den Blaauwen*

*Bacterial Cell Biology and Physiology, Swammerdam Institute for Life Sciences, Faculty of
Science, University of Amsterdam, Amsterdam, The Netherlands.*

**Corresponding author*

Manuscript in preparation

Abstract

The rod-shape of *E. coli* is maintained by a protein complex, comprising RodZ, MreB, MreC, MreD, PBP2 and RodA, called elongasome, which guides the synthesis and incorporation of peptidoglycan into the cylindrical wall of the cell. As a core component of the elongasome, RodA has been recently identified as the glycosyltransferase that polymerizes the glycan strands using Lipid II during peptidoglycan synthesis. However, how RodA activity is coordinated with other elongasome components and how its activity is regulated remains largely unknown. Here, using the model organism *E. coli*, we introduced single mutations into *E. coli* RodA based on the studies of its homologues in other species, and investigated how these mutations influence RodA and its role in the elongasome by *in vivo* functionality, localization and interaction studies. We found that most of these investigated residues are also essential in *E. coli* RodA, while they did neither influence RodA localization nor its interaction with PBP2. Further investigations revealed interactions between RodA and MreCD, and some mutations disrupted these interactions and abolished the MreB cellular localization pattern. Together with our previous observations that MreCD have a role in regulation of PBP2 and elongasome activity, our results suggest that interactions between RodA and MreCD are crucial for MreCD driven elongasome activity and organization.

Introduction

The Peptidoglycan layer is unique to most bacterial species and forms the major determinant of bacterial cell shape¹. It protects bacteria from osmotic pressure damage and scaffolds many important inner and outer membrane proteins²⁻⁴. Bacteria that are defective in peptidoglycan synthesis show irregular morphology and often cell lyse. The essential role of peptidoglycan makes its biosynthesis pathway a key target of antibiotics used to combat bacterial infections⁵. Nowadays, the rapid increase and spread of antibiotic resistance calls for the discovery of new and effective antibiotics, which quest could profit from a better understanding of peptidoglycan synthesis in bacteria.

Peptidoglycan is a mesh-like macromolecule consisting of alternating *N*-acetylmuramic acid (MurNAc)–pentapeptides and *N*-acetylglucosamine (GlcNAc) residues that polymerize with β -(1,4) bonds between the sugars to form glycan strands that are cross-linked between the peptide side chains^{1,6,7}. In *E. coli*, *in vivo* assembly of peptidoglycan initiates from the cytoplasmic steps that synthesize the nucleotide precursors UDP-GlcNAc and UDP-MurNAc-pentapeptide⁸. These precursors are subsequently assembled to form lipid II on the inner leaflet of the cytoplasmic membrane^{9,10}, and transported across the cytoplasmic membrane by a lipid II flippase¹¹. On the periplasmic side of the inner membrane, lipid II is polymerized and cross-linked by the glycosyltransferase (GTase) activity and transpeptidase (TPase) activity from the peptidoglycan synthesizing proteins^{12,13}.

In most bacteria, penicillin binding proteins (PBPs) were thought to be the major providers of the GTase and TPase activities for synthesis of the peptidoglycan mesh. In the model organism *E. coli*, based on their function, PBPs are usually classified into three classes: the bifunctional classes A PBPs (PBP1A, PBP1B and PBP1C) that contain a GTase domain as well as a TPase domain, the class B PBPs (PBP2 and PBP3) that only have TPase activity, and class C PBPs that mainly provide hydrolytic functions during peptidoglycan insertion, maturation and recycling¹³. Recently, RodA and FtsW, two homologous proteins of the SEDS (shape, elongation, division and sporulation) family, were characterized as GTase¹⁴⁻¹⁷. RodA, together with

other essential proteins, such as MreBCD, RodZ and PBP2, assemble into a complex called elongasome, to guide the synthesis and insertion of peptidoglycan into the cylindrical envelope^{7,18–20}. While FtsW, together with other proteins, such as FtsA, FtsZ, FtsEX, FtsK, FtsBLQ, PBP3 and FtsN, form the divisome at midcell that promotes the septum formation and daughter cell separation^{21,22}.

The discovery of RodA as a glycosyltransferase is historical. It was firstly identified as a bacterial cell shape determinant in a mutant that showed defects in cell morphology²³. The actual function and role of RodA in controlling the morphology of bacteria remained unknown for a long time. RodA interacts with PBP2 to form a stable subcomplex²⁴, and was assumed to be the lipid II flippase, because its homologues, FtsW from *E. coli* and RodA from *Corynebacterium glutamicum*, showed to some extent lipid II flipping activity^{25,26}. Only recently, *in vitro* biochemical evidence revealed that both RodA and FtsW have GTase activity using lipid II as substrate^{14,17}. The crystal structure of *Thermus thermophilus* RodA (RodA_{TT}) revealed that the protein has 10 trans-membrane helices with both its N-terminus and C-terminus localizing in the cytoplasm²⁷. How RodA functions as GTase and how this is coordinated with other elongasome proteins is still not clear. Especially, since previous studies identified many essential residues in *Bacillus subtilis* RodA (RodA_{BS}) and RodA_{TT} of which some influence the elongasome activity via unknown mechanisms rather than abolishing the RodA GTase activity^{14–16,27}. In this study, we introduced these mutations into *E. coli* RodA (RodA_{EC}), to investigate whether these residues are also essential in *E. coli*, and how they influence the function of RodA and the elongasome. Overall, our results reveal that a subset of the essential RodA amino acid residues are needed for the interactions between RodA and MreCD and that these interactions are essential for proper elongasome activity.

Results

Characterization of the *rodA*(TS) gene from the *E. coli* LMC882 strain that is used for complementation

To better study the function and role of *E. coli* RodA in the elongasome and peptidoglycan synthesis, a RodA temperature sensitive *E. coli* strain LMC882 was used for functionality analysis²³. This strain has a wild type rod-shaped phenotype at the permissive temperature of 30 °C, but a spherical phenotype at the non-permissive temperature of 42 °C, which can be complemented by expression of wild type RodA (RodA^{WT}) (Fig. 1A). The *rodA*(TS) gene was amplified by PCR from strain LMC882. Sequencing results revealed that the *rodA*(TS) gene contained two translational mutations that changed Gly276 into Asp and Ser326 into Asn in transmembrane helix 8 and 9, respectively (Fig. 1B). Interestingly, S326 was already reported to be essential for RodA_{EC} function²⁷, while G276D was also identified in the temperature sensitive FtsW_{EC} (G311D) that delocalized FtsW from midcell and blocked cell division in *E. coli*²⁸ (Fig. S1). The influence of these mutations on RodA function was further investigated below.

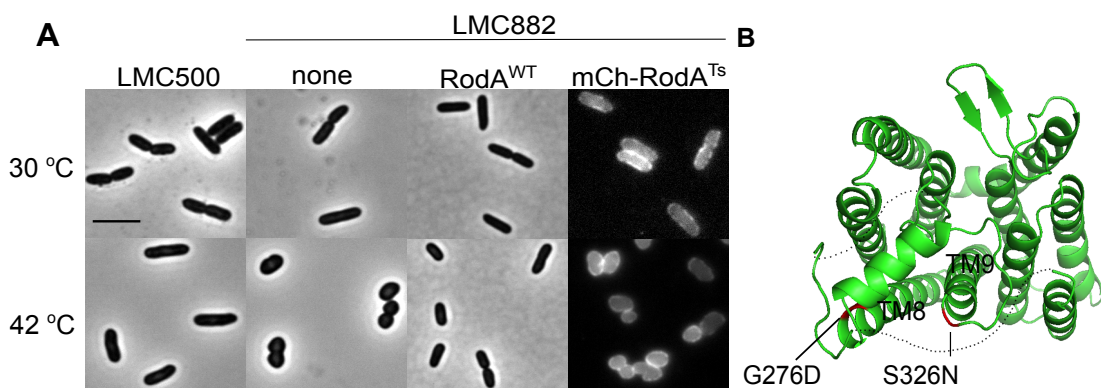


Figure 1. Characterization of the *rodA*(TS) gene from strain LMC882. **A.** Wild type RodA complements the morphological defects of LMC882 at the non-permissive temperature. Strains LMC500 (wild type control), LMC882 and LMC882 expressing non-fused RodA^{WT} or mcherry-RodA^{TS} were grown at permissive (30 °C) and non-permissive (42 °C) temperatures, and induced with 15 μ M IPTG for 2 mass doublings. Scale bar equals 5 μ m. **B.** Two point mutations (colored in red) were identified in RodA(TS) mutant by sequencing of the amplified *rodA*(TS) gene from three independent replicates. The structure of *E. coli* RodA was modeled from *Thermus thermophilus* RodA 6BAR²⁷ using Phyre 2²⁹ and edited with PyMol (view of the top of RodA from the periplasmic side).

Conserved residues in *E. coli* RodA protein

Previous functional studies on RodA_{BS} and FtsW_{EC} have revealed some essential residues for their function^{14,26–28}. Interestingly, most of these residues are also conserved in RodA_{EC} (Fig. S1). To investigate whether these residues are essential for RodA_{EC} and how they would influence its function, a total of 22 single mutations were introduced. In addition, one extra mutation at residue L240 was also introduced, as it was shown to be

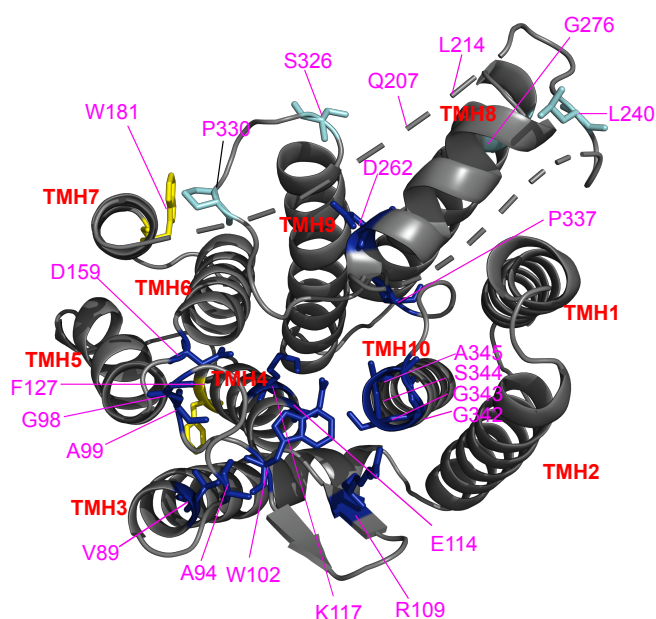


Figure 2. Residues mutated in *E. coli* RodA in this study. Structure of *E. coli* RodA (view of the top of RodA from the periplasmic side) was modeled from RodA_{TT} 6BAR²⁷ using Phyre 2²⁹ and edited with PyMol. Residues located close to or in the central cavity of RodA were colored blue. Residues locate outside the central cavity but close to the predicted protein interaction interface were colored cyan. Residues that were replaced with stop codons to generate the two truncate mutants were colored in yellow. Dashed lines present the missing regions of the published structure in the periplasmic loops.

important to maintain *E. coli* rod-shape morphology but not for RodA GTase activity²⁷. Preferably, these selected residues were mutated to alanine, or to glycine if they were originally alanine, or to other types of residues as applied in the studies of FtsW_{EC} (Fig. 2 and Table 1). Functionality of these mutants was detected by their ability to complement the RodA temperature sensitive

strain LMC882. Except for a few functional mutants (RodA^{A94G}, RodA^{L240S} and RodA^{P337A}), most of these mutations resulted into the loss of RodA function and even showed dominant negative effects (Fig. 3), which was in agreement with the studies on RodA_{BS} and FtsW_{EC}^{14,27,28}. Although a previous study reported that mutations of residues L240 and S326 resulted in morphological defects of *E. coli* (especially L240)²⁷, our results showed the opposite situation in which RodA^{L240S} is largely functional while RodA^{S326N} is very toxic (Fig. 3A and C). FtsW_{EC} mutants that only contain the first four or first six transmembrane helices were shown to be able to flip lipid II *in vitro*²⁶, while the two corresponding *E. coli* RodA truncates, RodA^{F127stop} and RodA^{W181stop}, were found to be not functional *in vivo* (Fig. 3B).

Table 1. Properties of RodA variants used in this study.

RodA variants	Location ^a	Functionality	Localization	Protein stability	MreB localization
WT		+	+	+	+
V89A	TMH3 (periplasmic end)	-	+	+	ND ^b
A94G	Periplasmic loop	+	+	+	ND
G98A	Periplasmic loop	-	+	+	ND
A99G	Periplasmic loop	Dominant negative	+	+	ND
W102A	Periplasmic loop	-	+	+	ND
R109A	Periplasmic loop	Dominant negative	+	+	ND
E114A	TMH4 (periplasmic end)	Dominant negative	+	+	ND
K117N	TMH4 (periplasmic end)	-	+	+	ND
F127stop	Cytoplasmic loop after TMH4	-	±	-	ND
D159A	TMH5 (periplasmic end)	Dominant negative	+	+	ND
W181stop	Cytoplasmic loop after TMH6	-	+	±	ND
Q207R	Periplasmic loop	Dominant negative	+	+	ND
L214A	Periplasmic loop	-	+	+	-
L240A	Periplasmic loop	+	+	+	+
D262A	Periplasmic loop	Dominant negative	+	+	ND
G276D	TMH8 (periplasmic end)	Dominant negative	+	+	ND
S326N	TMH9 (periplasmic end)	Dominant negative	+	+	-
P330A	Periplasmic loop	-	+	+	ND
P337A	Periplasmic loop	+	+	+	ND
G342A	TMH10 (periplasmic end)	-	+	+	ND
G343A	TMH10 (periplasmic end)	Dominant negative	+	-	ND
S344A	TMH10 (periplasmic end)	-	+	+	ND
A345G	TMH10 (periplasmic end)	Dominant negative	+	+	-

^a. Location of mutated residues was defined based on the modeled structure of RodA_{EC} from the published structure of *T. thermophilus* RodA 6BAR³⁰ using Phyre 2²⁹.

^b. Not detected.

Localization and structural stability of RodA mutants

To investigate how these mutations influenced the function of *E. coli* RodA, their localization was analyzed by fusing mCherry to the N-terminus of each variant^{16,24}. Expression from plasmid of the fused proteins in the wild type

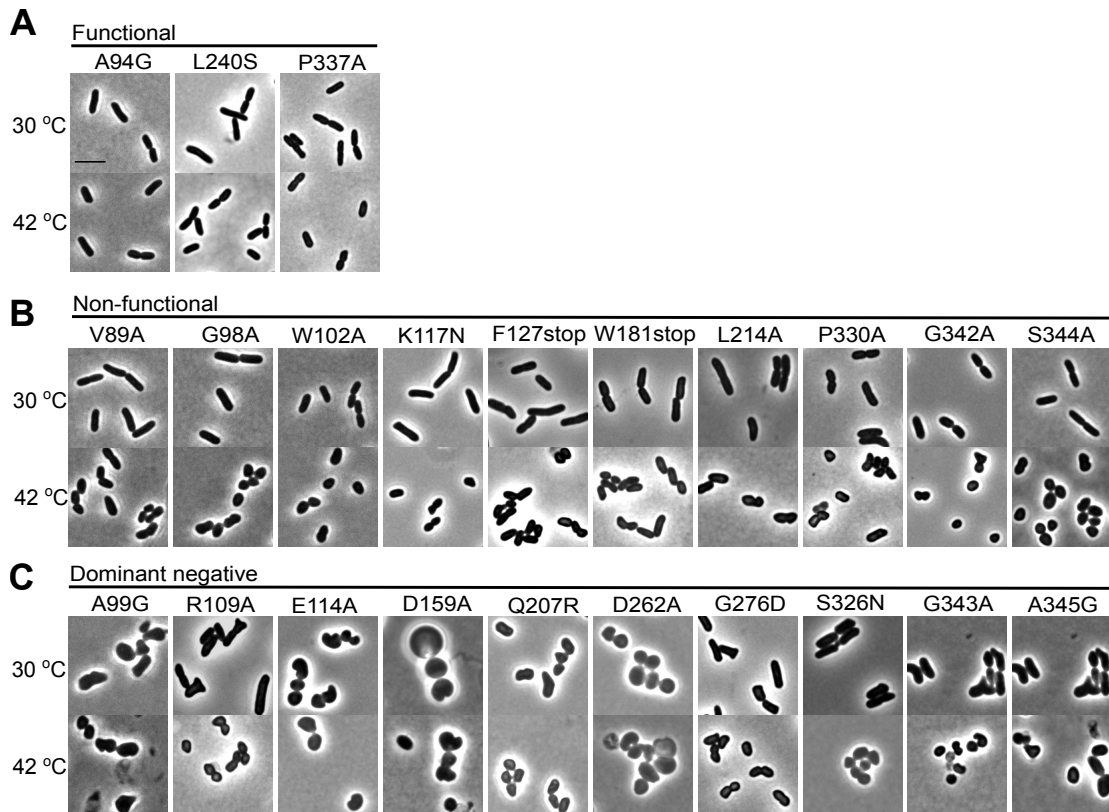


Figure 3. Complementation of RodA mutants. RodA temperature sensitive strain LMC882 was transformed with plasmids expressing RodA variants under control of the IPTG inducible $p_{\text{trc99A-down}}$ promoter, and grown in LB medium at both 30 °C and 42 °C for 2 mass doublings, with induction of 15 μM IPTG. **A.** Complementation of functional RodA variants. **B.** Complementation of non-functional RodA variants. **C.** Complementation of the dominant negative RodA variants. Images are representative of at least three independent experiments. Scale bar equals 5 μm .

strain was induced with 15 μM IPTG for 2 mass doubling at both 30 °C and 42 °C. The membrane localization of the mCh-RodA proteins was not influenced by most of these mutations at both growth conditions (Fig. 4 and Table 1) irrespective of their ability to complement the RodA function. This suggests that the folding and membrane insertion of these RodA mutants was not affected at both growth conditions. However, the inactive truncate mutant RodA^{F127stop} and the dominant negative mutant RodA^{G342A} showed lower fluorescence signal intensity, and a large extent of cytoplasmic fluorescence signal was also observed, especially for RodA^{F127stop} (Fig. 4 B and C). An immunoblot using whole cell extracts of the wild type strain expressing the mCh-RodA mutants was developed with antibodies against mCh to assess the stability of these RodA variants. In agreement with the localization results,

the mCherry signal was significantly reduced only for the mutant RodA^{F127stop} and RodA^{G342A} at both growth conditions, and for RodA^{W181stop} at 42 °C (Fig. S2), suggesting potential defects in stability of these mutants. All other mutants were stably expressed indicating that their inability to complement the RodA(TS) strain could be attributed to a loss of enzymatic activity or protein interaction.

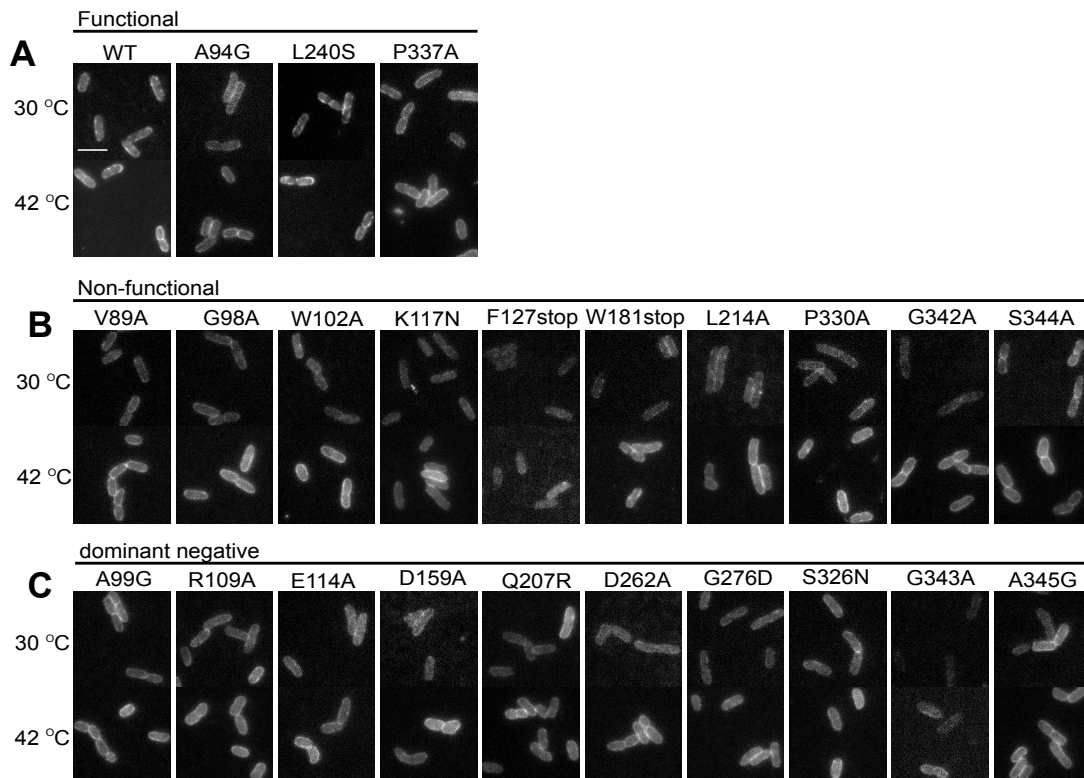


Figure 4. Localization of RodA mutants. LMC500 strain was transformed with plasmids expressing mCherry fused RodA variants under control of the IPTG inducible $p_{trc99A-down}$ promoter, and grown in LB medium at both 30 °C and 42 °C for 2 mass doublings, with induction of 15 μ M IPTG. Figure layout was the same as in figure 3. Images are representative of two independent experiments. Scale bar equals 5 μ m.

Interactions between RodA variants and PBP2

RodA and PBP2 form a stable subcomplex that functions in cylindrical peptidoglycan synthesis^{24,31}. Since most of the tested essential residues were not important for RodA localization and structural stability, it was possible that they influenced the RodA-PBP2 interaction. Therefore, FRET (Förster Resonance Energy Transfer) experiments were applied to detect the

interaction between mCherry fused RodA variants and mKO fused PBP2^{24,32,33} (Fig. 3 and Fig. S3). To account for possible interactions between proteins due to crowding in the cytoplasmic membrane a peptidoglycan synthesis unrelated integral membrane protein GlpT was fused to mKO and combined with mCh-RodA as negative control²⁴. A directly fused mCherry-mKO tandem was used as positive control. The acceptor FRET efficiency (E_f) of all the FRET samples was calculated using our previously published algorithm^{24,33}. The calculated E_f values for the tandem, RodA-GlpT and RodA^{WT}-PBP2 were $33.0 \pm 3.9\%$, $3.3 \pm 0.6\%$ and $12.9 \pm 1.8\%$, respectively (Fig. 5), which is in agreement with the previous reported data (Chapter 3). Except for RodA^{F127stop}, RodA^{W181stop} and RodA^{G343A}, the calculated E_f values for the interaction between PBP2 and the RodA variants were similar to that of PBP2 and RodA^{WT} (Fig. 5 and Table 2), indicating that these residues were not essential for their interaction with PBP2. Mutant RodA^{W181stop}, which can form a relatively stable truncated protein at 30 °C (Supplementary Fig. S2), showed a significantly reduced E_f value of $6.2 \pm 1.6\%$, suggesting the essentiality of transmembrane helices 7-10 in the interaction between RodA and PBP2. This is in agreement with prediction that the transmembrane helices 8 and 9 are involved in the interaction between RodA and PBP2²⁷. The remaining E_f value of $6.2 \pm 1.6\%$ between this truncate and PBP2 suggests that the periplasmic regions of PBP2 and RodA also contribute to their interaction, as reported (Chapter 3). Although interaction of PBP2-RodA^{F127stop} and PBP2-RodA^{G343A} yielded the calculated E_f values of still $9.4 \pm 3.0\%$ and even $20.5 \pm 2.3\%$, respectively (Fig. 5 and Table 2), these are likely the consequence of the reduced number of RodA^{F127stop} and RodA^{G343A} acceptor molecules that are surrounded by many energy donating PBP2 molecules (Fig. S3).

In the divisome, FtsW (GTase activity)¹⁷, PBP3 (TPase activity)¹² and PBP1B (both TGase and TPase activities)^{34,35} form a ternary subcomplex, and the interaction between them plays an important role in septal synthesis^{36,37}. Since RodA, PBP2 and PBP1A provide the same activities^{15,16,31,38,39} in the elongasome as FtsW, PBP3 and PBP1B in divisome, respectively, we wondered whether RodA interacts with PBP1A and

Essential interaction between RodA and MreCD proteins

Table 2. Summary of the calculated acceptor FRET efficiencies (E_f) from spectral FRET measurements for listed samples.

Parameter	Proteins expressed		E_f (%)	SD (%)	No. ^a
	pTHV037	pSAV057			
Positive control*					
Tandem	Empty vector	mKO-mCh	31.0	4.0	22
Negative control*					
RodA ^{WT} -GlpT	mCh-RodA ^{WT}	mKO-(GGG) ₂ -GlpT	1.1	3.5	24
Biological interactions					
RodA ^{WT} - PBP2 ^{WT}	mCh- RodA ^{WT}	mKO-PBP2 ^{WT}	12.9	1.8	16
RodA ^{A94G} - PBP2 ^{WT}	mCh- RodA ^{A94G}	mKO-PBP2 ^{WT}	13.8	1.8	8
RodA ^{L240S} - PBP2 ^{WT}	mCh- RodA ^{L240S}	mKO-PBP2 ^{WT}	15.5	0.4	2
RodA ^{P337A} -PBP2 ^{WT}	mCh- RodA ^{P337A}	mKO-PBP2 ^{WT}	13.8	0.3	4
RodA ^{V89A} - PBP2 ^{WT}	mCh- RodA ^{V89A}	mKO-PBP2 ^{WT}	14.3	0.8	8
RodA ^{G98A} - PBP2 ^{WT}	mCh- RodA ^{G98A}	mKO-PBP2 ^{WT}	14.7	1.3	8
RodA ^{W102A} - PBP2 ^{WT}	mCh- RodA ^{W102A}	mKO-PBP2 ^{WT}	13.6	1.7	7
RodA ^{K117N} - PBP2 ^{WT}	mCh- RodA ^{K117N}	mKO-PBP2 ^{WT}	11.5	1.8	4
RodA ^{F127stop} - PBP2 ^{WT}	mCh- RodA ^{F127stop}	mKO-PBP2 ^{WT}	9.4	3.0	4
RodA ^{W181stop} - PBP2 ^{WT}	mCh- RodA ^{W181stop}	mKO-PBP2 ^{WT}	6.2	1.6	4
RodA ^{L214A} - PBP2 ^{WT}	mCh- RodA ^{L214A}	mKO-PBP2 ^{WT}	15.5	3.4	8
RodA ^{P330A} - PBP2 ^{WT}	mCh- RodA ^{P330A}	mKO-PBP2 ^{WT}	12.8	2.3	4
RodA ^{G342A} - PBP2 ^{WT}	mCh- RodA ^{G342A}	mKO-PBP2 ^{WT}	15.9	4.9	4
RodA ^{S244A} - PBP2 ^{WT}	mCh- RodA ^{S244A}	mKO-PBP2 ^{WT}	14.7	3.9	4
RodA ^{A99G} - PBP2 ^{WT}	mCh- RodA ^{A99G}	mKO-PBP2 ^{WT}	15.2	1.7	4
RodA ^{R109A} - PBP2 ^{WT}	mCh- RodA ^{R109A}	mKO-PBP2 ^{WT}	12.5	1.9	4
RodA ^{E114A} - PBP2 ^{WT}	mCh- RodA ^{E114A}	mKO-PBP2 ^{WT}	15.6	1.9	7
RodA ^{D159A} - PBP2 ^{WT}	mCh- RodA ^{D159A}	mKO-PBP2 ^{WT}	15.8	2.4	8
RodA ^{Q207R} - PBP2 ^{WT}	mCh- RodA ^{Q207R}	mKO-PBP2 ^{WT}	12.7	1.2	4
RodA ^{D262A} - PBP2 ^{WT}	mCh- RodA ^{D262A}	mKO-PBP2 ^{WT}	12.5	5.0	4
RodA ^{G276D} - PBP2 ^{WT}	mCh- RodA ^{D276D}	mKO-PBP2 ^{WT}	11.2	1.8	4
RodA ^{S326N} - PBP2 ^{WT}	mCh- RodA ^{S326N}	mKO-PBP2 ^{WT}	12.8	0.3	4
RodA ^{G343A} - PBP2 ^{WT}	mCh- RodA ^{G343A}	mKO-PBP2 ^{WT}	20.5	2.3	4
RodA ^{A345G} - PBP2 ^{WT}	mCh- RodA ^{A345G}	mKO-PBP2 ^{WT}	14.4	5.9	4
RodA ^{WT} - MreC	mCh-RodA ^{WT}	mKO- MreC	4.0	1.4	2
RodA ^{Q207R} - MreC	mCh- RodA ^{Q207R}	mKO- MreC	1.5	1.1	2
RodA ^{L214A} - MreC	mCh- RodA ^{L214A}	mKO- MreC	2.6	0.0	2
RodA ^{S326N} - MreC	mCh- RodA ^{S326N}	mKO- MreC	4.4	0.9	2
RodA ^{WT} - MreD	mCh-RodA ^{WT}	mKO- MreD	6.3	1.2	2
RodA ^{Q207R} - MreD	mCh- RodA ^{Q207R}	mKO- MreD	5.6	0.6	2
RodA ^{L214A} - MreD	mCh- RodA ^{L214A}	mKO- MreD	4.6	0.5	2
RodA ^{S326N} - MreD	mCh- RodA ^{S326N}	mKO- MreD	3.5	0.8	2

^a, Number of samples detected;

*, Here all measured positive and negative controls are averaged. In the figures the controls are included that belong to the corresponding measurements.

whether the mutations in RodA would disrupt this interaction. Detecting interactions between PBP1A and RodA (both wild type and some mutants) by FRET yielded similar Ef_A values as for the RodA-GlpT negative control sample (Fig. S4), indicating the absence of measurable direct interaction between RodA and PBP1A. This is in agreement with the reported data that PBP1A showed distinct dynamics from that of other elongasome components such as RodA, PBP2 and MreB¹⁵.

Almost all the tested mutations in RodA interrupted its function, but did not influence the RodA membrane localization, stability or its interaction with PBP2. According to the modeled structure of *E. coli* RodA, the residues V89, G98, A99, W102, R109, E114, D159, D262, P337, G342, G343, S344 and A345 that are colored in blue (Fig. 2), are situated at either the potential lipid II binding pocket or in the proposed central cavity²⁷. Given the fact that mutating some of these residues clearly abolished RodA GTase activity^{14–16,27}, it is likely that these essential residues are all involved directly in the activity of RodA. The essential residues Q207, L214, G276, S326 and P330 that are colored in cyan (Fig. 2) are situated at the far side of the lipid II binding pocket and central cavity of RodA, but close to the potential protein-protein interaction interface (TMH8 and TMH9)²⁷. Although it was predicted in a previous study that mutations in this site likely uncouple the coordination of glycan strand elongation and peptide cross-linking²⁷, our results suggest that this uncoupling is not due to a loss of interaction with PBP2 (Fig. 4).

MreB cellular localization was abolished in presence of RodA mutants

MreB is one of the core proteins of the elongasome^{19,40,41}. It was shown to polymerize into short filaments that rotate underneath the cylindrical membrane in a circumferential motion^{20,42}, to organize the synthesis and insertion of peptidoglycan into the cylindrical wall^{40–43}. Since our result so far showed that most of these mutations in *E. coli* RodA did not support elongation, we reasoned that MreB localization might be also disturbed. Therefore, MreB localization was determined in the RodA(TS) strain LMC882 expressing non-functional mutants (RodA^{L214A}, RodA^{S326N} and RodA^{A324G}) and the functional mutants (RodA^{WT} and RodA^{L240S}) at both 30 °C and 42 °C

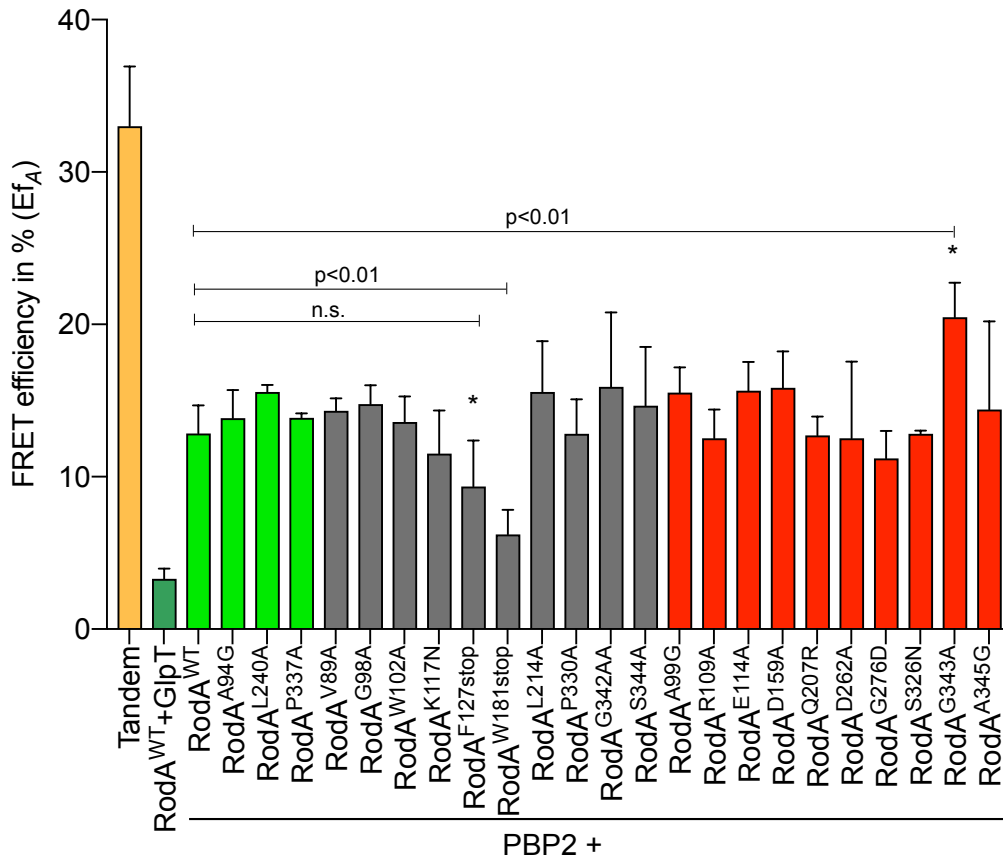


Figure 5. Interaction between mCherry fused RodA variants and mKO fused PBP2 detected by FRET *in vivo*. LMC500 strain was transferred with plasmids expressing each FRET pair and grown in Gb4 at 28 °C to steady state, and induced with 15 μM IPTG for 2 mass doublings. Acceptor FRET efficiency (Ef_A) was calculated from the spectral measurements. Green bars: functional RodA variants; grey bars: non-functional RodA mutants; red bars: dominant negative RodA mutants. *: Instable mutant. P value determined with Student's t test (n.s.: not significant; p<0.01: very significant). Results are the average of at least two independent experiments, error bars represent standard deviation.

(Fig. 6 and Table 1). Detection of MreB localization in cells expressing functional RodA variants showed its typical helical-like pattern (Fig. 6A and C). Central cavity mutant RodA^{G345A} that is likely GTase defective (Fig. 2), showed a complete disruption of MreB localization at both growth conditions (Fig. 6E), which is in agreement with the observation that MreB localization and dynamic rotation are dependent on the RodA peptidoglycan synthesizing activity^{15,44}. More importantly, the mutants RodA^{L214A} and RodA^{S326N} that are likely not involved in the GTase activity also abolished MreB cellular localization at both temperatures (Fig. 6B and D), indicating that these two

mutants (possibly also RodA^{Q207R}, RodA^{G276D} and RodA^{P330A}) uncoupled MreB from peptidoglycan synthesis.

Interaction between RodA variants and MreCD proteins

Although it was shown already that MreB interacts directly with RodA (Chapter 3), residues Q207, L214, G276, S326 and P330 are situated at the periplasmic surface of RodA (Fig. 2), indicating that they cannot be involved in the interaction with MreB. Thus, the disruption of MreB localization by these RodA mutants was likely achieved through loss of other intermediary proteins. RodZ interacts strongly with MreB and was shown to link MreB proteins to the peptidoglycan synthesizing RodA-PBP2 complex^{44–46}. Therefore, the interaction between RodA and RodZ was detected by FRET. However, no direct interaction was found (Fig. S4), which is in agreement with the previously reported bacterial two-hybrid data⁴⁶. These results indicate that the disruption of MreB localization by these RodA mutants was likely not through the RodZ protein.

As essential components of the elongasome, the function and role of MreC and MreD remains poorly understood. Previous studies showed that MreCD form a ternary complex together with MreB, whereby MreB interacts with MreC but not with MreD¹⁹. RodZ was reported to interact strongly with MreC as well as with MreD⁴⁶. Our recent data revealed that MreC and MreD competitively activate and inactivate PBP2 peptidoglycan synthesis, respectively, which functions likely as the check point for elongasome activation and regulation (Chapter 3). Possibly, mutation of residues Q207, L214, G276, S326 and P330 disrupt the function of MreC and/or MreD. Therefore, FRET experiments were performed to detect the interaction between some of the RodA variants and the MreCD proteins (Fig. 7 and Table 2). A calculated E_f value of $4.0 \pm 1.4\%$ indicated the direct interaction between RodA^{WT} and MreC. Mutants RodA^{R207R} and RodA^{L214A} showed reduced E_f values of $1.5 \pm 1.1\%$ and $2.6 \pm 0.01\%$, respectively, indicating that their interaction with MreC was abolished (Fig. 7 and Table 2). Mutant RodA^{S326N} interacted with MreC like wild type with an E_f of $4.4 \pm 0.9\%$. A

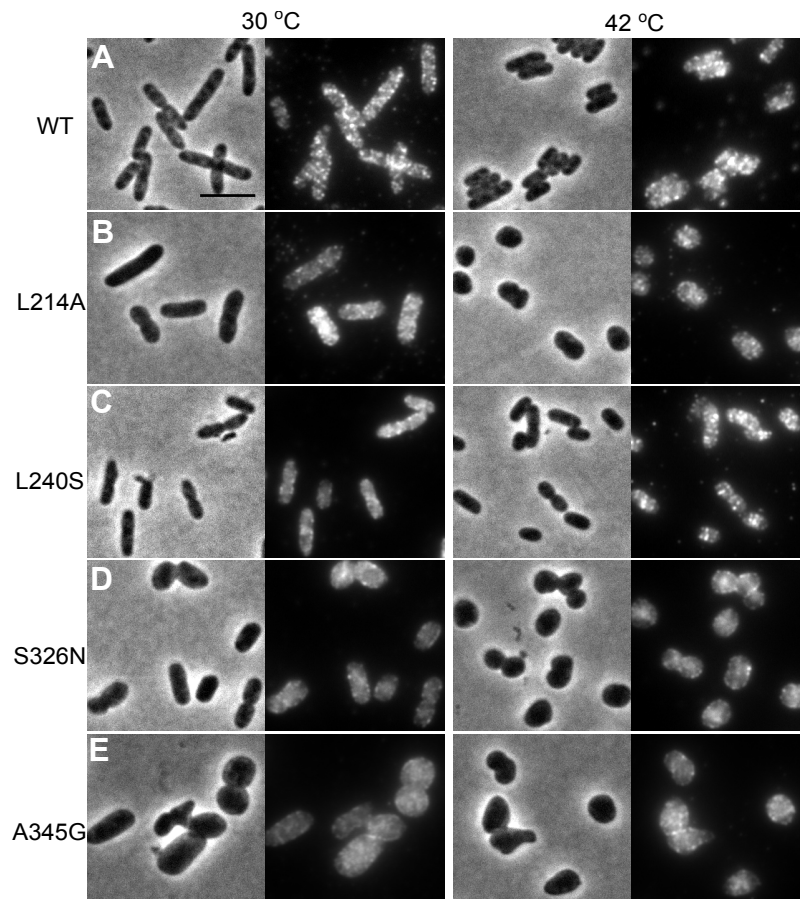


Figure 6. Effects of RodA mutations on MreB cellular localization. The LMC882 *rodA*(TS) strain was transformed with the plasmids expressing RodA variants under control of the *P_{trc99A-down}* promoter, and grown in LB medium at both 30 °C and 42 °C for 2 mass doublings, with induction of 15 μ M IPTG. MreB localization was determined by anti-MreB antibody. (A and C) Functional variants RodA^{WT} and RodA^{L240S} showed the typical helix-like localization pattern of MreB. (B, D and E) Inactive mutants RodA^{L214A}, RodA^{S326} and RodA^{A345G} abolish MreB cellular localization. Scale bar equals 5 μ m.

direct interaction between RodA^{WT} and MreD was also detected as the calculated Ef_A value of $6.3 \pm 1.2\%$ (Fig. 7). Comparing with RodA^{WT}, mutants RodA^{Q207R} and RodA^{L214A} had slightly reduced affinity for MreD with Ef_A values of $5.6 \pm 0.6\%$ and $4.6 \pm 0.5\%$, respectively. While RodA^{S326N} clearly had a reduced affinity for MreD with an Ef_A value of $3.5 \pm 0.8\%$ (Fig. 7). Together, these results indicate that the interaction between RodA and MreCD proteins is essential for *E. coli*, and mutation of the conserved residues Q207, L214, G276, S326 and P330 will likely reduce this interaction, and results into the growth and morphological defects (Fig. 3).

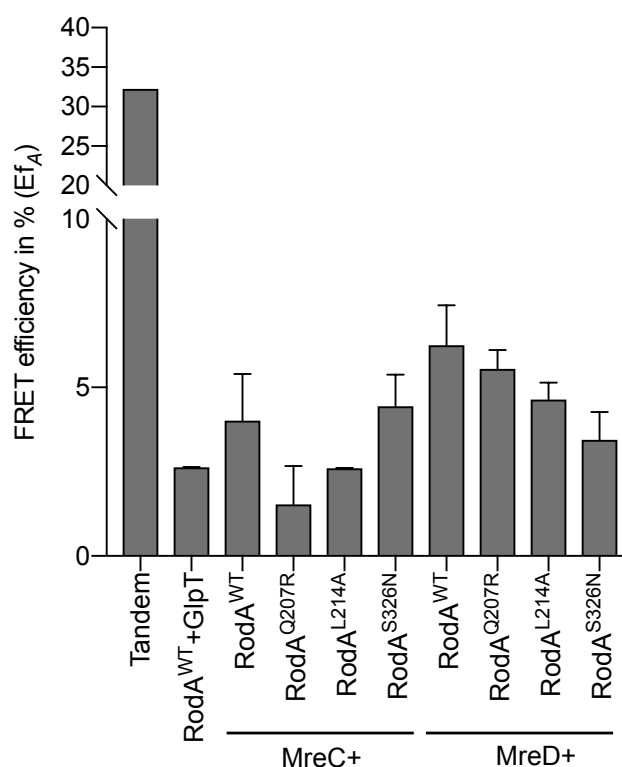


Figure 7. Interaction between mCh-RodA variants and mKO-MreC or mKO-MreD proteins detected by FRET *in vivo*. LMC500 strain was transformed with plasmids expressing each FRET pair, and grown in Gb4 minimal medium at 28 °C to steady state. Expression of the proteins was Induced with 15 μ M IPTG for 2 mass doublings. Acceptor FRET efficiency (E_{f_A}) was calculated based on the FRET spectra measurements.

Discussion

Organization of elongasome

The rod-shape of *E. coli* is maintained by the protein complex called elongasome, which guides the synthesis and incorporation of peptidoglycan into the cylindrical cell wall during cell growth. The elongasome contains many essential proteins, such as MreB, MreC, MreD, PBP2, RodA and RodZ. The actin homologous protein MreB polymerizes into short filaments that rotate along the cylindrical membrane in a circumferential motion, and is believed to guide the position of insertion of new peptidoglycan^{20,40,47–49}. RodA and PBP2 form a stable peptidoglycan synthesis subcomplex that provides the essential GTase and TPase activities, respectively. MreB filaments are reported to be linked to the RodA-PBP2 proteins via the essential bitopic inner membrane

protein RodZ. Also, interaction studies indicated MreB interacts with MreC but not with MreD¹⁹, while RodZ interacts with all MreBCD proteins⁴⁶. Our results in chapter 3 suggested an MreC-MreD balance dependent activation and inhibition of RodA-PBP2, which likely corresponds to the mechanism of peptidoglycan synthesis during length growth.

Potential roles of the essential residues of RodA

How RodA performs its GTase activity and coordinates with other elongasome proteins remained largely unknown. In this study, we investigated the functionality, localization and interaction of RodA_{EC} by mutating selected residues (Table 1), based on the studies of its homologues^{14,27,28}. In agreement with these studies, our results showed that most of these residues (except A94, L240 and P337) are also immutable in RodA_{EC}, and mutation of these residues result into the loss of RodA function and consequently morphological defects (Fig. 3). However, their localization and protein stability were not affected (Fig. 4 and Fig. S2). Surprisingly, the mutations did not affect the interaction between RodA and PBP2 either, which is the principle interaction partner of RodA.(Fig. 5), even though some residues were predicted to be important for coordination of glycan strand polymerization and peptide cross-linking. It can be concluded that the activity of RodA is likely not important for its interaction with PBP2. Since the activity of PBP2 is also not required for the interaction with RodA (Chapter 3), the two proteins probably form a permanent complex as was observed for FtsW and PBP3^{28,50}.

According to the modeled structure of RodA_{EC}, these residues can be divided into two groups (Fig. 2): the first group contains residues that are located in the potential substrate binding groove or central cavity, and the second group contains residues that are situated close to the predicted protein interaction surface (around the transmembrane helices 8 and 9) (Fig. 2). Together with the published data, our results suggest that the residues of the first group are likely involved in the GTase activity of RodA, while the residues in second group likely influence part of the assembly or regulation of the elongasome.

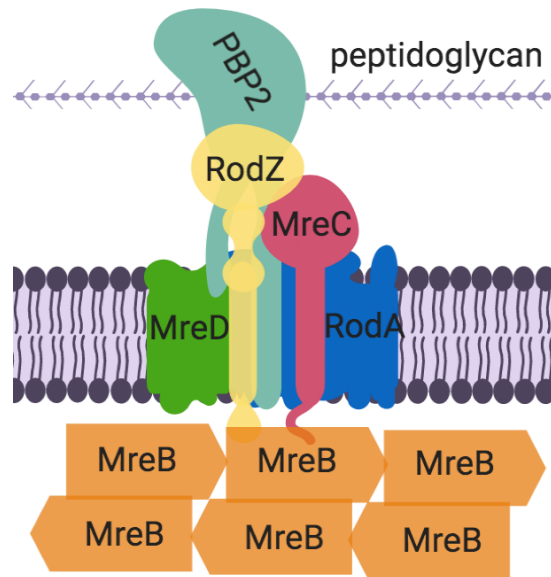


Figure 8. Model of organization of elongasome. At the heart of elongasome, RodA and PBP2 form a stable subcomplex, and they both interact with proteins MreC and MreD (at the predicted protein interaction interface of RodA that are close to the TMH8 and TMH9 region). The balance between MreC and MreD determines the activity of PBP2. RodZ interacts strongly with MreB and to decreasing extents with MreC-MreD-PBP2 proteins, while MreB interacts strongly with MreC and RodZ but not with MreD. These direct interactions of RodZ and MreC with MreD and RodA/PBP2 provide likely the forces that link MreB to the peptidoglycan synthesis, and thus coordinate elongasome assembly and peptidoglycan synthesis.

Further investigations showed that the residues in the second group also disrupted MreB cellular localization. This is not likely through abolishing RodA GTPase activity (especially RodA^{S326N}) but possibly through loss of the interaction with other elongasome subunits, since these periplasmic-side residues cannot be involved in the direct interaction with MreB. After assaying the interaction of some of these mutants with PBP1A, RodZ, MreC and MreD, finally our results revealed essential interactions between RodA and MreCD, which were disrupted by the second group of mutations in RodA (Fig. 7). This is in agreement with our previous observations that MreCD proteins play an important role in the regulation of PBP2 activity and subsequent peptidoglycan synthesis. Possibly, disruption of the interaction between MreCD and RodA will abolish the regulation by MreCD of PBP2 and elongasome activity.

Using our previous data and available published data, we suggest a model of elongasome organization and peptidoglycan synthesis coordination (Fig. 8). RodA and PBP2 form a stable peptidoglycan synthesis subcomplex. RodA interacts with MreCD and PBP2 at the predicted interaction surface around its transmembrane helices 8 and 9 region. While both MreC and MreD interact with PBP2 and competitively regulate PBP2 activity. RodZ interacts strongly with MreBCD proteins, while additionally, MreB interacts with MreC but not with MreD. The interaction between these intermediary elongasome proteins likely links up MreB and RodA/PBP2, and thus coordinates the elongasome organization and position of peptidoglycan synthesis.

Materials and methods

Medium and growth conditions

Rich medium LB (10 g tryptone, 5 g yeast extract and 10 g NaCl, per liter) and minimal medium Gb4 (6.33 g K₂HPO₄, 2.95 g KH₂PO₄, 1.05 g (NH₄)₂SO₄, 0.10 g MgSO₄·7H₂O, 0.28 mg FeSO₄·7H₂O, 7.1 mg Ca(NO₃)₂·4H₂O, 4 mg thiamine, 2 mg uracil, 2 mg lysine, 2 mg thymine, and 0.5% glucose, per liter, pH 7.0) were used for bacterial cultures as indicated. Concentrations of antibiotics applied when needed: 100 µg mL⁻¹ ampicillin, 25 µg mL⁻¹ chloramphenicol.

Strains, plasmids and primers

Strains and plasmids used in this study were listed in Supplementary Table 1. Primers used in this study were listed in Supplementary Table 2. To characterize the *rodA*(TS) gene, primers priXL83 and priXL84 were used in PCR to amplify a 4.5 kb DNA fragment that covered the *rodA*(TS) gene region from LMC882 genome. Primers priXL82 and priXL83 were used for sequencing. Three independent replicates were performed. Plasmids were constructed as following:

RodA mutant plasmids. Plasmids expressing mCherry fused RodA mutants were generated from plasmid pSAV047-RodA by site direct mutagenesis PCR using the primer pair for each mutant listed in

Supplementary Table 2. To construct plasmids expressing mCherry-RodA^{TS}, the *rodA*(TS) gene was firstly amplified from LMC882 genome using primers priXL89 and priXL60, and subsequently cloned into pSAV047-RodA plasmid with restriction enzymes *EcoRI* and *HindIII*. To construct the plasmids expressing non-fused RodA mutants, the wild type *rodA* gene was firstly amplified with primers priXL59 and priXL60, and cloned into plasmid pSAV057 with restriction enzymes *EcoRI* and *HindIII*, to generate plasmid pXL63. Site direct mutagenesis PCR was performed using pXL63 as template with the primer pair for each mutant, to generate the plasmids expressing non-fused RodA mutants.

pXL29. Plasmid pXL28 and pWA004 were digested with *EcoRI* and *HindIII* restriction enzymes, the generated (GGS)₂-GlpT expressing gene and pSAV057-mKO linear vector were ligated together to generate the mKO-(GGS)₂-GlpT expressing plasmid.

pXL163 and pXL170. To construct these plasmids expressing mKO-MreC and mKO-MreD fusion proteins, primer pairs, priXL282 and priXL286, priXL283 and priXL299, were used to amplify the *mreC* and *mreD* gene from the MG1655 genome. PCR products were cloned into plasmid pSAV057-mKO with restriction enzymes *EcoRI* and *HindIII*.

pXL171. To construct the plasmid expressing mKO-RodZ, primers rene39 and rene40 were used to amplify the *rodZ* gene from MG1655 genome. PCR products were cloned into plasmid pSAV057-mKO with restriction enzymes *EcoRI* and *HindIII*.

Functionality test and localization of RodA mutants

Complementation experiments were performed to test the functionality of RodA mutants. The RodA temperature sensitive strain LMC882 was transformed with plasmids expressing non-fused RodA mutants. Strains were grown in LB medium at 30 °C with glucose and chloramphenicol overnight. Cultures were diluted 1:1000 into fresh LB medium with glucose and chloramphenicol at 30 °C to OD₆₀₀ around 0.2 to 0.3. Cultures were further diluted 1:5 into fresh LB medium with chloramphenicol and 15 μM IPTG, and grown at both 30 °C and 42 °C for 2 mass doublings. Cells were fixed with

FAGA (2.8% formaldehyde and 0.04% glutaraldehyde, final concentration) for 15 minutes and pelleted down at 7000 rpm at room temperature for 10 minutes. Cell pellets were washed with PBS buffer (pH 7.2) for three times. Morphology of strains expressing each RodA mutants was imaged by phase contrast microscopy.

To test the localization of RodA mutants, plasmids expressing mCherry fused RodA variants were transformed to the wild type LMC500 strain, and similar growth experiments were performed as above. Localization of each mutant was imaged by widefield fluorescence microscopy.

Protein stability of RodA mutants tested by immunoblotting

To test the protein stability of RodA mutants, extract of LMC500 cells expressing mCherry fused RodA mutants was immunoblotted using mCherry recognizing antibodies. Same growth experiments were firstly applied at both 30 °C and 42 °C as mentioned above to OD₆₀₀ around 0.2 to 0.3 (no fixation). A volume of 2 ml of cell cultures were collected by centrifugation at 7000 rpm at 4 °C for 10 minutes. Cell pellets were washed three times with ice-cold PBS buffer, and then resuspended in 5x SDS-PAGE sample buffer (2.5 ml 1M Tris, PH 8.3, 1 g SDS, 1 g DTT, 5 ml glycerol, and 5 mg bromo phenolblue, per 10 ml), to an OD₄₅₀ of 1 (OD₆₀₀ of 1.0 equals OD₄₅₀ of 1.7). Samples were incubated at room temperature (no boiling) for 1 hour to avoid protein aggregation. Subsequently, 4 µl of the samples were loaded and run on a 12% SDS polyacrylamide gel. Immunoblotting was performed using anti-mCherry polyclonal antibody (Fisher, Catalog # PA5-34974, 1:1000 or 1:2000 as indicated) to detect the mCherry fused RodA variants.

Immunolocalization of MreB

LMC882 cells expressing non-fused RodA mutants were grown at 30 °C and 42 °C as described above. After induction with 15 µM IPTG for 2 mass doublings, cells were fixed with FAGA (2.8% formaldehyde and 0.04% glutaraldehyde final concentration) for 15 minutes, and washed 3 times with PBS buffer. *In vivo* immunolabelling of MreB was performed as described

previously⁵¹. Cells were incubated with blocking reagents (Boehringer) (0.5% (w/v) in PBS buffer) at 37 °C for 30 min, to block the non-specific binding sites. After pelleted down at 7000 rpm for 10 min, cells were incubated with affinity-purified polyclonal antibodies against MreB (diluted in blocking buffer) at 37°C for 60 min. After washing three times with PBS containing 0.05% (v/v) Tween-20, cells were further incubated with secondary antibody (Donkey anti-rabbit conjugated with Cy3 (Jackson), diluted in blocking buffer) at 37 °C for 30 min. After washing two more times in PBS containing 0.05% Tween-20 and one time with PBS buffer, cells were re-suspended in PBS and kept in dark before imaging by widefield fluorescence microscopy.

FRET experiments to test the protein interaction

Protein interactions were detected with FRET experiments as described previously⁵². In brief, mCherry and mKO were used as acceptor and donor fluorophores, respectively. LMC500 strain was co-transformed with the two plasmids pair expressing the proteins to be detected. All FRET strains were grown in Gb4 medium to steady state at 28 °C, and induced with 15 µM IPTG for 2 mass doublings before FAGA fixation. After fixation, cells of each culture were collected by centrifugation at 7000 rpm at room temperature, and washed 3 times with PBS buffer (pH 7.2). Subsequently, all samples were protected from light and incubated at 37 °C overnight to allow maturation of the mKO chromophore and then stored at 4 °C for 1 day before measured with spectrofluorimeter (Photon Technology International, NJ). Emission spectra of acceptor and donor fluorophores were measured through 6-nm slit widths with 1 second integration time per scanned nm for 3 times averaging. Filters f 587/11 nm (587/11 nm BrightLine single band-pass filter, Semrock, New York, NY, USA) and 600nm long-pass (LP) filter (Chroma Technology Corp., Bellows Falls, VT) were used for excitation and emission of acceptor fluorophore (mCherry), while 541/12 nm (Semrock) and 550 nm long pass (Chroma) filters were used for mKO excitation and emission, respectively. For calculation, measurement of PBS buffer was subtracted from all samples, and the empty-cell reference was subtracted from the donor and acceptor spectra. The FRET efficiencies were calculated as described previously^{24,33}.

Microscopy and images analysis

Fixed bacteria cells were loaded on the 1.3% agarose pads (w/v in Gb4 medium) and imaged with an Olympus BX-60 fluorescence microscope equipped with an UPlanApo 100×/N.A. 1.35 oil Iris Ph3 objective, or with a Nikon Eclipse Ti microscope equipped with a C11440-22CU Hamamatsu ORCA camera, a CFI Plan Apochromat DM 100× oil objective, an Intensilight HG 130W lamp and the NIS elements software (version 4.20.01). Images were acquired using the Micro Manager 1.4 plugin for ImageJ, and analyzed with Coli-Inspector supported by the ObjectJ plugin for ImageJ (version 1.49v)⁵³.

Acknowledgements

X.L. was supported by the Chinese Scholarship Council (File No. 201406220123). X.L. and T.B. designed all the experiments. X.L. performed all experiments and collected data. X.L. and T.B. analyzed the results and wrote the manuscript.

Conflicting interests

The authors declare no conflicting interests.

References

1. Vollmer, W., Blanot, D. & De Pedro, M. A. Peptidoglycan structure and architecture. *FEMS Microbiol. Rev.* **32**, 149–167 (2008).
2. Mattei, P. J., Neves, D. & Dessen, A. Bridging cell wall biosynthesis and bacterial morphogenesis. *Curr. Opin. Struct. Biol.* **20**, 749–755 (2010).
3. Gray, A. N. *et al.* Coordination of peptidoglycan synthesis and outer membrane constriction during Escherichia coli cell division. *Elife* **4**, 1–29 (2015).
4. Demchick, P. & Koch, A. L. The permeability of the wall fabric of Escherichia coli and Bacillus subtilis. *J. Bacteriol.* **178**, 768 LP – 773 (1996).
5. Koch, A. L. Bacterial Wall as Target for Attack. *Clin. Microbiol. Rev.* **16**, 673 LP – 687 (2003).
6. de Jonge, B. *et al.* Peptidoglycan synthesis during the cell cycle of Escherichia coli: Composition and mode of insertion. *J. Bacteriol.* **171**, 5783–5794 (1989).
7. Den Blaauwen, T., De Pedro, M. A., Nguyen-Distèche, M. & Ayala, J. A. Morphogenesis of rod-shaped sacculi. *FEMS Microbiol. Rev.* **32**, 321–344 (2008).
8. Barreteau, H. *et al.* Cytoplasmic steps of peptidoglycan biosynthesis. *FEMS Microbiol. Rev.* **32**, 168–207 (2008).
9. van Heijenoort, J. Lipid Intermediates in the Biosynthesis of Bacterial Peptidoglycan. *Microbiol. Mol. Biol. Rev.* **71**, 620–635 (2007).
10. Bouhss, A., Trunkfield, A. E., Bugg, T. D. H. & Mengin-Lecreux, D. The biosynthesis of peptidoglycan lipid-linked intermediates. *FEMS Microbiology Reviews* **32**, 208–233 (2008).
11. Sham, L.-T. *et al.* MurJ is the flippase of lipid-linked precursors for peptidoglycan biogenesis. *Science (80-.)*. **345**, 220–222 (2014).
12. Sauvage, E., Kerff, F., Terrak, M., Ayala, J. A. & Charlier, P. The penicillin-binding proteins: Structure and role in peptidoglycan biosynthesis. *FEMS Microbiol. Rev.* **32**, 234–258 (2008).
13. Macheboeuf, P., Contreras-Martel, C., Job, V., Dideberg, O. & Dessen, A. Penicillin binding proteins: Key players in bacterial cell cycle and drug resistance processes. *FEMS Microbiol. Rev.* **30**, 673–691 (2006).
14. Meeske, A. J. *et al.* SEDS proteins are a widespread family of bacterial cell wall polymerases. *Nature* 1–15 (2016). doi:10.1038/nature19331
15. Cho, H. *et al.* Bacterial cell wall biogenesis is mediated by SEDS and PBP polymerase families functioning semi-Autonomously. *Nat. Microbiol.* **1**, (2016).
16. Emami, K. *et al.* RodA as the missing glycosyltransferase in Bacillus subtilis and antibiotic discovery for the peptidoglycan polymerase pathway. *Nat. Microbiol.* **2**, 1–8 (2017).
17. Taguchi, A. *et al.* FtsW is a peptidoglycan polymerase that is functional only in complex with its cognate penicillin-binding protein. *Nat. Microbiol.* (2019).

doi:10.1038/s41564-018-0345-x

18. Shiomi, D., Sakai, M. & Niki, H. Determination of bacterial rod shape by a novel cytoskeletal membrane protein. *EMBO J.* **27**, 3081–3091 (2008).
19. Kruse, T., Bork-Jensen, J. & Gerdes, K. The morphogenetic MreBCD proteins of *Escherichia coli* form an essential membrane-bound complex. *Mol. Microbiol.* **55**, 78–89 (2005).
20. Strahl, H., Bürmann, F. & Hamoen, L. W. The actin homologue MreB organizes the bacterial cell membrane. *Nat. Commun.* **5**, 1–11 (2014).
21. Aarsman, M. E. G. *et al.* Maturation of the *Escherichia coli* divisome occurs in two steps. *Mol. Microbiol.* **55**, 1631–1645 (2005).
22. Goehring, N. W. & Beckwith, J. Diverse paths to midcell: Assembly of the bacterial cell division machinery. *Curr. Biol.* **15**, 514–526 (2005).
23. Matsuzawa, H., Hayakawa, K., Sato, T. & Imahori, K. Characterization and genetic analysis of a mutant of *Escherichia coli* K-12 with rounded morphology. *J. Bacteriol.* **115**, 436–442 (1973).
24. van der Ploeg, R., Goudelis, S. T. & den Blaauwen, T. Validation of FRET assay for the screening of growth inhibitors of *Escherichia coli* reveals elongasome assembly dynamics. *Int. J. Mol. Sci.* **16**, 17637–17654 (2015).
25. Sieger, B., Schubert, K., Donovan, C. & Bramkamp, M. The lipid II flippase RodA determines morphology and growth in *Corynebacterium glutamicum*. *Mol. Microbiol.* **90**, 966–982 (2013).
26. Mohammadi, T. *et al.* Specificity of the transport of lipid II by FtsW in *Escherichia coli*. *J. Biol. Chem.* **289**, 14707–14718 (2014).
27. Sjødt, M. *et al.* Structure of the peptidoglycan polymerase RodA resolved by evolutionary coupling analysis. *Nature* (2018). doi:10.1038/nature25985
28. Pastoret, S. *et al.* Functional Analysis of the Cell Division Protein FtsW of *Escherichia coli*. *J. Bacteriol.* **186**, 8370–8379 (2004).
29. Kelley, L. A. & Sternberg, M. J. E. Protein structure prediction on the Web: a case study using the Phyre server. *Nat. Protoc.* **4**, 363 (2009).
30. Contreras-Martel, C. *et al.* Molecular architecture of the PBP2-MreC core bacterial cell wall synthesis complex. *Nat. Commun.* **8**, 1–10 (2017).
31. Rohs, P. D. A. *et al.* A central role for PBP2 in the activation of peptidoglycan polymerization by the bacterial cell elongation machinery. *PLoS Genet.* **14**, 1–25 (2018).
32. Meiresonne, N. Y., van der Ploeg, R., Hink, M. A. & den Blaauwen, T. Activity-related conformational changes in D,D-carboxypeptidases revealed by in vivo periplasmic Förster resonance energy transfer assay in *Escherichia coli*. *MBio* **8**, 1–18 (2017).
33. Van der Ploeg, R. *et al.* Colocalization and interaction between elongasome and divisome during a preparative cell division phase in *Escherichia coli*. *Mol. Microbiol.* **87**, 1074–1087 (2013).

34. Lysis of *Escherichia coli* by beta-lactam antibiotics: deletion analysis of the role of penicillin-binding proteins 1A and 1B. *J Gen Microbiol.* **131**, 2839–45. (1985).
35. Ranjit, D. K., Jorgenson, M. A. & Young, K. D. PBP1B Glycosyltransferase and Transpeptidase Activities Play Different Essential Roles during the De Novo Regeneration of Rod Morphology in *Escherichia coli*. *J Biol Chem* **199**, 1–17 (2017).
36. Boes, A., Olatunji, S., Breukink, E. & Terrak, M. Regulation of the peptidoglycan polymerase activity of PBP1b by antagonist actions of the core divisome proteins FtsBLQ and FtsN. *MBio* **10**, 1–16 (2019).
37. den Blaauwen, T. & Luirink, J. Checks and Balances in Bacterial Cell Division. *MBio* **10**, 1–6 (2019).
38. Den Blaauwen, T., Aarsman, M. E. G., Vischer, N. O. E. & Nanninga, N. Penicillin-binding protein PBP2 of *Escherichia coli* localizes preferentially in the lateral wall and at mid-cell in comparison with the old cell pole. *Mol. Microbiol.* **47**, 539–547 (2003).
39. Takasuga, A. *et al.* Identification of the penicillin-binding active site of penicillin-binding protein 2 of *Escherichia coli*. *J. Biochem.* **104**, 822–826 (1988).
40. Errington, J. Bacterial morphogenesis and the enigmatic MreB helix. *Nat Rev Micro* **13**, 241–248 (2015).
41. Shi, H., Bratton, B. P., Gitai, Z. & Huang, K. C. How to Build a Bacterial Cell: MreB as the Foreman of *E. coli* Construction. *Cell* **172**, 1294–1305 (2018).
42. Bratton, B. P., Shaevitz, J. W., Gitai, Z. & Morgenstein, R. M. MreB polymers and curvature localization are enhanced by RodZ and predict *E. coli*'s cylindrical uniformity. *Nat. Commun.* **9**, (2018).
43. Schirner, K. *et al.* Lipid-linked cell wall precursors regulate membrane association of bacterial actin MreB. *Nat. Chem. Biol.* **11**, 38–45 (2015).
44. Morgenstein, R. M. *et al.* RodZ links MreB to cell wall synthesis to mediate MreB rotation and robust morphogenesis. *Proc Natl Acad Sci U S A* **112**, 12510–12515 (2015).
45. Colavin, A., Shi, H. & Huang, K. C. RodZ modulates geometric localization of the bacterial actin MreB to regulate cell shape. *Nat. Commun.* **9**, 1280 (2018).
46. Bendezú, F. O., Hale, C. A., Bernhardt, T. G. & De Boer, P. A. J. RodZ (YfgA) is required for proper assembly of the MreB actin cytoskeleton and cell shape in *E. coli*. *EMBO J.* **28**, 193–204 (2009).
47. Garner, E. C. *et al.* Coupled, circumferential motions of the cell wall synthesis machinery and MreB filaments in *B. subtilis*. *Science (80-.)*. **333**, 222–5 (2011).
48. White, C. L. & Gober, J. W. MreB: Pilot or passenger of cell wall synthesis? *Trends Microbiol.* **20**, 74–79 (2012).
49. van den Ent, F., Izoré, T., Bharat, T. A. M., Johnson, C. M. & Löwe, J. Bacterial actin MreB forms antiparallel double filaments. *Elife* **2014**, 1–22 (2014).
50. Leclercq, S. *et al.* Interplay between Penicillin-binding proteins and SEDS proteins promotes bacterial cell wall synthesis. *Sci. Rep.* **7**, 43306 (2017).

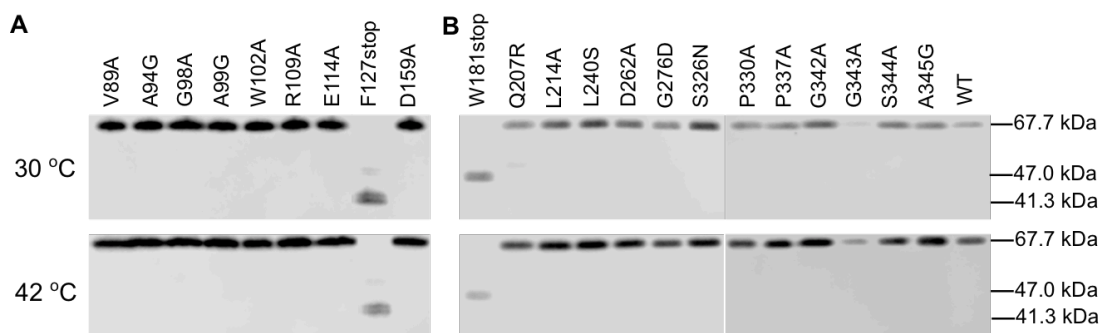
51. Karczmarek, A. *et al.* DNA and origin region segregation are not affected by the transition from rod to sphere after inhibition of Escherichia coli MreB by A22. *Mol. Microbiol.* **65**, 51–63 (2007).
52. Meiresonne, N. Y., Alexeeva, S., van der Ploeg, R. & den Blaauwen, T. Detection of Protein Interactions in the Cytoplasm and Periplasm of Escherichia coli by Förster Resonance Energy Transfer. *Bio-protocol* **8**, e2697 (2018).
53. Vischer, N. O. E. *et al.* Cell age dependent concentration of Escherichia coli divisome proteins analyzed with ImageJ and ObjectJ. *Front. Microbiol.* **6**, 1–18 (2015).

Supplementary information

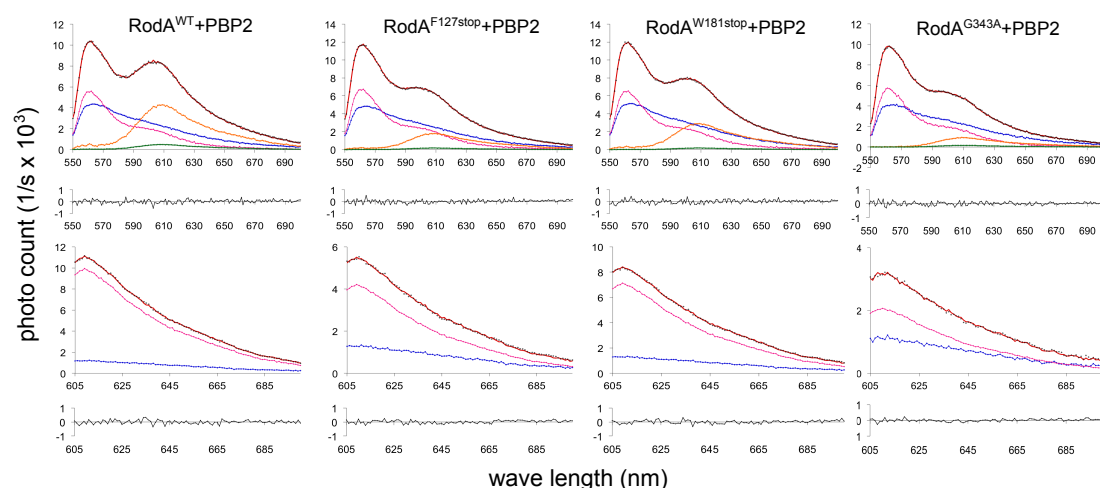
RodA_BS	0	----MSRYKKQQSEFFYQ-----GDLIFIFGVFFIIS	27
FtsW_EC	0	MRLSLPRLKMPRLPGFSILVWISTALKGWVMGSREKDTDSLIMYDRITLLWLTFGIAAIGF	60
RodA_EC	0	-----MTDNPNKTF-W-----DKVHLDPTMLLILLALLVYSAL	33
RodA_TT	0	-----VAPARFNWLAIDW-----GLVFLVAAIVALGF	27
RodA_BS	28	VVSIYAAGQFGQYGNTDWI---QQIVFYLLGAVAITVLLYFDLEQLEKLSLYIFIIIGIL	83
FtsW_EC	61	IMVTSASMPIGQRLTNDPFFFAKRDRGVYLILAFILAITLRLPMEFWQRYSATMLLGSII	120
RodA_EC	34	VIWSASGQDIGMME-----RKIGQIAMGLVIMVVMQIPPRVYEGWAPYLYIICII	84
RodA_TT	28	VNLGSAAPDPALLY-----RQSVALLGLLLAFLLQFLSRRRLFGLAYPLYGASLL	78
RodA_BS	84	SLIILKISPESIA PIKGAKS WFRIGRITIQ PSEF FMKVGLIMMLASVIGKANPKGVRTL	143
FtsW_EC	121	LLMIVLV---VGSVKGASRWIDLGLLRIQPAEITKLSLFCYIANYLVRKGDVFRNNLR	176
RodA_EC	85	LLVAVDA---FGAISKGAQRWLDLGIIVRFQ PSET AKIAVPLMVARF INR --DVCPPSLK	138
RodA_TT	79	LLALVLV---VGREINGARAWFVLG PLQ F QPL E LAK LGLLLALAKAL-----EGRPIAR	129
RodA_BS	144	DDIHLLLKIAGVAVIP-VGILIMQ-DAGTAGICMFIIVLMVFMMSGIN-WKLIATAGSGI	200
FtsW_EC	177	G---FLKPMGVILVLA-V-LLLAQPDIGTVVVLVFTTTLAMFLAGAKLWQFIATII-GMGI	230
RodA_EC	139	N---TGIAL-VLIFMP-TLLVAAQPDIGTSILVALSGLFVLFSLGLS-WRLI---GVAV	188
RodA_TT	130	V---WDYALPALLTLPVVGLLLLQPDIGGALVVLF GVFVVVFVRGLP-WRHL ----LVGL	181
RodA_BS	201	LLISLILLVMINFPDVAKS VGI Q DY QIKRVTS W VSASNETQEDSNDSWQVDQAIMAIGSG	260
FtsW_EC	231	SAVVLLIL-----AEPYRIRRVTA FW ---NPWEDPFGSGYQLTQSLMA FGR G	274
RodA_EC	189	VLVAAFIPILWFF-----LMHDYQ RQ RVMMLL---DPESDPLGAGYHIIQSKIAIGSG	238
RodA_TT	182	FALALLVPTAVWP-----NLKPY QR ERVLIVL---DPYRDPLGQGFQVIQSTIAIGSG	231
RodA_BS	261	GILNGISNLKV---YVPEST DF IFSIIGESFGFIGCAIVVIMFFFLIYRLVVLIDKI	316
FtsW_EC	275	ELWGOGLGNSVQ-KLEYLPEAHTDFIFAIIG EE LGVVVLALLMVFFVAFRAMS IGR KA	333
RodA_EC	239	G R KGWLHGTSQLEFLPERHTDFIFAVLAEELGLVGILILLALYILLIMRGLWIAARA	298
RodA_TT	232	GLFGKYGQGTQAQLGFIPFRHTDFVFSVWAE EW GFVGVVGLLGLYGLLLARLFALALAC	291
RodA_BS	317	HPFNRFASFFCVGYTALIV-IHTFQNI GM NIGIMPVTGIPLLFVSY CGSS TLSTLIGFGI	375
FtsW_EC	334	LEIDHRFSGFLACSIGIWFSFOALVNVGAAAGML PT KGLT LP LISYGGSSLLIMSTAIMM	393
RodA_EC	299	QTTFGRV--MAGGLMLILF-VYVFNIGMV GL LPVVG VL PLVSYGGSSALIVLMAGFGI	355
RodA_TT	292	PRLSDRL--FLSGFAGMLG-FQVVVNLGVALGVMPVTGTL LP LFSYGGSSLIATL AGL L	348
RodA_BS	376	VYNASVQLTKYRSYLFNS--- 393	
FtsW_EC	394	LLRIDYETRLEKAQAFVRGSR 414	
RodA_EC	356	VMSIHTHRKMLS KS V----- 370	
RodA_TT	349	VLLVHRDRYQD----- 359	

Supplementary figure 1. Alignment of *Escherichia coli* RodA with its homologues using MUSCLE (Multiple Sequence Alignment) tool. Definition of the listed species: BS: *Bacillus subtilis*, EC: *Escherichia coli*, TT: *Thermus thermophilus*. Immutable residues are bold faced and colored in red (immutable residues reported in *Bacillus subtilis* RodA^{1,2}), blue (mutations analyzed in *E. coli* FtsW) and pink (mutations identified in *E. coli* RodA³). A given column has one color, which indicates the average BLOSUM62 score of pairs of letters in the column: light blue ≥ 3 , dark blue ≥ 1 , light gray ≥ 0.2 , no color otherwise.

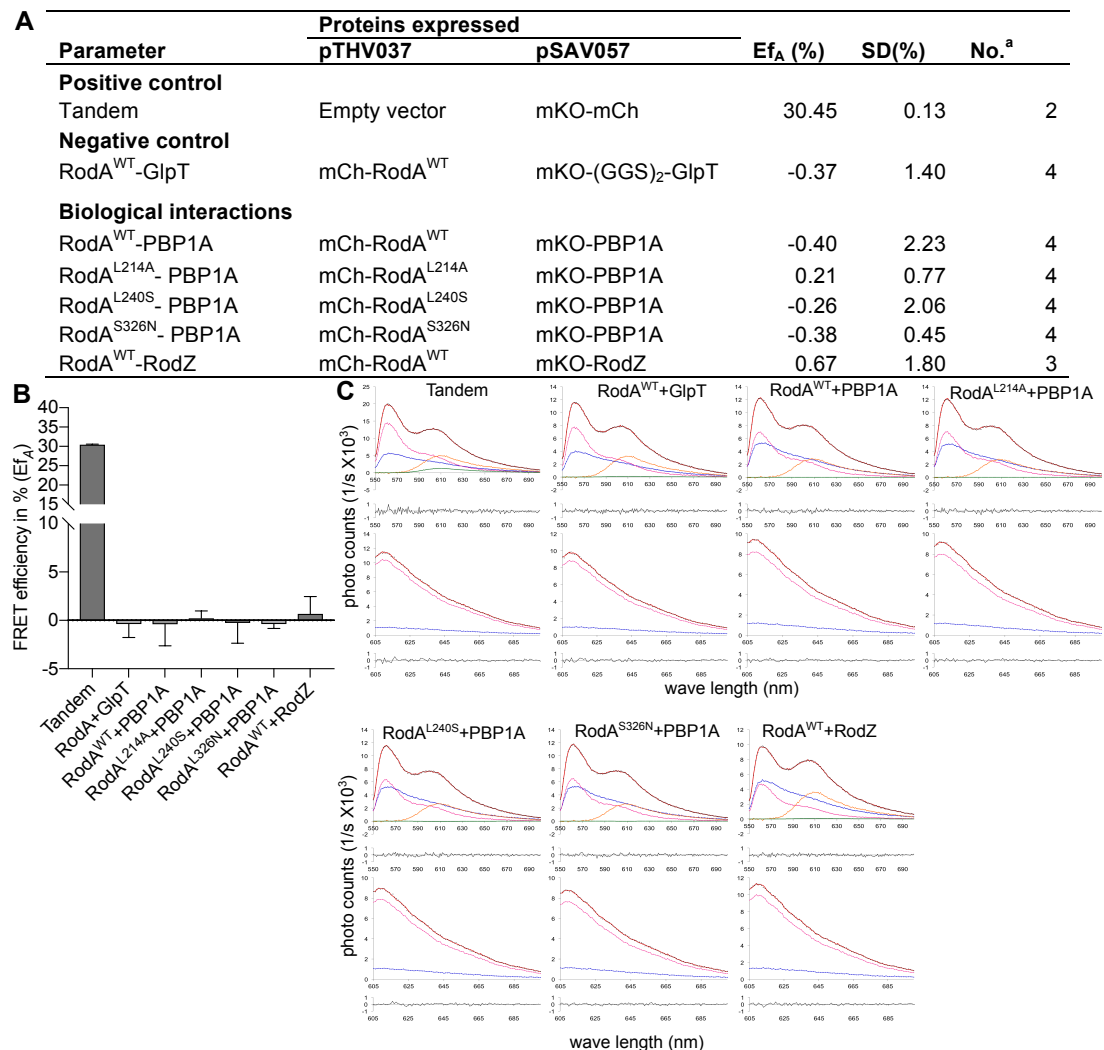
Essential interaction between RodA and MreCD proteins



Supplementary figure 2. Detection of RodA mutants by Immunoblotting. (A) Anti-mCherry antibody (1:1000) was used to detect the fusion proteins at 30 °C and 42 °C. The mCherry fused RodA mutants were detected at 67.7kDa. The truncate mutant mCherry-RodA^{F127stop} was detected at 41.3 kDa, and showed reduced blotting signals. (B) Anti-mCherry antibody (1:2000) was used to detect the fusion proteins at 30 °C and 42 °C. The truncate mutant mCherry-RodA^{W181stop} was detected at 47.0 kDa. Mutants RodA^{W181stop} and RodA^{G342A} showed reduced blotting signals.

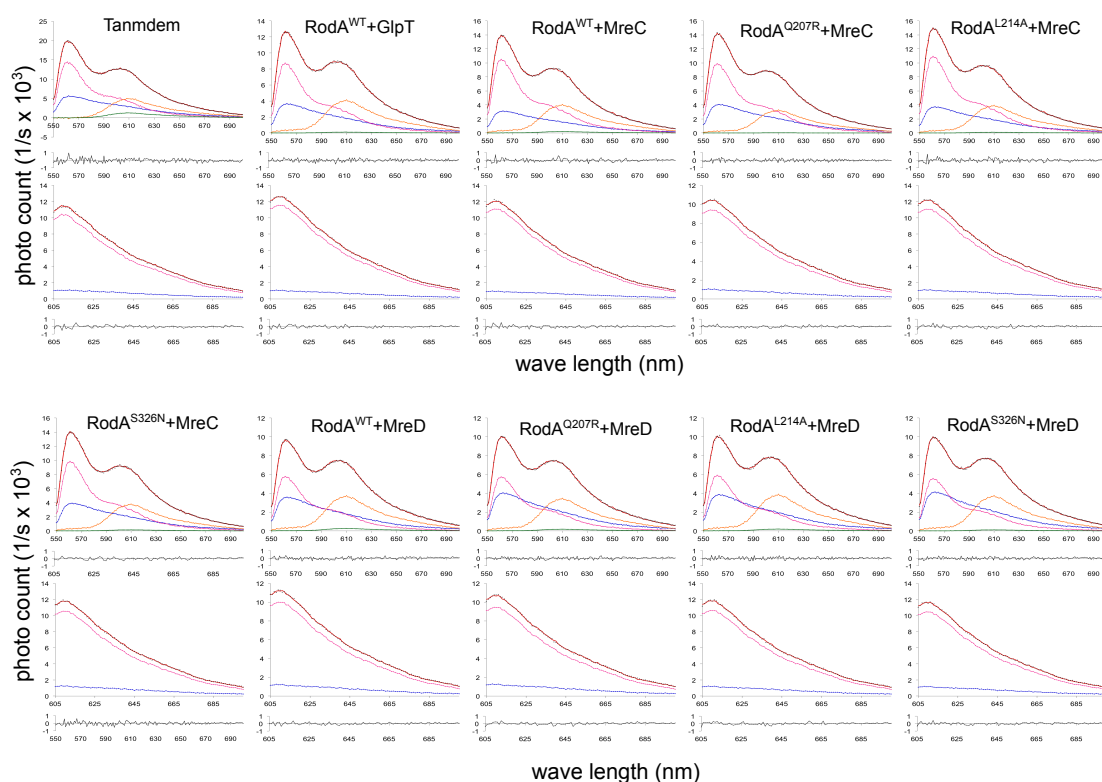


Supplementary figure 3. Overview of the unmixing data of the selected FRET groups. The FRET pairs listed above the graphs apply to the spectral data beneath them. For each pair the upper panel contains the measured spectrum excited at 538 nm in black dots, the calculated spectrum and its unmixed components; blue is background, magenta is mKO, orange is mCherry and green is the sensitized emission. The middle panel is the measured spectrum of mCherry excited at 590 nm in black dots, the calculated spectrum and its unmixed components; blue is background and magenta is mCherry. The bottom panel shows the residuals of the measured and calculated spectrum. Mutants RodA^{F127stop} and RodA^{G343A} showed defects on protein structure stability, as their measured spectrum shows significantly reduced mCherry intensity.



Supplementary figure 4. Interaction between RodA variants and PBP1A and RodZ detected by FRET. **A.** Summary of FRET experiments applied to detect the interaction of listed protein pairs. ^a. Number of sample measured. **B.** Acceptor FRET efficiency (Ef_A) between mCh-RodA variants and mKO-PBP1A or mKO-RodZ calculated from the spectral FRET measurements. **C.** Overview of the unmixing data of all the FRET pairs showed in the table. The FRET pairs listed above the graphs apply to the spectral data beneath them. Panels as in supplementary figure 3. Results are representative of two independent experiments.

Essential interaction between RodA and MreCD proteins



Supplementary figure 5. Overview of the unmixing data of the FRET samples listed in Figure 4. FRET pairs listed above the graphs apply to the spectral data beneath them. Panels as in supplementary figure 3.

Supplementary table 1. Strains and plasmids used in this study.

	Relevant properties	References
Strains		
DH5 α	<i>supE44, ΔlacU169, (Φ80lacZΔM15), hsdR17, recA1, endA1, gyrA9,6 thi-1, relA1</i>	Lab stock
LMC500 (MC4100 <i>lysA</i>)	<i>F araD139, Δ(argF-lac)U169, deoC1, flbB5301, ptsF25 rbsR, relA1, rpsL150, lysA1</i>	Lab stock ⁴
LMC882	<i>his, purB, proA, thi, lacY, rpsL, rodA(Ts)-52, zbe::Tn10</i>	Lab stock ⁵
Plasmids		
pTHV037	pTRC99A with a weakened P _{trc99A-down} promoter. pBR322 ori, ampicillin resistance	Lab stock ⁶
pSAV057	pTRC99A with a weakened P _{trc99A-down} promoter. p15A ori, chloramphenicol resistance	Lab stock ⁶
pSAV058	pSAV057 expressing mKO gene	Lab stock ⁶
pSAV050	pSAV057 expressing mCherry-mKO tandem protein	Lab stock ⁶

pSAV047-RodA	pTHV037 expressing mCh-RodA fusion protein linked with five codons	Lab stock ⁶
pWA004	pSAV057 expressing mKO-PBP2 fusion protein	Lab stock ⁶
pBB004	pSAV057 expressing mKO-PBP1A fusion protein	Lab stock ⁷
pXL29	pSAV057 expressing mKO-(GGG) ₂ -GlpT fusion protein	This work
pXL36	pTHV037 expressing mCh-RodA ^{R109A} fusion protein	This work
pXL37	pTHV037 expressing mCh-RodA ^{K117N} fusion protein	This work
pXL38	pTHV037 expressing mCh-RodA ^{F127stop} fusion protein	This work
pXL39	pTHV037 expressing mCh-RodA ^{W181stop} fusion protein	This work
pXL40	pTHV037 expressing mCh-RodA ^{Q207R} fusion protein	This work
pXL41	pTHV037 expressing mCh-RodA ^{G276D} fusion protein	This work
pXL42	pTHV037 expressing mCh-RodA ^{P330A} fusion protein	This work
pXL43	pTHV037 expressing mCh-RodA ^{P337A} fusion protein	This work
pXL44	pSAV057 expressing non-fused RodA ^{R109A} protein	This work
pXL45	pSAV057 expressing non-fused RodA ^{K117N} protein	This work
pXL46	pSAV057 expressing non-fused RodA ^{F127stop} protein	This work
pXL47	pSAV057 expressing non-fused RodA ^{W181stop} protein	This work
pXL48	pSAV057 expressing non-fused RodA ^{Q207R} protein	This work
pXL49	pSAV057 expressing non-fused RodA ^{G276D} protein	This work
pXL50	pSAV057 expressing non-fused RodA ^{P330A} protein	This work
pXL51	pSAV057 expressing non-fused RodA ^{P337A} protein	This work
pXL57	pTHV037 expressing mCh-RodA(TS) fusion protein	This work
pXL63	pSAV057 expressing non-fused RodA ^{W1} protein	This study
pXL96	pSAV057 expressing non-fused RodA ^{V89A} protein	This work
pXL97	pSAV057 expressing non-fused RodA ^{A94G} protein	This work
pXL98	pSAV057 expressing non-fused RodA ^{G98A} protein	This work
pXL99	pSAV057 expressing non-fused RodA ^{A99G} protein	This work
pXL100	pSAV057 expressing non-fused RodA ^{W102A} protein	This work
pXL101	pSAV057 expressing non-fused RodA ^{E114A} protein	This work
pXL102	pSAV057 expressing non-fused RodA ^{U159A} protein	This work
pXL103	pSAV057 expressing non-fused RodA ^{L214A} protein	This work
pXL104	pSAV057 expressing non-fused RodA ^{U262A} protein	This work
pXL105	pSAV057 expressing non-fused RodA ^{G342A} protein	This study
pXL106	pSAV057 expressing non-fused RodA ^{G343A} protein	This work
pXL107	pSAV057 expressing non-fused RodA ^{S344A} protein	This work
pXL108	pSAV057 expressing non-fused RodA ^{A345G} protein	This study
pXL111	pTHV037 expressing mCh-RodA ^{V89A} fusion protein	This work
pXL112	pTHV037 expressing mCh-RodA ^{A94G} fusion protein	This work
pXL113	pTHV037 expressing mCh-RodA ^{G98A} fusion protein	This work

Essential interaction between RodA and MreCD proteins

pXL114	pTHV037 expressing mCh-RodA ^{A99G} fusion protein	This work
pXL115	pTHV037 expressing mCh-RodA ^{W102A} fusion protein	This work
pXL116	pTHV037 expressing mCh-RodA ^{E114A} fusion protein	This work
pXL117	pTHV037 expressing mCh-RodA ^{D159A} fusion protein	This work
pXL118	pTHV037 expressing mCh-RodA ^{L214A} fusion protein	This work
pXL119	pTHV037 expressing mCh-RodA ^{D262A} fusion protein	This work
pXL120	pTHV037 expressing mCh-RodA ^{G342A} fusion protein	This work
pXL121	pTHV037 expressing mCh-RodA ^{G343A} fusion protein	This work
pXL122	pTHV037 expressing mCh-RodA ^{S344A} fusion protein	This work
pXL123	pTHV037 expressing mCh-RodA ^{A345G} fusion protein	This work
pXL154	pTHV037 expressing mCh-RodA ^{L240S} fusion protein	This work
pXL155	pTHV037 expressing mCh-RodA ^{S326N} fusion protein	This work
pXL156	pSAV057 expressing non-fused RodA ^{L240S} protein	This work
pXL157	pSAV057 expressing non-fused RodA ^{S326N} protein	This study
pXL163	pSAV057 expressing mKO-MreC fusion protein	This work
pXL170	pSAV057 expressing mKO-MreD fusion protein	This study
pXL171	pSAV057 expressing mKO-RodZ fusion protein	This study

Supplementary table 2. Primers used in this study.

Primer	Sequence 5'-3'	Description
priXL59	GCGCGAATTCATGACGGATAATCCGAATAAA	EcoRI-RodA-F
priXL60	GCGCAAGCTTTTACACGCTTTTCGACAACAT	HindIII-RodA-R
priXL61	GGCTGGACCTAGGTATTGTTGCCTTTCAGCCGTGC	RodA-R109A-F
priXL62	CGACGGCTGAAAGGCAACAATACCTAGGTCCAGCC	RodA-R109A-R
priXL63	ATTGCCAATATAGCCGTACCACTGATGGTCGCGAGATT TATCAACCGC	RodA-K117N-F
priXL64	GCGGTTGATAAATCTCGCGACCATCAGTGGTACGGCT ATATTGGCAAT	RodA-K117N-R
priXL65	CCGTACCACTGATGGTCGCGAGATAAATCAACCGCG	RodA-F127stop- F
priXL66	CGCGGTTGATTTATCTCGCGACCATCAGTGGTACGG	RodA-F127stop- R
priXL67	GGCCTTAGCTAGCGTCTGATTGGC	RodA-W181stop- F
priXL68	GCCAATCAGACGCTAGCTAAGGCC	RodA-W181stop- R
priXL69	ATGCATGATTACCGTCGCCAGCGC	RodA-Q207R-F
priXL70	GCGCTGGCGACGGTAATCATGCAT	RodA-Q207R-R
priXL71	AGCTGGGACTAGTGGACATTCTGATTCTGC	RodA-G276D-F

Chapter 4

priXL72	GCAGAATCAGAATGTCCACTAGTCCCAGCT	RodA-G276D-R
priXL73	GTATGGTAAGCGGAATTCTGGCGGTTGTA	RodA-P330A-F
priXL74	TACAACCGCCAGAATTCCGCTTACCATAC	RodA-P330A-R
priXL75	TTCCGCTCGCACTGGTCTCATATGGAGGATCGG	RodA-P337A-F
priXL76	CCGATCCTCCATATGAGACCAGTGCGAGCGGAA	RodA-P337A-R
priXL82	ACGGTATGTACGGTGTTGCTAAC	RodAts-Seq-2
priXL83	TGTGTCGGATCGAATGCTTCGC	RodAts-seq-3
priXL84	TTCGCGTTGACCAGGGGTGT	RodAts-seq-1
priXL89	CCCGAATTCAACAACAACATGACGGATAATCCGAATAA A	EcoRI-linker- RodA-F
priXL105	GTTTTTTTATTCGGATTATCCGTCAT	GA-FPs-RodAts- R1
priXL106	CAGGAAAATGTTGTCGAAAAGC	GA-FPs-RodAts- F1
priXL107	ATGACGGATAATCCGAATAAAAAACAT	GA-FPs-RodAts- F2
priXL108	TTACACGCTTTTCGACAACATTTTCCTG	GA-FPs-RodAts- R2
priXL195	AAGCATCTGCCGCCACTAGTAAAATAATACAG	RodA-V89A-F
priXL196	CTGTATTATTTTACTAGTGGCGGCAGATGCTT	RodA-V89A-R
priXL197	GTGGCGGTGCGACGCTTTCCGGTGGCATCTCTAAAGG	RodA-A94C-F
priXL198	CTTTAGAGATGCCACCGAAAGCGTCGACCGCCACC	RodA-A94C-R
priXL199	TTCGGTGCGATATCTAAAGCTGCTCAACGCTGGCT	RodA-K97C-F
priXL200	CAGCGTTGAGCAGCTTTAGATATCGCACCGAAAGC	RodA-K97C-R
priXL201	TTCGGTGCGATATCTAAAGGTGGTCAACGCTGGCTG	RodA-A99G-F
priXL202	GCCAGCGTTGACCACCTTTAGATATCGCACCGAAAGC	RodA-A99G-R
priXL203	ATACCGAGATCTAGAGCGCGTTGAGCACC	RodA-W102A-R
priXL204	GGTGCTCAACGCGCTCTAGATCTCGGTATTG	RodA-W102A-F
priXL205	AGCCGTCGGCAATTGCCAAAATAGC	RodA-E114A-F
priXL206	GCTATTTTGGCAATTGCCGACGGCT	RodA-E114A-R
priXL207	CAACGAGGATACTAGTTCCAGGGCAGGCTGTGCAGC	RodA-D159A-R
priXL208	CACAGCCTGCCCTGGGAACTAGTATCCTCGTTGCGC	RodA-D159A-F
priXL209	GGTCCAGGGCCATCATGACGCGCTGGCGCTGG	RodA-L214A-R
priXL210	CGCCAGCGCGTCATGATGGCCCTGGACCCGG	RodA-L214A-F
priXL211	CGCCATACTGCTTTTATCTTCGCGGTAATG	RodAD262-F
priXL212	CAGTACCGCGAAGATAAAAGCAGTATGGCG	RodAD262-R
priXL213	ATTAGCGCGGATCCAGCATAACTGACCAG	RodA-G342A-R
priXL214	CTGGTCAGTTATGCTGGATCCGCGCTAATTG	RodA-G342A-F
priXL215	CAATTAGCGCTGATGCTCCATAACTGACC	RodA-G343A-R
priXL216	GGTCAGTTATGGAGCATCAGCGCTAATTG	RodA-G343A-F

Essential interaction between RodA and MreCD proteins

priXL217	CACAATTAGCGCTGCTCCTCCATAA	RodA-S344A-R
priXL218	TTATGGAGGAGCAGCGCTAATTGTG	RodA-S344A-F
priXL219	GGAGGATCCGGGCTAATTGTGCTG	RodA-A345G-F
priXL220	CAGCACAATTAGCCCGGATCCTCC	RodA-A345G-R
priXL270	TCCGGCGGATCCCGCGGCAAA	RodA-L240S-F
priXL271	TTTGCCGCGGGATCCGCCGGA	RodA-L240S-R
priXL272	TATTGGTATGGTAAATGGAATTCTGCCGGTTGTAG	RodA-S326N-F
priXL273	CTACAACCGGCAGAATTCCATTTACCATACCAAT	RodA-S326N-R
rene39	GGGGGAATTCATGAATACTGAAGCC	EcoRI-RodZ-F
rene40	CCCCAAGCTTTTACTGCGCCGGTGATTG	HindIII-RodZ-R
priXL282	CCCGAATTCAACAACAACATGAAGCCAATTTTGTAGCCG TGG	EcoRI-MreCD-F
priXL283	GCGCAAGCTTTTATTGCACTGCAAAGCTGCTGAC	HindIII-MreCD-R
priXL286	GCGCAAGCTTTTATTGCCCTCCCGGCGCACG	HindIII-MreC-R
priXL299	GCGCGAATTCAACAACAACGTGGCGAGCTATCGTAGC CA	EcoRI-NNN- MreD-F

Reference

1. Meeske, A. J. *et al.* SEDS proteins are a widespread family of bacterial cell wall polymerases. *Nature* 1–15 (2016). doi:10.1038/nature19331
2. Pastoret, S. *et al.* Functional Analysis of the Cell Division Protein FtsW of *Escherichia coli*. *J. Bacteriol.* **186**, 8370–8379 (2004).
3. Sjødt, M. *et al.* Structure of the peptidoglycan polymerase RodA resolved by evolutionary coupling analysis. *Nature* (2018). doi:10.1038/nature25985
4. Taschner, P. E., Huls, P. G., Pas, E. & Woldringh, C. L. Division behavior and shape changes in isogenic *ftsZ*, *ftsQ*, *ftsA*, *pbpB*, and *ftsE* cell division mutants of *Escherichia coli* during temperature shift experiments. *J. Bacteriol.* **170**, 1533–1540 (1988).
5. Matsuzawa, H., Hayakawa, K., Sato, T. & Imahori, K. Characterization and genetic analysis of a mutant of *Escherichia coli* K-12 with rounded morphology. *J. Bacteriol.* **115**, 436–442 (1973).
6. van der Ploeg, R., Goudelis, S. T. & den Blaauwen, T. Validation of FRET assay for the screening of growth inhibitors of *Escherichia coli* reveals elongasome assembly dynamics. *Int. J. Mol. Sci.* **16**, 17637–17654 (2015).
7. Van der Ploeg, R. *et al.* Colocalization and interaction between elongasome and divisome during a preparative cell division phase in *Escherichia coli*. *Mol. Microbiol.* **87**, 1074–1087 (2013).

CHAPTER

5

General Discussion

Flipping lipid II across the cytoplasmic membrane

Interactions between elongasome proteins

Regulation of peptidoglycan synthesis by elongasome and divisome

As the key component of bacterial cell wall, peptidoglycan determines the shape of bacteria, and protects them from threats of their surroundings^{1,2}. Therefore its synthesis is tightly controlled and regulated during the bacteria cell cycle. Defects in peptidoglycan synthesis usually deforms bacteria and results eventually in cell lyse, that is why a large group of antibiotics discovered so far target the proteins involving in bacterial peptidoglycan synthesis³⁻⁶. Although in clinical therapies antibiotics has saved countless lives from bacterial infections, many bacteria have developed strategies to survive and become resistant when exposed to antibiotics⁷⁻⁹. The rising number of “super bacteria” that are resistant to all available antibiotics has already ring the alarm for speeding up the discovery of new antibiotics, which quest could profit from a better understanding of peptidoglycan synthesis.

Flipping lipid II across the cytoplasmic membrane

The peptidoglycan mesh is built at the outer side of the bacterial cytoplasmic membrane, while the precursor lipid II is synthesized inside the cytoplasm. The essential step of flipping lipid II across the cytoplasmic membrane makes the involved protein an important potential target for antibiotics. Only recently, the conserved essential integral membrane protein MurJ has been proved to have the lipid II flipping activity *in vivo*^{10,11}. Different crystal structures suggested that the flipping step is coupled to a conformational change of MurJ from inward open to outward open¹²⁻¹⁴. However, how and where MurJ performs its function remained unclear. This promoted us to visualize the MurJ behavior *in vivo*, and to gain more insights in peptidoglycan synthesis.

This was achieved by constructing functional fusions of fluorescent proteins to the N-terminus of MurJ in **Chapter 2**. MurJ localizes in the cylindrical membrane and also at the division site, which is in agreement with its function as lipid II flippase, since peptidoglycan synthesis is needed both for length growth and cell division. Interestingly, the midcell recruitment of MurJ is simultaneously with lipid II synthesis proteins MraY and MurG but slightly after the recruitment of the last core divisome protein FtsN. This timing is very logical because lipid II is synthesized by MraY and MurG on the inner leaflet of the cytoplasmic membrane, and subsequently flipped across

membrane by flippase MurJ. More importantly, the midcell localization of MurJ is dependent on the mature core divisome (arrival of FtsN). FtsN is thought to competitively overcome the inhibition of the PG synthesizing complex PBP1B-PBP3-FtsW^{15,16} and therefore initiates PG synthesis. The flipping of lipid II is thus critically coordinated with the activity of the divisome and peptidoglycan synthesis. Further investigations revealed that MurJ midcell localization is likely substrate depended rather than protein-protein interaction depended. This is supported by the facts that: (i) The essential MurJ function could be replaced with other flippases that share no sequence and structure similarities with MurJ¹⁷⁻¹⁹. (ii) The depletion of lipid II either by D-cycloserine inhibition of lipid II synthesis, or by inactivation of PBP3 and FtsW, delocalized MurJ from midcell. (iii) The divisome proteins that are recruited through protein-protein interactions remain assembled when PBP3 or FtsW are inactivated. (iv) No direct interaction could be detected between MurJ and other divisome components. Additionally, we found that the activity of MurJ is not needed for its recruitment at midcell, as inactivation of MurJ either by directly mutating essential charged residues or by adding MTSES to functional cysteine variants still allowed its localization at midcell. Given the evidence that MurJ midcell recruitment is substrate-dependent, this would indicate that these inactivated MurJ variants could still recognize lipid II but not be able to flip it. This is conflict with the *in vitro* evidence that MTSES reduces the lipid II binding affinity of the MurJ A29C variant²⁰. Considering that *in vitro* data in detergents are not always comparable with *in vivo* situation (e.g. the conflicting lipid II binding data)²¹, it is possible that after binding with MTSES, A29C variant could still recognize lipid II sufficiently to localize it to midcell.

Interactions between elongasome proteins

The synthesis and incorporation of peptidoglycan into the cylindrical cell wall is organized by a protein complex called elongasome, of which the assembly and activity regulation is still to a large extent unknown. So far, the published data have revealed that actin-like protein MreB can polymerize into short filaments that rotates along the cylindrical membrane in a circumferential motion, which is believed to organize the insertion of new peptidoglycan into

the existing wall²²⁻²⁴. The glycosyltransferase RodA and transpeptidase PBP2 form a subcomplex²⁵, while MreB, MreC and MreD form an essential membrane-bound ternary complex (MreB only interacts with MreC but not with MreD)²⁶. MreC can interact with itself to form a dimer or higher polymers, while MreD cannot interact with itself²⁶. The bitopic membrane protein RodZ interacts strongly with itself and MreB, and to decreasing extents with MreC, MreD and PBP2²⁶. The interaction between RodZ and MreB enhances the assembly and localization of MreB polymers and links MreB to the peptidoglycan synthesis proteins RodA-PBP2²⁷⁻²⁹. These scattered data (Fig. 1) are not enough to give a clear view on elongasome organization and regulation.

In **chapter 3**, we showed that the interaction between RodA and PBP2 is independent of their activities, but requires the transmembrane helix (TMH) of PBP2, which is in agreement with the evolutionary coupled co-variation of these regions³⁰. In addition, periplasmic parts of both proteins are needed for an optimal interaction. Our further investigations revealed that both MreC and MreD interact with PBP2 (Fig. 1) and competitively regulate PBP2 activity. PBP2 and RodA were observed to be able to interact with themselves³¹ (Fig. 1), suggesting that the proteins might be functional as at least a dimer of dimers. This would allow the insertion of multiple glycan strand simultaneously as has been often suggested as model for glycan strand insertion^{32,33}.

Besides its glycosyltransferase activity, RodA seems also to determine elongasome activity through coordination with other elongasome components. Some mutations in RodA would abolish bacterial elongation without interfering with its own glycosyltransferase activity³⁰. We firmly believed that further study on RodA would gain more insights about bacterial cell growth and peptidoglycan synthesis. Therefore in **chapter 4**, when we introduced mutations to the 23 potential essential residues of *E. coli* RodA, its localization, protein stability and interaction with PBP2 was mostly not influenced, in spite of the defects in RodA function and cell morphology. Eventually, we identified essential interactions between RodA with MreC and MreD proteins. Mutations at the potential interaction interface of RodA disrupted its interactions with MreC or MreD, which consequently abolished the cellular localization pattern of MreB. Together with the identified interactions between other elongasome

components (Fig. 1), these additional interactions also support the idea that MreB motion is linked to peptidoglycan synthesis²⁷, likely through RodZ-MreCD proteins. Since we revealed the potential regulatory mechanism of MreCD proteins on PBP2 activity (**Chapter 3**), it is possible that the disruption between RodA mutants and MreCD proteins could also influence the MreCD regulatory effects on PBP2. To validate this, further *in vivo* three-plasmids FRET experiments need to be performed between these mutated RodA variants and PBP2, in the presence of MreC or MreD. It is expected to observe disruptions in the regulatory effects of MreC and MreD on the RodA-PBP2 FRET efficiency.

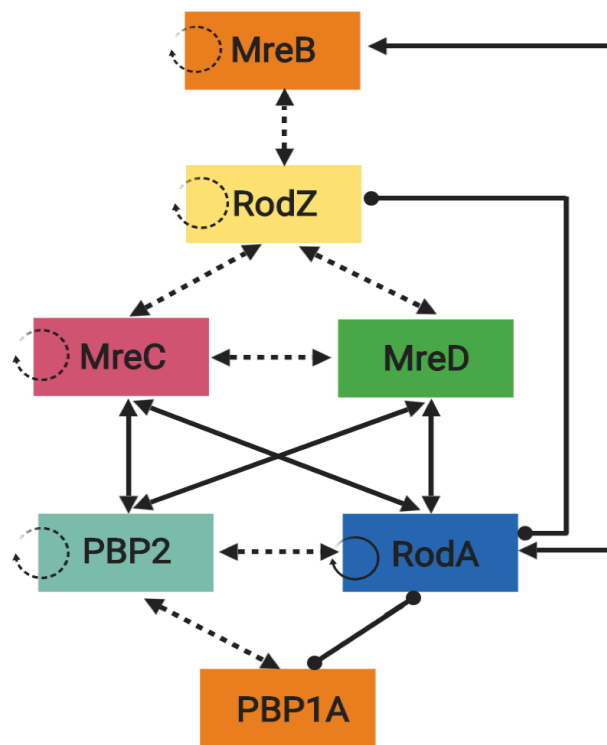


Figure 1. Interaction between elongasome proteins. Double arrowed dashed lines represent the interaction published in previous studies. Double arrowed solid lines represent the interaction identified in this thesis. Double dotted lines indicate no interaction detected in this thesis. Circle dashed and solid arrows represent the self-interaction published previously or identified in this thesis, respectively.

Regulation of peptidoglycan synthesis by elongasome and divisome

Peptidoglycan synthesis at the right time and right place is an important factor for bacterial survival. Therefore, it is not surprising that bacteria employ strict and tight regulatory mechanisms to control peptidoglycan synthesis. It has been shown in *E. coli* that, during cell division, the key divisome proteins FtsBLQ and FtsN competitively regulate the activity of peptidoglycan synthesizing proteins FtsW, PBP3 and PBP1B. At the heart of divisome, FtsBLQ proteins form a subcomplex that recruits FtsW-PBP3 and keeps PBP3, FtsW and PBP1B inactive or at a basal level of activity. While the accumulation of FtsN, which is the last core divisome protein that is recruited to mid cell, could finally competitively activate FtsW, PBP3 and PBP1B, and initiate septal peptidoglycan synthesis^{15,16,34}.

As the machinery that controls peptidoglycan synthesis in the cylindrical cell wall, the elongasome shares many similarities with the divisome. For example, they both employ a cytoskeleton-like protein (MreB and FtsZ in elongasome and divisome, respectively) to organize their assembly^{24,35}. And they both recruit a group of proteins, RodA-PBP2-PBP1A and FtsW-PBP3-PBP1B that have similar activities in elongasome and divisome, respectively, to synthesize peptidoglycan^{4,21,34,36-39}. Surprisingly, our study in **chapter 3** indicated a similar regulatory mechanism of peptidoglycan synthesis in the elongasome as in the divisome. The essential inner membrane protein MreD keeps RodA-PBP2 inactive, while they are activated by the accumulation of MreC. In agreement with this, both FtsN and MreC have been shown to interact with themselves, and (possibly) accumulate at each protein complex^{26,40,41}, and the number of FtsN and MreC are twice higher than the number of FtsBLQ and MreC molecules⁴². Therefore, It is seems logical that they share similar regulatory mechanisms of peptidoglycan synthesis.

To further validate this, future *in vitro* study of S2d (analog of the lipid II peptide moiety) hydrolysis experiments could to be performed, as it has been done for PBP3¹⁵. PBP2 could be expressed, purified and mixed with S2d⁴³ in reaction buffer¹⁵. To allow assessment of the influence of MreC and MreD on

the activity of PBP2, PBP2 should be reconstituted in vesicles in the presence of MreC or MreCD, preferably including RodA as well. PBP2 TPase activity could be monitored in presence of MreC or MreCD by measuring the absorbance at 330 nm with a plate reader. It is expected to observe that MreC stimulates PBP2 activity by increasing the absorbance, while MreD inhibits this stimulation and reduces the absorbance. Alternatively, *in vivo* experiments could also be possibly performed by analyzing the peptidoglycan structures to monitor PBP2 activity⁴⁴. Under the precondition that the TPase activity of all PBPs except PBP2 is blocked (i.e. by cefsoludin) in *E. coli* cells in osmotic protective environment, the peptidoglycan could be isolated from cells that expressing MreC only or MreCD proteins together, and be further analyzed by HPLC to detect the degree of cross-linking in peptidoglycan structure. It is expected to observe that in the presence of MreC, cells have higher extent of cross-linking, while in presence of MreD will reduce the degree of cross-linking.

References

1. Mattei, P. J., Neves, D. & Dessen, A. Bridging cell wall biosynthesis and bacterial morphogenesis. *Curr. Opin. Struct. Biol.* **20**, 749–755 (2010).
2. Demchick, P. & Koch, A. L. The permeability of the wall fabric of *Escherichia coli* and *Bacillus subtilis*. *J. Bacteriol.* **178**, 768 LP – 773 (1996).
3. Suzuki, H., Nishimura, Y. & Hirota, Y. On the process of cellular division in *Escherichia coli*: a series of mutants of *E. coli* altered in the penicillin-binding proteins. *Proc. Natl. Acad. Sci. U. S. A.* **75**, 664–668 (1978).
4. Lysis of *Escherichia coli* by beta-lactam antibiotics: deletion analysis of the role of penicillin-binding proteins 1A and 1B. *J Gen Microbiol.* **131**, 2839–45. (1985).
5. Zervosen, A., Sauvage, E., Frère, J. M., Charlier, P. & Luxen, A. Development of new drugs for an old target - The penicillin binding proteins. *Molecules* **17**, 12478–12505 (2012).
6. James T. Park, L. B. B. L. FL-1060: A new penicillin with a unique mode of action. *Biochem. Biophys. Res. Commun.* **51**, 863–868 (1973).
7. Neudorf, K. D. *et al.* Antibiotic resistance genes in municipal wastewater treatment systems and receiving waters in Arctic Canada. *Sci. Total Environ.* **598**, 1085–1094 (2017).
8. Pernot, L. *et al.* A PBP2x from a Clinical Isolate of *Streptococcus pneumoniae* Exhibits an Alternative Mechanism for Reduction of Susceptibility to β -Lactam Antibiotics. *J. Biol. Chem.* **279**, 16463–16470 (2004).
9. Foster, T. J. Antibiotic resistance in *Staphylococcus aureus*. Current status and future prospects. *FEMS Microbiol. Rev.* 430–449 (2017). doi:10.1093/femsre/fux007
10. Sham, L.-T. *et al.* MurJ is the flippase of lipid-linked precursors for peptidoglycan biogenesis. *Science (80-.)*. **345**, 220–222 (2014).
11. Chamakura, K. R. *et al.* A viral protein antibiotic inhibits lipid II flippase activity. *Nat. Microbiol.* (2017). doi:10.1038/s41564-017-0023-4
12. Kuk, A. C. Y., Hao, A., Guan, Z. & Lee, S. Y. Visualizing conformation transitions of the Lipid II flippase MurJ. *Nat. Commun.* **10**, (2019).
13. Butler, E. K., Davis, R. M., Bari, V., Nicholson, P. A. & Ruiz, N. Structure-function analysis of MurJ reveals a solvent-exposed cavity containing residues essential for peptidoglycan biogenesis in *Escherichia coli*. *J. Bacteriol.* **195**, 4639–4649 (2013).
14. Kuk, A. C. Y., Mashalidis, E. H. & Lee, S. Y. Crystal structure of the MOP flippase MurJ in an inward-facing conformation. *Nat. Struct. Mol. Biol.* **24**, 171–176 (2017).
15. Boes, A., Olatunji, S., Breukink, E. & Terrak, M. Regulation of the peptidoglycan polymerase activity of PBP1b by antagonist actions of the core divisome proteins FtsBLQ and FtsN. *MBio* **10**, 1–16 (2019).
16. den Blaauwen, T. & Luirink, J. Checks and Balances in Bacterial Cell Division. *MBio* **10**, 1–6 (2019).

17. Ruiz, N. Streptococcus pyogenes YtgP (Spy-0390) complements Escherichia coli strains depleted of the putative peptidoglycan flippase MurJ. *Antimicrob. Agents Chemother.* **53**, 3604–3605 (2009).
18. Meeske, A. J. *et al.* MurJ and a novel lipid II flippase are required for cell wall biogenesis in Bacillus subtilis. *Proc. Natl. Acad. Sci. U. S. A.* **112**, 6437–42 (2015).
19. Elhenawy, W. *et al.* The o-antigen flippase wzk can substitute for MurJ in peptidoglycan synthesis in helicobacter pylori and Escherichia coli. *PLoS One* **11**, 1–16 (2016).
20. Bolla, J. R. *et al.* Direct observation of the influence of cardiolipin and antibiotics on lipid II binding to MurJ. *Nat. Chem.* **10**, 363–371 (2018).
21. Leclercq, S. *et al.* Interplay between Penicillin-binding proteins and SEDS proteins promotes bacterial cell wall synthesis. *Sci. Rep.* **7**, 43306 (2017).
22. van den Ent, F., Izoré, T., Bharat, T. A. M., Johnson, C. M. & Löwe, J. Bacterial actin MreB forms antiparallel double filaments. *Elife* **2014**, 1–22 (2014).
23. Errington, J. Bacterial morphogenesis and the enigmatic MreB helix. *Nat Rev Micro* **13**, 241–248 (2015).
24. Strahl, H., Bürmann, F. & Hamoen, L. W. The actin homologue MreB organizes the bacterial cell membrane. *Nat. Commun.* **5**, 1–11 (2014).
25. van der Ploeg, R., Goudelis, S. T. & den Blaauwen, T. Validation of FRET assay for the screening of growth inhibitors of escherichia coli reveals elongasome assembly dynamics. *Int. J. Mol. Sci.* **16**, 17637–17654 (2015).
26. Kruse, T., Bork-Jensen, J. & Gerdes, K. The morphogenetic MreBCD proteins of Escherichia coli form an essential membrane-bound complex. *Mol. Microbiol.* **55**, 78–89 (2005).
27. Morgenstein, R. M. *et al.* RodZ links MreB to cell wall synthesis to mediate MreB rotation and robust morphogenesis. *Proc Natl Acad Sci U S A* **112**, 12510–12515 (2015).
28. Colavin, A., Shi, H. & Huang, K. C. RodZ modulates geometric localization of the bacterial actin MreB to regulate cell shape. *Nat. Commun.* **9**, 1280 (2018).
29. Bratton, B. P., Shaevitz, J. W., Gitai, Z. & Morgenstein, R. M. MreB polymers and curvature localization are enhanced by RodZ and predict E. coli's cylindrical uniformity. *Nat. Commun.* **9**, (2018).
30. Sjodt, M. *et al.* Structure of the peptidoglycan polymerase RodA resolved by evolutionary coupling analysis. *Nature* (2018). doi:10.1038/nature25985
31. Van der Ploeg, R. *et al.* Colocalization and interaction between elongasome and divisome during a preparative cell division phase in Escherichia coli. *Mol. Microbiol.* **87**, 1074–1087 (2013).
32. Moreno, E. *et al.* Surgical treatment of Zenker's diverticulum: Review of our experience. *Gullet* **2**, 19–23 (1992).
33. Scheffers, D.-J. & Pinho, M. G. Bacterial Cell Wall Synthesis: New Insights from

- Localization Studies. *Microbiol. Mol. Biol. Rev.* **69**, 585 LP – 607 (2005).
34. Ranjit, D. K., Jorgenson, M. A. & Young, K. D. PBP1B Glycosyltransferase and Transpeptidase Activities Play Different Essential Roles during the De Novo Regeneration of Rod Morphology in Escherichia coli. *J Biol Chem* **199**, 1–17 (2017).
 35. Sun, Q. & Margolin, W. FtsZ Dynamics during the Division Cycle of Live Escherichia coli Cells. *J. Bacteriol.* **180**, 2050–2056 (1998).
 36. Den Blaauwen, T., Aarsman, M. E. G., Vischer, N. O. E. & Nanninga, N. Penicillin-binding protein PBP2 of Escherichia coli localizes preferentially in the lateral wall and at mid-cell in comparison with the old cell pole. *Mol. Microbiol.* **47**, 539–547 (2003).
 37. Meeske, A. J. *et al.* SEDS proteins are a widespread family of bacterial cell wall polymerases. *Nature* 1–15 (2016). doi:10.1038/nature19331
 38. Cho, H. *et al.* Bacterial cell wall biogenesis is mediated by SEDS and PBP polymerase families functioning semi-Autonomously. *Nat. Microbiol.* **1**, (2016).
 39. Aarsman, M. E. G. *et al.* Maturation of the Escherichia coli divisome occurs in two steps. *Mol. Microbiol.* **55**, 1631–1645 (2005).
 40. Gerding, M. A. *et al.* Self-enhanced accumulation of FtsN at division sites and roles for other proteins with a SPOR domain (DamX, DedD, and RlpA) in Escherichia coli cell constriction. *J. Bacteriol.* **191**, 7383–7401 (2009).
 41. Lutkenhaus, J. FtsN - Trigger for septation. *J. Bacteriol.* **191**, 7381–7382 (2009).
 42. Li, G. W., Burkhardt, D., Gross, C. & Weissman, J. S. Quantifying absolute protein synthesis rates reveals principles underlying allocation of cellular resources. *Cell* **157**, 624–635 (2014).
 43. Kelly, J. A., Waley, S. G., Adam, M. & Frère, J. M. Crystalline enzyme kinetics: activity of the Streptomyces R61 d-alanyl-d-alanine peptidase. *Biochim. Biophys. Acta (BBA)/Protein Struct. Mol.* **1119**, 256–260 (1992).
 44. Silva, A. M. *et al.* The fluorescent D-Amino Acid NADA as a tool to study the conditional activity of transpeptidases in Escherichia coli. *Front. Microbiol.* **9**, 1–15 (2018).

Summary

In this thesis, we carried out several studies using genetics, microscopy, biochemistry and protein interaction detecting assay FRET, to investigate the synthesis and regulation of peptidoglycan in the model organism *E. coli*, and gained some new insights that could be beneficial for future antibiotic development.

In **chapter 1** the composition of bacterial cell envelope was overviewed and the structure and biosynthesis of peptidoglycan was introduced, which is an important component of bacterial cell wall. We focused on and emphasized several unclear key points about peptidoglycan synthesis, which are also the research questions of our studies in this thesis. (i) How does the lipid II flippase MurJ perform its function *in vivo*? (ii) How is the elongasome organized? (iii) How is peptidoglycan synthesis regulated during bacterial length growth?

In **chapter 2**, we focused on the lipid II flippase MurJ, and showed how MurJ functions during peptidoglycan synthesis based on its *in vivo* function and localization study. We firstly constructed functional N-terminal fusion of MurJ, and visualized that it localizes in the lateral wall and also at midcell. The timing of MurJ midcell localization is slightly later than that of the last divisome protein FtsN, but simultaneously together with that of lipid II synthesis proteins MraY and MurG. MurJ midcell localization requires the maturation of divisome, lipid II synthesis and activity of peptidoglycan synthesizing proteins PBP3 and FtsW. But its own lipid II flipping activity is not required for its localization. These results indicate MurJ midcell localization is substrate dependent, and its recruitment is tightly regulated by divisome activity.

In **chapter 3** and **chapter 4**, we aimed to reveal the organization of the elongasome, and its coordination with peptidoglycan synthesis. In **chapter 3**, we firstly investigated the interaction between RodA and PBP2, and found out that both the transmembrane and periplasmic regions of PBP2 are needed to form a permanent subcomplex that is independent on their function. For the first time, we found that both MreC and MreD interact with PBP2 *in vivo*, and MreC affects the interaction between PBP2 and RodA, which likely

corresponded to the activation of PBP2, while MreD competitively inhibits this activation. The balance between MreC and MreD regulates the conformational changes of PBP2 and its activity, and consequently the diameter of bacteria. These results revealed a potential regulation mechanism of elongasome activity and cylindrical peptidoglycan synthesis, which is similar to the reported mechanism in divisome.

In **chapter 4**, we focused on the glycosyltransferase RodA, and aimed to reveal how RodA influence elongasome organization and activity, in addition to its function in lipid II polymerization. We replaced 23 potential essential residues in RodA by other amino acids, and investigated their influence on RodA function, localization, protein stability and RodA-PBP2 interaction. We found that most of these residues are essential for RodA function, while RodA localization, protein stability and its interaction with PBP2 are mostly not influenced. Based on the crystal structure of RodA, we grouped these residues into two classes, and concluded that residues of first class are likely directly involved in the RodA glycosyltransferase activity, because they locate close or in the central cavity of RodA. Further investigations on the residues of the second class revealed that they are important for MreB localization, and the abolished MreB localization by these mutations is achieved through the disruption on RodA interactions with MreC and MreD. These results indicate that the RodA interaction with MreC and MreD is essential for MreB and elongasome function and is also likely important for the proper regulatory function of MreCD on PBP2 activity. These results give more details on elongasome organization and peptidoglycan synthesis regulation.

In **chapter 5**, we discussed our results together with the available published data, and answered the research questions of our studies. Our studies have gained more insight in peptidoglycan biosynthesis in bacteria, and provide more information for future novel antibiotics development.

Samenvatting

In dit proefschrift hebben we verschillende studies uitgevoerd met behulp van genetica, microscopie en biochemische- en eiwitinteractietechnieken om de synthese en regulatie van peptidoglycaan in modelorganisme *E. coli* te onderzoeken. Hierbij hebben we enkele nieuwe inzichten opgedaan die gunstig kunnen zijn voor de ontwikkeling van nieuwe antibiotica in de toekomst.

Hoofdstuk 1 behandelt de samenstelling van de bacteriële celenvelop en de structuur en biosynthese van peptidoglycaan, een belangrijk onderdeel van de bacteriële celwand. We concentreren ons op en benadrukken enkele onduidelijke kernpunten over peptidoglycaansynthese, die ook de onderzoeksvragen zijn van onze studies in dit proefschrift: (i) Hoe werkt de Lipide II flippase MurJ zijn functie *in vivo*? (ii) Hoe is het elongasoom georganiseerd? (iii) Hoe wordt de synthese van peptidoglycaan gereguleerd tijdens de lengtegroei van de bacterie?

In **hoofdstuk 2** hebben we ons gericht op de lipid II flippase MurJ en laten we zien hoe MurJ functioneert tijdens peptidoglycaansynthese op basis van een *in vivo* functie- en lokalisatieonderzoek. We construeerden een functionele N-terminale fusie van MurJ en visualiseerden de lokalisatie ervan in de laterale celwand en in de midcel. De timing van MurJ-midcellokalisatie is enigszins later dan die van het laatste divisoomewit FtsN, maar gelijktijdig samen met die van Lipide II-synthese-eiwitten MraY en MurG. MurJ-midcellokalisatie vereist de ontwikkeling van het divisoom, van de lipid II-synthese en activiteit van peptidoglycaansyntheseëiwitten PBP3 en FtsW, maar de eigen lipid II-flippingactiviteit is niet vereist voor de lokalisatie van MurJ. Deze resultaten geven aan dat de midcellokalisatie van MurJ afhankelijk is van het substraat en dat de recrutering ervan nauw wordt gereguleerd door activiteit van het divisoom.

In **hoofdstuk 3** en **hoofdstuk 4** onderzoeken we de organisatie van het elongasoom en de coördinatie ervan met peptidoglycaansynthese. In **hoofdstuk 3** hebben we eerst de interactie tussen RodA en PBP2 onderzocht en ontdekt dat er interactie is tussen deze twee in zowel de transmembraan- als de periplasmatische delen, om een permanent subcomplex te vormen dat

onafhankelijk is van hun functie. Voor de eerste keer vonden we dat zowel MreC als MreD *in vivo* interactie vertonen met PBP2. Ook heeft MreC een stimulerend effect op de PBP2-conformatie, wat overeenkomt met de activering van PBP2, terwijl MreD deze activering competitief remt. De balans tussen MreC en MreD reguleert de verandering in conformatie van PBP2 en daarmee de activiteit en bijgevolg ook de diameter van bacteriën. Deze resultaten onthullen een mogelijk regulatiemechanisme van activiteit van het elongasoom en van cilindrische peptidoglycaansynthese, die vergelijkbaar is met het gerapporteerde mechanisme in het divisoom.

In **hoofdstuk 4** richten we ons op de glycosyltransferase RodA, en laten we zien hoe RodA invloed heeft op de organisatie en activiteit van het elongasoom, ondanks de functie ervan bij Lipide II-polymerisatie. We construeerden 23 mutaties in de potentieel essentiële residuen in RodA en onderzochten hun invloed op de functie, lokalisatie en eiwitstabiliteit van RodA en op RodA-PBP2-interactie. We ontdekten dat de meeste van deze residuen essentieel zijn voor de functie van RodA, terwijl ze geen invloed hebben op lokalisatie, eiwitstabiliteit en de interactie met PBP2. Gebaseerd op de kristalstructuur van RodA hebben we deze residuen in twee klassen gegroepeerd en we hebben geconcludeerd dat residuen van de eerste klasse waarschijnlijk direct betrokken zijn bij de RodA-glycosyltransferaseactiviteit, omdat ze zich dichtbij of in de centrale holte van RodA bevinden. Verder onderzoek naar de residuen van tweede klasse onthulde dat ze belangrijk zijn voor MreB-lokalisatie. De ontbrekende MreB-lokalisatie door deze mutaties wordt bereikt door de verstoring van RodA-interacties met MreC en MreD. Deze resultaten geven aan dat RodA-interactie met MreC en MreD essentieel is voor de functie van MreB en het elongasoom. Deze interactie is waarschijnlijk ook belangrijk voor de juiste regulerende functie van MreCD op PBP2-activiteit. Deze resultaten bieden een gedetailleerder beeld van de organisatie van het elongasoom en de regulatie van peptidoglycaansynthese.

In **hoofdstuk 5** bespreken we onze resultaten in het licht van de beschikbare gepubliceerde data en beantwoorden we de onderzoeksvragen van onze studies. Ons onderzoek heeft meer inzicht gegeven in de biosynthese van peptidoglycaan in bacteriën en biedt aanknopingspunten voor de ontwikkeling van nieuwe antibiotica in de toekomst.

Acknowledgement

I have heard many times that PhD studies are fulfilled with stresses and pains, especially when you are also starting a life in a totally new place. While I would say that I had enjoyed a wonderful and unforgettable PhD research life in Amsterdam, which is just because I am lucky enough to have all the help and supports from the people who had ever participated in this journey. After over 40,000 words summarizing my PhD researches, I would like to include few hundreds more to express my sincerest gratitude to these people.

In the first place, I would like to thank my supervisor Tanneke den Blaauwen, for all her warm help and support in the past few years, not only on my researches, but also on the life outside of lab. I really appreciate her patience and understanding during the tough moments during the research, and her constructive insights to solve complicated research questions. Her professionalism has taught me how to be a good and independent researcher. I am especially thankful for her efforts and help during the paper work of my manuscripts and thesis, with so many versions of editing, correcting. I was very much touched at the time when I knew that she was suffering from a serious headache but still working on my thesis, because she wanted to help as much as possible. The past few months was a tough period for me due to the many changes in my life, I am also very thankful for her suggestions and help on my visa issue and job seeking. I cannot feel luckier to work together with her. I would also very much like to extend my sincerely thanks to my co-promotor Leendert Hamoen, for his instructive suggestions and discussions in scientific researches. Also, I appreciate that he is always supportive and willing to help, especially during the tough moments during the lab relocation.

I would like to thank all the former and current members of our Bacterial Cell Biology and Physiology group, Jolanda, Tjalling, Annelies, Norbert, Pranav, Alejandro, Michaela, Gaurav, Nils, Laura, Terrens, Edward, Yongqiang, Jinglan, Biwen, Elisa, Laureen, Xinwei, Zihao, Yaozu and all the students. All of them had given me plenty of help in the lab, and thanks to all these lovely people, the lab is running smoothly and very well organized. I enjoyed very much of the positive and united atmosphere in our lab. I had

learned many from all of you, which will benefit for rest of my life. I enjoyed the scientific part during the lab hours, and also appreciate these unforgettable moments we had together outside of lab. We share, we care, we support and we contribute. These nice people together make our lab a dream place to join.

I would like also to express my grateful to the committee members. Thank you all for your critical reading and efforts to improve this thesis. And also thank your time to come to my defense. Specially, many thanks to Prof. Waldemar Vollmer. I appreciate very much for your constructive suggestions and collaborations on my project, and for your help and efforts during the manuscript preparation.

Outside of my research hours, I had developed strong friendship with some other people who I would also like to thank too, no matter where they are working now. Dongdong Zheng and Yuan Gao, we met at the national airport of Beijing for first time, together with Yongqiang, and we made this fancy journey together starting from the same flight. After landed, I eventually made friends with some nice people here. Jun Xiao, Yiwei Sun, Si Wen, Zijian Zhou, Xiaoqin Liu, Huan Zhou, Yang Hu, Ludan Tan, Muhe Diao, Wei Du, Hui Xiong, Xiaotang Di, Xinyi Li, Yixuan Cao, Yanfei Zhang, Qinglong Meng, WenYang Wu, Yumei Wang, Songyu Yang, Shilin Zeng, Chao Ding, Qiong Li, Qianqian Zhang, Xia Fang, Wei Quan, Zhaochun Ren, Yanfang Feng, Que Chen, Guowei Lv, Ambuj, Vishnu, Arivanda and many others. Thank you all for participating this fancy journey in the past few years. We had so much fun together, sporting, play games, travelling, and celebrating Chinese festivals. Additionally, many thanks to Jun, Yiwei, Zijian, Yang, Huan, Feifei and Si, for your warm help during the last few months. It is amazing and lucky to have those friends sharing the life with me. I will certainly remember all the beautiful moments we had spent together.

In the end, I would like to thank my family members in Chinese. 感谢我的爸爸妈妈多年来对我的养育之恩。过去的几年，虽然我很少能和你们团聚，虽然远隔万水千山，但是你们无时无刻不在关心牵挂我，你们的每一句叮嘱儿子都记在心里。感谢你们一直以来的辛劳付出。我亲爱的老婆张琳琳，感谢你这些年来的相伴和照顾，从我们相知，相识，到步入婚姻的殿堂，到一起迎来我们可爱的宝宝桐桐。你的一路相伴，给了我最大的勇气和动力。有你在的这

段时间里，海外的求学生活充满了快乐，感谢你带给我一个温暖幸福的家。同时，也非常感谢我的岳父岳母以及奶奶，感谢你们的信任和支持，把你们的掌上明珠琳琳许配给我。感谢岳父岳母过去几个月长途跋涉来到荷兰，照顾我们，照顾桐桐。此外，非常感谢我的姐姐和姐夫。我感到很幸福，有姐姐姐夫宜家在一直关心爱护我们。在过去的十年里，一直都是你们照顾爸妈。也非常感谢其他家人对我的关心和照顾。祝愿我所有的最亲爱的家人，身体健康，幸福美满。

Xiaolong

Amsterdam, 2019